Technische Universität München
Fakultät für Informatik

Lehrstuhl für Sensorbasierte Robotersysteme
und Intelligente Assistenzsysteme

Multi-Dimensional Nonlinear Oscillation Control of Compliantly Actuated Robots

Dipl.-Ing. (FH) Dominic Lakatos

Vollständiger Abdruck der von der Fakultät für Informatik der Technischen Universität München zur Erlangung des akademischen Grades eines Doktors der Naturwissenschaften (Dr. rer. nat.) genehmigten Dissertation.

Vorsitzende(r):	Prof. Dr.-Ing. Matthias Althoff
Prüfer der Dissertation:	
	1. Prof. Dr.-Ing. Alin Albu-Schäffer
	2. Prof. Dr. Marco Hutter
	3. Prof. Dr. Stefano Stramigioli

Diese Dissertation wurde am 29.06.2017 bei der Technischen Universität München eingereicht und durch die Fakultät für Informatik am 15.12.2017 angenommen.

Preface

This doctoral thesis is based on investigations undertaken at the Institute of Robotics and Mechatronics of the German Aerospace Center (DLR) in Oberpfaffenhofen, Germany.

I would like to express my deepest gratitude to my supervisor and mentor Alin Albu-Schäffer for his guidance, the inspiring discussions we had on numerous evenings (and also weekends) throughout the course of this work, and his infectious enthusiasm for everything related to dynamics and many more surrounding and further topics. My special thanks go to the leader of my department Christian Ott, who gave me the opportunity to freely work on the topic of this thesis, and supported me with many ideas and critical but constructive questions. I would like to thank my former colleague and good friend Florian Petit for the fruitful collaboration and all the fun we had together in investigating compliantly actuated robots. Furthermore, many thanks to all my other colleagues Maxime Chalon, Alexander Dietrich, Gianluca Garofalo, Martin Görner, Manuel Keppler, Christian Rode (guest researcher), Philipp Stratmann, M. Can Özparpucu, Alexander Werner, etc., with whom I had a lot of interesting and inspiring discussions. My particular thanks go to Florian Schmidt, Werner Friedl, Florian Loeffl, Daniel Seidel, Jan Cremer, Robert Burger, Thomas Gumpert, all my former students, and all so excellent co-workers from the mechanics and electronics workshops.

I would like to appreciate the support of Alexander Dietrich, M. Can Özparpucu, Alessandro Giordano, Philipp Stratmann, and Johannes Engelsberger in proofreading this thesis.

This thesis is dedicated to Alexandra (one of the bravest and kindest person I ever met), my beloved daughter Magdalena, and my (male) dog Molly.

Abstract

To increase performance and energetic efficiency, robot design recently evolved from classical, rigid to intrinsically compliant actuation. The introduction of elastic elements enables the absorption of external impact forces, and it offers the capability of buffering and directedly releasing kinetic energy. Therefore, the instantaneously retrievable power at the link side of the joint is not limited by the restricted input power of the motor. These properties can be exploited in the execution of highly dynamical, cyclic, and periodic motion tasks such as hammering, pick-and-place with robotic manipulators, walking, jumping, or running with versatile, articulated legs. Although compliant actuators are promising regarding performance and efficiency, they turn the plant into a multi-dimensional, nonlinear, oscillatory system, of which the analysis and control is a challenging task.

This thesis contributes to the theory of energy-efficient limit cycle generation, dimensionality reduction of nonlinear systems, natural dynamics-based, modal controllers, and the application to legged system design and control. A new, robust control principle is proposed, which solves the problem of resonance-like excitation in the single-degree-of-freedom, nonlinear oscillator case. Thereby, existence, uniqueness, and attractiveness of resulting periodic orbits are proven based on novel statements, which contribute to hybrid dynamical system and contraction theory. To generalize these findings to multiple dimensions, classical results of theoretical mechanics suggest to reduce the dimensionality of the oscillatory dynamics to one. This proposition is further supported by empirical evidence of biologists that fundamental principles of legged locomotion are based upon oscillatory movements, which evolve on lower-dimensional submanifolds than the configuration space of articulated legs. The well-established method of modal analysis solves the problem of dimensionality reduction for the linear case. However, the multibody dynamics of articulated robots is strongly nonlinear, and therefore, linear modal analysis is not applicable straightforwardly. A novel theory of oscillation modes of nonlinear dynamics is proposed here, which solves the problem at hand for the general case. The main theorem on oscillation modes provides algebraically verifiable conditions, for which a one-dimensional submanifold of some configuration space represents an invariant set of the considered dynamical system. By means of this finding a method is introduced which allows to embody low-order, desired task dynamics as oscillation modes in the mechanical design of the robotic system. To exploit the natural oscillatory behavior, as given by oscillation modes, appropriate control methods are crucial. For this purpose, four different modal control methods are introduced, which address the demands of feasibility, versatility, robustness,

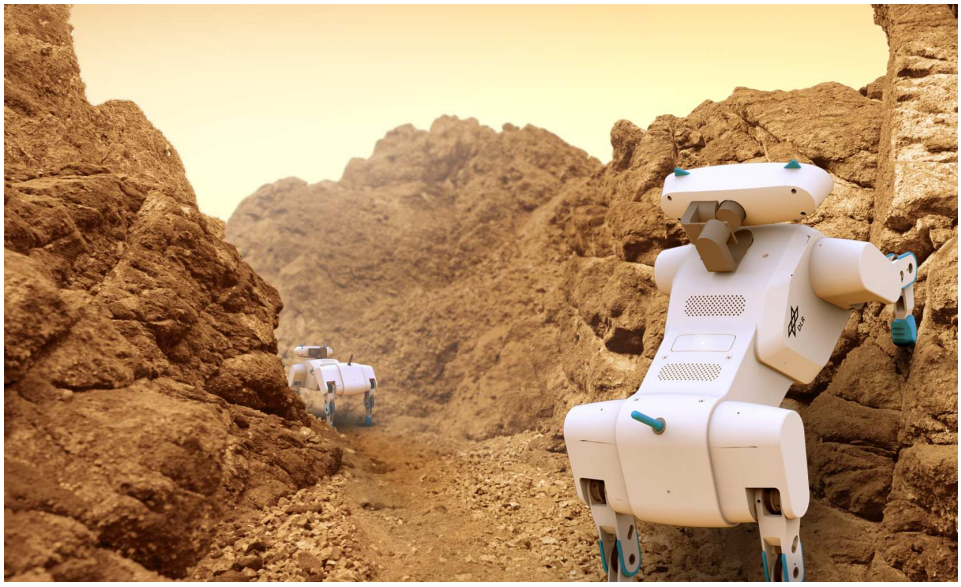

and efficiency with varying priority. The control methods are validated in simulations and experiments. A proof of concept is performed by applying the theoretical results to the design and control of legged robots. Thereby, the performance and efficiency of the approach is experimentally validated in various dynamic locomotion gaits with compliantly actuated quadrupedal and bipedal robots. This is a fine step towards the vision to create a versatile and efficient system, which can efficiently move in rather simple terrain but has simultaneously the capability to climb, jump, and crawl in rough and challenging terrain, being therefore able to reach areas, where *no other system* could go before.

Contents

Nomenclature

$\boldsymbol{A}$	Matrix, e. g., $\boldsymbol{A} \in \mathbb{R}^{m \times n}$
$\boldsymbol{b}$	Column matrix, e. g., $\boldsymbol{b} \in \mathbb{R}^{n}$
$\dot{\boldsymbol{q}}$	Total time derivative, i. e., $\dot{\boldsymbol{q}} = \frac{\mathrm{d}\boldsymbol{q}}{\mathrm{d}t}$
$\mathcal{M}$	Point-set, Manifold
$\mathcal{TM}$	Tangent bundle corresponding to $\mathcal{M}$, e. g., $(\boldsymbol{q}, \dot{\boldsymbol{q}}) \in \mathcal{TM}$
$\boldsymbol{q}$	Local coordinates of $\mathcal{M}$
$\mathbb{R}$	Real numbers
$\mathbb{R}^n$	n-dimensional Euclidian space
t	Time

List of Figures

List of Tables

CHAPTER 1

Introduction

1.1. Motivation

The phenomena of *nonlinear oscillations* fascinate engineers and mathematicians since the discovery of the oscillators of *Duffing* [Duf18] and *van der Pol* [VdP26], [VdP27] and maybe even longer. They arose as models in continuum mechanics and electrical circuit theory, respectively [GH83]. Oscillations, e. g., of particles or electrical charges, are motions, where parts of the same trajectory are retraced repeatedly. This general definition implies the interchange of kinetic and potential energy. As such, in robotics nonlinear oscillations became important at least since the intentional addition of compliance to the generally nonlinear multibody dynamics of classically rigid robots. The idea of realizing a desired visco-elastic behavior by control originates from the necessity of universally applicable robots to *stably* interact with uncertain or even unknown environments [Hog85]. To overcome the bandwidth limitations of any control system, robot development evolved from rigid towards compliant actuation—implementing elasticities by real, physical springs [PW95]. These elastic elements in combination with the inherent damping contained in any real system act as low-pass filter on external forces, which compared to rigidly actuated systems, substantially increase the mechanical robustness of the plant. In particular, the elastic energy storage can be exploited to buffer and directedly release kinetic energy. Thereby, task performance can be increased, and energetic efficiency can be gained compared to rigid actuation, since the instantaneously retrievable output power of the joints is not limited by the maximum power input related to the motors. The capability to store potential energy independently of the configuration of the links can be particularly exploited in oscillatory motion tasks such as throwing and pick-and-place for manipulator arms, or walking, jumping, and running in case of legged systems. For the latter class of tasks, the above-mentioned energy saving properties are even of major importance. Such mobile, legged systems gain significant advantages over wheeled vehicles: they are able to efficiently move in rather simple terrain, while fulfilling still the requirements to maneuver in highly demanding environments, where rover like systems cannot be operated properly.

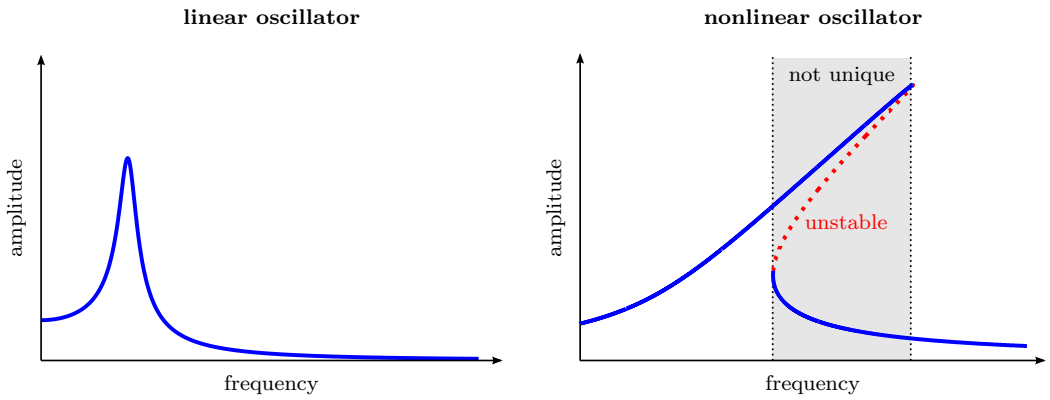

Figure 1.1.: Comparison of the amplitude-frequency characteristics: linear vs. nonlinear oscillator.

1.2. Problem statement and objectives

Although the step from rigid towards compliant actuation is promising regarding performance and efficiency, it turns the dynamics of the plant into a nonlinear and oscillatory one, of which the analysis and control is a challenging task. Even the single-degree-of-freedom oscillators of Duffing [Duf18] and van der Pol [VdP26], [VdP27] are improperly understood yet [GH83, p. 66], although they probably belong to the most studied nonlinear systems of the last century. In case of forced linear oscillations such as of mass-spring-damper systems, the concept of resonance is well studied, as particular solutions can be obtained in closed form. In contrast, for nonlinear oscillators such as the forced Duffing oscillator [Duf18], approximative solutions based on perturbation methods [Nay73] reveal a substantially different resonance behavior as known from linear oscillation theory. For instance, the system exhibits multiple resonance states, and the amplitude and frequency of the steady-state response depend on the amplitude and frequency of the excitation as well as on the initial conditions [NM79]. This fundamentally different behavior of nonlinear oscillators (compared to linear systems) makes the prediction of periodic and resonance-like motions a non-trivial problem (Fig. 1.1).

By turning from single to multi-degrees-of-freedom (DOF) nonlinear oscillatory systems, the situation becomes even worse. For instance, solutions of the conservative (elastic) double pendulum, as representative of the most simplest multi-DOF, nonlinear oscillator, can behave chaotically. Under certain conditions on the Hamiltonian[1], an energy-conservative one-DOF system displays periodic solutions, which correspond to level sets of energy. However, in case of multi-DOF systems, such level sets are not necessarily closed. This is as in general the level sets of multi-DOF systems have a dimensionality greater than one. Accordingly, the existence of periodic solutions can be ensured solely for one-DOF oscillators. From these considerations it becomes clear that for studying multi-dimensional nonlinear oscillations, the concept of reducing the dimensionality of dynamical systems to a single DOF dynamics is crucial.

However, even if a multi-DOF system features an invariant subset of reduced dimensionality, as mentioned above, then its exploitation by control requires still the explicit knowledge of its "shape". The shape of such an invariant manifold depends on the model

[1]For instance, if the Hamiltonian is a strongly convex function of the generalized coordinate and the conjugate momentum variable

of the corresponding dynamical system, which, for a real plant cannot be assumed to be exactly known. Additionally, even if the motion of the considered system can be nominally controlled to evolve in the invariant manifold, disturbances may occur. As such, either the system itself or the control needs to feature a certain attractiveness of the invariant manifold.

To be able to exploit the natural oscillatory behavior, the "shape" of the corresponding invariant manifold needs to match to the evolution of the task. Due to the nonlinearity of the considered dynamical systems, this matching procedure is challenging.

In summary, the main objective of this thesis is to address the following questions:

- How can single-DOF, compliantly actuated, nonlinear, second-order systems be efficiently controlled to display attractive closed orbits?
- What are the preconditions for multi-dimensional nonlinear oscillations, i. e., under which conditions collapses the natural dynamics of compliantly actuated multibody systems to a single second-order differential equation?
- How to efficiently control compliantly actuated robots to display oscillatory or periodic motions?
- Are there ways to embody a certain desired natural dynamics behavior of reduced dimensionality into the plant, and how can such system-inherent properties be exploited in the execution of robotic tasks?

Ultimate goals of this thesis are gaining the understanding for natural motions of highly nonlinear multibody systems with elastic elements in the joints, and exploiting the acquired insights to increase performance and efficiency in the execution of particular tasks. Thereby, the application of articulated, legged locomotion is intended to serve as the main benchmark.

1.3. Related work

This section provides an overview of related work in the field of nonlinear oscillations and the control of robotic system with elasticities in the joints. Thereby, the starting point of investigations of this thesis is identified.

1.3.1. Compliantly actuated robotic systems

In the last decades, numerous robotic systems with elasticities in the power-trains of the joints have been developed. For the goal of analyzing and controlling naturally arising oscillations, the distinction of *flexible-joint robots* [Rea94] and *compliantly actuated robots* [ASEG$^+$08] is of concern, whereas the latter are often treated in the context of so-called *variable stiffness actuators (VSA)*, see [CVS12] and [WGE$^+$16] for recent overviews. While the rather high stiffness[2] of flexible-joint robots arises mainly as a side effect of reducing weight and achieving superior controllability of the torques in the joints [HASH$^+$01], the rather low intrinsic stiffness of compliantly actuated robots is intended to match the bandwidth of desired tasks [ASEF$^+$11]. Again, one of the primary goals of this thesis is exploiting the natural oscillatory behavior in the execution of particular tasks. As such, only the class of compliantly actuated systems (with rather low intrinsic stiffness matching

[2]The term "stiffness" is used here for simplicity, although this quantity is non-tensorial (cf. Definition 2.3).

to considered tasks) is of interest. Nevertheless, both classes of multibody systems with elasticities in the joints can be treated in the general framework of statically controllable, under-actuated Euler-Lagrange systems [ASWE+10], [ASOP12].

1.3.2. Basic control

In compliantly actuated systems, the motion of the links is controlled via springs by moving the motors. However, in general, electrical motors are able to generate high velocities but rather low torques such that gear-boxes are required, which, in turn, are subject to energetic losses. In general, the dissipated power increases with increasing velocities. As such, a strategy to efficiently move the links is given by moving the motors as few as possible. This can be achieved by directly controlling the motion of the motors, e. g., by utilizing the methods of [Tom91], [OKL95], [ZDLS04], [ASOP12]. As these controllers feedback exclusively control-input-collocated variables (i. e., motor positions and velocities), they perform very robustly even in case of significant model uncertainties. Thus, these motor position controllers serve as a basis to control nonlinear oscillations in compliantly actuated systems. Although, these controllers are able to statically regulate the link configuration, in some situations, it is required to specifically increase the damping by control. This is as efficient power-trains of compliantly actuated systems are designed such that damping in parallel to the springs (connecting motors and links) is as low as possible. The related methods aiming at the solution to the link-side damping problem can be classified in the basic approaches of full-state-feedback-based gain scheduling [ASH01], [PAS11], [SMCT+13], cascaded structures or integrator backstepping [OASKH03], [OL99], [Ott08, Chapt. 6.2], extensions of the Slotine and Li controller [SW88] to the flexible joint case [Spo89], and feedback linearization [DLL98], [PMDL08]. The methods based on full-state feedback control are validated to perform in experiments. However, a stability analysis is not provided in the general nonlinear case. All other approaches come with a comprehensive stability analysis, but experimental validations on the relevant class of compliantly actuated systems are lacking.

1.3.3. One-dimensional oscillations

A central issue of this thesis is the excitation and maintenance of oscillations in nonlinear, compliantly actuated systems. As mentioned in Sect. 1.2, this is already in the single-DOF case a challenging task. The control methods implementing a limit cycle behavior in robotic systems reported so far are mainly based on the principles of van der Pol oscillators [VdP26], e. g., [SD08], [GOAS13], and central pattern generators (CPG) [Ijs01], [BI04], [IC07], [BI08], whereas the latter approaches realize basically a (harmonic) excitation acting on the spring. The limit cycle controllers proposed in [SD08] and [GOAS13] realize a nonlinear damping term, which increases the system energy if the state evolves inside the limit cycle, and decreases it outside the limit cycle. A theoretical difficulty of this approach is that for the stability analysis, it is assumed that damping forces (which are inherent in any real plant) are canceled a priori. The idea of a CPG is to generate a periodic pattern, which is feed-forward to the plant as reference motor position. The extension to the classical CPG approach [BI08] considers further feedback of the plant to adapt the frequency of the generated pattern to a resonance-like steady state. Although, the concept of adapting the resonance frequency of the plant seems to be promising w. r. t. the goal of exploiting the natural dynamics behavior, it suffers from the unpredictability of periodic and resonance-like motions of forced nonlinear oscillators (cf. Sect. 1.2).

1.3.4. Normal modes

A precondition for the step from single to multi-dimensional, natural, periodic motions is given if the (multi-dimensional) system of second-order differential equations features two-dimensional (2-D), invariant subsets of its state space. The concept of modal decomposition, which is well known from linear vibration and control theory, provides a powerful tool to separate high-dimensional linear systems into 1-D decoupled ones. However, the dynamics of articulated multibody systems at hand is nonlinear in general, such that the classical modal decomposition cannot be conducted. The problem of describing periodic solutions of systems of nonlinear second-order equations has been treated in the literature in the context of so-called *normal modes* [Ros66], [Ran71], [Ran74], [CVS90], [SP93]. Thereby, the definition of *Rosenberg* of normal modes [Ros66] applies to conservative systems consisting of nonlinear (and coupled) elasticities but constant masses. Although, e. g., in [Ran74] and [CVS90], explicit parameterizations have been found in the two-DOF case, the Rosenberg definition of normal modes cannot track the class of articulated multibody systems at hand, where the indispensable nonlinearity is mainly the result of the rotation of bodies. In principle, such systems could be treated by the more general formulation of nonlinear normal modes, as proposed by *Shaw and Pierre* [SP93]. However, the procedure to determine normal modes, as proposed in [SP93], involves a set of nonlinear, partial differential equations, for which even the existence of solutions can be proven only in particular, symmetrical cases. As such, no appropriate method has been reported so far, which solves the problem of dimensionality reduction for the compliantly actuated systems of interest.

1.3.5. Control of multi-dimensional nonlinear oscillations

Although the analysis of natural, nonlinear, oscillatory, or periodic motions is currently mainly unresolved, there remains the alternative to implement them in compliantly actuated systems by (feedback) control. The control methods reported so far, which realize explosive and periodic motions in multiple-joint robotic systems, are based on numerical optimal control [BHV11], [BPH$^+$12], [HHAS12], [BPH$^+$13], shaping attractive 2-D manifolds by feedback control [GAP01], [CEU02], [WGK03], [DS03], [GOAS13], tracking of periodic reference trajectories/patterns [BI08], [UGK14], and inter-limb synchronization control [FvdSS14], just to name a few from each category. The approaches reported in [BHV11], [BPH$^+$12], [HHAS12], [BPH$^+$13] exploit the natural dynamics behavior of compliantly actuated robotic arms in throwing a ball. A current limitation of numerical-optimization-based methods is that computational costs and number of local minima explode with the number of degrees of freedom. As such, the reported experiments are conducted with systems, where only two joints are involved in the motion. The methods in [GAP01], [CEU02], [WGK03], [DS03], [GOAS13], scale to higher dimensional systems and a variety of periodic tasks. Despite their generality, the approaches do not include a directed method to take the natural oscillatory behavior of the plant into account. The approach of adaptive frequency oscillators as proposed in [BI08] extends the idea of central pattern generators [Ijs01] by a feedback, which enables the closed-loop system to adapt to an inherent frequency of the plant. However, in realization of adaptive frequency oscillators for compliant quadrupedal robots [BI08], the "optimal" inter-joint distribution of pattern amplitudes (and phase relations) are determined by manual search. The concepts proposed in [UGK14] and [FvdSS14] solve the problem of efficient periodic motion generation most closely. Both methods utilize the control input of variable stiffnesses to adapt

to multi-DOF periodic motions. In [UGK14], linear elasticities are considered in parallel to the actuators and a periodic reference trajectory is tracked. The power-continuous controller introduced by [FvdSS14] synchronizes the nominal motion of two oscillators. For both approaches it remains open to show to which extent the natural oscillatory behavior of multibody systems with elasticities can be exploited, since the inertial dynamics of the robotic links is not explicitly taken into account.

1.4. Contributions and overview

This thesis investigates the theoretical foundations of nonlinear oscillations, transfers gained insights to the design and control of compliantly actuated robotic systems, and verifies the proposed concepts in applications to tasks of robotic arms and legged systems. The key methodologies are validated in experiments with at least one of the robotic systems: DLR Hand Arm System [GASB+11], the compliant biped C-Runner [LWL+16], or the compliantly actuated quadruped Bert (Sect. 7.1.1), whereby, the latter hardware system has been developed in the course of this thesis. In addition to these technical aspects, based on theoretical findings of this thesis, it was possible to generate new hypotheses in neural motor control [LAS14a], [SLAS16] and to substantiate the evidence of existing empirical models in biomechanics [LFAS17].

To deepen the understanding of mechanical systems and their natural oscillatory or periodic solutions, the geometry of the underlying physics is indispensable. Therefore, Chapt. 2 provides an overview of the differential geometric concepts of theoretical mechanics. Although, the mathematical theory is well-known from the literature [LR89], [Fra03], [Arn13], the description is recapitulated from a robotics and control point of view. In particular, geometrical interpretations of relevant physical principles and effects are highlighted. In Chapt. 3, the compliantly actuated mechanical systems of interest are introduced and generalized w. r. t. the formulation of [ASOP12] to the case of underactuation at rigid-body level. Moreover, basic concepts to control the static equilibrium conditions are investigated. In particular, a novel control method is introduced, which implements a damping term for the dynamics of indirectly actuated states. This controller preserves the structure of the plant-inherent elasticity and performs very robustly on real-hardware systems therefore.

The central contribution of this thesis is the theory on reducing the dimensionality of natural (uncontrolled) evolutions of compliantly actuated multibody systems to one. This concept of one-dimensional (1-D), invariant submanifolds of configurations is referred to as *oscillation modes*. On the basis of this fundamental theory, the proposed approach of controlling naturally arising, nonlinear oscillations consists of the "trinity" of newly introduced methodologies and concepts of *limit cylcle control*, *oscillation modes*, and *modal control* (Fig. 1.2). In Chapt. 4, a control principle is introduced, which switches the potential energy based on thresholding the elastic tension. This way, limit cycles are generated by exciting the natural oscillatory dynamics of planar, non-conservative Euler-Lagrange systems. Considering the equilibrium configuration of the potential as control input (which is a reliable assumption utilizing the basic control to be described in Sect. 3.2), the controller feedbacks solely measurements of the state at position level, and it requires, if anything, the knowledge of a static model of the plant. Due to the switching nature of the control law, the resulting closed-loop dynamics represents a hybrid dynamical system. By investigating the stability properties of such planar systems, novel interpretations of ordinary statements to prove the existence and convergence of hybrid closed orbits are found. To

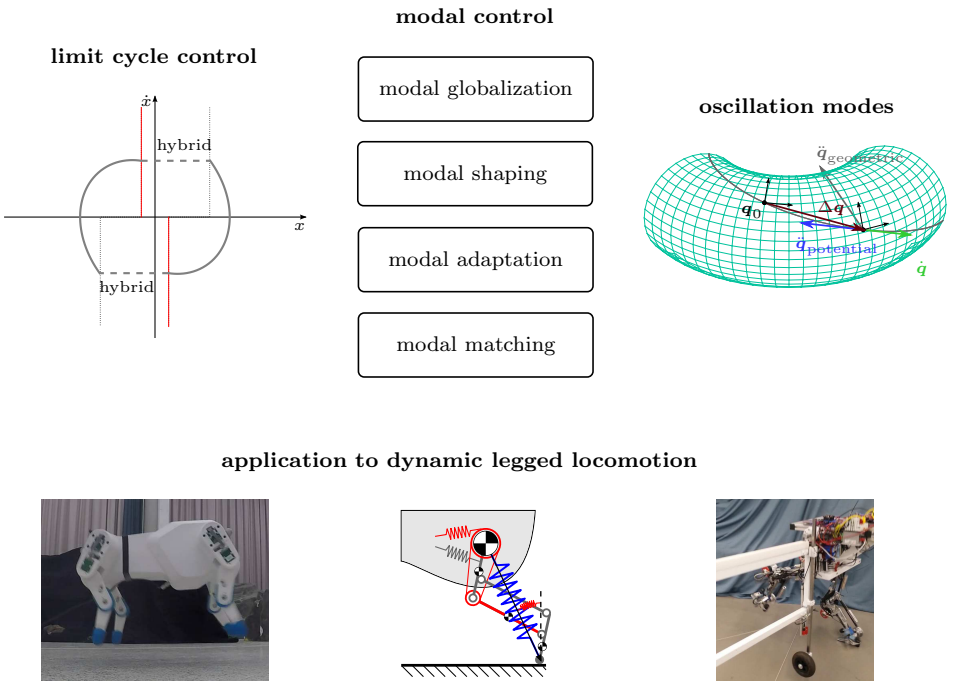

Figure 1.2.: Theory of Multi-Dimensional Nonlinear Oscillation Control and applications.

transfer the principles of one-dimensional limit cycle generation to the multi-dimensional case, the problem of dimensionality reduction needs to be solved. Yet, tackling this problem in the general case is not trivial. Although the well-established method of modal decomposition solves the problem in the linear case, especially the multibody dynamics of articulated robotic systems is strongly nonlinear, and therefore, linear modal analysis is not applicable. The novel theory on oscillation modes of nonlinear dynamics, as introduced in Chapt. 5, solves the problem of dimensionality reduction in the general multibody case. The contributed theorems on oscillation modes provide algebraically verifiable conditions, for which a one-dimensional submanifold of the configuration space represents an invariant set of the considered *uncontrolled* system. This stands in stark contrast to the concept of normal modes [SP93], where the invariance conditions arise as a set of nonlinear partial differential equations. Based on the proposed directly testable conditions on oscillation modes, a method is proposed in Sect. 5.2, which enables to embody fundamental low-order template model dynamics of robotic tasks in the design of the mechanical system. To exploit the natural oscillatory dynamics of compliantly actuated systems (which are represented by oscillation modes) in the execution of real-world tasks, one needs to trade off between the requirements of *feasibility*, *versatility*, *robustness*, and *performance respectively efficiency*. Each of the four modal control methods, as contributed in Chapt. 6, is best suited at least for one of these aims. Modal globalization control (Sect. 6.1) applies to any (statically controllable) compliantly actuated system, as the controller makes the local linear oscillation properties globally valid. The practical feasibility of the method has been validated in experiments on the DLR Hand Arm System. Moreover, a strict Lyapunov function approach is introduced in the context of modal globalization control, which allows to prove exponential stability for a class of parameter-varying second-order systems. Modal shaping control, as proposed in Sect. 6.2, is intended to increase the versatility of possible tasks, where performance or efficiency is of paramount importance. The control

effort of this method is minimalistic in a sense that the controller is not active, when the natural motion of the plant coincides with the shaped mode. The approach is conceptually validated in simulations of compliantly actuated, quadrupedal jumping tasks. The method of modal adaptation (Sect. 6.3) may be regarded as the next core contribution of this thesis. Based on sole observations of the motion of configuration variables, it is able to extract the oscillation modes of the plant. The combination of modal adaptation and switching-based limit cycle control (as mentioned above) yields a powerful tool to excite periodic motions evolving in the oscillation modes without model-parameter knowledge of the plant. The performance and efficiency of the method has been validated in several experimental applications on the DLR Hand Arm System as well as on a compliantly actuated robotic leg [SLAS16]. A further seminal finding is the hypothesis that the controller structure can be realized by a biologically plausible network of neurons [LAS14a], [SLAS16]. Finally, the concept of modal matching, as introduced in Sect. 6.4 combines the aims of versatility and efficiency. The method exploits the nonlinearity of compliantly actuated multibody systems to match and control the direction of local eigenvectors to a given task. A first proof of concept of this approach is performed by simulation of a compliantly actuated leg in a directed jumping task. A by-product of the modal matching methodology is a task-dynamics formulation based on holonomic constraints.

Chapter 7 is dedicated to the applications of the general theory of oscillation modes, limit cycle, and modal control in legged locomotion (Fig. 1.2). A widely accepted and empirically validated hypothesis of biologists claims that the high-dimensional, nonlinear dynamics anchored in a complex legged animal collapses to strongly reduced-order template model dynamics [FK99], [HFKG06], like the spring-loaded inverted pendulum (SLIP) model [Bli89]. By the methodology of oscillation mode embodiment, examples are discovered, which validate that the dynamics of the SLIP model can be anchored in the elastic multibody dynamics of articulated legs. In particular, Sect. 7.1 and 7.2 provides realizations of such template model dynamics in the real compliantly actuated quadrupedal and bipedal robots Bert and C-Runner, respectively. Thereby, first experimental verifications by a dynamic pronk, trot and walk are performed on real robotic analog systems. As such, the theory contributed by this thesis supports and substantiates the hypotheses of the biologists.

The investigations and findings reported here yielded five journal articles, ten conference papers in the main robotic and control congresses (Table 1.1), and three patents, of which [KLO17] is accepted and [LAS], [LFAS] are currently under review.

Reference	Description
Journal, [LPAS14]	D. Lakatos, F. Petit, and A. Albu-Schäffer. Nonlinear Oscillations for Cyclic Movements in Human and Robotic Arms. *IEEE Transactions on Robotics*, 30(4):865–879, Aug. 2014.
Journal, [LAS16]	D. Lakatos and A. Albu-Schäffer. Modal Matching: An Approach to Natural Compliant Jumping Control. *IEEE Robotics and Automation Letters*, 1(1):274–281, Jan. 2016.
Journal, [SLAS16]	P. Stratmann, D. Lakatos, and A. Albu-Schäffer. Neuromodulation and Synaptic Plasticity for the Control of Fast Periodic Movement: Energy Efficiency in Coupled Compliant Joints via PCA. *Frontiers in Neurorobotics*, 10(2):1–20, Mar. 2016.
Journal, [SLOAS17]	P. Stratmann, D. Lakatos, M. C. Özparpucu, and A. Albu-Schäffer. Legged Elastic Multibody Systems: Adjusting Limit Cycles to Close-to-Optimal Energy Efficiency. *IEEE Robotics and Automation Letters*, 2(2):436–443, Apr. 2017.
Journal, [LFAS17]	D. Lakatos, W. Friedl, and A. Albu-Schaffer. Eigenmodes of Nonlinear Dynamics: Definition, Existence, and Embodiment into Legged Robots with Elastic Elements. *IEEE Robotics and Automation Letters*, 2(2):1062–1069, Apr. 2017.
Conference, [LPAS13]	D. Lakatos, F. Petit, and A. Albu-Schäffer. Nonlinear Oscillations for Cyclic Movements in Variable Impedance Actuated Robotic Arms. In *IEEE Int. Conf. on Robotics and Automation*, pages 508–515, May 2013.
Conference, [LGP+13a]	D. Lakatos, G. Garofalo, F. Petit, C. Ott, and A. Albu-Schäffer. Modal Limit Cycle Control for Variable Stiffness Actuated Robots. In *IEEE Int. Conf. on Robotics and Automation*, pages 4934–4941, May 2013.
Conference, [LGP+13b]	D. Lakatos, M. Görner, F. Petit, A. Dietrich, and A. Albu-Schäffer. A Modally Adaptive Control for Multi-Contact Cyclic Motions in Compliantly Actuated Robotic Systems. In *IEEE/RSJ Int. Conf. on Intelligent Robots and Systems*, pages 5388–5395, Nov. 2013.
Conference, [LGDAS14]	D. Lakatos, G. Garofalo, A. Dietrich, and A. Albu-Schäffer. Jumping Control for Compliantly Actuated Multilegged Robots. In *IEEE Int. Conf. on Robotics and Automation*, pages 4562–4568, May 2014.
Conference, [LAS14a]	D. Lakatos and A. Albu-Schaffer. Neuron model interpretation of a cyclic motion control concept. In *IEEE RAS & EMBS Int. Conf. on Biomedical Robotics and Biomechatronics*, pages 905–910, Aug. 2014.
Conference, [LAS14b]	D. Lakatos and A. Albu-Schäffer. Switching based limit cycle control for compliantly actuated second-order systems. In *Proc. of the IFAC World Congress*, pages 6392–6399, Aug. 2014.
Conference, [LRSAS14]	D. Lakatos, C. Rode, A. Seyfarth, and A. Albu-Schäffer. Design and Control of Compliantly Actuated Bipedal Running Robots: Concepts to Exploit Natural System Dynamics. In *IEEE-RAS Int. Conf. on Humanoid Robots (Humanoids)*, pages 930–937, Nov. 2014.
Conference, [LSFAS15]	D. Lakatos, D. Seidel, W. Friedl, and A. Albu-Schäffer. Targeted Jumping of Compliantly Actuated Hoppers based on Discrete Planning and Switching Control. In *IEEE/RSJ Int. Conf. on Intelligent Robots and Systems*, pages 5802–5808, 2015.
Conference, [KLOAS16]	M. Keppler, D. Lakatos, C. Ott, and A. Albu-Schäffer. A Passivity-Based Approach for Trajectory Tracking and Link-Side Damping of Compliantly Actuated Robots. In *IEEE Int. Conf. on Robotics and Automation*, pages 1079–1086, May 2016. **Best Automation Paper Award Finalist.**
Conference, [LASRL16]	D. Lakatos, A. Albu-Schäffer, C. Rode, and F. Loeffl. Dynamic Bipedal Walking by Controlling only the Equilibrium of Intrinsic Elasticities. In *IEEE-RAS Int. Conf. on Humanoid Robots (Humanoids)*, pages 1282–1289, Nov. 2016.

Table 1.1.: Main publications covered by this thesis.

CHAPTER 2

Differential Geometric Fundamentals of Mechanics

To analyze and control periodic motions of mechanical systems, the concepts of manifolds, tensors, and submanifolds are crucial. Especially, the analysis and control of intrinsically periodic tasks, e. g., in legged locomotion can be substantially simplified, in case their dynamics is represented in different curvy-linear coordinates which generally dissent from the coordinates where the actuation physically takes place. Therefore, the concept of differentiable manifolds suggests clear rules how to transform physical quantities (required to describe the dynamics) between these coordinate systems and formalize the way how these so-called tensor-fields are differentiated. Periodicity requirements as well as environmental contacts (appearing in legged locomotion) constrain the motion of mechanical systems to evolve on a lower-dimensional space than its configuration manifold. But also basic principles of energy-efficient limit cycle generation rely on such a dimensionality reduction. Therefore, the concept of (holonomic) motion constraints is introduced, which can be conveniently handled by the notion of submanifolds. In the following, the differential geometric concepts are briefly introduced from an application point of view only. For rigorous definitions and a comprehensive description, the reader is referred to [Fra03].

2.1. Differentiable manifolds

The requirement to introduce the notion of a manifold arises when a space is considered which cannot be completely covered by a single coordinate system.[1] The idea of a manifold is to cover the point set of interest by a family of local coordinate systems such that two intersecting coordinate "patches" can be continuously related to each other [Fra03]. The existence of such coordinate patches depends on topological properties of the surface (described by the point set) [LR89]. Since this thesis focuses on the application of the differential-geometric concepts to analyze dynamical systems and to design controllers, the topological requirements for the existence of such coordinate neighborhoods will be considered as given. This means that the surfaces treated here are so-called *differentiable manifolds*, where such properties are guaranteed by definition.

In the following, the differentiable manifold will be defined based on a common exam-

[1] Note that the Euclidean space $\mathbb{R}^n$ can be always covered by a single Cartesian coordinate system.

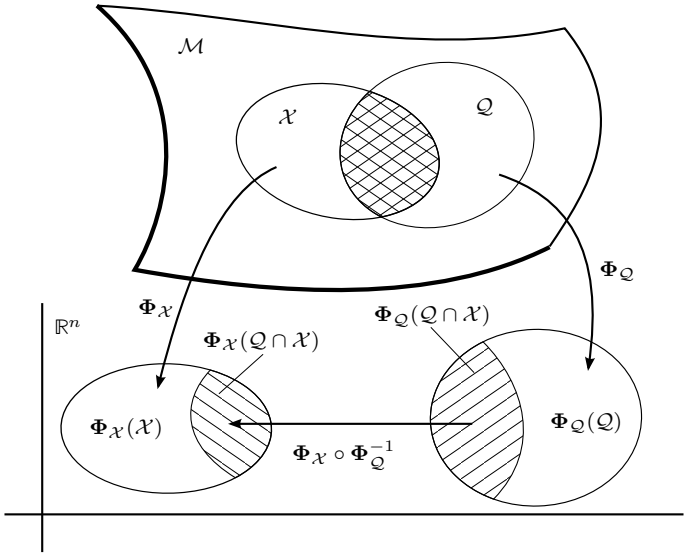

Figure 2.1.: Definition of a manifold.

ple in multibody systems, where the manifold consists of a covering by two (or more) coordinate neighborhoods: the joint or configuration and the task coordinates[2] (Fig. 2.1). This intuitive example can be easily extended to an arbitrary countable set of coordinate neighborhoods.

Definition 2.1 (Manifold)**.** *A n-dimensional manifold is a point set*[3] $\mathcal{M} = \mathcal{Q} \cup \mathcal{X} \cup \ldots$ *which is covered by a family of local coordinate systems, for instance, the patch of the configuration coordinates $\mathcal{Q}$ and the patch of the task coordinates $\mathcal{X}$. The point set is called locally $\mathbb{R}^n$ (Euclidean) in a sense that for each subset $\mathcal{Q}$ and $\mathcal{X}$ there are one-to-one correspondences $\mathbf{\Phi}_{\mathcal{Q}} : \mathcal{Q} \to \mathbb{R}^n$ and $\mathbf{\Phi}_{\mathcal{X}} : \mathcal{X} \to \mathbb{R}^n$ with open subsets $\mathbf{\Phi}_{\mathcal{Q}}$ and $\mathbf{\Phi}_{\mathcal{X}}$ of $\mathbb{R}^n$, respectively. In other words, the manifold (not necessarily embedded in $\mathbb{R}^n$) is such that to each point $\boldsymbol{r} \in \mathcal{M}$, one can assign the n real numbers $\boldsymbol{q} := (q^1, \ldots, q^n)$ and $\boldsymbol{x} := (x^1, \ldots, x^n)$, if the point belongs to the coordinate neighborhood of the configuration coordinates $\boldsymbol{r} \in \mathcal{Q}$ and task coordinates $\boldsymbol{r} \in \mathcal{X}$, respectively. The intersection of the two coordinate patches $\mathcal{Q} \cap \mathcal{X}$ is assumed to be non-empty such that for $\boldsymbol{r} \in \mathcal{Q} \cap \mathcal{X}$ one can express the relation of the configuration coordinates $\boldsymbol{q}$ and task coordinates $\boldsymbol{x}$ in the form*

$$\boldsymbol{x} = \boldsymbol{x}(\boldsymbol{q}) := \mathbf{\Phi}_{\mathcal{X}} \circ \mathbf{\Phi}_{\mathcal{Q}}^{-1}(\boldsymbol{q})\,, \tag{2.1}$$

with the inverse transformation

$$\boldsymbol{q} = \boldsymbol{q}(\boldsymbol{x}) := \mathbf{\Phi}_{\mathcal{Q}} \circ \mathbf{\Phi}_{\mathcal{X}}^{-1}(\boldsymbol{x})\,. \tag{2.2}$$

Definition 2.2 (Differentiable manifold)**.** *If additionally to the requirements of Definition 2.1, the functions of* (2.1) *and* (2.2) *are of class $\mathcal{C}^\infty$, i. e., infinitely times differentiable $\forall \boldsymbol{r} \in \mathcal{Q} \cap \mathcal{X}$, the manifold $\mathcal{M}$ is called a n-dimensional differentiable manifold.*

In the following, it is assumed that differentiable manifolds are treated, where the above requirements are satisfied by definition.

[2] In some particular cases, the task-coordinates correspond end-effector positions of a manipulator.
[3] More precisely, it is a topological space [Fra03].

2.2. Tensors on manifolds

If one is concerned with velocities, forces, and inertias of nonlinear systems represented in different coordinate neighborhoods, the notion of a tensor is essential. First, a general tensor is defined from a view point of coordinate transformations and then particular tensors are introduced, which are required to model, analyze, and control the class of systems considered here. Finally, the non-tensorial concept of an affine connection is briefly treated, which typically appears in nonlinear Euler-Lagrange dynamics.

2.2.1. Tensors and tensor fields

To describe general tensorial quantities, the concept of a matrix, i. e., a two-index quantity, is not sufficient anymore. Therefore, lower-case Latin indices such as $j, h, k, \ldots$ are considered. Additionally, the following summation convention is used: if the same index appears twice in a term, summation over that index is implied. Since we are concerned with n-dimensional manifolds, the summation range is $1 \ldots n$.

The following general definition of a tensor is taken from [LR89]:

Definition 2.3 (Tensor)**.** *A set of n^{r+s} quantities $Q^{h_1 \cdots h_r}{}_{k_1 \cdots k_s}$ constitute the components of a tensor of type (r, s) (r contravariant, s covariant)[4] at a point $\boldsymbol{r}$ of a differentiable manifold $\mathcal{M}$, if, under the coordinate transformation* (2.1)*, these quantities transform according to the law*

$$X^{j_1 \cdots j_r}{}_{l_1 \cdots l_s} = \frac{\partial x^{j_1}}{\partial q^{h_1}} \cdots \frac{\partial x^{j_r}}{\partial q^{h_r}} \frac{\partial x^{k_1}}{\partial q^{l_1}} \cdots \frac{\partial x^{k_s}}{\partial q^{l_s}} Q^{h_1 \cdots h_r}{}_{k_1 \cdots k_s} \,. \tag{2.3}$$

Most of the tensors required in this thesis can be treated in the context of matrix operations. However, the index notation is advantageous, since it intrinsically denotes the type of the tensor[5]. Since the matrix notation is more common in robotics and control theory, both notations will be introduced and the index notation will only be used if the context requires it.

Two types of vectorial quantities are considered:

Definition 2.4 (Velocity vector)**.** *A set of n quantities $\dot{q}^h$ constitute the components of a vector of type $(1, 0)$ (contravariant vector) at a point $\boldsymbol{r}$ of a differentiable manifold $\mathcal{M}$, if, under the coordinate transformation* (2.1)*, these quantities transform according to the law*

$$\dot{x}^j = \frac{\partial x^j}{\partial q^h} \dot{q}^h \,. \tag{2.4}$$

The transformation law of a velocity vector $\dot{\boldsymbol{q}}$ can be expressed as the matrix operation

$$\dot{\boldsymbol{x}} = \boldsymbol{J}(\boldsymbol{q}) \dot{\boldsymbol{q}} \,, \tag{2.5}$$

where

$$\boldsymbol{J}(\boldsymbol{q}) := \frac{\partial \boldsymbol{x}(\boldsymbol{q})}{\partial \boldsymbol{q}} \tag{2.6}$$

represents the Jacobian matrix of the coordinate transformation (2.1)*.*

[4] Note that the indices of tensorial quantities are not horizontally aligned to preserve the order: first contravariant (superscript) and second covariant (subscript).

[5] Note that tensors of rank $r + s > 2$ cannot be expressed in matrix notation anymore. An example is the curvature tensor of a manifold which consist of rank 3.

The velocity is a particular example of a so-called tangent vector. The set of all tangent vectors at a point $\boldsymbol{r}$ of the manifold forms a n-dimensional vector space, the so-called tangent space $\mathcal{M}_{\boldsymbol{r}}$.

Definition 2.5 (Co-vector (force))**.** *A set of n quantities τ_h constitute the components of a vector of type $(0,1)$ (covariant vector) at a point $\boldsymbol{r}$ of a differentiable manifold $\mathcal{M}$, if, under the coordinate transformation (2.1), these quantities transform according to the law*

$$f_j = \frac{\partial q^h}{\partial x^j}\tau_h \,. \tag{2.7}$$

The inverse of the transformation law (2.7), i. e., the so-called pull-back, can be expressed as the matrix operation

$$\boldsymbol{\tau} = \boldsymbol{J}(\boldsymbol{q})^T \boldsymbol{f} \,, \tag{2.8}$$

where the Jacobian matrix $\boldsymbol{J}(\boldsymbol{q})$ is defined by (2.6).

The force is a general example of a so-called co-tangent vector (or briefly co-vector). The set of all co-vectors at a point $\boldsymbol{r}$ of the manifold forms also a n-dimensional vector space, the so-called dual tangent space $\mathcal{M}^\star_{\boldsymbol{r}}$.

Remark 2.1 (Gradient)**.** *A particular example of a co-vector is the gradient. Let U be a scalar field on a subset $\mathcal{S}$ of the manifold $\mathcal{M}$. Suppose that $\mathcal{S}$ is not contained in a single coordinate patch such that the point $\boldsymbol{r} \in \mathcal{W}$ is in a coordinate overlap, $\boldsymbol{r} \in \mathcal{Q} \cap \mathcal{X}$. The partial derivatives $\partial U(q^k)/\partial q^h$ constitute the components of a covariant vector which can be immediately seen by applying the chain rule*

$$\frac{\partial U(x^l)}{\partial x^j} = \frac{\partial q^h}{\partial x^j}\frac{\partial U(q^k(x^l))}{\partial q^h} \,. \tag{2.9}$$

The comparison of (2.9) and (2.7) reveals that the gradient $\partial U(q^k)/\partial q^h$ is a co-vector. Its transformation can be analogously expressed as the matrix operation[6]

$$\frac{\partial U(\boldsymbol{x})}{\partial \boldsymbol{x}}^T = \boldsymbol{J}(\boldsymbol{q})^{-T}\frac{\partial U(\boldsymbol{q})}{\partial \boldsymbol{q}}^T \,,$$

where the dependency on $\boldsymbol{q}$ can be removed by (2.2).

An additional important tensorial quantity appearing in the dynamics of nonlinear mechanical systems is the so-called inertia tensor. This tensor of type $(0,2)$ can be characterized by a quotient theorem as described in [LR89]:

Theorem 2.1 ([LR89])**.** *If the n^2 quantities M_{hk} are such that for any contravariant vector $\dot{q}^h$ at a point $\boldsymbol{r}$ of the manifold $\mathcal{M}$, $M_{hk}\dot{q}^h\dot{q}^k$ is a scalar, then the symmetric parts $\frac{1}{2}(M_{hk} + M_{kh})$ of M_{hk} are the components of a tensor of type $(0,2)$.*

The following can be deduced from this theorem:

Corollary 2.1. *If in addition to the requirements of Theorem 2.1, the quantities M_{hk} are symmetric, i. e., $M_{hk} = M_{kh}$, then M_{hk} are the components of a type $(0,2)$ tensor.*

Remark 2.2 (Inertial tensor)**.** *If the quantities M_{hk} of Corollary 2.1 are such that the scalar $M_{hk}\dot{q}^h\dot{q}^k$ is positive definite, then the components M_{hk} are sometimes referred to as inertia tensor.*

In Riemannian geometry, the inertia tensor has a particular meaning which is also of major importance for the analysis and construction of Lyapunov stability.

[6] The transposed operator $(\cdot)^T$ denotes that the gradient $\partial U(\boldsymbol{q})/\partial \boldsymbol{q}$ is a row in matrix notation.

2.2.2. Riemannian metric

The concept of a metric for the differentiable manifold $\mathcal{M}$ allows to measure the length of vectors and co-vectors, the angle between two vectors (of equal type), or the arc length of a curve [Arn13]. The following definitions of the notion of a metric will be performed based on the length of a contravariant vector. Thereby, only matrix operations (instead of index operations) will be conducted.

Definition 2.6 (Length of a vector)**.** *Let $\dot{\boldsymbol{q}}$ be a contravariant vector in the tangent space $\mathcal{M}_{\boldsymbol{r}}$ of a point $\boldsymbol{r}$ of the manifold $\mathcal{M}$, for which the coordinates of that point $\boldsymbol{r}$ are $\boldsymbol{q}$. Then, analogously to the expression of a length in Euclidean space, the length of that vector, denoted $\|\dot{\boldsymbol{q}}\|$, can be expressed by the modulus of a function $f(\boldsymbol{q}, \dot{\boldsymbol{q}})$ which is:*

1. *sufficiently smooth*[7] *in all its arguments,*
2. *invariant under any coordinate transformation on $\mathcal{M}$, and*
3. *positively homogeneous of the first degree in the argument $\dot{\boldsymbol{q}}$, i. e.,*

$$f(\boldsymbol{q}, c\dot{\boldsymbol{q}}) = cf(\boldsymbol{q}, \dot{\boldsymbol{q}}) \,, \quad \forall c > 0 \,. \tag{2.10}$$

Such a function $f(\boldsymbol{q}, \dot{\boldsymbol{q}})$ can be constructed by differentiating one half of this squared function w. r. t. the vector $\dot{\boldsymbol{q}}$ which yields [LR89]

$$\frac{1}{2}\frac{\partial^2 f^2(\boldsymbol{q}, \dot{\boldsymbol{q}})}{\partial \dot{\boldsymbol{q}}^2} = \frac{\partial f(\boldsymbol{q}, \dot{\boldsymbol{q}})}{\partial \dot{\boldsymbol{q}}}^T \frac{\partial f(\boldsymbol{q}, \dot{\boldsymbol{q}})}{\partial \dot{\boldsymbol{q}}} + f(\boldsymbol{q}, \dot{\boldsymbol{q}}) \frac{\partial^2 f(\boldsymbol{q}, \dot{\boldsymbol{q}})}{\partial \dot{\boldsymbol{q}}^2} \tag{2.11}$$

Since, Euler's theorem on homogeneous functions implies that

$$\frac{\partial f(\boldsymbol{q}, \dot{\boldsymbol{q}})}{\partial \dot{\boldsymbol{q}}} \dot{\boldsymbol{q}} = f(\boldsymbol{q}, \dot{\boldsymbol{q}}) \,,$$
$$\frac{\partial^2 f(\boldsymbol{q}, \dot{\boldsymbol{q}})}{\partial \dot{\boldsymbol{q}}^2} \dot{\boldsymbol{q}} = \boldsymbol{0} \,,$$

it follows from (2.11) that

$$f^2(\boldsymbol{q}, \dot{\boldsymbol{q}}) = \dot{\boldsymbol{q}}^T \frac{1}{2} \frac{\partial^2 f^2(\boldsymbol{q}, \dot{\boldsymbol{q}})}{\partial \dot{\boldsymbol{q}}^2} \dot{\boldsymbol{q}} \,, \tag{2.12}$$

which suggests the notation

$$f^2(\boldsymbol{q}, \dot{\boldsymbol{q}}) = \dot{\boldsymbol{q}}^T \boldsymbol{M}(\boldsymbol{q}, \dot{\boldsymbol{q}}) \dot{\boldsymbol{q}} \,,$$

where

$$\boldsymbol{M}(\boldsymbol{q}, \dot{\boldsymbol{q}}) := \frac{1}{2} \frac{\partial^2 f^2(\boldsymbol{q}, \dot{\boldsymbol{q}})}{\partial \dot{\boldsymbol{q}}^2} \,. \tag{2.13}$$

As a result, the length $\|\dot{\boldsymbol{q}}\|$ of any tangent vector $\dot{\boldsymbol{q}}$ of $\mathcal{M}_{\boldsymbol{r}}$ can be considered as the positive square root of

$$\|\dot{\boldsymbol{q}}\|^2 := |\dot{\boldsymbol{q}}^T \boldsymbol{M}(\boldsymbol{q}, \dot{\boldsymbol{q}}) \dot{\boldsymbol{q}}| \,.$$

[7] By sufficiently smooth it is meant that $f(\boldsymbol{q}, \dot{\boldsymbol{q}})$ is of $\mathcal{C}^r$, $r \geq 5$ [LR89]. Note that if $r \geq 5$, the curvature tensor associated with $f(\boldsymbol{q}, \dot{\boldsymbol{q}})$ is at least one times continuously differentiable.

From condition 2 of Definition 2.6 and by successive differentiation taking Schwarz' theorem (on the symmetry of the second-order partial derivatives) and Corollary 2.1 into account, it can be easily verified that the $n \times n$-matrix $\boldsymbol{M}$ defined in (2.13) is a tensor of type $(0, 2)$. Requiring additionally that $\boldsymbol{M}$ depends exclusively on positional coordinates of the manifold $\mathcal{M}$ such as $\boldsymbol{q}$ and that

$$\det(\boldsymbol{M}) \neq 0\,, \tag{2.14}$$

the notion of a Riemmanian metric can be introduced:

Definition 2.7 (Riemannian metric [Fra03])**.** *Let $\vec{v}$ be a tangent vector represented in a coordinate-free fashion. Then, a Riemannian metric on a manifold $\mathcal{M}$ assigns a positive definite inner product (quadratic form) $\langle \vec{v}, \vec{v} \rangle$ to each tangent space $\mathcal{M}_{\boldsymbol{r}}$. In local coordinates $\boldsymbol{q}$ of the coordinate neighborhood $\mathcal{Q}$, the inner product can be expressed as*

$$\langle \dot{\boldsymbol{q}}, \dot{\boldsymbol{q}} \rangle = \dot{\boldsymbol{q}}^T \boldsymbol{M}(\boldsymbol{q}) \dot{\boldsymbol{q}}\,, \tag{2.15}$$

where $\boldsymbol{M}(\boldsymbol{q})$ is called a metric tensor.

The notion of a tensor has been introduced based upon its transformation under a change of coordinates so far. However, from the concept of a metric it becomes clear that tensors are intrinsic quantities which can be introduced in a coordinate-free fashion. In particular, for the Definition 2.7 of the Riemannian metric which is an invariant quantity, it is necessary to introduce the vector as a coordinate-independent quantity denoted by $\vec{(\cdot)}$. This intrinsic concept of a metric leads us directly to the definition of the Riemannian manifold.

Definition 2.8 (Riemannian manifold [Fra03])**.** *A differentiable manifold equipped with a Riemannian metric is called a Riemannian manifold.*

Remark 2.3. *The definition of a Riemannian metric does not necessarily require the inner product in Definition 2.7 to be positive. If the positive definiteness condition is relaxed such that the inner product is only non-degenerate anymore*[8] *than the manifold equipped with this metric is called a pseudo-Riemannian manifold.*

This thesis considers only metrics, where the positive definiteness condition of Remark 2.2 is satisfied.

2.2.3. Covariant differentiation

In general, the derivation of the Euler-Lagrange equations representing, e. g., the dynamics of multi-body systems requires to differentiate a vector field on a differentiable manifold $\mathcal{M}$. The process of differentiation on a manifold is a generalization of the ordinary process of differentiation in $\mathbb{R}^n$. The main difference becomes clear by considering (for a moment) the example of a vector field $\boldsymbol{v}(\boldsymbol{q})$ in $\mathbb{R}^n$ defined along a parameterized curve $\boldsymbol{q} = \boldsymbol{q}(t) \in \mathbb{R}^n$ with time t [Fra03]. The ordinary derivative of this vector field along the curve is defined by

$$\frac{\mathrm{d}\boldsymbol{v}(t)}{\mathrm{d}t} = \lim_{\Delta t \to 0} \frac{\boldsymbol{v}(t + \Delta t) - \boldsymbol{v}(t)}{\Delta t}\,, \tag{2.16}$$

[8] This implies that the metric tensor is only regular, i. e., $\det(\boldsymbol{M}) \neq 0$ (cf. (2.14)).

where it can be seen that vectors at the different points $\boldsymbol{q}(t+\Delta t)$ and $\boldsymbol{q}(t)$ are related. This makes only sense in an affine space, where a vector can be translated parallel. If one is concerned with a vector field $\boldsymbol{v}(\boldsymbol{q})$ on a general manifold $\mathcal{M}$, then the vectors in (2.16) are even in the different tangent spaces $\boldsymbol{v}(t+\Delta t) \in \mathcal{M}_{\boldsymbol{q}(t+\Delta t)}$ respectively $\boldsymbol{v}(t) \in \mathcal{M}_{\boldsymbol{q}(t)}$. An important implication of this state of affairs is that the (time) derivatives

$$\dot{v}^h = \frac{\partial v^h}{\partial q^k}\dot{q}^k \tag{2.17}$$

of a vector field $v^h(\boldsymbol{q}(t))$ on a manifold $\mathcal{M}$ do not represent the components of a contravariant vector. Since $\dot{q}^k$ are of type $(1,0)$, the partial derivatives $\partial v^h/\partial q^k$ would need to be of type $(1,1)$. However considering the transformation of the vector field

$$w^j(\boldsymbol{x}) = \frac{\partial x^j}{\partial q^h} v^h(\boldsymbol{q})\,, \tag{2.18}$$

it can be seen, by partial differentiation,

$$\frac{\partial w^j}{\partial x^k} = \frac{\partial^2 x^j}{\partial q^l \partial q^h}\frac{\partial q^l}{\partial x^k} v^h + \frac{\partial x^j}{\partial q^h}\frac{\partial q^l}{\partial x^k}\frac{\partial v^h}{\partial q^l} \tag{2.19}$$

that $\partial v^h/\partial q^l$ is even not tensorial (cf. Definition 2.3).

The circumstance that the ordinary derivative of a vector field on a general manifold is not tensorial motivates the introduction of a more general concept of differentiation.

Definition 2.9 (Covariant derivative of a vector field)**.** *Let $v^h(q^k)$ be a contravariant vector field on a differentiable manifold $\mathcal{M}$. Then, the partial covariant derivative w. r. t. q^k can be expressed as*

$$\nabla_k v^j = \frac{\partial v^h}{\partial q^k} + \Gamma_h{}^j{}_k v^h\,, \tag{2.20}$$

where the three-index symbols $\Gamma_h{}^j{}_k$ are the connection coefficients on the differentiable manifold $\mathcal{M}$.

The notion of covariant differentiation involves the components of an affine connection $\Gamma_h{}^j{}_k$. Thereby, it is assumed that the manifold is equipped with such a connection. In accordance with the example of ordinary differentiation (2.16), the affine connection (to be defined later) specifies how to relate vectors of distinct (neighboring) tangent spaces of a general manifold. This process of translation is sometimes referred to as transportation by parallel displacement.

Definition 2.10 (Local parallelism of vectors)**.** *Let $v^j(q^k)$ be an arbitrary contravariant vector at the point $\boldsymbol{r}(q^k) \in \mathcal{M}$, a unique vector $v^j + \mathrm{d}v^j$ at the neighboring point $\boldsymbol{r}(q^k + \mathrm{d}q^k) \in \mathcal{M}$ is defined such that the covariant differential of the vector field is zero, i. e.,*

$$\mathrm{D}v^j = \nabla_k v^j \,\mathrm{d}q^k = \mathrm{d}v^j + \Gamma_h{}^j{}_k v^h \mathrm{d}q^k = 0\,, \tag{2.21}$$

where $\Gamma_h{}^j{}_k$ is to be evaluated at $\boldsymbol{r}(q^k)$, while $\mathrm{d}q^k$ refers to the displacement from $\boldsymbol{r}(q^k)$ to $\boldsymbol{r}(q^k + \mathrm{d}q^k)$. The vector $v^j + \mathrm{d}v^j$ constructed at $\boldsymbol{r}(q^k + \mathrm{d}q^k)$ is said to be parallel to the vector v^j at $\boldsymbol{r}(q^k)$ if $\mathrm{d}v^j$ satisfies the condition (2.21)*.*

The process of covariant differentiation—leading to the concept of parallelism—is defined for a general tensor field on an affinely connected space[9]:

Definition 2.11 (Covariant derivative of a tensor field)**.** *The partial covariant derivative of a general type (r,s) tensor field ${Q^{j_1\cdots j_r}}_{l_1\cdots l_s}$,*

$$\nabla_k {Q^{j_1\cdots j_r}}_{l_1\cdots l_s} = \frac{\partial {Q^{j_1\cdots j_r}}_{l_1\cdots l_s}}{\partial q^k} + \sum_{\alpha=1}^{r} {\Gamma_m}^{j_\alpha}{}_k {Q^{j_1\cdots j_{\alpha-1} m j_{\alpha+1}\cdots j_r}}_{l_1\cdots l_s} - \sum_{\beta=1}^{s} {\Gamma_{l_\beta}}^{m}{}_k {Q^{j_1\cdots j_r}}_{l_1\cdots l_{\beta-1} m l_{\beta+1}\cdots l_s}\,, \tag{2.22}$$

1. *is a type $(r,s+1)$ tensor field,*
2. *The covariant derivative is a linear operator, i. e., given the real numbers a and b,*

$$\nabla_m \left(a {X^{j_1\cdots j_r}}_{l_1\cdots l_s} + b {Y^{h_1\cdots h_r}}_{k_1\cdots k_s} \right) = a \nabla_m {X^{j_1\cdots j_r}}_{l_1\cdots l_s} + b \nabla_m {Y^{h_1\cdots h_r}}_{k_1\cdots k_s}\,.$$

3. *The covariant derivative of the product of two tensor fields follows a rule formally identically to the product rule of ordinary partial differentiation, i. e.,*

$$\nabla_m \left({X^{j_1\cdots j_r}}_{l_1\cdots l_s} {Y^{h_1\cdots h_r}}_{k_1\cdots k_s} \right) = \nabla_m {X^{j_1\cdots j_r}}_{l_1\cdots l_s} {Y^{h_1\cdots h_r}}_{k_1\cdots k_s} + {X^{j_1\cdots j_r}}_{l_1\cdots l_s} \nabla_m {Y^{h_1\cdots h_r}}_{k_1\cdots k_s}\,.$$

Note that the above properties do not completely specify the connection coefficients.

Definition 2.12 (Connection coefficients [LR89])**.** *Any set of three-index symbols ${\Gamma_h}^l{}_k$ is said to constitute the components of an affine connection on the differentiable manifold $\mathcal{M}$ if they transform under a change of coordinates* (2.1) *by*

$${}^\star{\Gamma_m}^j{}_p(\boldsymbol{x}) = \frac{\partial x^j}{\partial q^l}\frac{\partial q^h}{\partial x^m}\frac{\partial q^k}{\partial x^p}{\Gamma_h}^l{}_k(\boldsymbol{q}) - \frac{\partial^2 x^j}{\partial q^h \partial q^k}\frac{\partial q^h}{\partial x^m}\frac{\partial q^k}{\partial x^p}\,. \tag{2.23}$$

In case of a Riemannian manifold of Definition 2.8, there is a particular connection that relates parallel displacement with the Riemannian metric of Definition 2.7.

Definition 2.13 (Riemannian connection)**.** *The metric tensor $M_{hj}(\boldsymbol{r})$, $\det(M_{hj}(\boldsymbol{r})) \neq 0$ for all $\boldsymbol{r} \in \mathcal{M}$, defines a connection on the Riemannian manifold as introduced by Definition 2.8. In local coordinates $\boldsymbol{q}$ of the coordinate neighborhood $\mathcal{Q}$, its connection coefficients are given by the Christoffel symbols of the first kind and second kind*

$$\Gamma_{hlk} = \frac{1}{2}\left(\frac{\partial M_{lk}}{\partial q^h} + \frac{\partial M_{hl}}{\partial q^k} - \frac{\partial M_{hk}}{\partial q^l} \right) \tag{2.24}$$

and

$${\Gamma_h}^j{}_k = M^{jl}\Gamma_{hlk}\,, \tag{2.25}$$

respectively, where the contravariant tensor of rank two in (2.25)*, M^{jl} represents the inverse of the metric tensor M_{jl}.*

[9] An affinely connected space is a manifold equipped with an affine connection.

Especially the motion of our Euler-Lagrange systems considered here, takes place on a differentiable manifold equipped with a Riemannian connection. Such a so-called Levi-Civita connection has some important implications. A property of paramount importance for the stability analysis of nonlinear Euler-Lagrange systems relies on the following lemma:

Lemma 2.1 (Ricci's lemma [LR89])**.** *The covariant derivative of the metric tensor w. r. t. the connection* (2.25) *vanishes identically:*

$$\nabla_k M_{jh} = 0\,, \quad \nabla_k M^{jh} = 0\,. \tag{2.26}$$

Proof. Permuting the indices h and l in (2.24) and adding the result

$$\Gamma_{lhk} = \frac{1}{2}\left(\frac{\partial M_{hk}}{\partial q^l} + \frac{\partial M_{lh}}{\partial q^k} - \frac{\partial M_{lk}}{\partial q^h}\right)$$

to (2.24) and exploiting the symmetry property of Corollary 2.1, yields the identity

$$\Gamma_{hlk} + \Gamma_{lhk} = \frac{\partial M_{hl}}{\partial q^k}\,. \tag{2.27}$$

Furthermore, it follows from (2.22) of Definition 2.11 that the covariant derivative of the tensor field $M_{hl}(\boldsymbol{q})$ w. r. t. the Christoffel symbols (2.25) is given by

$$\nabla_k M_{hl} = \frac{\partial M_{hl}}{\partial q^k} - \Gamma_{hlk} - \Gamma_{lhk}\,, \tag{2.28}$$

where the inverse of the relation (2.25) has already been used. By considering the identity (2.27) in (2.28) it follows directly that $\nabla_k M_{hl} = 0$. The result $\nabla_k M^{hl} = 0$ can be obtained analogously. □

An additional important implication of the Riemannian connection is the property that parallel displacement preserves scalar products.

Remark 2.4. *Let $\boldsymbol{v}$ and $\boldsymbol{w}$ be vectors at the same point $\boldsymbol{r}$ of the Riemannian manifold equipped with a metric connection as introduced by Definition 2.13. Then, the scalar product $\langle \boldsymbol{v}, \boldsymbol{w} \rangle$ is preserved under transportation by parallel displacement, i. e., for a displacement from $\boldsymbol{r}(q^k)$ to $\boldsymbol{r}(q^k + \mathrm{d}q^k)$,*

$$\mathrm{d}\,\langle \boldsymbol{v}, \boldsymbol{w} \rangle = 0\,. \tag{2.29}$$

Proof. According to statement 2 of Definition 2.6, the scalar product of the vectors $\boldsymbol{v}$ and $\boldsymbol{w}$ is an invariant. Therefore, it can be written

$$\begin{aligned}\mathrm{d}\,\langle \boldsymbol{v}, \boldsymbol{w} \rangle &= \mathrm{D}\,\langle \boldsymbol{v}, \boldsymbol{w} \rangle = \mathrm{D}\left(\boldsymbol{v}^T \boldsymbol{M} \boldsymbol{w}\right) \\ &= \left(\mathrm{D}\boldsymbol{v}^T\right) \boldsymbol{M} \boldsymbol{w} + \boldsymbol{v}^T \left(\mathrm{D}\boldsymbol{M}\right) \boldsymbol{w} + \boldsymbol{v}^T \boldsymbol{M} \left(\mathrm{D}\boldsymbol{w}\right) = 0\,.\end{aligned}$$

The first and the third term in the three-term expression of the above equation are zero due to Definition 2.10. The second term is zero as a consequence of Lemma 2.1, since $\mathrm{D}M_{jh} = \nabla_k M_{jh} \mathrm{d}q^k = 0$. □

The concept of covariant differentiation of tensors on affinely connected spaces of the Riemannian manifold will be extensively exploited for the derivation of the Euler-Lagrange equation, describing the dynamics of the class of systems considered here.

2.3. Euler-Lagrange equations

The class of systems considered in this thesis satisfies certain Euler-Lagrange differential equations. These equations can be derived from Hamilton's principle [Gol65] by means of methods from the calculus of variations. To demonstrate the invariance property of the Euler-Lagrange equations under a change of coordinates, tensor calculus (on manifolds) will be exploited. On the basis of the notion of covariant differentiation, the matrix components form will be derived, which is common in robotics. Due to its fundamental importance, the Euler-Lagrange equations representing our physical systems of interest will be related geometrically to the concept of a Riemannian manifold.

2.3.1. Hamilton's principle

The following derivation introduces the Euler-Lagrange equations from a pure calculus point of view[10]. Afterwards, the result will be related to the physical problem which leads to Hamilton's principle.

Consider the problem of finding the path, where a given line integral along the path[11] possess an extremum.

Theorem 2.2 ([Arn13])**.** *Let $\mathcal{C}$ be a curve on the differentiable manifold $\mathcal{M}$ passing through the points $\boldsymbol{r}(t_1)$ and $\boldsymbol{r}(t_2)$, where $t_1 \leq t \leq t_2$ is a parameter. Assume that the curve $\mathcal{C}$ can be expressed in local coordinates $\boldsymbol{q}$ of the coordinate neighborhood $\mathcal{Q}$. Then, the curve $\mathcal{C} : \boldsymbol{q} = \boldsymbol{q}(t)$ is an extremum of the line integral*

$$J = \int_{t_1}^{t_2} L(\boldsymbol{q}(t), \dot{\boldsymbol{q}}(t))\mathrm{d}t \tag{2.30}$$

of all curves passing through the points $\boldsymbol{q}_1 = \boldsymbol{q}(t_1)$ and $\boldsymbol{q}_2 = \boldsymbol{q}(t_2)$, if and only if

$$\frac{\mathrm{d}}{\mathrm{d}t}\frac{\partial L}{\partial \dot{\boldsymbol{q}}} - \frac{\partial L}{\partial \boldsymbol{q}} = \boldsymbol{0} \tag{2.31}$$

along the curve $\boldsymbol{q}(t)$.

Remark 2.5 (Lagrangian)**.** *The function $L(\boldsymbol{q}(t), \dot{\boldsymbol{q}}(t))$ of Theorem 2.2 is defined on a path $\boldsymbol{q} = \boldsymbol{q}(t)$, where $\dot{\boldsymbol{q}} = \mathrm{d}\boldsymbol{q}(t)/\mathrm{d}t$. This function is referred to as Lagrange function or Lagrangian.*

Remark 2.6. *Note that the Lagrange functions $L(\boldsymbol{q}(t), \dot{\boldsymbol{q}}(t))$ considered here correspond to mechanical systems which obviate an explicit dependency on time t. This stands in contrast to the general theory usually considered in calculus of variations [LR89].*

The proof of Theorem 2.2 is intended to replace its explanation.

Proof. Let us parameterize the variation of the path w. r. t. the extremum path by α such that

$$\boldsymbol{q}(t, \alpha) = \boldsymbol{q}(t, 0) + \alpha\boldsymbol{\eta}(t)\,, \tag{2.32}$$

[10] The derivation uses mainly matrix notations. Index notations are only considered if the content makes it unavoidable.

[11] In calculus, this kind of functions are called functionals, since their domain is the infinitesimal space of curves [Arn13].

where $\boldsymbol{q}(t,0)$ denotes the extremum path. The functions $\boldsymbol{\eta}(t)$ are defined to vanish at t_1 and t_2. As a result the path integral (2.30) depends also on α such that the condition for an extremum is

$$\left.\frac{\mathrm{d}J(\alpha)}{\mathrm{d}\alpha}\right|_{\alpha=0} = 0\,. \tag{2.33}$$

Then, considering the family of paths (2.32) in (2.30) and differentiating the resulting integrand, it is found that

$$\frac{\mathrm{d}J}{\mathrm{d}\alpha} = \int_{t_1}^{t_2} \left(\frac{\partial L}{\partial \boldsymbol{q}}\frac{\partial \boldsymbol{q}}{\partial \alpha} + \frac{\partial L}{\partial \dot{\boldsymbol{q}}}\frac{\partial \dot{\boldsymbol{q}}}{\partial \alpha}\right)\mathrm{d}t\,. \tag{2.34}$$

Integrating the second integral by parts, i. e.,

$$\begin{aligned}\int_{t_1}^{t_2} \frac{\partial L}{\partial \dot{\boldsymbol{q}}}\frac{\partial \dot{\boldsymbol{q}}}{\partial \alpha}\mathrm{d}t &= \int_{t_1}^{t_2} \frac{\partial L}{\partial \dot{\boldsymbol{q}}}\frac{\partial^2 \boldsymbol{q}}{\partial t \partial \alpha}\mathrm{d}t \\ &= \left.\frac{\partial L}{\partial \dot{\boldsymbol{q}}}\frac{\partial \boldsymbol{q}}{\partial \alpha}\right|_{t_1}^{t_2} - \int_{t_1}^{t_2} \frac{\mathrm{d}}{\mathrm{d}t}\left(\frac{\partial L}{\partial \dot{\boldsymbol{q}}}\right)\frac{\partial \boldsymbol{q}}{\partial \alpha}\mathrm{d}t\end{aligned}$$

and taking into account that all the varied paths pass through the points $\boldsymbol{q}(t_1)$ and $\boldsymbol{q}(t_2)$, i. e., the first term of the partial integrated expression vanishes, it follows that (2.34) reduces to

$$\frac{\mathrm{d}J}{\mathrm{d}\alpha} = \int_{t_1}^{t_2} \left(\frac{\partial L}{\partial \boldsymbol{q}} - \frac{\mathrm{d}}{\mathrm{d}t}\frac{\partial L}{\partial \dot{\boldsymbol{q}}}\right)\frac{\partial \boldsymbol{q}}{\partial \alpha}\mathrm{d}t\,. \tag{2.35}$$

Now, introducing the differential quantities,

$$\delta \boldsymbol{q} := \left.\frac{\partial \boldsymbol{q}}{\partial \alpha}\right|_{\alpha=0} \mathrm{d}\alpha\,, \tag{2.36}$$

referred to as virtual displacement, respectively

$$\delta J := \left.\frac{\partial J}{\partial \alpha}\right|_{\alpha=0} \mathrm{d}\alpha\,, \tag{2.37}$$

referred to as the infinitesimal variation of J about the extremum path, it can be deduced that

$$\delta J = \int_{t_1}^{t_2} \left(\frac{\partial L}{\partial \boldsymbol{q}} - \frac{\mathrm{d}}{\mathrm{d}t}\frac{\partial L}{\partial \dot{\boldsymbol{q}}}\right)\delta \boldsymbol{q}\mathrm{d}t = 0\,. \tag{2.38}$$

The virtual displacements δq_i in (2.38) are independent since the variables q_i are independent. Therefore, from the fundamental lemma of the calculus of variation [JLJ98] it can be concluded that in order that the path $\boldsymbol{q}(t)$ constitutes an extremum to the fundamental integral (2.30), it is necessary that the Euler-Lagrange equations

$$\boldsymbol{E}(L) = \frac{\mathrm{d}}{\mathrm{d}t}\frac{\partial L}{\partial \dot{\boldsymbol{q}}} - \frac{\partial L}{\partial \boldsymbol{q}} \tag{2.39}$$

vanish identically along the path. □

Hamilton's principle of least action follows directly from Theorem 2.2:

Theorem 2.3 ([Arn13])**.** *Motions of the mechanical system* $\boldsymbol{E}(L) = \mathbf{0}$ *(where the Euler-Lagrange equations* $\boldsymbol{E}(L)$ *are defined by* (2.39)*) coincide with extrema of the line integral*

$$J = \int_{t_1}^{t_2} L \mathrm{d}t$$

where $L = T - U$ *is the difference between the kinetic and potential energy.*

Proof. The proof of the above theorem is a direct consequence of Theorem 2.2. □

Note that the above Theorem is referred to as "Hamilton's principle of least action". This is as the action $\boldsymbol{q}(t)$ is a minimum value of the action integral $\int_{t_1}^{t_2} L \mathrm{d}t$ in many cases [Arn13, p. 60]. In the sequel of this thesis physically motivated Lagrange functions as in Theorem 2.3 will be considered, where the action is a minimum.

2.3.2. Tensorial properties

The path integral (2.30) of Theorem 2.2 respectively 2.3 is of fundamental importance for the control systems considered here. Therefore, it will be investigated if this path integral is invariant under a change of coordinates (2.1). This is the case if the Lagrangian is a scalar relative to (2.1), i. e., if

$$L^\star(x^j, \dot{x}^j) = L(q^h(x^j), \dot{q}^h(x^j, \dot{x}^j)) \tag{2.40}$$

for all values of $(x^j, \dot{x}^j)$. According to Remark 2.1 this would be the case if $\partial L / \partial q^h$ would represent the components of the gradient co-vector which is not true as will become clear immediately.

Remark 2.7. *The derivatives* $\partial L / \partial q^h$ *do not form the components of a tensor. This can be seen by differentiating the relation* (2.40) *w. r. t.* x^j*:*

$$\frac{\partial L^\star}{\partial x^j} = \frac{\partial L}{\partial q^h}\frac{\partial q^h}{\partial x^j} + \frac{\partial L}{\partial \dot{q}^h}\frac{\partial \dot{q}^h}{\partial x^j} = \frac{\partial L}{\partial q^h}\frac{\partial q^h}{\partial x^j} + \frac{\partial L}{\partial \dot{q}^h}\frac{\partial^2 q^h}{\partial x^j \partial x^l}\dot{x}^l \,, \tag{2.41}$$

where in the last step the identity

$$\frac{\partial \dot{q}^h}{\partial x^j} = \frac{\partial^2 q^h}{\partial x^j \partial x^l}\dot{x}^l \tag{2.42}$$

which can be derived from

$$\dot{q}^h = \frac{\partial q^h}{\partial x^j}\dot{x}^j = \dot{q}^h(x^j, \dot{x}^j) \,, \tag{2.43}$$

has been exploited.

The above state of affairs motivates the introduction of a generalized gradient of L:

Definition 2.14. *The Euler-Lagrange equations*

$$\boldsymbol{E}(L) = \frac{\mathrm{d}}{\mathrm{d}t}\frac{\partial L}{\partial \dot{\boldsymbol{q}}} - \frac{\partial L}{\partial \boldsymbol{q}}$$

represent a generalized gradient of the Lagrangian L*.*

Lemma 2.2. *The Euler-Lagrange equations $\boldsymbol{E}(L)$ constitute the components of a covariant vector.*

Proof [LR89]. Consider the derivative of the relation (2.40) w. r. t. $\dot{x}^j$,

$$\frac{\partial L^\star}{\partial \dot{x}^j} = \frac{\partial L}{\partial \dot{q}^h}\frac{\partial \dot{q}^h}{\partial \dot{x}^j} = \frac{\partial L}{\partial \dot{q}^h}\frac{\partial q^h}{\partial x^j}\,, \tag{2.44}$$

where in the last step the identity

$$\frac{\partial \dot{q}^h}{\partial \dot{x}^j} = \frac{\partial q^h}{\partial x^j} \tag{2.45}$$

resulting from (2.43) has been substituted. Differentiate the result (2.44) with respect to time and take the relation (2.42) into account, i. e.,

$$\frac{\mathrm{d}}{\mathrm{d}t}\left(\frac{\partial L^\star}{\partial \dot{x}^j}\right) = \frac{\mathrm{d}}{\mathrm{d}t}\left(\frac{\partial L}{\partial \dot{q}^h}\right)\frac{\partial q^h}{\partial x^j} + \frac{\partial L}{\partial \dot{q}^h}\frac{\partial \dot{q}^h}{\partial x^j} = \frac{\mathrm{d}}{\mathrm{d}t}\left(\frac{\partial L}{\partial \dot{q}^h}\right)\frac{\partial q^h}{\partial x^j} + \frac{\partial L}{\partial \dot{q}^h}\frac{\partial^2 q^h}{\partial x^j \partial x^l}\dot{x}^l\,. \tag{2.46}$$

Then, subtracting (2.41) from the result, yields the relation

$$\frac{\mathrm{d}}{\mathrm{d}t}\left(\frac{\partial L^\star}{\partial \dot{x}^j}\right) - \frac{\partial L^\star}{\partial x^j} = \frac{\partial q^h}{\partial x^j}\left[\frac{\mathrm{d}}{\mathrm{d}t}\left(\frac{\partial L}{\partial \dot{q}^h}\right) - \frac{\partial L}{\partial q^h}\right] \tag{2.47}$$

which is clearly the transformation law of a covariant vector (cf. (2.7)). □

2.3.3. Matrix components

In this thesis, the particular class of Euler-Lagrange systems as introduced by Theorem 2.3 is considered extensively. In local coordinates $\boldsymbol{q}$ of the coordinate neighborhood $\mathcal{Q}$ (of the manifold $\mathcal{M}$), the Lagrangian comprises

$$L(\boldsymbol{q}, \dot{\boldsymbol{q}}) = T(\boldsymbol{q}, \dot{\boldsymbol{q}}) - U(\boldsymbol{q})\,, \tag{2.48}$$

the kinetic energy

$$T(\boldsymbol{q}, \dot{\boldsymbol{q}}) = \frac{1}{2}\dot{\boldsymbol{q}}^T \boldsymbol{M}(\boldsymbol{q})\dot{\boldsymbol{q}} \tag{2.49}$$

and potential energy $U(\boldsymbol{q})$, where the latter depends only on the positional coordinates $\boldsymbol{q}$. Note that the former expression is related to the Riemannian metric introduced by Definition 2.7. The Euler-Lagrange equations corresponding to the Lagrangian (2.48) can be written in the form

$$E_j(L) = \frac{\mathrm{d}}{\mathrm{d}t}\left(\frac{\partial T}{\partial \dot{q}^j}\right) - \frac{\partial T}{\partial q^j} + \frac{\partial U}{\partial q^j} \tag{2.50}$$

Taking (2.49) into account, it follows that

$$\frac{\partial T}{\partial \dot{q}^j} = M_{hj}\dot{q}^h\,,$$
$$\frac{\partial T}{\partial q^j} = \frac{1}{2}\frac{\partial M_{hk}}{\partial q^j}\dot{q}^h\dot{q}^k$$

such that the first two terms of the Euler-Lagrange equations (2.50) can be rewritten as

$$E_j(T) = \frac{\mathrm{d}}{\mathrm{d}t}\left(\frac{\partial T}{\partial \dot{q}^j}\right) - \frac{\partial T}{\partial q^j} = M_{hj}\ddot{q}^h + \frac{\partial M_{hj}}{\partial q^k}\dot{q}^h\dot{q}^k - \frac{1}{2}\frac{\partial M_{hk}}{\partial q^j}\dot{q}^h\dot{q}^k \tag{2.51}$$

$$= M_{hj}\ddot{q}^h + \Gamma_{hjk}\dot{q}^h\dot{q}^k \tag{2.52}$$

$$= M_{hj}\left(\ddot{q}^h + \Gamma_l{}^h{}_k\dot{q}^l\dot{q}^k\right), \tag{2.53}$$

where in the last two steps the Christoffel symbols (2.24) respectively (2.25) have been consulted, i. e.,

$$\left(\frac{\partial M_{hj}}{\partial q^k} - \frac{1}{2}\frac{\partial M_{hk}}{\partial q^j}\right)\dot{q}^h\dot{q}^k = \frac{1}{2}\left(\frac{\partial M_{hj}}{\partial q^k} + \frac{\partial M_{hj}}{\partial q^k} - \frac{\partial M_{hk}}{\partial q^j}\right)\dot{q}^h\dot{q}^k \tag{2.54}$$

$$= \frac{1}{2}\left(\frac{\partial M_{jk}}{\partial q^h} + \frac{\partial M_{hj}}{\partial q^k} - \frac{\partial M_{hk}}{\partial q^j}\right)\dot{q}^h\dot{q}^k \tag{2.55}$$

$$= \Gamma_{hjk}\dot{q}^h\dot{q}^k\,. \tag{2.56}$$

As can be seen from (2.55), the Christoffel symbols constitute a particular factorization of the term $\left(\partial M_{hj}/\partial q^k - \frac{1}{2}\partial M_{hk}/\partial q^j\right)\dot{q}^h\dot{q}^k$. This factorization suggests the introduction of the so-called Coriolis/centrifugal matrix:

Definition 2.15 (Coriolis/centrifugal matrix)**.** *The product*

$$C_{hj}(\boldsymbol{q}, \dot{\boldsymbol{q}}) = \Gamma_{hjk}(\boldsymbol{q})\dot{q}^k \tag{2.57}$$

is said to constitute the components of the $n \times n$ Coriolis/centrifugal matrix.

On the basis of this definition and Remark 2.2, the Euler-Lagrange equations (2.52) can be expressed as

$$\boldsymbol{E}(T) = \boldsymbol{M}(\boldsymbol{q})\ddot{\boldsymbol{q}} + \boldsymbol{C}(\boldsymbol{q}, \dot{\boldsymbol{q}})\dot{\boldsymbol{q}}\,, \tag{2.58}$$

where the following proposition of Lemma 2.1 holds:

Proposition 2.1. *Given the components of the Coriolis/centrifugal matrix introduced by Definition 2.15, then the identity*

$$\dot{\boldsymbol{M}} = \boldsymbol{C} + \boldsymbol{C}^T \tag{2.59}$$

holds along a path $\boldsymbol{q} = \boldsymbol{q}(t)$.

Proof. Rewriting (2.59) in index notion, i. e.,

$$\frac{\partial M_{hj}}{\partial q^k}\dot{q}^k = \Gamma_{hjk}\dot{q}^k + \Gamma_{jhk}\dot{q}^k\,,$$
$$\frac{\partial M_{hj}}{\partial q^k} = \Gamma_{hjk} + \Gamma_{jhk}\,,$$

it can be immediately seen that the last equation equals (2.27) of Lemma 2.1. □

Finally, the concept of covariant differentiation can be recapitulated from the Euler-Lagrange equations (2.53):

Remark 2.8. *Note that the Euler-Lagrange equations* (2.53) *can be expressed as the covariant derivative*

$$E_j(T) = M_{hj}\frac{\mathrm{D}\dot{q}^h}{\mathrm{D}t} \tag{2.60}$$

or in matrix notation as

$$\boldsymbol{E}(T) = \boldsymbol{M}\frac{\mathrm{D}\dot{\boldsymbol{q}}}{\mathrm{D}t}\,. \tag{2.61}$$

The entire Euler-Lagrange system (2.50) *can be compactly written as*

$$E_j(L) = M_{hj}\frac{\mathrm{D}\dot{q}^h}{\mathrm{D}t} + \frac{\partial U}{\partial q^j}\,. \tag{2.62}$$

It should be further noted that since the Euler-Lagrange co-vector resulting from Hamilton's principle of least action (cf. Theorem 2.3) can be exclusively derived based on tensorial operations, its components are intrinsic (physical) quantities which can be formulated in coordinate-free fashion.

2.3.4. Geometrical interpretation

The Euler-Lagrange equations, where the Lagrangian consists only of kinetic energy, i. e., $L = T$, can be interpreted from a view-point of Riemannian geometry. Using the indirect approach adopted from [LR89] it can be shown that any path on a Riemannian manifold, or equivalently, any trajectory of a physical system which consists of kinetic energy only and satisfies the Euler-Lagrange equations

$$\boldsymbol{E}(T) = \frac{\mathrm{D}\dot{\boldsymbol{q}}}{\mathrm{D}t} = \boldsymbol{0}\,, \tag{2.63}$$

is a geodesic of the Riemannian space (according to Definition 2.8). A geodesic is an extremum to the path integral

$$J = \int_{t_1}^{t_2} f(\boldsymbol{q}, \dot{\boldsymbol{q}})\mathrm{d}t\,, \tag{2.64}$$

where $f(\boldsymbol{q}, \dot{\boldsymbol{q}})$ measures the length of the vector $\dot{\boldsymbol{q}}$ according to Definition 2.6. In most cases (or all cases considered in this thesis), this extremum is a minimum such that the corresponding Euler-Lagrange equations define the "shortest" path connecting two points on the Riemannian manifold.

In the following, it will be shown that an extremum of

$$J = \int_{t_1}^{t_2} T(\boldsymbol{q}, \dot{\boldsymbol{q}})\mathrm{d}t \tag{2.65}$$

is equivalently also an extremum of (2.64). Therefore, it is noted that the kinetic energy,

$$T(\boldsymbol{q}, \dot{\boldsymbol{q}}) = \frac{1}{2}f(\boldsymbol{q}, \dot{\boldsymbol{q}})^2 = \frac{1}{2}\dot{\boldsymbol{q}}^T\boldsymbol{M}(\boldsymbol{q})\dot{\boldsymbol{q}}\,, \tag{2.66}$$

is one-half the squared length of the vector $\dot{\boldsymbol{q}}$. From this relation it is found that

$$f\frac{\partial f}{\partial \dot{\boldsymbol{q}}} = \frac{\partial T}{\partial \dot{\boldsymbol{q}}}\,,$$

$$\frac{\mathrm{d}f}{\mathrm{d}t}\frac{\partial f}{\partial \dot{\boldsymbol{q}}} + f\frac{\mathrm{d}}{\mathrm{d}t}\left(\frac{\partial f}{\partial \dot{\boldsymbol{q}}}\right) = \frac{\mathrm{d}}{\mathrm{d}t}\left(\frac{\partial T}{\partial \dot{\boldsymbol{q}}}\right)$$

and using (2.39) that

$$f\boldsymbol{E}(f) = \boldsymbol{E}(T) - \frac{\mathrm{d}f}{\mathrm{d}t}\frac{\partial f}{\partial \dot{\boldsymbol{q}}}\,. \tag{2.67}$$

Furthermore, differentiating the relation (2.66) taking Lemma 2.1 into account, i. e.,

$$2f\frac{\mathrm{d}f}{\mathrm{d}t} = \frac{\mathrm{d}}{\mathrm{d}t}\left(\dot{\boldsymbol{q}}^T\boldsymbol{M}\dot{\boldsymbol{q}}\right) = \frac{\mathrm{D}}{\mathrm{D}t}\left(\dot{\boldsymbol{q}}^T\boldsymbol{M}\dot{\boldsymbol{q}}\right) = 2\dot{\boldsymbol{q}}^T\boldsymbol{M}\frac{\mathrm{D}\dot{\boldsymbol{q}}}{\mathrm{D}t}$$

it follows using the extremum condition of the kinetic energy integral (2.65), (2.63) that

$$f\frac{\mathrm{d}f}{\mathrm{d}t} = 0$$

which is equivalent to

$$f(\boldsymbol{q}, \dot{\boldsymbol{q}}) = c = \text{const.} \tag{2.68}$$

Considering this result and (2.63) in (2.67) it follows that $\boldsymbol{E}(f) = \boldsymbol{0}$ if $\boldsymbol{E}(T) = \boldsymbol{0}$. Accordingly an extremum of the kinetic energy path integral (2.65) is equivalently a geodesic of the Riemannian manifold, i. e., it is the shortest path connecting two points on a Riemannian manifold.

2.4. Submanifolds

In general, the motion of the considered Euler-Lagrange systems takes place on a n-dimensional manifold $\mathcal{M}^n$. However, if (holonomic) constraints are imposed on the system, the motion evolves on a lower dimensional manifold. Such constraints can be, e. g., contact or periodicity constraints.

An example of a submanifold is to constrain the motion on a sphere such that it evolves on the equator. A sphere is a two-dimensional manifold, while the equator is a circle, i. e., it is an one-dimensional submanifold. If a trajectory evolving on the equator is such that the arc length increases over time, then the corresponding motion is periodic.

2.4.1. Embedded submanifolds

The definition and the main theorem of an embedded submanifold, i. e., a submanifold of a manifold, are exactly as in case of a submanifold of euclidean space, if the point set of the manifold is replaced by the euclidean space. Therefore, only the former case is considered.

Definition 2.16 (Submanifold)**.** *An embedded submanifold $\mathcal{W}^{n-r} \subset \mathcal{M}^n$ of a manifold $\mathcal{M}^n$ can be locally described by the r differentiable functions*

$$\begin{aligned} \phi^1(\boldsymbol{q}) &= 0 \\ &\vdots \\ \phi^r(\boldsymbol{q}) &= 0 \end{aligned} \tag{2.69}$$

which depend on the coordinates $\boldsymbol{q}$ of the coordinate neighborhood $\mathcal{Q}$. These functions are independent in a sense that the Jacobian matrix $\partial\boldsymbol{\phi}/\partial\boldsymbol{q}$ has rank r at each point of the locus (2.69)*.*

Note that the same submanifold could also be defined in terms of different coordinates as long as the coordinate patches are intersecting in the region of interest. This can be done by introducing the differential of a map between manifolds.

Definition 2.17 (Differential of a map [Fra03])**.** *The differential $\boldsymbol{\phi}_\star$ of the map $\boldsymbol{\phi} : \mathcal{M}^n \to \mathcal{V}^r$ is the linear transformation $\boldsymbol{\phi}_\star : \mathcal{M}^n_{\boldsymbol{r}} \to \mathcal{V}^r_{\boldsymbol{\phi}(\boldsymbol{r})}$ defined as follows. Let $\boldsymbol{r} = \boldsymbol{r}(t)$ be a parameterized curve on the manifold $\mathcal{M}^n$ and let $\boldsymbol{v} \in \mathcal{M}^n_{\boldsymbol{r}}$, where $\boldsymbol{v} = \dot{\boldsymbol{r}}$, be the velocity vector. Then,*

$$\boldsymbol{\phi}_\star \boldsymbol{v} = \frac{\mathrm{d}\boldsymbol{\phi}(\boldsymbol{r}(t))}{\mathrm{d}t}\,,$$

is the velocity vector of the image curve $\boldsymbol{\phi}(\boldsymbol{r})$ on $\mathcal{V}^r$. In local coordinates $\boldsymbol{q}$ of $\mathcal{M}^n$ and $\boldsymbol{y}$ of $\mathcal{V}^r$, this linear transformation is the Jacobian matrix

$$\boldsymbol{\phi}_\star = \frac{\partial \boldsymbol{\phi}}{\partial \boldsymbol{q}}(\boldsymbol{r}) = \frac{\partial \boldsymbol{y}}{\partial \boldsymbol{q}}(\boldsymbol{r})\,. \tag{2.70}$$

On the basis of this definition, the main theorem on embedded submanifolds can be introduced.

Theorem 2.4 ([Fra03])**.** *Let $\boldsymbol{\phi} : \mathcal{M}^n \to \mathcal{V}^r$ be a map between manifolds of different dimensions $n > r$ and suppose that for some $\boldsymbol{s} \in \mathcal{V}^r$ the inverse map $\boldsymbol{\phi}^{-1}(\boldsymbol{s}) \subset \mathcal{M}^n$ is not empty. Suppose further that the differential of the map $\boldsymbol{\phi}_\star$ introduced by Definition 2.17 has rank r at each point of $\boldsymbol{\phi}^{-1}(\boldsymbol{s})$. Then, $\boldsymbol{\phi}^{-1}(\boldsymbol{s})$ defines a $(n-r)$-dimensional submanifold of $\mathcal{M}^n$.*

The notion of an embedded submanifold can be used to constrain the motion of an Euler-Lagrange system as will be shown next.

2.4.2. Hamilton's principle with holonomic constraints

Consider the case where the motion of a mechanical system is constrained to move on a submanifold $\mathcal{W}^{n-r}$ of $\mathcal{M}^n$. This happens, e. g., when a free floating system gets in contact with the ground and the impact is such that the contact point is constrained to maintain its position. The submanifold is defined by r constraint functions ϕ^j which satisfy the assumptions of Theorem 2.4. In the following, the case is considered where these functions depend on the local coordinates $\boldsymbol{q}$ for simplicity[12]. The following result is a well-known modification of the Theorem 2.2 respectively 2.3 (see, e. g., [SC70]).

Theorem 2.5. *Motions of the constraint mechanical system, where the Lagrangian L is defined by Theorem 2.3,*

$$\frac{\mathrm{d}}{\mathrm{d}t}\frac{\partial L}{\partial \dot{\boldsymbol{q}}} - \frac{\partial L}{\partial \boldsymbol{q}} = -\boldsymbol{\lambda}^T \frac{\partial \boldsymbol{\phi}}{\partial \boldsymbol{q}} \tag{2.71}$$

satisfying

$$\boldsymbol{\phi}(\boldsymbol{q}) = \boldsymbol{0}\,, \tag{2.72}$$

[12] In general, the constraints $\boldsymbol{\phi}$ can be expressed w. r. t. to any coordinates of the manifold $\mathcal{M}$ as long as the corresponding coordinate patch covers the region of interest.

coincide with extrema of the action integral

$$J^\star = \int_{t_1}^{t_2} \left(L + \boldsymbol{\lambda}^T \boldsymbol{\phi}\right) \mathrm{d}t = \int_{t_1}^{t_2} L^\star \mathrm{d}t\,, \tag{2.73}$$

where $\boldsymbol{\lambda}$ *are suitable chosen Lagrange multipliers.*

Proof. To proof the above theorem, a similar variation as in the proof of Theorem 2.2 will be considered, i. e.,

$$\delta J^\star = \int_{t_1}^{t_2} \left(\frac{\partial J^\star}{\partial \alpha}\mathrm{d}\alpha + \frac{\partial J^\star}{\partial \boldsymbol{\lambda}}\mathrm{d}\boldsymbol{\lambda}\right) \mathrm{d}t = 0\,. \tag{2.74}$$

From the second term of the integrand it follows directly that

$$\frac{\partial L^\star}{\partial \boldsymbol{\lambda}} = \mathbf{0} \quad \Longrightarrow \quad \boldsymbol{\phi}(\boldsymbol{q}) = \mathbf{0}\,, \tag{2.75}$$

which shows that the constraints are satisfied. The first term of the integrand in (2.74) leads to the Euler-Lagrange equations

$$\frac{\partial L^\star}{\partial \boldsymbol{q}} - \frac{\mathrm{d}}{\mathrm{d}t}\frac{\partial L^\star}{\partial \dot{\boldsymbol{q}}} = \mathbf{0}\,, \tag{2.76}$$

for the modified Lagrangian $L^\star$. Substituting $L^\star = L + \boldsymbol{\lambda}^T\boldsymbol{\phi}$ from (2.73) leads to

$$\frac{\partial L}{\partial \boldsymbol{q}} - \frac{\mathrm{d}}{\mathrm{d}t}\frac{\partial L}{\partial \dot{\boldsymbol{q}}} = \frac{\mathrm{d}}{\mathrm{d}t}\left(\boldsymbol{\lambda}^T\frac{\partial \boldsymbol{\phi}}{\partial \dot{\boldsymbol{q}}}\right) - \boldsymbol{\lambda}^T\frac{\partial \boldsymbol{\phi}}{\partial \boldsymbol{q}}\,. \tag{2.77}$$

Since the constraint functions $\boldsymbol{\phi}(\boldsymbol{q})$ depend only on $\boldsymbol{q}$, i. e., the first term on the right hand side vanishes, the above equations equal (2.71). □

Remark 2.9 (Initial conditions and degrees of freedom)**.** *The constrained Euler-Lagrange system* (2.71) *represents* n *second-order differential equations. They give rise to* $2n$ *integration constants of which* $2r$ *are determined by the constraint equations* (2.72) *and their time derivative* $\dot{\boldsymbol{\phi}} = \mathbf{0}$*. The remaining* $2(n-r)$ *integration constants are determined by initial conditions. One may say that* r *of* n *degrees of freedom are eliminated by the holonomic constraints* (2.72)*. The latter statement coincides with the definition of a submanifold (cf. Theorem 2.4).*

2.5. Conclusion

This chapter introduces the notion of a differentiable manifold from a dynamics and control perspective of multi-body mechanical systems. On this differentiable manifold the concept of tensors are derived based on their transformation properties under a change of coordinates. A particular tensor is the inertia matrix which constitutes a metric to measure the length on a Riemannian manifold. The necessity of dynamics derivations to differentiate vector fields on a manifold leads to the concept of covariant differentiation which assumes that the manifold is equipped with an affine connection. Introducing the coefficients of a Riemannian connection (which are known as the Christoffel symbols), the Euler-Lagrange equations describing the dynamics of the mechanical systems of interest are compactly derived from Hamilton's principle of least action by means of common tools of the calculus of variation. Due to its tantamount importance in the dynamics of legged and periodic locomotion, the notion of a submanifolds is briefly introduced. Therefore, this chapter forms the foundations for the analysis and the derivation of mechanical periodic motion control systems.

CHAPTER 3

Modeling and Basic Control

Compliantly actuated mechanical systems represent a sub-class of under-actuated Euler-Lagrange dynamics, where directly and indirectly actuated degrees of freedom are connected via elastic elements. The capability of such dynamics to convert between kinetic and elastic potential energy are the cause for an intrinsic oscillatory behavior. The primary goal of this thesis is analyzing and controlling such multi-dimensional, nonlinear oscillations. To this end, first, a general description of under-actuated Euler-Lagrange dynamics is presented. Then, this formulation is specified in greater detail via the concept of static controllability, which yields conditions on the potential of the Lagrangian, and defines the compliantly actuated systems of interest. The intrinsic oscillatory behavior of such dynamics can be excited and altered by changing its equilibrium configurations and damping properties. Therefore, basic joint-level control methods are proposed which can be applied to access these properties by controlling configuration variables and their transient behavior without changing the structure of the plant-inherent Lagrangian.

3.1. Under-actuated Euler-Lagrange systems

The most general class of dynamics considered here are the so-called under-actuated Euler-Lagrange systems [ASWE+10, ASOP12], satisfying

$$\frac{\mathrm{d}}{\mathrm{d}t}\left(\frac{\partial L(\boldsymbol{z},\dot{\boldsymbol{z}})}{\partial \dot{\boldsymbol{z}}}\right) - \frac{\partial L(\boldsymbol{z},\dot{\boldsymbol{z}})}{\partial \boldsymbol{z}} = \boldsymbol{\tau}_{\mathrm{gen}} - \boldsymbol{d}(\boldsymbol{z},\dot{\boldsymbol{z}})\,, \tag{3.1}$$

where the left hand side is a consequence of Hamilton's principle of least action (Theorem 2.3). Thus, the Lagrangian

$$L(\boldsymbol{z},\dot{\boldsymbol{z}}) = T(\boldsymbol{z},\dot{\boldsymbol{z}}) - U(\boldsymbol{z}) \tag{3.2}$$

is the difference of the kinetic energy $T(\boldsymbol{z},\dot{\boldsymbol{z}})$ and potential energy $U(\boldsymbol{z})$. By the term "under-actuated" it is meant that the local coordinates $\boldsymbol{z} = (\boldsymbol{\theta}^T, \boldsymbol{q}^T)^T \in \mathbb{R}^{m+n}$ of the configuration manifold $\mathcal{M}^{m+n}$ can be divided into directly actuated states $\boldsymbol{\theta} \in \mathbb{R}^m$ and indirectly actuated states $\boldsymbol{q} \in \mathbb{R}^n$ at position level, where m and n are positive integers. Accordingly, the generalized forces $\boldsymbol{\tau}_{\mathrm{gen}} = (\boldsymbol{u}^T, \boldsymbol{\tau}_{\mathrm{ext}}^T)^T \in \mathbb{R}^{m+n}$ can be divided into the

control input $\boldsymbol{u} \in \mathbb{R}^m$ and the externally applied generalized force $\boldsymbol{\tau}_{\text{ext}} \in \mathbb{R}^n$. Finally, the non-conservative, generalized force $\boldsymbol{d}(\boldsymbol{z}, \dot{\boldsymbol{z}})$ is assumed to be dissipative:

Assumption 3.1. *For any continuous path $\boldsymbol{z} = \boldsymbol{z}(t)$ on the configuration manifold $\mathcal{M}^{m+n}$, $\dot{\boldsymbol{z}}^T \boldsymbol{d}(\boldsymbol{z}, \dot{\boldsymbol{z}}) > 0$ for all $\dot{\boldsymbol{z}} \neq \boldsymbol{0}$ and $\boldsymbol{d}(\boldsymbol{z}, \dot{\boldsymbol{z}}) = \boldsymbol{0}$ only if $\dot{\boldsymbol{z}} = \boldsymbol{0}$ holds.*

This assumption is the only restriction invoked for the general under-actuated Euler-Lagrange system (3.1).

According to Remark 2.2 and Definition 2.15, the under-actuated Euler-Lagrange system (3.1) can be expressed in terms of the matrix components

$$\bar{\boldsymbol{M}}(\boldsymbol{z})\ddot{\boldsymbol{z}} + \bar{\boldsymbol{C}}(\boldsymbol{z}, \dot{\boldsymbol{z}})\dot{\boldsymbol{z}} + \frac{\partial U(\boldsymbol{z})}{\partial \boldsymbol{z}}^T = \boldsymbol{\tau}_{\text{gen}} - \boldsymbol{d}(\boldsymbol{z}, \dot{\boldsymbol{z}})\,, \tag{3.3}$$

where $\bar{\boldsymbol{M}}(\boldsymbol{z})$ is the symmetric, positive definite $(m+n) \times (m+n)$ inertia matrix and $\bar{\boldsymbol{C}}(\boldsymbol{z}, \dot{\boldsymbol{z}})$ is the $(m+n) \times (m+n)$ Coriolis/centrifugal matrix introduced by Definition 2.15, where the following property can be deduced from Proposition 2.1:

Corollary 3.1. *For any continuous path $\boldsymbol{z} = \boldsymbol{z}(t)$ on the configuration manifold $\mathcal{M}^{m+n}$, the matrix $\dot{\bar{\boldsymbol{M}}} - 2\bar{\boldsymbol{C}}$ is skew symmetric in a sense that $\dot{\boldsymbol{z}}^T \left(\dot{\bar{\boldsymbol{M}}} - 2\bar{\boldsymbol{C}} \right) \dot{\boldsymbol{z}}$ vanishes identically.*

This property is of major importance in the stability and passivity analysis of general Euler-Lagrange systems. It holds for any sub-class of the Euler-Lagrange systems introduced in the remainder of this chapter.

Proof. The proof of the above corollary follows directly from Proposition 2.1 and a lemma (see, e. g., [VdS12]) which states that the matrix $\dot{\bar{\boldsymbol{M}}} - 2\bar{\boldsymbol{C}}$ is skew symmetric if and only if the equality $\dot{\bar{\boldsymbol{M}}} = \bar{\boldsymbol{C}} + \bar{\boldsymbol{C}}^T$ holds. □

3.1.1. Compliantly actuated mechanical system

A particular sub-class of under-actuated Euler-Lagrange systems which is in the main focus of the following investigations is given by the so-called compliantly actuated mechanical systems. Thereby, the potential energy $U(\boldsymbol{z})$ is further specified.

Definition 3.1 (Compliant actuation)**.** *The under-actuated Euler-Lagrange system as introduced by* (3.3) *is said to constitute a compliantly actuated mechanical system if the potential energy*

$$U(\boldsymbol{z}) = U_{\text{g}}(\boldsymbol{z}) + U_{\text{e}}(\boldsymbol{z}) \tag{3.4}$$

comprises a gravitational potential $U_{\text{g}}(\boldsymbol{z})$ (which is allowed to vanish on the entire manifold $\mathcal{M}^{m+n}$) and a positive semi-definite elastic potential

$$U_{\text{e}}(\boldsymbol{z}) \geq 0\,, \quad \forall \boldsymbol{z} \in \mathbb{R}^{m+n}\,, \tag{3.5}$$

where for at least one $h \in \{1, \ldots, m\}$ and for at least one $j \in \{1, \ldots, n\}$, the "elastic coupling",

$$\frac{\partial^2 U_{\text{e}}}{\partial \theta^h \partial q^j} = \frac{\partial^2 U_{\text{e}}}{\partial q^j \partial \theta^h} \neq 0\,, \quad \frac{\partial^2 U_{\text{e}}}{\partial {\theta^h}^2} > 0\,, \quad \frac{\partial^2 U_{\text{e}}}{\partial {q^j}^2} > 0\,, \quad \forall \boldsymbol{z} \in \mathbb{R}^{m+n} \tag{3.6}$$

is non-zero (and finite).

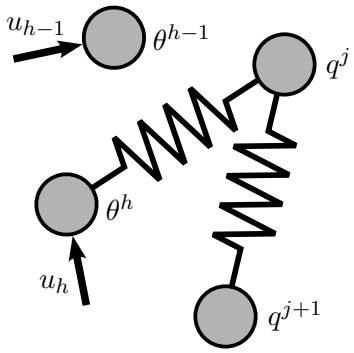

Figure 3.1.: Compliant actuation and static controllability of the state q^j by the control input u_h via θ^h.

Note that the above definition implies that the elastic potential U_e is such that at least one of the indirectly actuated states q^j is statically controllable via a directly actuated state θ^h at position level. Loosely speaking, at least one of the actuator inertias is connected at least to one of the link inertias via a spring (cf. Fig. 3.1). An example of a not fully statically controllable system is given by the elastic pendulum, where a point-mass is suspended on a radially acting spring.

In the following, the compliantly actuated system is specified further such that the number of statically controllable indirectly actuated states p equals or is lower than the number of directly actuated states m at position level. Furthermore for the simplicity of the description, it is assumed that all of the indirectly actuated states are statically controllable, i. e., $p = n$. Then, properties naturally arising for mechanical systems—when rigid bodies are connected via springs—are assumed. Therefore, basic definitions to evaluate the boundedness of matrices are introduced in advance.

Definition 3.2. *Given a square and symmetric real matrix $\boldsymbol{A}$, then the minimum and maximum eigenvalue of $\boldsymbol{A}$ are denoted by $\lambda_{\min}(\boldsymbol{A})$ and $\lambda_{\max}(\boldsymbol{A}) \geq \lambda_{\min}(\boldsymbol{A})$, respectively.*

Definition 3.3. *Given any real matrix $\boldsymbol{A}$, then the minimum and maximum singular value of $\boldsymbol{A}$ are denoted by $\sigma_{\min}(\boldsymbol{A})$ and $\sigma_{\max}(\boldsymbol{A}) \geq \sigma_{\min}(\boldsymbol{A})$, respectively.*

Assumption 3.2. *The gradient $\partial U_\mathrm{e}/\partial \boldsymbol{q}$ is strictly monotonic in $\boldsymbol{q}$ in a sense that there exists constants $c_1, c_2 > 0$ such that*

$$\inf_{\boldsymbol{z}\in\mathbb{R}^{m+n}} \lambda_{\min}\left(\frac{\partial^2 U_\mathrm{e}(\boldsymbol{\theta},\boldsymbol{q})}{\partial \boldsymbol{q}^2}\right) > c_1\,, \tag{3.7}$$

$$\sup_{\boldsymbol{z}\in\mathbb{R}^{m+n}} \lambda_{\max}\left(\frac{\partial^2 U_\mathrm{e}(\boldsymbol{\theta},\boldsymbol{q})}{\partial \boldsymbol{q}^2}\right) < c_2\,, \tag{3.8}$$

keep bounded.

This property ensures that given any fixed $\boldsymbol{\theta}$, the equations[1] $-(\partial U_\mathrm{e}/\partial \boldsymbol{q})^T = \boldsymbol{\tau}$ have always a unique solution for $\boldsymbol{q}$. The assumption which ensures that given any fixed $\boldsymbol{q}$, $-(\partial U_\mathrm{e}/\partial \boldsymbol{q})^T = \boldsymbol{\tau}$ have always a unique solution for $\boldsymbol{\theta}$ can be formulated similarly.

[1]The negative sign is a convention that the generalized elastic force $\boldsymbol{\tau}$ is an "applied" force.

Assumption 3.3. *The gradient $\partial U_\mathrm{e}/\partial \boldsymbol{q}$ is strictly monotonic in $\boldsymbol{\theta}$ in a sense that there exists constants $c_3, c_4 > 0$ such that*

$$\inf_{\boldsymbol{z}\in\mathbb{R}^{m+n}} \sigma_{\min}\left(\frac{\partial^2 U_\mathrm{e}(\boldsymbol{\theta},\boldsymbol{q})}{\partial \boldsymbol{q}\partial\boldsymbol{\theta}}\right) > c_3\,, \tag{3.9}$$

$$\sup_{\boldsymbol{z}\in\mathbb{R}^{m+n}} \sigma_{\max}\left(\frac{\partial^2 U_\mathrm{e}(\boldsymbol{\theta},\boldsymbol{q})}{\partial \boldsymbol{q}\partial\boldsymbol{\theta}}\right) < c_4\,, \tag{3.10}$$

keep bounded.

The above property also implies that all of the indirectly actuated states are statically controllable. This in turn means that the generalized force produced by the springs is controllable which is a requirement for the control approaches presented in Sect. 3.3.

Assumption 3.4. *The gradient $\partial U_\mathrm{e}/\partial \boldsymbol{\theta}$ is strictly monotonic in $\boldsymbol{\theta}$ in a sense that there exists constants $c_5, c_6 > 0$ such that*

$$\inf_{\boldsymbol{z}\in\mathbb{R}^{m+n}} \lambda_{\min}\left(\frac{\partial^2 U_\mathrm{e}(\boldsymbol{\theta},\boldsymbol{q})}{\partial \boldsymbol{\theta}^2}\right) > c_5\,, \tag{3.11}$$

$$\sup_{\boldsymbol{z}\in\mathbb{R}^{m+n}} \lambda_{\max}\left(\frac{\partial^2 U_\mathrm{e}(\boldsymbol{\theta},\boldsymbol{q})}{\partial \boldsymbol{\theta}^2}\right) < c_6\,, \tag{3.12}$$

keep bounded.

The remaining assumptions guarantee the existence of a unique static equilibrium and are therefore imposed on the potential function including gravity.

Assumption 3.5. *There exists constants $c_7, c_8 > 0$ such that*

$$\inf_{\boldsymbol{z}\in\mathbb{R}^{m+n}} \lambda_{\min}\left(\frac{\partial^2 U(\boldsymbol{\theta},\boldsymbol{q})}{\partial \boldsymbol{q}^2}\right) > c_7\,, \tag{3.13}$$

$$\sup_{\boldsymbol{z}\in\mathbb{R}^{m+n}} \lambda_{\max}\left(\frac{\partial^2 U(\boldsymbol{\theta},\boldsymbol{q})}{\partial \boldsymbol{q}^2}\right) < c_8\,, \tag{3.14}$$

keep bounded.

Loosely speaking, condition (3.13) ensures that the compliantly actuated system does not collapse statically under the influence of gravity, if the actuator positions are hold to constant.

Assumption 3.6. *There exists constants $c_9, c_{10} > 0$ such that*

$$\inf_{\boldsymbol{z}\in\mathbb{R}^{m+n}} \sigma_{\min}\left(\frac{\partial^2 U(\boldsymbol{\theta},\boldsymbol{q})}{\partial \boldsymbol{q}\partial\boldsymbol{\theta}}\right) > c_9\,, \tag{3.15}$$

$$\sup_{\boldsymbol{z}\in\mathbb{R}^{m+n}} \sigma_{\max}\left(\frac{\partial^2 U(\boldsymbol{\theta},\boldsymbol{q})}{\partial \boldsymbol{q}\partial\boldsymbol{\theta}}\right) < c_{10}\,, \tag{3.16}$$

keep bounded.

These assumptions suggest the definition of a static equivalent of the indirectly actuated states at position level as introduced in the following.

Definition 3.4. *Let*

$$\boldsymbol{f}_{\mathrm{q}}(\boldsymbol{\theta},\boldsymbol{q}) := \frac{\partial U(\boldsymbol{\theta},\boldsymbol{q})}{\partial \boldsymbol{q}}^{T}, \tag{3.17}$$

then the mapping $\bar{\boldsymbol{q}} : \mathbb{R}^m \to \mathbb{R}^n$ *are such that*

$$\boldsymbol{f}_{\mathrm{q}}(\boldsymbol{\theta},\bar{\boldsymbol{q}}(\boldsymbol{\theta})) = \boldsymbol{0}, \quad \forall \boldsymbol{\theta} \in \mathbb{R}^m. \tag{3.18}$$

Remark 3.1. *As a result of the implicit function theorem, the existence of the functions* $\bar{\boldsymbol{q}} = \bar{\boldsymbol{q}}(\boldsymbol{\theta})$ *is guaranteed due to Assumption 3.5.*

Considering an argumentation adopted from [ASOP12] (and if $m = n$) it can be shown that $\bar{\boldsymbol{q}} = \bar{\boldsymbol{q}}(\boldsymbol{\theta})$ is a diffeomorphism.

Proposition 3.1. *In case* $m = n$*, the mapping* $\bar{\boldsymbol{q}} : \mathbb{R}^n \to \mathbb{R}^n$ *introduced by Definition 3.4 is a global diffeomorphism.*

Proof. In order to show that the mapping $\bar{\boldsymbol{q}} : \mathbb{R}^n \to \mathbb{R}^n$ is a diffeomorphism, the Jacobian $\partial\bar{\boldsymbol{q}}(\boldsymbol{\theta})/\partial\boldsymbol{\theta}$ needs to be shown to be always nonsingular, i. e., it has to be shown that

$$\sup_{\boldsymbol{\theta}\in\mathbb{R}^m} \left\| \left(\frac{\partial \bar{\boldsymbol{q}}(\boldsymbol{\theta})}{\partial \boldsymbol{\theta}} \right)^{-1} \right\| < \infty, \tag{3.19}$$

keeps bounded[2] from above [Zei86, Corollary 4.41, p. 174]. By differentiating condition (3.18) it can be seen that the Jacobian matrix of the mapping $\bar{\boldsymbol{q}}$ takes the form

$$\boldsymbol{J}_{\bar{\mathrm{q}}}(\boldsymbol{\theta}) := \frac{\partial \bar{\boldsymbol{q}}(\boldsymbol{\theta})}{\partial \boldsymbol{\theta}} = -\left(\frac{\partial^2 U(\boldsymbol{\theta},\boldsymbol{q})}{\partial \boldsymbol{q}^2}\bigg|_{\boldsymbol{q}=\bar{\boldsymbol{q}}} \right)^{-1} \frac{\partial^2 U(\boldsymbol{\theta},\boldsymbol{q})}{\partial \boldsymbol{q}\partial\boldsymbol{\theta}}\bigg|_{\boldsymbol{q}=\bar{\boldsymbol{q}}}. \tag{3.20}$$

The inverse of this Jacobian matrix

$$\left\|\boldsymbol{J}_{\bar{\mathrm{q}}}(\boldsymbol{\theta})^{-1}\right\| \leq \left\| \left(\frac{\partial^2 U(\boldsymbol{\theta},\boldsymbol{q})}{\partial \boldsymbol{q}\partial\boldsymbol{\theta}}\bigg|_{\boldsymbol{q}=\bar{\boldsymbol{q}}} \right)^{-1} \right\| \left\| \frac{\partial^2 U(\boldsymbol{\theta},\boldsymbol{q})}{\partial \boldsymbol{q}^2}\bigg|_{\boldsymbol{q}=\bar{\boldsymbol{q}}} \right\| \leq c_8/c_9, \tag{3.21}$$

keeps bounded due to Assumptions 3.5 and 3.6. □

Remark 3.2. *Proposition 3.1 can be extended to the more general case:* $m > n$*. This can be accomplished by introducing* $m - n$ *holonomic constraints* $\boldsymbol{\phi}(\boldsymbol{\theta}) = \boldsymbol{0}$*, where the constraint Jacobian matrix* $\partial\boldsymbol{\phi}(\boldsymbol{\theta})/\partial\boldsymbol{\theta}$ *is of full rank (cf. Theorem 2.4).*

The remaining assumption on the potential $U(\boldsymbol{\theta},\boldsymbol{q})$ is made mainly for the case of classical actuator position PD control.

Assumption 3.7. *There exists a constant* $c_{11} \in \mathbb{R}$ *such that*

$$\inf_{\boldsymbol{z}\in\mathbb{R}^{m+n}} \lambda_{\min}\left(\frac{\partial^2 U(\boldsymbol{\theta},\boldsymbol{q})}{\partial \boldsymbol{\theta}^2} \right) > c_{11}. \tag{3.22}$$

[2] The matrix norm $\|\cdot\|$ is assumed to be the induced Euclidean norm.

This assumption is not required (for the stability analysis), if instead of the actuator configuration, the homeomorphic static equivalent of the indirectly actuated states (cf. Definition 3.4) is considered as control variable.

Remark 3.3 (Variable stiffness actuation)**.** *It is worth mentioning that no assumptions have been made yet on the number of directly and indirectly actuated states at position level m and n, respectively. In particular, the additional degrees of freedom in case $m > n$ can be exploited to alter the characteristics of the generalized spring force, i. e., the relation between a displacement $\Delta\boldsymbol{q}$ w. r. t. an equilibrium point $\boldsymbol{q}_0$ and the resulting generalized force*

$$\boldsymbol{\tau} = - \left. \frac{\partial U_\mathrm{e}(\boldsymbol{\theta}, \boldsymbol{q})}{\partial \boldsymbol{q}} \right|^T_{\boldsymbol{q}=\boldsymbol{q}_0+\Delta\boldsymbol{q}} . \tag{3.23}$$

The possibility to independently alter the "shape" of the elastic potential in addition to its minimum is known as the principle of variable stiffness actuation (VSA), see, e. g., [ASEG+08].

The concept of variable stiffness actuation is a special case of the more general concept of compliant actuation treated here. The former is circumstantial for this thesis and therefore will not be treated in detail.

Finally, for simplicity and for readability, the derivation of the basic joint-level control approaches treated in this thesis assumes the case, where the number of directly actuated states m equals the number of statically controllable indirectly actuated states p and the number of indirectly actuated states n, at position level respectively, i. e., $m = p = n$.

3.1.2. Reduced compliantly actuated mechanical system

The general model (3.3) taking Definition 3.1 into account can be decomposed as

$$\begin{bmatrix} \boldsymbol{B}(\boldsymbol{z}) & \boldsymbol{S}(\boldsymbol{z}) \\ \boldsymbol{S}(\boldsymbol{z})^T & \boldsymbol{M}(\boldsymbol{z}) \end{bmatrix} \begin{pmatrix} \ddot{\boldsymbol{\theta}} \\ \ddot{\boldsymbol{q}} \end{pmatrix} + \bar{\boldsymbol{C}}(\boldsymbol{z}, \dot{\boldsymbol{z}})\dot{\boldsymbol{z}} + \frac{\partial U_\mathrm{g}}{\partial \boldsymbol{z}}^T + \frac{\partial U_\mathrm{e}}{\partial \boldsymbol{z}}^T = \begin{pmatrix} \boldsymbol{u} \\ \boldsymbol{\tau}_\mathrm{ext} \end{pmatrix} - \boldsymbol{d}(\boldsymbol{z}, \dot{\boldsymbol{z}}) , \tag{3.24}$$

where $\boldsymbol{B}$ is the $(m \times m)$ inertia matrix of the actuators, $\boldsymbol{M}$ is the $(n \times n)$ inertia matrix of the links, and $\boldsymbol{S}$ represent the inertia coupling. The general model (3.24) is required to describe, e. g., the inertial coupling through linkages in parallel to elasticities (cf. the elbow joint of the DLR Hand Arm System [GASB+11]).

On the basis of the following assumptions, the model (3.24) can be reduced [Spo87]:

Assumption 3.8. *The rotors of the actuators are modeled as uniform rotational symmetric rigid bodies, where the rotation and symmetry axes of each actuator coincide.*

This assumption is valid for many compliantly actuated robotic systems having solely rotational electric motors as actuators and no multi-bar linkages with parallel elastic actuation. In particular, assumption 3.8 implies that the inertia matrix $\bar{\boldsymbol{M}}(\boldsymbol{q})$ as well as the gravity potential $U_\mathrm{g}(\boldsymbol{q})$ depend exclusively on the indirectly actuated states at position level $\boldsymbol{q}$ and the inertia of the actuators $\boldsymbol{B}$ is constant (see, [DT96] for a proof), i. e.,

$$\begin{bmatrix} \boldsymbol{B} & \boldsymbol{S}(\boldsymbol{q}) \\ \boldsymbol{S}(\boldsymbol{q})^T & \boldsymbol{M}(\boldsymbol{q}) \end{bmatrix} \begin{pmatrix} \ddot{\boldsymbol{\theta}} \\ \ddot{\boldsymbol{q}} \end{pmatrix} + \bar{\boldsymbol{C}}(\boldsymbol{q}, \dot{\boldsymbol{q}})\dot{\boldsymbol{z}} + \begin{pmatrix} \boldsymbol{0} \\ \frac{\partial U_\mathrm{g}}{\partial \boldsymbol{q}}^T \end{pmatrix} + \frac{\partial U_\mathrm{e}}{\partial \boldsymbol{z}}^T = \begin{pmatrix} \boldsymbol{u} \\ \boldsymbol{\tau}_\mathrm{ext} \end{pmatrix} - \boldsymbol{d}(\boldsymbol{z}, \dot{\boldsymbol{z}}) . \tag{3.25}$$

Since also the metric tensor $\bar{\boldsymbol{M}}(\boldsymbol{q})$ defines a Riemannian connection according to Definition 2.13, the Coriolis/centrifugal matrix $\bar{\boldsymbol{C}}(\boldsymbol{q}, \dot{\boldsymbol{q}})$ can be computed such that it depends solely on $\boldsymbol{q}$ and $\dot{\boldsymbol{q}}$.

Assumption 3.9. *The kinetic energy of the rotors of the actuators is dominated by the relative motion w. r. t. their parent links such that the part of the kinetic energy of the rotors corresponding to the motion of the parental links can be neglected.*

This assumption is valid in case of many robotic manipulators, where gear boxes with high transmission ratios reduce the angular velocity of the rotors of the actuators and in case, where the actuators are placed on non-moving or slowly-moving parts of the robot, e. g., in case of legged robots, where the links of the legs are actuated via motors in the trunk. According to Assumption 3.9, the model (3.25) reduces further to

$$\boldsymbol{B}\ddot{\boldsymbol{\theta}} + \frac{\partial U_{\mathrm{e}}}{\partial \boldsymbol{\theta}}^T + \boldsymbol{d}_{\theta}(\boldsymbol{z}, \dot{\boldsymbol{z}}) = \boldsymbol{u}\,, \tag{3.26}$$

$$\boldsymbol{M}(\boldsymbol{q})\ddot{\boldsymbol{q}} + \boldsymbol{C}(\boldsymbol{q}, \dot{\boldsymbol{q}})\dot{\boldsymbol{q}} + \frac{\partial U_{\mathrm{g}}}{\partial \boldsymbol{q}}^T + \frac{\partial U_{\mathrm{e}}}{\partial \boldsymbol{q}}^T + \boldsymbol{d}_{\mathrm{q}}(\boldsymbol{z}, \dot{\boldsymbol{z}}) = \boldsymbol{\tau}_{\mathrm{ext}}\,, \tag{3.27}$$

where the generalized dissipative force has been subdivided into

$$\begin{bmatrix} \boldsymbol{d}_{\theta}(\boldsymbol{z}, \dot{\boldsymbol{z}}) \\ \boldsymbol{d}_{\mathrm{q}}(\boldsymbol{z}, \dot{\boldsymbol{z}}) \end{bmatrix} := \boldsymbol{d}(\boldsymbol{z}, \dot{\boldsymbol{z}})\,. \tag{3.28}$$

If it is further assumed in (3.26) and (3.27) that

$$\boldsymbol{d}_{\theta} = \boldsymbol{d}_{\theta}(\boldsymbol{z}, \dot{\boldsymbol{\theta}})\,, \quad \dot{\boldsymbol{\theta}}^T \boldsymbol{d}_{\theta}(\boldsymbol{z}, \dot{\boldsymbol{\theta}}) > 0\,, \forall \dot{\boldsymbol{\theta}} \neq \boldsymbol{0}\,, \quad \boldsymbol{d}_{\theta}(\boldsymbol{z}, \dot{\boldsymbol{\theta}}) = \boldsymbol{0} \iff \dot{\boldsymbol{\theta}} = \boldsymbol{0}\,, \tag{3.29}$$

$$\boldsymbol{d}_{\mathrm{q}} = \boldsymbol{d}_{\mathrm{q}}(\boldsymbol{q}, \dot{\boldsymbol{q}})\,, \quad \dot{\boldsymbol{q}}^T \boldsymbol{d}_{\mathrm{q}}(\boldsymbol{q}, \dot{\boldsymbol{q}}) > 0\,, \forall \dot{\boldsymbol{q}} \neq \boldsymbol{0}\,, \quad \boldsymbol{d}_{\mathrm{q}}(\boldsymbol{q}, \dot{\boldsymbol{q}}) = \boldsymbol{0} \iff \dot{\boldsymbol{q}} = \boldsymbol{0}\,, \tag{3.30}$$

than the system (3.26) and (3.27) is further feedback linearizable by static state feedback while the general model (3.24) requires dynamic state feedback to achieve the same result [DT96].

Assumption 3.9 and 3.8 are particularly important for damping injection into the indirectly actuated state dynamics via generalized actuator force input presented in Sect. 3.3.3.

3.2. Actuator position control

Due to losses in the conversion from electrical to mechanical power at a required generalized force and velocity level[3] which are reflected in the dynamic model by a term of the form (3.29), the most efficient way to move the indirectly actuated inertial degrees of freedom of the general mechanical system (3.24) is to move the actuators as few as possible. This motion can be controlled directly by controlling the configuration coordinates of the actuators, i. e., by driving the actual to the desired positions $\boldsymbol{\theta} \to \boldsymbol{\theta}_{\mathrm{des}}$. It is worth mentioning that by controlling the generalized force acting on the indirectly actuated inertial degrees of freedom, i. e., $\partial U_{\mathrm{e}}/\partial \boldsymbol{q}$, it is not transparent how much the actuators move and how much losses are produced. A further advantage of actuator position control is given by the property that under certain controller-gain assumptions, the singular-perturbed, controlled actuator dynamics [KKO86] can be neglected.

In the following, the problem of driving the actual actuator configuration $\boldsymbol{\theta}$ of the system (3.24) implying Assumptions 3.5 and 3.6 to a desired configuration $\boldsymbol{\theta}_{\mathrm{des}}$ is considered. This can be achieved by a PD control of the form

$$\boldsymbol{u} = -\boldsymbol{K}_{\mathrm{P}}\tilde{\boldsymbol{\theta}} - \boldsymbol{K}_{\mathrm{D}}\dot{\boldsymbol{\theta}}\,, \tag{3.31}$$

[3] Note that the losses are especially high, when gear-boxes with high transmission ratios are present.

where $\tilde{\boldsymbol{\theta}} := \boldsymbol{\theta} - \boldsymbol{\theta}_{\mathrm{des}}$ is defined as the control error and $\boldsymbol{K}_{\mathrm{P}}, \boldsymbol{K}_{\mathrm{D}}$ are symmetric and positive definite $n \times n$ controller gain matrices. Note that the control (3.31) requires no model-knowledge of potential forces of the plant. The resulting closed-loop dynamics takes the form

$$\bar{\boldsymbol{M}}(\boldsymbol{z})\ddot{\boldsymbol{z}} + \bar{\boldsymbol{C}}(\boldsymbol{z}, \dot{\boldsymbol{z}})\dot{\boldsymbol{z}} + \begin{bmatrix} \boldsymbol{K}_{\mathrm{D}}\dot{\boldsymbol{\theta}} + \boldsymbol{K}_{\mathrm{P}}\tilde{\boldsymbol{\theta}} + \boldsymbol{f}_{\theta}(\boldsymbol{\theta}, \boldsymbol{q}) \\ \boldsymbol{f}_{\mathrm{q}}(\boldsymbol{\theta}, \boldsymbol{q}) \end{bmatrix} = \begin{bmatrix} \boldsymbol{0} \\ \boldsymbol{\tau}_{\mathrm{ext}} \end{bmatrix} - \boldsymbol{d}(\boldsymbol{z}, \dot{\boldsymbol{z}}) \,, \tag{3.32}$$

where

$$\boldsymbol{f}_{\theta}(\boldsymbol{\theta}, \boldsymbol{q}) = \frac{\partial U(\boldsymbol{\theta}, \boldsymbol{q})}{\partial \boldsymbol{\theta}}^{T} \,, \tag{3.33}$$

$$\boldsymbol{f}_{\mathrm{q}}(\boldsymbol{\theta}, \boldsymbol{q}) = \frac{\partial U(\boldsymbol{\theta}, \boldsymbol{q})}{\partial \boldsymbol{q}}^{T} \,. \tag{3.34}$$

3.2.1. Equilibrium condition

In case of free motion, i. e., $\boldsymbol{\tau}_{\mathrm{ext}} = \boldsymbol{0}$, the static equilibrium conditions $\dot{\boldsymbol{z}} = \boldsymbol{0}$ of the closed-loop dynamics (3.32) become

$$\boldsymbol{K}_{\mathrm{P}}\tilde{\boldsymbol{\theta}} + \boldsymbol{f}_{\theta}(\boldsymbol{\theta}, \boldsymbol{q}) = \boldsymbol{0} \,, \tag{3.35}$$

$$\boldsymbol{f}_{\mathrm{q}}(\boldsymbol{\theta}, \boldsymbol{q}) = \boldsymbol{0} \,. \tag{3.36}$$

The equations (3.35) and (3.36) have exactly one solution $\boldsymbol{z}_{\star} = (\boldsymbol{\theta}_{\star}, \boldsymbol{q}_{\star})$, where $\boldsymbol{q}_{\star} = \bar{\boldsymbol{q}}(\boldsymbol{\theta}_{\star})$ according to Definition 3.4, if the potential

$$U_{\mathrm{P}}(\boldsymbol{z}) = U(\boldsymbol{\theta}, \boldsymbol{q}) + \frac{1}{2}\tilde{\boldsymbol{\theta}}^{T}\boldsymbol{K}_{\mathrm{P}}\tilde{\boldsymbol{\theta}} \tag{3.37}$$

is a strictly convex function defined on $\mathbb{R}^{2n}$. Strict convexity of U_{P} can be shown by showing that the Hessian of the potential

$$\boldsymbol{H}_{\mathrm{P}}(\boldsymbol{z}) := \frac{\partial^2 U_{\mathrm{P}}}{\partial \boldsymbol{z}^2} = \begin{bmatrix} \frac{\partial^2 U}{\partial \boldsymbol{\theta}^2} + \boldsymbol{K}_{\mathrm{P}} & \frac{\partial^2 U}{\partial \boldsymbol{q}\partial \boldsymbol{\theta}} \\ \frac{\partial^2 U}{\partial \boldsymbol{q}\partial \boldsymbol{\theta}} & \frac{\partial^2 U}{\partial \boldsymbol{q}^2} \end{bmatrix} \tag{3.38}$$

is positive definite. This in turn leads to a lower bound on the controller gain matrix

$$\boldsymbol{K}_{\mathrm{P}} + \frac{\partial^2 U}{\partial \boldsymbol{\theta}^2} \succ \frac{\partial^2 U}{\partial \boldsymbol{q}\partial \boldsymbol{\theta}} \left(\frac{\partial^2 U}{\partial \boldsymbol{q}^2} \right)^{-1} \frac{\partial^2 U}{\partial \boldsymbol{q}\partial \boldsymbol{\theta}}^{T} \,, \tag{3.39}$$

where by the relational operator in the above equation it is meant that

$$\lambda_{\min}\left(\boldsymbol{K}_{\mathrm{P}} + \frac{\partial^2 U}{\partial \boldsymbol{\theta}^2} \right) > \lambda_{\max}\left(\frac{\partial^2 U}{\partial \boldsymbol{q}\partial \boldsymbol{\theta}} \left(\frac{\partial^2 U}{\partial \boldsymbol{q}^2} \right)^{-1} \frac{\partial^2 U}{\partial \boldsymbol{q}\partial \boldsymbol{\theta}}^{T} \right) \,, \quad \forall \boldsymbol{z} \in \mathbb{R}^{2n} \,. \tag{3.40}$$

According to Assumptions 3.5, 3.6 and 3.7 the condition on $\boldsymbol{K}_{\mathrm{P}}$, (3.40) can be expressed as

$$\lambda_{\min}\left(\boldsymbol{K}_{\mathrm{P}} + \frac{\partial^2 U}{\partial \boldsymbol{\theta}^2} \right) > c_{10}^2 / c_7 \tag{3.41}$$

or more precisely if $\partial^2 U / \partial \boldsymbol{\theta}^2$ is a definite matrix the condition (3.40) can be expressed as

$$\lambda_{\min}\left(\boldsymbol{K}_{\mathrm{P}} \right) > c_{10}^2 / c_7 - c_{11} \,. \tag{3.42}$$

This result can be summarized as follows.

Proposition 3.2. *The closed-loop system* (3.32) *has an unique equilibrium point* $\boldsymbol{z} = \boldsymbol{z}_\star$ *and* $\dot{\boldsymbol{z}} = \boldsymbol{0}$*, if the controller gain matrix* $\boldsymbol{K}_\mathrm{P}$ *satisfies condition* (3.42)*.*

Proof. A sketch of a proof is given above. □

Remark 3.4. *It can be easily verified from* (3.35) *that in the limit case*

$$\lim_{\lambda_{\min}(\boldsymbol{K}_\mathrm{P})\to\infty} \boldsymbol{\theta}_\star = \boldsymbol{\theta}_\mathrm{des}\,. \tag{3.43}$$

Due to changing static equilibrium conditions, e. g., discontinuously changing contact situations appearing in legged systems, the assumption of the limit case mentioned in Remark 3.4 is practically the most relevant case.

3.2.2. Stability

Stability of the closed-loop dynamics (3.32) can be deduced based in a simpler Lyapunov function as in the case of the actuator position PD controls including gravity compensation based on desired values as proposed by [Tom91].

Proposition 3.3. *The equilibrium point* $\{\boldsymbol{z} = \boldsymbol{z}_\star, \dot{\boldsymbol{z}} = \boldsymbol{0}\}$ *of the closed-loop dynamics* (3.32)*, where* $\boldsymbol{K}_\mathrm{P}$ *is chosen according to condition* (3.42) *and* $\boldsymbol{\tau}_\mathrm{ext} = \boldsymbol{0}$*, is globally asymptotically stable in a sense of Lyapunov.*

Proof. Consider a Lyapunov function candidate

$$V(\boldsymbol{z}, \dot{\boldsymbol{z}}) = T(\boldsymbol{z}, \dot{\boldsymbol{z}}) + V_\mathrm{P}(\boldsymbol{z})\,, \tag{3.44}$$

comprising the kinetic energy $T(\boldsymbol{z}, \dot{\boldsymbol{z}}) = \frac{1}{2}\dot{\boldsymbol{z}}^T \bar{\boldsymbol{M}}(\boldsymbol{z})\dot{\boldsymbol{z}}$ of the open-loop system (3.24) and the potential energy of the closed-loop dynamics (3.32)

$$V_\mathrm{P}(\boldsymbol{z}) = U_\mathrm{P}(\boldsymbol{z}) - U_\mathrm{P}(\boldsymbol{z}_\star)\,. \tag{3.45}$$

Herein, $U_\mathrm{P}(\boldsymbol{z})$ is a potential function given by (3.37) which is strictly convex since $\boldsymbol{K}_\mathrm{P}$ is chosen according to condition (3.42). The additional constant term $U_\mathrm{P}(\boldsymbol{z}_\star)$ in (3.45) has the value of the potential function at the minimum $\boldsymbol{z}_\star$ of $U_\mathrm{P}(\boldsymbol{z})$ such that $V_\mathrm{P}(\boldsymbol{z})$ is positive definite in $\boldsymbol{z}$. Since the kinetic energy $T(\boldsymbol{z}, \dot{\boldsymbol{z}})$ is positive definite in $\dot{\boldsymbol{z}}$, the sum, $V(\boldsymbol{z}, \dot{\boldsymbol{z}}) = T(\boldsymbol{z}, \dot{\boldsymbol{z}}) + V_\mathrm{P}(\boldsymbol{z})$, considered as Lyapunov function candidate (cf. (3.44)) is positive definite in the system states $(\boldsymbol{z}, \dot{\boldsymbol{z}})$. In order to show that $V(\boldsymbol{z}, \dot{\boldsymbol{z}})$ is a Lyapunov function, its derivative along the solution of (3.32) has to be shown to be at least negative semi-definite. This can be done by direct calculations

$$\begin{aligned}
\dot{V}(\boldsymbol{z}, \dot{\boldsymbol{z}}) &= \dot{\boldsymbol{z}}^T \bar{\boldsymbol{M}}(\boldsymbol{z})\ddot{\boldsymbol{z}} + \frac{1}{2}\dot{\boldsymbol{z}}^T \dot{\bar{\boldsymbol{M}}}(\boldsymbol{z})\dot{\boldsymbol{z}} + \dot{\boldsymbol{z}}^T \frac{\partial U(\boldsymbol{z})}{\partial \boldsymbol{z}}^T + \dot{\boldsymbol{\theta}}^T \boldsymbol{K}_\mathrm{P}\tilde{\boldsymbol{\theta}} \\
&= \dot{\boldsymbol{z}}^T \left[-\bar{\boldsymbol{C}}(\boldsymbol{z}, \dot{\boldsymbol{z}}) + \frac{1}{2}\dot{\bar{\boldsymbol{M}}}(\boldsymbol{z})\right] \dot{\boldsymbol{z}} - \dot{\boldsymbol{\theta}}^T \boldsymbol{K}_\mathrm{D}\dot{\boldsymbol{\theta}} - \dot{\boldsymbol{z}}^T \boldsymbol{d}(\boldsymbol{z}, \dot{\boldsymbol{z}}) \\
&= -\dot{\boldsymbol{\theta}}^T \boldsymbol{K}_\mathrm{D}\dot{\boldsymbol{\theta}} - \dot{\boldsymbol{z}}^T \boldsymbol{d}(\boldsymbol{z}, \dot{\boldsymbol{z}}) \leq 0\,,
\end{aligned} \tag{3.46}$$

where in the last step Corollary 3.1 has been used. Note that $\dot{V}(\boldsymbol{z}, \dot{\boldsymbol{z}})$ is non-positive due to Assumption 3.1. As a result, the equilibrium point $\{\boldsymbol{z} = \boldsymbol{z}_\star, \dot{\boldsymbol{z}} = \boldsymbol{0}\}$ is stable in a sense of Lyapunov [SL91, Theorem 3.2, p. 62].

This result can be extended to the case of asymptotic stability: By hypothesis of Assumption 3.1, $-\dot{\boldsymbol{\theta}}^T \boldsymbol{K}_\mathrm{D} \dot{\boldsymbol{\theta}} - \dot{\boldsymbol{z}}^T \boldsymbol{d}(\boldsymbol{z}, \dot{\boldsymbol{z}}) = 0$ only if $\dot{\boldsymbol{z}} = \boldsymbol{0}$. But $\dot{\boldsymbol{z}} = \boldsymbol{0}$ implies that

$$\ddot{\boldsymbol{z}} = -\bar{\boldsymbol{M}}(\boldsymbol{z})^{-1} \begin{bmatrix} \boldsymbol{K}_\mathrm{P} \tilde{\boldsymbol{\theta}} + \boldsymbol{f}_\theta(\boldsymbol{\theta}, \boldsymbol{q}) \\ \boldsymbol{f}_\mathrm{q}(\boldsymbol{\theta}, \boldsymbol{q}) \end{bmatrix}$$

which is non-zero as long as $\boldsymbol{z} \neq \boldsymbol{z}_\star$ according to Proposition 3.2. The system cannot remain in the set $\mathcal{R} = \{\boldsymbol{z}, \dot{\boldsymbol{z}} \in \mathbb{R}^{2n} \,|\, \dot{\boldsymbol{z}} = \boldsymbol{0}\}$ except at the equilibrium point $\{\boldsymbol{z} = \boldsymbol{z}_\star, \dot{\boldsymbol{z}} = \boldsymbol{0}\}$ since the largest invariant set in $\mathcal{R}$ is the equilibrium point $\{\boldsymbol{z} = \boldsymbol{z}_\star, \dot{\boldsymbol{z}} = \boldsymbol{0}\}$ itself. Therefore, the system is locally asymptotically stable according to La Salle's invariance principle [SL91, Theorem 3.4, p. 69].

Furthermore, the potential energy $U_\mathrm{P}(\boldsymbol{z})$ is a strictly convex function in $\boldsymbol{z}$ (due to Assumption 3.5, 3.6, and Proposition 3.2) and the kinetic energy $T(\boldsymbol{z}, \dot{\boldsymbol{z}})$ is a strictly convex function in $\dot{\boldsymbol{z}}$. Thus, the sum $V(\boldsymbol{z}, \dot{\boldsymbol{z}})$ is strictly convex in $\boldsymbol{z}$ and $\dot{\boldsymbol{z}}$. Since this result holds globally, $V(\boldsymbol{z}, \dot{\boldsymbol{z}})$ is radially unbounded, i. e., $V(\boldsymbol{z}, \dot{\boldsymbol{z}}) \to \infty$ if $\|\boldsymbol{z}\| \to \infty$ or $\|\dot{\boldsymbol{z}}\| \to \infty$ and the above argumentation holds globally (cf. [SL91, Theorem 3.5, p. 73]). Therefore, in case of free motion, i. e., $\boldsymbol{\tau}_\mathrm{ext} = \boldsymbol{0}$, the equilibrium point $\{\boldsymbol{z} = \boldsymbol{z}_\star, \dot{\boldsymbol{z}} = \boldsymbol{0}\}$ of the system (3.32) is globally asymptotically stable. □

Remark 3.5 (Robustness)**.** *Besides the lower-bound on the gain matrix $\boldsymbol{K}_\mathrm{P}$, the controller* (3.31) *requires no model parameter knowledge of the plant. In particular, $\boldsymbol{K}_\mathrm{P}$ can be chosen a priori conservatively high enough such that any static and dynamic model errors can be completely avoided in the feedback loop. Thus, the simple control approach* (3.31) *is the most robust solution for the class of statically controllable under-actuated Euler-Lagrange systems described by* (3.24)*.*

3.2.3. Singular perturbed reduced closed-loop system

An additional implication of the high-gain control (3.31) which allows to consider a reduced order closed-loop dynamics equations of (3.32) can be deduced from the singular perturbation theory [KKO86]. This is an approximate method applicable for systems which have a so-called two-times-scales property. Thereby, the basic idea is to split up the dynamics in two coupled subsystems comprising a fast and a slow part. Under certain assumptions (see, e. g., so-called Tychonov's theorem [Kha02]), the dynamics of the fast subsystem can be neglected. A comprehensive description of the method is out of the scope of this thesis. However, the proposed fundamental control concept is based on the singular perturbed reduced dynamics of (3.32), therefore in the following, the idea is briefly sketched.

For the simplicity of notation consider the reduced model (3.26), (3.27) under the actuator position PD control (3.31),

$$\boldsymbol{B}\ddot{\boldsymbol{\theta}} + \boldsymbol{K}_\mathrm{D}\dot{\boldsymbol{\theta}} + \boldsymbol{K}_\mathrm{P}\tilde{\boldsymbol{\theta}} + \boldsymbol{f}_\theta(\boldsymbol{\theta}, \boldsymbol{q}) + \boldsymbol{d}_\theta(\boldsymbol{z}, \dot{\boldsymbol{z}}) = \boldsymbol{0} \tag{3.47}$$

$$\boldsymbol{M}(\boldsymbol{q})\ddot{\boldsymbol{q}} + \boldsymbol{C}(\boldsymbol{q}, \dot{\boldsymbol{q}})\dot{\boldsymbol{q}} + \boldsymbol{f}_\mathrm{q}(\boldsymbol{\theta}, \boldsymbol{q}) + \boldsymbol{d}_\mathrm{q}(\boldsymbol{z}, \dot{\boldsymbol{z}}) = \boldsymbol{\tau}_\mathrm{ext}\,. \tag{3.48}$$

By introducing $\boldsymbol{K}_\mathrm{P} = \boldsymbol{K}_\epsilon/\epsilon$, the actuator dynamics (3.47) can be brought to the singular perturbation form

$$\epsilon\ddot{\boldsymbol{\theta}} + \epsilon\boldsymbol{B}^{-1}\left[\boldsymbol{K}_\mathrm{D}\dot{\boldsymbol{\theta}} + \boldsymbol{f}_\theta(\boldsymbol{\theta}, \boldsymbol{q}) + \boldsymbol{d}_\theta(\boldsymbol{z}, \dot{\boldsymbol{z}})\right] = -\boldsymbol{B}^{-1}\boldsymbol{K}_\epsilon\tilde{\boldsymbol{\theta}}\,, \tag{3.49}$$

which in the limit case $\epsilon \to 0$ results in $\boldsymbol{B}^{-1}\boldsymbol{K}_\epsilon\tilde{\boldsymbol{\theta}} \approx \boldsymbol{0}$, i. e., $\boldsymbol{\theta} \approx \boldsymbol{\theta}_\mathrm{des}$. Thus, the dynamics (3.47), (3.48) reduces approximately to

$$\boldsymbol{M}(\boldsymbol{q})\ddot{\boldsymbol{q}} + \boldsymbol{C}(\boldsymbol{q}, \dot{\boldsymbol{q}})\dot{\boldsymbol{q}} + \boldsymbol{f}_\mathrm{q}(\boldsymbol{\theta}_\mathrm{des}, \boldsymbol{q}) + \boldsymbol{d}_\mathrm{q}(\boldsymbol{q}, \boldsymbol{\theta}_\mathrm{des}, \dot{\boldsymbol{q}}) = \boldsymbol{\tau}_\mathrm{ext}\,. \tag{3.50}$$

Note that an analogous singular perturbation reduction can also be performed for the more general closed-loop dynamics (3.32).

3.3. Damping injection into the indirectly actuated state dynamics

Compliantly actuated mechanical systems are generally designed such that friction and damping effects acting in parallel to the springs connecting actuators and links are as small as possible. The reason for this design criterion is the concept to couple the actuators and the links mainly via elasticities. This energy transmission path would become inefficient if it is subjected to non-negligible dissipative losses. In particular, elastic transmissions with low friction and damping properties often display a weakly damped behavior seen from the indirectly actuated coordinates, since, e. g., in robotic systems the bearing of the spring mechanisms can often not be strictly separated from the bearing of the connected links. Therefore, low damping in the elastic transmission results often in low damping of the indirectly actuated states dynamics. However, as will be discussed later in Sect. 5.3.3, control approaches which mainly exploit the natural system dynamics require a certain amount of damping (in the indirectly actuated state dynamics) to regulate model uncertainties and external disturbances (see, the author's previous work [LPAS14]). Thus a method is required to exclusively inject damping w. r. t. to the indirectly actuated states[4] by control.

Several control methods to achieve a desired dynamics of the indirectly actuated state variables for compliantly actuated mechanical systems have been considered so far. Solutions based on the feedback of only directly actuated variables (i. e., states of the actuator dynamics) have been introduced in [Tom91], [OKL95], [ZDLS04], and [OASK$^+$04] for flexible joint robots[5] and have been further extended to the case of nonlinear elasticities in [ASOP12]. Since these control methods consider only variables in the feedback which are collocated with the control input, they perform very robustly against model uncertainties, but in turn have limitations in the convergence properties of the indirectly actuated states. A further class of controllers which aim at improved convergence properties of the indirectly actuated states utilize a full-state feedback as it has been introduced for constant joint stiffness in [ASH01] and extended to the case of nonlinear elasticities in [PAS11]. Another related approach which addresses the gain scheduling design of full-state feedback control in VSA has been reported in [SMCT$^+$13]. As the methods in [ASH01], [PAS11], [SMCT$^+$13] suggest only a design of the state feedback gains, the approach does not rely on the knowledge of an accurate dynamics model. However, while the approach of [ASH01] is supported by a stability statement, in [PAS11] and [SMCT$^+$13], a stability analysis is not provided. This is as the stability statement in [ASH01] relies on the assumption of constant stiffness. As such, the theory cannot be straightforwardly generalized to the case of nonlinear elastic transmissions as appearing in variable stiffness mechanisms [VASB$^+$13].

Further methods to achieve desired dynamics of the indirectly actuated states for the under-actuated mechanical system are based on cascaded structures [OASKH03], integrator backstepping [OL99], [Ott08, Chap. 6.2], extensions of the well known Slotine and Li

[4] Note that actuator side damping can be implemented directly via the control input which is also used for the actuator PD control (3.31). Also note that damping acting between the indirectly and directly actuated states is not desired since it counteracts the efficiency of the elastic energy transmission.

[5] The terminology of *flexible joint robots* refers in literature to robots with serial, linear springs in the power train.

controller [SW88] to the flexible joint case [Spo89], and feedback linearization [DLL98], [PMDL08], [DLF10]. A comprehensive overview of the first three methods are given in [BOL95]. To achieve the desired dynamics of the indirectly actuated states, these methods substantially change the original dynamics of the plant. The approach introduced in [OASKH03] first decouples the dynamics of the generalized elastic forces from the dynamics of the indirectly actuated states and then implements a desired behavior of the indirectly actuated states via a tracking controller for the generalized elastic force acting on the indirectly actuated inertial degrees of freedom. The approaches of [OL99] and [Ott08, Chap. 6.2] apply the constructive design method of integrator backstepping to the case of flexible joint robots. Assuming the knowledge of a complete model of the plant, the methods in [OASKH03], [OL99], and [Ott08, Chap. 6.2] are theoretically well-founded, since they are accompanied by a comprehensive stability analysis. Additionally, they can be straightforwardly generalized to the case of nonlinear elasticities. However, the knowledge of a complete model of the plant is a strong assumption from a point of view of controller robustness. This becomes evident if structural changes of the original plant dynamics are performed based upon the knowledge of a complete model of the plant.

The methods proposed in the following, achieve an additional damping term in the indirectly actuated state dynamics, while preserving the structure of the kinetic and potential energy of the plant. First, the desired indirectly actuated state dynamics including the additional generalized damping force is formulated in terms of the reduced model (3.27). Then, on the basis of the singular perturbation assumption of Section 3.2.3, a simple method is presented, which requires only model-knowledge of the elastic potential of the plant to achieve the desired additional damping term. Finally, the control input which implements the desired damping via the actuator dynamics (3.26) is introduced. This approach preserves the structure of the original plant dynamics (3.26), (3.27), except for the desired damping term [KLOAS16]. Therefore, the solution to eliminate the steady-state control error under the influence of gravity [ASOP12] can be directly adopted. Both control approaches are accompanied with a stability proof.

3.3.1. Problem statement

Consider the dynamics of the indirectly actuated coordinates (3.27) under the assumption (3.30),

$$\boldsymbol{M}(\boldsymbol{q})\ddot{\boldsymbol{q}} + \boldsymbol{C}(\boldsymbol{q},\dot{\boldsymbol{q}})\dot{\boldsymbol{q}} + \boldsymbol{d}_{\mathrm{q}}(\boldsymbol{q},\dot{\boldsymbol{q}}) + \boldsymbol{f}_{\mathrm{q}}(\boldsymbol{\theta},\boldsymbol{q}) = \boldsymbol{\tau}_{\mathrm{ext}}\,. \tag{3.51}$$

The goal is to achieve an additional damping term

$$\boldsymbol{d}_{\mathrm{q,inj}} = \boldsymbol{d}_{\mathrm{q,inj}}(\boldsymbol{q},\dot{\boldsymbol{q}})\,, \quad \dot{\boldsymbol{q}}^T\boldsymbol{d}_{\mathrm{q,inj}}(\boldsymbol{q},\dot{\boldsymbol{q}}) > 0\,, \forall \dot{\boldsymbol{q}} \neq \boldsymbol{0}\,, \quad \boldsymbol{d}_{\mathrm{q,inj}}(\boldsymbol{q},\dot{\boldsymbol{q}}) = \boldsymbol{0} \iff \dot{\boldsymbol{q}} = \boldsymbol{0}\,, \tag{3.52}$$

such that the indirectly actuated state dynamics takes the form

$$\boldsymbol{M}(\boldsymbol{q})\ddot{\boldsymbol{q}} + \boldsymbol{C}(\boldsymbol{q},\dot{\boldsymbol{q}})\dot{\boldsymbol{q}} + \boldsymbol{d}_{\mathrm{q}}(\boldsymbol{q},\dot{\boldsymbol{q}}) + \boldsymbol{f}_{\mathrm{q}}(\boldsymbol{\eta},\boldsymbol{q}) + \boldsymbol{d}_{\mathrm{q,inj}}(\boldsymbol{q},\dot{\boldsymbol{q}}) = \boldsymbol{\tau}_{\mathrm{ext}}\,. \tag{3.53}$$

A comparison of (3.51) and (3.53) reveals that the family of mappings $\boldsymbol{\eta}_{\boldsymbol{q},\dot{\boldsymbol{q}}}(\boldsymbol{\theta}) : \mathbb{R}^n \times \mathbb{R}^n$, as implicitly defined by

$$\boldsymbol{f}_{\mathrm{q}}(\boldsymbol{\theta},\boldsymbol{q}) = \boldsymbol{f}_{\mathrm{q}}(\boldsymbol{\eta},\boldsymbol{q}) + \boldsymbol{d}_{\mathrm{q,inj}}(\boldsymbol{q},\dot{\boldsymbol{q}})\,, \tag{3.54}$$

implement the additional damping term (3.52). As a result of Assumption 3.6, for any $\boldsymbol{q},\dot{\boldsymbol{q}} \in \mathbb{R}^n$, (3.54) can be uniquely solved either for $\boldsymbol{\eta}$ or for $\boldsymbol{\theta}$.

Proposition 3.4. *The family of mappings* $\boldsymbol{\eta}_{\boldsymbol{q},\dot{\boldsymbol{q}}}(\boldsymbol{\theta}) : \mathbb{R}^n \to \mathbb{R}^n$ *defined by* (3.54) *under Assumption 3.6, where the constants* $\boldsymbol{q}, \dot{\boldsymbol{q}} \in \mathbb{R}^n$ *parametrize the mappings, represent global diffeomorphisms.*

Proof. In order to show that for any constant $\boldsymbol{q}, \dot{\boldsymbol{q}} \in \mathbb{R}^n$, $\boldsymbol{\eta}_{\boldsymbol{q},\dot{\boldsymbol{q}}}(\boldsymbol{\theta}) : \mathbb{R}^n \to \mathbb{R}^n$ is a diffeomorphism, the Jacobian $\partial\boldsymbol{\eta}(\boldsymbol{\theta})/\partial\boldsymbol{\theta}$ needs to be shown to be always nonsingular, i. e., it has to be shown that

$$\sup_{\boldsymbol{\theta}\in\mathbb{R}^n} \left\| \left(\frac{\partial \boldsymbol{\eta}_{\boldsymbol{q},\dot{\boldsymbol{q}}}(\boldsymbol{\theta})}{\partial \boldsymbol{\theta}} \right)^{-1} \right\| < \infty \,, \tag{3.55}$$

keeps bounded[6] from above [Zei86, Corollary 4.41, p. 174]. By differentiating condition (3.54) w. r. t. $\boldsymbol{\theta}$ (taking into account that $\boldsymbol{\eta} = \boldsymbol{\eta}_{\boldsymbol{q},\dot{\boldsymbol{q}}}(\boldsymbol{\theta})$) it can be seen that the Jacobian matrix of the mappings $\boldsymbol{\eta}_{\boldsymbol{q},\dot{\boldsymbol{q}}}(\boldsymbol{\theta})$ take the form

$$\boldsymbol{J}_\eta(\boldsymbol{\theta}) := \frac{\partial \boldsymbol{\eta}_{\boldsymbol{q},\dot{\boldsymbol{q}}}(\boldsymbol{\theta})}{\partial \boldsymbol{\theta}} = \left(\frac{\partial^2 U(\boldsymbol{\theta},\boldsymbol{q})}{\partial \boldsymbol{\theta}\partial \boldsymbol{q}}\bigg|_{\boldsymbol{\theta}=\boldsymbol{\eta}} \right)^{-1} \frac{\partial^2 U(\boldsymbol{\theta},\boldsymbol{q})}{\partial \boldsymbol{\theta}\partial \boldsymbol{q}} \,. \tag{3.56}$$

The inverse of this Jacobian matrix

$$\left\| \boldsymbol{J}_\eta(\boldsymbol{\theta})^{-1} \right\| \leq \left\| \left(\frac{\partial^2 U(\boldsymbol{\theta},\boldsymbol{q})}{\partial \boldsymbol{q}\partial \boldsymbol{\theta}} \right)^{-1} \right\| \left\| \frac{\partial^2 U(\boldsymbol{\theta},\boldsymbol{q})}{\partial \boldsymbol{q}\partial \boldsymbol{\theta}}\bigg|_{\boldsymbol{\theta}=\boldsymbol{\eta}} \right\| \leq c_{10}/c_9 \,, \tag{3.57}$$

keeps bounded due to Assumptions 3.6. □

Remark 3.6. *In the following, the family of mappings* $\boldsymbol{\eta}_{\boldsymbol{q},\dot{\boldsymbol{q}}}(\boldsymbol{\theta})$ *will be denoted as* $\boldsymbol{\eta}(\boldsymbol{\theta},\boldsymbol{q},\dot{\boldsymbol{q}})$ *while keeping in mind that for any constant* $\boldsymbol{q}, \dot{\boldsymbol{q}} \in \mathbb{R}^n$*, there is a bijective relation between* $\boldsymbol{\theta}$ *and* $\boldsymbol{\eta}$*.*

Remark 3.7. *The above proof can be straightforwardly extended to the case where the injected damping term* $\boldsymbol{d}_{\mathrm{q,inj}} = \boldsymbol{d}_{\mathrm{q,inj}}(\boldsymbol{\theta},\boldsymbol{q},\dot{\boldsymbol{q}})$ *depends also on the actuator positions* $\boldsymbol{\theta}$*. This would lead to boundedness conditions on the partial derivatives* $\partial\boldsymbol{d}_{\mathrm{q,inj}}/\partial\boldsymbol{\theta}$*. Such a dependency occurs in case of nonlinear, spring load or stiffness*[7] *dependent damping.*

Due to the change of coordinate defined by (3.54), the problem of damping injection into the indirectly actuated state dynamics can be solved by regulating $(\boldsymbol{\eta},\boldsymbol{q})$ instead of $(\boldsymbol{\theta},\boldsymbol{q})$. Thereby, the structure of the plant potential U is preserved. This agrees with the basic idea to change the natural dynamics of the plant only to a minimum extend by control.

3.3.2. Implementation via actuator position input

Consider the actuator position PD controlled dynamics (3.50) under the assumption (3.30) where the two time-scales property of Section 3.2.3 holds, i. e.,

$$\boldsymbol{M}(\boldsymbol{q})\ddot{\boldsymbol{q}} + \boldsymbol{C}(\boldsymbol{q},\dot{\boldsymbol{q}})\dot{\boldsymbol{q}} + \boldsymbol{f}_{\mathrm{q}}(\boldsymbol{\theta}_{\mathrm{des}},\boldsymbol{q}) + \boldsymbol{d}_{\mathrm{q}}(\boldsymbol{q},\dot{\boldsymbol{q}}) = \boldsymbol{\tau}_{\mathrm{ext}} \,. \tag{3.58}$$

[6] The matrix norm $\|\cdot\|$ is assumed to be the induced Euclidean norm.

[7] The dependency on $\boldsymbol{\theta}$ due to the stiffness occurs only if the intrinsic stiffness properties are such that they also depend on $\boldsymbol{\theta}$.

The control input of the above system is the actuator position $\boldsymbol{\theta}_{\mathrm{des}}$. It can be easily verified that the input transformation

$$\boldsymbol{\theta}_{\mathrm{des}} = \boldsymbol{g}_{\mathrm{q}}(\boldsymbol{f}_{\mathrm{q}}(\boldsymbol{\eta}_{\mathrm{des}}, \boldsymbol{q}) + \boldsymbol{d}_{\mathrm{q,inj}}(\boldsymbol{q}, \dot{\boldsymbol{q}}), \boldsymbol{q})\,, \tag{3.59}$$

leads to the desired closed-loop dynamics

$$\boldsymbol{M}(\boldsymbol{q})\ddot{\boldsymbol{q}} + \boldsymbol{C}(\boldsymbol{q}, \dot{\boldsymbol{q}})\dot{\boldsymbol{q}} + \boldsymbol{f}_{\mathrm{q}}(\boldsymbol{\eta}_{\mathrm{des}}, \boldsymbol{q}) + \boldsymbol{d}_{\mathrm{q}}(\boldsymbol{q}, \dot{\boldsymbol{q}}) + \boldsymbol{d}_{\mathrm{q,inj}}(\boldsymbol{q}, \dot{\boldsymbol{q}}) = \boldsymbol{\tau}_{\mathrm{ext}}\,. \tag{3.60}$$

Thereby, the inverse mapping $\boldsymbol{g}_{\mathrm{q}}(\boldsymbol{\tau}, \boldsymbol{q}) : \mathbb{R}^n \times \mathbb{R}^n \to \mathbb{R}^n$ in (3.59) is defined such that $\boldsymbol{\theta} = \boldsymbol{g}_{\mathrm{q}}(\boldsymbol{\tau}, \boldsymbol{q})$, if and only if $\boldsymbol{\tau} = \boldsymbol{f}_{\mathrm{q}}(\boldsymbol{\theta}, \boldsymbol{q})$. Note that Proposition 3.4 provides a sufficient condition for the global existence of the input transformation (3.59). Further note that by virtue of (3.52) it follows from (3.59) that if $\dot{\boldsymbol{q}} = \boldsymbol{0}$ or equivalently if $\boldsymbol{d}_{\mathrm{q,inj}} = \boldsymbol{0}$, $\boldsymbol{\eta}_{\mathrm{des}} = \boldsymbol{\theta}_{\mathrm{des}}$.

In case of free motion, i. e., $\boldsymbol{\tau}_{\mathrm{ext}} = \boldsymbol{0}$, the system (3.60) can be shown to be asymptotically stable for any constant actuator reference positions $\boldsymbol{\eta}_{\mathrm{des}} \in \mathbb{R}^n$. The problem of selecting $\boldsymbol{\eta}_{\mathrm{des}}$ such that a desired equilibrium configuration $\boldsymbol{q}_{\mathrm{des}}$ is achieved will be addressed in Sect. 3.3.3.

Proposition 3.5. *The equilibrium point* $\{\boldsymbol{q} = \bar{\boldsymbol{q}}(\boldsymbol{\eta}_{\mathrm{des}}), \dot{\boldsymbol{q}} = \boldsymbol{0}\}$ *of the system* (3.60)*, where* $\boldsymbol{\tau}_{\mathrm{ext}} = \boldsymbol{0}$*, is globally asymptotically stable.*

Proof. Consider a Lyapunov function candidate of the form

$$V(\boldsymbol{q}, \dot{\boldsymbol{q}}) = T(\boldsymbol{q}, \dot{\boldsymbol{q}}) + U(\boldsymbol{\eta}_{\mathrm{des}}, \boldsymbol{q}) - U(\boldsymbol{\eta}_{\mathrm{des}}, \bar{\boldsymbol{q}}(\boldsymbol{\eta}_{\mathrm{des}}))\,, \tag{3.61}$$

where for any constant $\boldsymbol{\eta}_{\mathrm{des}} \in \mathbb{R}^m$, $U(\boldsymbol{\eta}_{\mathrm{des}}, \boldsymbol{q})$ is minimal at $\boldsymbol{q} = \bar{\boldsymbol{q}}(\boldsymbol{\eta}_{\mathrm{des}})$ according to Definition 3.4 and Assumption 3.5. Since the kinetic energy $T(\boldsymbol{q}, \dot{\boldsymbol{q}}) = \frac{1}{2}\dot{\boldsymbol{q}}^T\boldsymbol{M}(\boldsymbol{q})\dot{\boldsymbol{q}}$ is positive definite in $\dot{\boldsymbol{q}}$ and $U(\boldsymbol{\eta}_{\mathrm{des}}, \boldsymbol{q}) - U(\boldsymbol{\eta}_{\mathrm{des}}, \bar{\boldsymbol{q}}(\boldsymbol{\eta}_{\mathrm{des}}))$ is positive definite in $\boldsymbol{q}$, $V(\boldsymbol{q}, \dot{\boldsymbol{q}})$ is positive definite in $(\boldsymbol{q}, \dot{\boldsymbol{q}})$. In order that $V(\boldsymbol{q}, \dot{\boldsymbol{q}})$ is a Lyapunov function, its derivative along the solution of (3.60) has to be at least negative semi-definite. The straight forward computation taking Corollary 3.1 into account yields

$$\dot{V}(\boldsymbol{q}, \dot{\boldsymbol{q}}) = \dot{\boldsymbol{q}}^T \left(\boldsymbol{d}_{\mathrm{q}}(\boldsymbol{q}, \dot{\boldsymbol{q}}) + \boldsymbol{d}_{\mathrm{q,inj}}(\boldsymbol{q}, \dot{\boldsymbol{q}})\right) \leq 0\,, \tag{3.62}$$

where the negative semi-definiteness can be concluded due to the assumptions on the dissipation terms (3.30) and (3.52). As a result the equilibrium point $\{\boldsymbol{q} = \bar{\boldsymbol{q}}(\boldsymbol{\eta}_{\mathrm{des}}), \dot{\boldsymbol{q}} = \boldsymbol{0}\}$ of the system (3.60) is stable in a sense of Lyapunov [SL91, Theorem 3.2, p. 62].

This result can be extended to the case of asymptotic stability: By hypothesis of the assumptions (3.30) and (3.52), $\dot{\boldsymbol{q}}^T \left(\boldsymbol{d}_{\mathrm{q}}(\boldsymbol{q}, \dot{\boldsymbol{q}}) + \boldsymbol{d}_{\mathrm{q,inj}}(\boldsymbol{q}, \dot{\boldsymbol{q}})\right) = 0$ only if $\dot{\boldsymbol{q}} = \boldsymbol{0}$. But $\dot{\boldsymbol{q}} = \boldsymbol{0}$ implies that $\ddot{\boldsymbol{q}} = -\boldsymbol{M}(\boldsymbol{q})^{-1}\boldsymbol{f}_{\mathrm{q}}(\boldsymbol{\eta}_{\mathrm{des}}, \boldsymbol{q})$ which is non-zero as long as $\boldsymbol{q} \neq \bar{\boldsymbol{q}}(\boldsymbol{\eta}_{\mathrm{des}})$. The system cannot remain in the set $\mathcal{R} = \{\boldsymbol{q}, \dot{\boldsymbol{q}} \in \mathbb{R}^m \mid \dot{\boldsymbol{q}} = \boldsymbol{0}\}$ except at the equilibrium point $\{\boldsymbol{q} = \bar{\boldsymbol{q}}(\boldsymbol{\eta}_{\mathrm{des}}), \dot{\boldsymbol{q}} = \boldsymbol{0}\}$ since the largest invariant set in $\mathcal{R}$ is the equilibrium point itself. Therefore, the system is locally asymptotically stable according to La Salle's invariance principle [SL91, Theorem 3.4, p. 69].

Furthermore, due to Assumption 3.5, $U(\boldsymbol{\eta}_{\mathrm{des}}, \boldsymbol{q})$ is a strictly convex function in $\boldsymbol{q}$ and the kinetic energy $T(\boldsymbol{q}, \dot{\boldsymbol{q}})$ is a strictly convex function in $\dot{\boldsymbol{q}}$. Thus, $V(\boldsymbol{q}, \dot{\boldsymbol{q}})$ is a strictly convex function of $(\boldsymbol{q}, \dot{\boldsymbol{q}})$. Since this result holds globally, $V(\boldsymbol{q}, \dot{\boldsymbol{q}})$ is radially unbounded, i. e., $V(\boldsymbol{q}, \dot{\boldsymbol{q}}) \to \infty$ if $\|\boldsymbol{q}\| \to \infty$ or $\|\dot{\boldsymbol{q}}\| \to \infty$, the above argumentation holds globally (cf. [SL91, Theorem 3.5, p. 73]). Therefore, in case of free motion, i. e.$\boldsymbol{\tau}_{\mathrm{ext}} = \boldsymbol{0}$, the equilibrium point $\{\boldsymbol{q} = \bar{\boldsymbol{q}}(\boldsymbol{\eta}_{\mathrm{des}}), \dot{\boldsymbol{q}} = \boldsymbol{0}\}$ of the system (3.60) is globally asymptotically stable. □

3.3.3. Implementation via generalized actuator force input

In the following, a method is presented which achieves the additional damping term $\boldsymbol{d}_{\mathrm{q,inj}}(\boldsymbol{q}, \dot{\boldsymbol{q}})$ (defined by (3.52)) for the plant dynamics (3.26), (3.27) under assumptions (3.29), (3.30) via the generalized actuator force input $\boldsymbol{u}$. The proposed controller extends the author's previous work [KLOAS16][8] to the case of general potential functions $U(\boldsymbol{\theta}, \boldsymbol{q})$ (cf. Sect. 3.1.1 under assumption $m = n = p$) such as bi-articular mechanisms, where $\partial U(\boldsymbol{\theta}, \boldsymbol{q})/\partial \boldsymbol{q} \neq -\partial U(\boldsymbol{\theta}, \boldsymbol{q})/\partial \boldsymbol{\theta}$ and combines the result with the method of [ASOP12].

Consider the actuator dynamics

$$\boldsymbol{B}\ddot{\boldsymbol{\theta}} + \boldsymbol{f}_{\theta}(\boldsymbol{\theta}, \boldsymbol{q}) = \boldsymbol{u}\,, \tag{3.63}$$

where for the potential force $\boldsymbol{f}_{\theta}(\boldsymbol{\theta}, \boldsymbol{q})$ the notation (3.33) is used. The indirectly actuated state dynamics (3.53) (containing the injected damping term $\boldsymbol{d}_{\mathrm{q,inj}}(\boldsymbol{q}, \dot{\boldsymbol{q}})$) can be achieved by choosing the control input $\boldsymbol{u}$ such that the actuator dynamics (3.63) under the change of coordinates (3.54) takes the form:

$$\boldsymbol{B}\ddot{\boldsymbol{\eta}} + \boldsymbol{f}_{\theta}(\boldsymbol{\eta}, \boldsymbol{q}) = \bar{\boldsymbol{u}}\,. \tag{3.64}$$

Herein, $\bar{\boldsymbol{u}} \in \mathbb{R}^n$ is the control input of the dynamics (3.64), (3.53), which implements the additional damping term $\boldsymbol{d}_{\mathrm{q,inj}}(\boldsymbol{q}, \dot{\boldsymbol{q}})$. The required control input $\boldsymbol{u}$ can be derived by differentiating the change of coordinates (3.54) twice w. r. t. time. The first derivative can be expressed as

$$\boldsymbol{J}_{\eta}(\boldsymbol{\theta}, \boldsymbol{\eta}, \boldsymbol{q})\dot{\boldsymbol{\theta}} + \boldsymbol{\gamma}(\boldsymbol{\theta}, \boldsymbol{\eta}, \boldsymbol{q}, \dot{\boldsymbol{q}}, \ddot{\boldsymbol{q}}) = \dot{\boldsymbol{\eta}}\,, \tag{3.65}$$

where the Jacobian matrix $\boldsymbol{J}_{\eta}(\boldsymbol{\theta}, \boldsymbol{\eta}, \boldsymbol{q})$ is defined by (3.56) and

$$\boldsymbol{\gamma}(\boldsymbol{\theta}, \boldsymbol{\eta}, \boldsymbol{q}, \dot{\boldsymbol{q}}, \ddot{\boldsymbol{q}}) = \left(\frac{\partial \boldsymbol{f}_{\mathrm{q}}(\boldsymbol{\eta}, \boldsymbol{q})}{\partial \boldsymbol{\eta}}\right)^{-1} \left[\left(\frac{\partial \boldsymbol{f}_{\mathrm{q}}(\boldsymbol{\theta}, \boldsymbol{q})}{\partial \boldsymbol{q}} - \frac{\partial \boldsymbol{f}_{\mathrm{q}}(\boldsymbol{\eta}, \boldsymbol{q})}{\partial \boldsymbol{q}}\right)\dot{\boldsymbol{q}} - \dot{\boldsymbol{d}}_{\mathrm{q,inj}}(\boldsymbol{q}, \dot{\boldsymbol{q}})\right] \tag{3.66}$$

can be interpreted as a bias of the velocity mapping (3.65). The time derivative of (3.65),

$$\boldsymbol{J}_{\eta}(\boldsymbol{\theta}, \boldsymbol{\eta}, \boldsymbol{q})\ddot{\boldsymbol{\theta}} + \dot{\boldsymbol{J}}_{\eta}(\boldsymbol{\theta}, \boldsymbol{\eta}, \boldsymbol{q})\dot{\boldsymbol{\theta}} + \dot{\boldsymbol{\gamma}}(\boldsymbol{\theta}, \boldsymbol{\eta}, \boldsymbol{q}, \dot{\boldsymbol{q}}, \ddot{\boldsymbol{q}}) = \ddot{\boldsymbol{\eta}}\,,$$

evaluated along the solution of (3.63) and (3.64) (i. e., substituting $\ddot{\boldsymbol{\theta}}$ and $\ddot{\boldsymbol{\eta}}$ by (3.63) and (3.64), respectively) yields the control law

$$\begin{aligned}\boldsymbol{u} =& \boldsymbol{f}_{\theta}\left(\boldsymbol{g}_{\mathrm{q}}\left(\boldsymbol{f}_{\mathrm{q}}(\boldsymbol{\eta}, \boldsymbol{q}) + \boldsymbol{d}_{\mathrm{q,inj}}(\boldsymbol{q}, \dot{\boldsymbol{q}}), \boldsymbol{q}\right), \boldsymbol{q}\right) \\ &+ \boldsymbol{B}\boldsymbol{J}_{\eta}(\boldsymbol{\theta}, \boldsymbol{\eta}, \boldsymbol{q})^{-1}\left[\boldsymbol{B}^{-1}\left(\bar{\boldsymbol{u}} - \boldsymbol{f}_{\theta}(\boldsymbol{\eta}, \boldsymbol{q})\right) - \dot{\boldsymbol{J}}_{\eta}(\boldsymbol{\theta}, \boldsymbol{\eta}, \boldsymbol{q})\dot{\boldsymbol{\theta}} - \dot{\boldsymbol{\gamma}}(\boldsymbol{\theta}, \boldsymbol{\eta}, \boldsymbol{q}, \dot{\boldsymbol{q}}, \ddot{\boldsymbol{q}})\right]\,,\end{aligned} \tag{3.67}$$

which leads to the closed-loop dynamics (3.64), (3.53).

Remark 3.8. *The control approach* (3.67) *can be straightforwardly extended to the case, where actuator-side friction of the form* (3.29) *is considered. However, this requires the knowledge of an explicit friction model*[9]*. Considering a priori observer based friction compensation as proposed by [TASLH08] would avoid this problem and validates the assumption made for the actuator dynamics* (3.63)*.*

[8] More precisely, the regulation case of [KLOAS16] without dynamic gravity cancellation is considered.
[9] Considering actuator-side friction in the control law (3.67) requires to compute the term $\boldsymbol{d}_{\theta}(\boldsymbol{\eta}, \boldsymbol{q}, \dot{\boldsymbol{\eta}})$.

Steady-state solution

In the following, the problem of regulating the indirectly actuated state variables $\boldsymbol{q}$ of the system (3.64), (3.53) at a desired configuration $\boldsymbol{q}_{\mathrm{des}}$ is considered. This can be achieved by a PD-like feedback of the control input collocated variables $\bar{\boldsymbol{q}}(\boldsymbol{\eta}), \dot{\boldsymbol{\eta}}$:

$$\bar{\boldsymbol{u}} = \boldsymbol{f}_{\theta}(\boldsymbol{\eta}, \bar{\boldsymbol{q}}(\boldsymbol{\eta})) - \boldsymbol{J}_{\bar{q}}(\boldsymbol{\eta})^T \boldsymbol{K}_{\mathrm{P}} \left(\bar{\boldsymbol{q}}(\boldsymbol{\eta}) - \boldsymbol{q}_{\mathrm{des}}\right) - \boldsymbol{K}_{\mathrm{D}} \dot{\boldsymbol{\eta}} \,. \tag{3.68}$$

Herein, $\bar{\boldsymbol{q}}(\boldsymbol{\eta})$ and the corresponding Jacobian matrix $\boldsymbol{J}_{\bar{q}}(\boldsymbol{\eta})$ are defined by Definition 3.4 and (3.20) (replacing the argument $\boldsymbol{\theta}$ by $\boldsymbol{\eta}$), respectively and $\boldsymbol{K}_{\mathrm{P}}, \boldsymbol{K}_{\mathrm{D}}$ are symmetric and positive definite controller gain matrices. The control law (3.68) equals formally the controller proposed in [ASOP12]. The difference to the cited work is that (3.68) is formulated in terms of $\boldsymbol{\eta}$, which already implements the additional damping term $\boldsymbol{d}_{\mathrm{q,inj}}(\boldsymbol{q}, \dot{\boldsymbol{q}})$ injected into the indirectly actuated state dynamics.

In case of free motion, i. e., $\boldsymbol{\tau}_{\mathrm{ext}} = \boldsymbol{0}$, the static equilibrium conditions $\dot{\bar{\boldsymbol{z}}} = (\dot{\boldsymbol{\eta}}, \dot{\boldsymbol{q}}) = \boldsymbol{0}$ of the closed-loop dynamics (3.64), (3.53), and (3.68) become

$$\boldsymbol{f}_{\theta}(\boldsymbol{\eta}, \boldsymbol{q}) = \boldsymbol{f}_{\theta}(\boldsymbol{\eta}, \bar{\boldsymbol{q}}(\boldsymbol{\eta})) - \boldsymbol{J}_{\bar{q}}(\boldsymbol{\eta})^T \boldsymbol{K}_{\mathrm{P}} \left(\bar{\boldsymbol{q}}(\boldsymbol{\eta}) - \boldsymbol{q}_{\mathrm{des}}\right) , \tag{3.69}$$

$$\boldsymbol{f}_{\mathrm{q}}(\boldsymbol{\eta}, \boldsymbol{q}) = \boldsymbol{0} \,. \tag{3.70}$$

Due to Definition 3.4, the only solution of (3.70) is $\boldsymbol{q} = \bar{\boldsymbol{q}}$. Substituting this result into (3.69) it follows that $\bar{\boldsymbol{q}} = \boldsymbol{q}_{\mathrm{des}}$. Since $\bar{\boldsymbol{q}}(\boldsymbol{\eta})$ is a diffeomorphism (cf. Proposition 3.1), $\boldsymbol{\eta} = \boldsymbol{\eta}_{\mathrm{des}}$ results. Therefore, it can be concluded that (3.69) and (3.70) have exactly the only solution $\boldsymbol{\eta} = \boldsymbol{\eta}_{\mathrm{des}}$ and $\boldsymbol{q} = \boldsymbol{q}_{\mathrm{des}}$.

Stability and passivity

In the following, the stability and passivity properties of the system (3.64), (3.53), and (3.68) are analyzed based upon considerations of [ASOP12]. Thereby, the configuration variables are denoted by $\bar{\boldsymbol{z}} = (\boldsymbol{\eta}, \boldsymbol{q})$.

Proposition 3.6. *In case of free motion, i. e.,* $\boldsymbol{\tau}_{\mathrm{ext}} = \boldsymbol{0}$*, the equilibrium point* $\{\bar{\boldsymbol{z}} = \bar{\boldsymbol{z}}_{\mathrm{des}}, \dot{\bar{\boldsymbol{z}}} = \boldsymbol{0}\}$ *of the closed-loop dynamics* (3.64)*,* (3.53)*, and* (3.68) *is globally asymptotically stable.*

Proof. Consider a Lyapunov function candidate of the form

$$V(\bar{\boldsymbol{z}}, \dot{\bar{\boldsymbol{z}}}) = T(\bar{\boldsymbol{z}}, \dot{\bar{\boldsymbol{z}}}) + U(\boldsymbol{\eta}, \boldsymbol{q}) + V_{\mathrm{C}}(\boldsymbol{\eta}, \bar{\boldsymbol{q}}(\boldsymbol{\eta})) \,, \tag{3.71}$$

which comprises the kinetic and potential energy $T(\bar{\boldsymbol{z}}, \dot{\bar{\boldsymbol{z}}}) = \frac{1}{2}\left(\dot{\boldsymbol{\eta}}^T \boldsymbol{B} \dot{\boldsymbol{\eta}} + \dot{\boldsymbol{q}}^T \boldsymbol{M}(\boldsymbol{q}) \dot{\boldsymbol{q}}\right)$ and $U(\boldsymbol{\eta}, \boldsymbol{q})$ of the dynamics (3.64), (3.53), respectively and a "candidate storage function",

$$V_{\mathrm{C}}(\boldsymbol{\eta}, \bar{\boldsymbol{q}}(\boldsymbol{\eta})) = -U(\boldsymbol{\eta}, \bar{\boldsymbol{q}}(\boldsymbol{\eta})) + \frac{1}{2} \left(\bar{\boldsymbol{q}}(\boldsymbol{\eta}) - \boldsymbol{q}_{\mathrm{des}}\right)^T \boldsymbol{K}_{\mathrm{P}} \left(\bar{\boldsymbol{q}}(\boldsymbol{\eta}) - \boldsymbol{q}_{\mathrm{des}}\right) , \tag{3.72}$$

for the controller (3.68). In order to show that $V(\bar{\boldsymbol{z}}, \dot{\bar{\boldsymbol{z}}})$ is a Lyapunov function, it is required to show that $V(\bar{\boldsymbol{z}}, \dot{\bar{\boldsymbol{z}}})$ is positive definite in its arguments and that the derivative $\dot{V}(\bar{\boldsymbol{z}}, \dot{\bar{\boldsymbol{z}}})$ along the solution of (3.64), (3.53), and (3.68) is at least negative semi-definite.

The first term of (3.71) is positive definite in $\dot{\bar{\boldsymbol{z}}}$, i. e., $T(\bar{\boldsymbol{z}}, \dot{\bar{\boldsymbol{z}}}) > 0$, for all $\dot{\bar{\boldsymbol{z}}} \neq \boldsymbol{0}$ and $T(\bar{\boldsymbol{z}}, \dot{\bar{\boldsymbol{z}}}) = 0$ if and only if $\dot{\bar{\boldsymbol{z}}} = \boldsymbol{0}$, for all $\bar{\boldsymbol{z}} \in \mathbb{R}^{2n}$. In order to show that $V(\bar{\boldsymbol{z}}, \dot{\bar{\boldsymbol{z}}})$ is positive definite in all its arguments, it remains to show that $U(\boldsymbol{\eta}, \boldsymbol{q}) + V_{\mathrm{C}}(\boldsymbol{\eta}, \bar{\boldsymbol{q}}(\boldsymbol{\eta})) > 0$, for all $\bar{\boldsymbol{z}} \neq \bar{\boldsymbol{z}}_{\mathrm{des}}$ and $U(\boldsymbol{\eta}, \boldsymbol{q}) + V_{\mathrm{C}}(\boldsymbol{\eta}, \bar{\boldsymbol{q}}(\boldsymbol{\eta})) = 0$ if and only if $\bar{\boldsymbol{z}} = \bar{\boldsymbol{z}}_{\mathrm{des}}$. To this end, consider first

the difference $\Delta U_{\mathrm{q}}(\boldsymbol{\eta}, \boldsymbol{q}) = U(\boldsymbol{\eta}, \boldsymbol{q}) - U(\boldsymbol{\eta}, \bar{\boldsymbol{q}})$. From Assumption 3.5 (i. e., $U(\boldsymbol{\eta}, \boldsymbol{q})$ is a strictly convex function of $\boldsymbol{q}$) and Definition 3.4 (i. e., $\boldsymbol{f}_{\mathrm{q}}(\boldsymbol{\eta}, \bar{\boldsymbol{q}}(\boldsymbol{\eta})) = \boldsymbol{0}$) for any given $\boldsymbol{\eta}$) it follows that $\Delta U_{\mathrm{q}}(\boldsymbol{\eta}, \boldsymbol{q}) > 0$ for all $\boldsymbol{q} \neq \bar{\boldsymbol{q}}$, which follows from the fact that $U(\boldsymbol{\eta}, \boldsymbol{q})$ has the only extremum, which is a minimum, at $\boldsymbol{q} = \bar{\boldsymbol{q}}$, for any given $\boldsymbol{\eta}$. Additionally, the strict convexity Assumption 3.5 in combination with the mean value theorem implies

$$\left|U(\boldsymbol{\eta}, \boldsymbol{q}_1) - U(\boldsymbol{\eta}, \boldsymbol{q}_2) - \boldsymbol{f}_{\mathrm{q}}(\boldsymbol{\eta}, \boldsymbol{q}_2)^T (\boldsymbol{q}_1 - \boldsymbol{q}_2)\right| \geq \frac{1}{2} c_7 \left\|\boldsymbol{q}_1 - \boldsymbol{q}_2\right\|^2 ,$$

for all $\boldsymbol{\eta}, \boldsymbol{q}_1, \boldsymbol{q}_2 \in \mathbb{R}^n$, where for $\boldsymbol{q}_1 = \boldsymbol{q}$ and $\boldsymbol{q}_2 = \bar{\boldsymbol{q}}(\boldsymbol{\eta})$, the above relation reduces to

$$\Delta U_{\mathrm{q}}(\boldsymbol{\eta}, \boldsymbol{q}) \geq \frac{1}{2} c_7 \left\|\boldsymbol{q} - \bar{\boldsymbol{q}}\right\|^2 .$$

Considering this result in (3.71), (3.72) it follows that

$$V(\bar{\boldsymbol{z}}, \dot{\bar{\boldsymbol{z}}}) \geq T(\bar{\boldsymbol{z}}, \dot{\bar{\boldsymbol{z}}}) + \frac{1}{2} c_7 \left\|\boldsymbol{q} - \bar{\boldsymbol{q}}\right\|^2 + \frac{1}{2} \left(\bar{\boldsymbol{q}}(\boldsymbol{\eta}) - \boldsymbol{q}_{\mathrm{des}}\right)^T \boldsymbol{K}_{\mathrm{P}} \left(\bar{\boldsymbol{q}}(\boldsymbol{\eta}) - \boldsymbol{q}_{\mathrm{des}}\right) \geq 0 . \tag{3.73}$$

It can be seen that the equality holds only if $\boldsymbol{q} = \bar{\boldsymbol{q}} = \boldsymbol{q}_{\mathrm{des}}$. According to Proposition 3.1, the mapping $\bar{\boldsymbol{q}}(\boldsymbol{\eta})$ is a diffeomorphism. This in turn implies $\boldsymbol{\eta} = \boldsymbol{\eta}_{\mathrm{des}}$. It can be concluded that $V(\bar{\boldsymbol{z}}, \dot{\bar{\boldsymbol{z}}}) = 0$, if and only if $\{\bar{\boldsymbol{z}} = \bar{\boldsymbol{z}}_{\mathrm{des}}, \dot{\bar{\boldsymbol{z}}} = \boldsymbol{0}\}$ holds.

In order that $V(\bar{\boldsymbol{z}}, \dot{\bar{\boldsymbol{z}}})$ is a Lyapunov function, it remains to show that $\dot{V}(\bar{\boldsymbol{z}}, \dot{\bar{\boldsymbol{z}}})$ is at least negative semi-definite. Consider therefore the Hamiltonian of the system (3.64), (3.53),

$$H(\bar{\boldsymbol{z}}, \dot{\bar{\boldsymbol{z}}}) = T(\bar{\boldsymbol{z}}, \dot{\bar{\boldsymbol{z}}}) + U(\boldsymbol{\eta}, \boldsymbol{q}) . \tag{3.74}$$

Its derivative along the solution of (3.64), (3.53) can be expressed as

$$\dot{H}(\bar{\boldsymbol{z}}, \dot{\bar{\boldsymbol{z}}}) = -\dot{\boldsymbol{q}}^T \left(\boldsymbol{d}_{\mathrm{q}}(\boldsymbol{q}, \dot{\boldsymbol{q}}) + \boldsymbol{d}_{\mathrm{q,inj}}(\boldsymbol{q}, \dot{\boldsymbol{q}})\right) + \bar{\boldsymbol{u}}^T \dot{\boldsymbol{\eta}} . \tag{3.75}$$

Consider further the derivative of the "candidate storage function" of the controller (3.72), which is given by

$$\begin{aligned} \dot{V}_{\mathrm{C}}(\boldsymbol{\eta}, \bar{\boldsymbol{q}}(\boldsymbol{\eta})) &= -\dot{\boldsymbol{\eta}}^T \left(\boldsymbol{f}_{\theta}(\boldsymbol{\eta}, \bar{\boldsymbol{q}}(\boldsymbol{\eta})) - \boldsymbol{J}_{\bar{q}}(\boldsymbol{\eta})^T \boldsymbol{K}_{\mathrm{P}} \left(\bar{\boldsymbol{q}}(\boldsymbol{\eta}) - \boldsymbol{q}_{\mathrm{des}}\right)\right) && (3.76) \\ &= -\bar{\boldsymbol{u}}^T \dot{\boldsymbol{\eta}} - \dot{\boldsymbol{\eta}}^T \boldsymbol{K}_{\mathrm{D}} \dot{\boldsymbol{\eta}} , && (3.77) \end{aligned}$$

since

$$\frac{\partial U(\boldsymbol{\eta}, \bar{\boldsymbol{q}}(\boldsymbol{\eta}))}{\partial \boldsymbol{\eta}} = \boldsymbol{f}_{\eta}(\boldsymbol{\eta}, \bar{\boldsymbol{q}}(\boldsymbol{\eta}))^T + \boldsymbol{f}_{\mathrm{q}}(\boldsymbol{\eta}, \bar{\boldsymbol{q}}(\boldsymbol{\eta}))^T \boldsymbol{J}_{\bar{q}}(\boldsymbol{\eta}) = \boldsymbol{f}_{\eta}(\boldsymbol{\eta}, \bar{\boldsymbol{q}}(\boldsymbol{\eta}))^T , \tag{3.78}$$

according to Definition 3.4 (i. e., $\boldsymbol{f}_{\mathrm{q}}(\boldsymbol{\eta}, \bar{\boldsymbol{q}}(\boldsymbol{\eta})) = \boldsymbol{0}$). The sum of both derivatives yields,

$$\dot{V}(\bar{\boldsymbol{z}}, \dot{\bar{\boldsymbol{z}}}) = -\dot{\boldsymbol{q}}^T \left(\boldsymbol{d}_{\mathrm{q}}(\boldsymbol{q}, \dot{\boldsymbol{q}}) + \boldsymbol{d}_{\mathrm{q,inj}}(\boldsymbol{q}, \dot{\boldsymbol{q}})\right) - \dot{\boldsymbol{\eta}}^T \boldsymbol{K}_{\mathrm{D}} \dot{\boldsymbol{\eta}} \leq 0 , \tag{3.79}$$

which is negative semi-definite due to the assumptions on the dissipation terms (3.30) and (3.52).

It follows that $V(\bar{\boldsymbol{z}}, \dot{\bar{\boldsymbol{z}}})$ is a Lyapunov function of the system (3.64), (3.53), and (3.68). As a result the equilibrium point $\{\bar{\boldsymbol{z}} = \bar{\boldsymbol{z}}_{\mathrm{des}}, \dot{\bar{\boldsymbol{z}}} = \boldsymbol{0}\}$ is stable in a sense of Lyapunov [SL91, Theorem 3.2, p. 62].

This result can be extended to the case of asymptotic stability: By hypothesis of assumptions (3.30), (3.52), and the positive definiteness of $\boldsymbol{K}_{\mathrm{D}}$, $-\dot{\boldsymbol{q}}^T \left(\boldsymbol{d}_{\mathrm{q}}(\boldsymbol{q}, \dot{\boldsymbol{q}}) + \boldsymbol{d}_{\mathrm{q,inj}}(\boldsymbol{q}, \dot{\boldsymbol{q}})\right) -$

$\dot{\boldsymbol{\eta}}^T \boldsymbol{K}_\mathrm{D} \dot{\boldsymbol{\eta}} = 0$ only if $\dot{\boldsymbol{q}} = \boldsymbol{0}$ and $\dot{\boldsymbol{\eta}} = \boldsymbol{0}$. But $\dot{\boldsymbol{q}} = \boldsymbol{0}$ implies that $\ddot{\boldsymbol{q}} = -\boldsymbol{M}(\boldsymbol{q})^{-1} \boldsymbol{f}_\mathrm{q}(\boldsymbol{\eta}, \boldsymbol{q})$, which is non-zero as long as $\boldsymbol{q} \neq \bar{\boldsymbol{q}}(\boldsymbol{\eta})$. Additionally, $\dot{\boldsymbol{\eta}} = \boldsymbol{0}$ implies that

$$\ddot{\boldsymbol{\eta}} = \boldsymbol{B}^{-1} \left(\boldsymbol{f}_\theta(\boldsymbol{\eta}, \bar{\boldsymbol{q}}(\boldsymbol{\eta})) - \boldsymbol{f}_\theta(\boldsymbol{\eta}, \boldsymbol{q}) - \boldsymbol{J}_{\bar{q}}(\boldsymbol{\eta})^T \boldsymbol{K}_\mathrm{P} \left(\bar{\boldsymbol{q}}(\boldsymbol{\eta}) - \boldsymbol{q}_\mathrm{des} \right) \right) ,$$

which is non-zero as long as $\boldsymbol{q} \neq \bar{\boldsymbol{q}}(\boldsymbol{\eta}) \neq \boldsymbol{q}_\mathrm{des}$. Since $\bar{\boldsymbol{q}}(\boldsymbol{\eta})$ is a diffeomorphism (cf. Proposition 3.1), the statement $\boldsymbol{q} \neq \bar{\boldsymbol{q}}(\boldsymbol{\eta}) \neq \boldsymbol{q}_\mathrm{des}$ is equivalent to $\bar{\boldsymbol{z}} \neq \bar{\boldsymbol{z}}_\mathrm{des}$. Therefore, the system cannot remain in the set $\mathcal{R} = \left\{ \bar{\boldsymbol{z}}, \dot{\bar{\boldsymbol{z}}} \in \mathbb{R}^{2n} \,|\, \dot{\bar{\boldsymbol{z}}} = \boldsymbol{0} \right\}$ except at the equilibrium point $\{ \bar{\boldsymbol{z}} = \bar{\boldsymbol{z}}_\mathrm{des}, \dot{\bar{\boldsymbol{z}}} = \boldsymbol{0} \}$, since the largest invariant set in $\mathcal{R}$ is the equilibrium point itself. Therefore, the system is locally asymptotically stable according to La Salle's invariance principle [SL91, Theorem 3.4, p. 69].

Furthermore, from (3.73) and the fact that $\bar{\boldsymbol{q}}(\boldsymbol{\eta})$ is a diffeomorphism (cf. Proposition 3.1), it follows that $V(\bar{\boldsymbol{z}}, \dot{\bar{\boldsymbol{z}}})$ is radially unbounded, i. e., $V(\bar{\boldsymbol{z}}, \dot{\bar{\boldsymbol{z}}}) \to \infty$ if $\|\bar{\boldsymbol{z}}\| \to \infty$ or $\|\dot{\bar{\boldsymbol{z}}}\| \to \infty$ and thus the above argumentation holds globally [SL91, Theorem 3.5, p. 73]. Therefore, in case of free motion, i. e., $\boldsymbol{\tau}_\mathrm{ext} = \boldsymbol{0}$, the equilibrium point $\{ \bar{\boldsymbol{z}} = \bar{\boldsymbol{z}}_\mathrm{des}, \dot{\bar{\boldsymbol{z}}} = \boldsymbol{0} \}$ of the system (3.64), (3.53), and (3.68) is globally asymptotically stable. □

Passivity of the closed-loop dynamics (3.64), (3.53), and (3.72) can be deduced by considering the Lyapunov function given by (3.71) as storage function.

Proposition 3.7. *The system* (3.64)*,* (3.53)*, and* (3.68) *can be represented as a passive map from the generalized external force* $\boldsymbol{\tau}_\mathrm{ext}$ *to the generalized velocity* $\dot{\boldsymbol{q}}$ *(which in most robotic systems represents the velocity of the bodies in interaction with the environment).*

Proof. Consider a storage function $S := V$, where V is defined in (3.71) and (3.72). Its derivative along the solution of the system (3.64), (3.53), and (3.68) satisfies

$$\dot{S} = -\dot{\boldsymbol{q}}^T \left(\boldsymbol{d}_\mathrm{q}(\boldsymbol{q}, \dot{\boldsymbol{q}}) + \boldsymbol{d}_\mathrm{q,inj}(\boldsymbol{q}, \dot{\boldsymbol{q}}) \right) - \dot{\boldsymbol{\eta}}^T \boldsymbol{K}_\mathrm{D} \dot{\boldsymbol{\eta}} + \dot{\boldsymbol{q}}^T \boldsymbol{\tau}_\mathrm{ext} \leq \dot{\boldsymbol{q}}^T \boldsymbol{\tau}_\mathrm{ext} \,. \tag{3.80}$$

Therefore, according to [VdS12, Definition 2.2.1, p. 19], the system (3.64), (3.53), and (3.68) represents a passive map from $\boldsymbol{\tau}_\mathrm{ext}$ to $\dot{\boldsymbol{q}}$. □

3.4. Summary

This chapter proposes a formulation of compliantly actuated mechanical systems as a sub-class of under-actuated Euler-Lagrange dynamics. This formulation is as general as it includes the case, where not all of the indirectly actuated states at position level are statically controllable. On the basis of this general model, a PD control in terms of the directly actuated states is presented which asymptotically stabilizes all statically controllable states without model parameter knowledge of the plant. For the PD controlled plant, a singular perturbation argumentation is presented, which allows to neglect the closed-loop actuator dynamics under certain controller gain assumptions. Even though this result is deemed as known in the robotic control community (yet not published, from the author's best knowledge), it forms the foundation of the analysis and control methodologies proposed in this thesis, since it allows to stabilize the statically controllable states of compliantly actuated mechanical systems, even in the presence of statically not-controllable states appearing in locomotion dynamics (such as the inverted pendulum dynamics). Moreover, a unified control framework to inject damping into the statically controllable state dynamics is proposed, which preserves the structure of the system-inherent Lagrangian. Two different implementation of the damping injection are proposed: implementation via actuator

position input and via generalized actuator force input. The former implementation is based on the singular perturbation result. It achieves the additional damping term and maintains the global asymptotic stability property, even in case where the original plant dynamics is not statically feedback-linearizable due to inertial couplings. The damping injection implementation via the generalized actuator force input considers the complete (statically feedback-linearizable) plant dynamics. A link-side tracking control variant of the damping-injection controller is presented in the author's previous work [KLOAS16]. Herein, a comprehensive, experimental validation of the approach is performed with the compliantly actuated robot DLR Hand Arm System [GASB$^+$11]. As in case of the former implementation, it preserves also the structure of the Lagrangian and therefore, the method of [ASOP12] to control the steady-state behavior of the indirectly actuated states can be directly applied. The proposed superposition completes the approach of [ASOP12] in a way that in addition to constructive energy shaping control it achieves desired damping, which directly influences the convergence behavior of all statically controllable states.

CHAPTER 4

Limit Cycle Control

Solving the problem of energy efficient limit cycle generation in planar, compliantly actuated systems represents a major step towards the main goal at hand. However, due to the generally nonlinear structure of the underlying second-order differential equation, this problem is not trivial and is far from being completely understood. A novel switching-based control principle is derived here, which is based upon observations of humans controlling an equivalent simulated dynamical system in a force-feedback setup. The resulting controller is able to generate a limit cycle without the knowledge of model-parameters of the plant. Due to the switching nature of the control law, the corresponding closed-loop dynamics represents a hybrid dynamical system of which the stability analysis yields novel interpretations of ordinary existence and convergence statements for continuous dynamics in the hybrid case.

4.1. Problem statement

Consider the planar, second-order system

$$M\ddot{q} + d(q-\theta,\dot{q}) + \left.\frac{\partial U(\phi)}{\partial \phi}\right|_{\phi=q-\theta} = 0\,. \tag{4.1}$$

Herein, $q, \dot{q} \in \mathbb{R}$ and $\theta \in \mathbb{R}$ represent the indirectly actuated states and the control input, respectively, and $M > 0$ denotes the inertia constant. The dynamics (4.1) may be regarded as the actuator PD controlled, singularly perturbed, compliantly actuated system (3.50), where $n = 1$. To reduce the complexity of the analysis, the following assumptions are made in (4.1):

Assumption 4.1. *The potential $U(\phi) : \mathbb{R} \to \mathbb{R}$ is a strictly convex, two-times continuously differentiable, positive definite, and even function in ϕ, i. e., $\partial^2 U(\phi)/\partial\phi^2 > 0$ for all $\phi \in \mathbb{R}$, $U(\phi) > 0$ for all $\phi \neq 0$, $U(\phi) = 0$ only if $\phi = 0$ and $U(-\phi) = U(\phi)$ for all $\phi \in \mathbb{R}$.*

Assumption 4.2. *The generalized damping force $d(\phi,\dot{q}) : \mathbb{R}^2 \to \mathbb{R}$, which is continuously differentiable in its arguments, is dissipative in a sense that $d(\phi,\dot{q})\dot{q} > 0$ for all $\dot{q} \neq 0$ and $d(\phi,\dot{q}) = 0$ only if $\dot{q} = 0$, for all $\phi \in \mathbb{R}$. Additionally, $d(\phi,\dot{q})$ is an odd and strictly increasing function of $\dot{q}$, i. e., $d(\phi,-\dot{q}) = -d(\phi,\dot{q})$.*

Compared to the model (3.50) with $n = 1$, the assumptions added for the planar system (with two state variables) (4.1) are basically conditions on the symmetry of the potential and damping terms, which halve the amount of cases to be distinguished in the following analysis of such nonlinear dynamics. Thereby, as will become clear during analysis of Sect. 4.6 and 4.7, the generality of the results is not lowered to a large extent.

The stability properties of the dynamics (4.1) with $\theta = \text{const.}$ rely only on the positive definiteness of $U(\phi)$ and $d(\phi, \dot{q})\dot{q}$ in ϕ and $\dot{q}$, respectively. This can be seen from the proof of the following proposition:

Proposition 4.1. *Let $\boldsymbol{x} = (q - \theta, \dot{q}) \in \mathbb{R}^2$ be the state of the dynamics (4.1). Then, for $\theta = \text{const.}$, the origin $\boldsymbol{x} = \mathbf{0}$ of (4.1) under Assumption 4.1 and 4.2 is globally asymptotically stable.*

Proof. The proof of this proposition is provided in the Appendix A.1. □

The objectives of this chapter are:

- Deriving a control such that the state trajectory is periodic;
- Exploiting mechanical resonance effects of the system.

To understand the challenging character of this problem in the case of nonlinear springs, consider a sinusoidal control signal $\theta(t) = \hat{\theta} \cos(\omega t)$ with amplitude $\hat{\theta}$ and frequency ω and compare qualitatively the behavior of the system (4.1) consisting of a linear spring with potential function

$$U(\phi) = \frac{1}{2} k_{\text{lin}} \phi^2 \tag{4.2}$$

and a cubic spring as an example of a nonlinear elasticity with potential function

$$U(\phi) = \frac{1}{2} k_{\text{lin}} \phi^2 + \frac{1}{4} k_{\text{cub}} \phi^4 , \tag{4.3}$$

where $k_{\text{lin}} > 0$ and $k_{\text{cub}} > 0$ denote the linear and cubic spring constants, respectively, and linear damping in both cases, i. e., $d(\phi, \dot{q}) = d_0 \dot{q}$ with $d_0 > 0$ constant-

4.1.1. Linear spring

The resulting system is a forced, linear oscillator

$$M\ddot{q} + d_0 \dot{q} + k_{\text{lin}} q = \hat{\theta} \cos(\omega t) \ .$$

A resonance oscillation can be achieved either by exciting the system with a frequency close to the natural frequency or, in case of a variable stiffness actuator joint, with a linear and adjustable spring by adjusting the stiffness such that the resulting natural frequency is close to the desired frequency of the task and excitation.

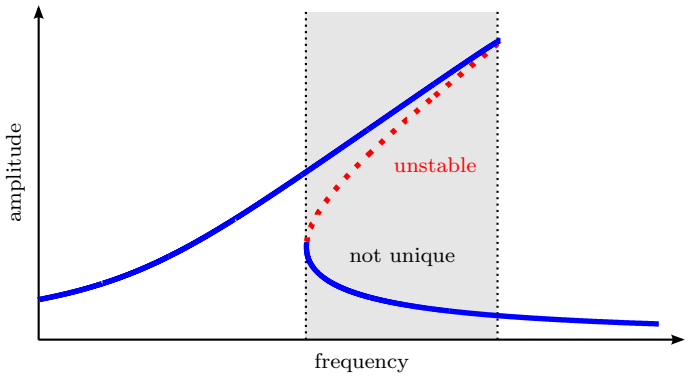

Figure 4.1.: Amplitude-frequency characteristics of a forced, nonlinear oscillator.

4.1.2. Nonlinear, cubic spring

The system represents a forced, nonlinear, parametrically excited oscillator with multi-frequency excitation [NM79]

$$M\ddot{q} + d_0\dot{q} + \left(k_{\text{lin}} + \frac{3k_{\text{cub}}\hat{\theta}^2}{2}\right) q + k_{\text{cub}}q^3 + \underbrace{3k_{\text{cub}}\hat{\theta}\left(\frac{\hat{\theta}}{2}\cos(2\omega t) - \cos(\omega t)\, q\right) q}_{\text{parametric excitation}}$$
$$= \left(k_{\text{lin}} + \frac{3k_{\text{cub}}\hat{\theta}^2}{4}\right)\hat{\theta}\cos(\omega t) + \underbrace{\frac{k_{\text{cub}}\hat{\theta}^3}{4}\cos(3\omega t)}_{\text{multi-frequency excitation}} .$$

Approximative solutions can be obtained partly using perturbation methods [Nay73], [PKB11]. The qualitative behavior is discussed in [NM79]:

- *Cubic nonlinearity:* the system exhibits multiple resonances; The amplitude and frequency of the steady-state response depend on the excitation (amplitude, frequency) and the *initial conditions* (Fig. 4.1).
- *Parametric excitation:* the system consists of rapidly varying parameters; small excitation amplitudes can produce large responses, even if the excitation frequency is not close to the linear, natural frequency.
- *Multi-frequency excitation:* more than one type of excitation may occur simultaneously.

These observations highlight that there is a substantial difference between the well-known linear case and the nonlinear case, making the prediction of periodic motions a non-trivial problem.

4.2. Related approaches

The related methods solving the problem of Sect. 4.1 can be mainly classified in two basic principles:

- the *Van der Pol oscillator* and

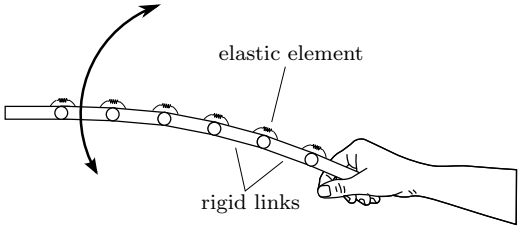

Figure 4.2.: Human induces periodic motions for a rod consisting of rigid links, which are connected via nonlinear, elastic elements.

- the *central pattern generator (CPG).*

On the basis of the seminal work of *Van der Pol* [VdP26], several control methods to implement a limit cycle behavior in robotic systems have been proposed by [SD08], [GOAS13], and the author's previous work [LGP$^+$13a]. These controllers implement the limit cycle generation by a nonlinear damping term (which, e. g., can be achieved applying the method of Sect. 3.3) that increases the system energy along trajectories inside the limit cycle and decreases the system energy outside the limit cycle. Thereby, the original dynamics of the plant is substantially changed: In particular, applying this approach to robotic systems entails additional energy losses in the actuators even in phases of positive damping, since the nonlinear damping is generated artificially by control. Moreover, the Van der Pol oscillator based control systems are exposed to theoretical difficulties, since the stability analysis of such systems assumes that the damping force inherent in any real plant is canceled a priori.

The CPG based approach has been invented by *Ijspeert et al.* [Ijs01], [BI04], [IC07] to control periodic motions of systems with usually a large number of degrees of freedom. As observed in neuro-control units of amphibians, periodic trajectories are generated by nonlinear (phase-)coupled oscillators. The periodic motion replicating this behavior in a robotic system is generated in an isolated (feed-forward) unit, the CPG, and commanded to the plant as desired joint positions. In contrast to the motivation of the work at hand, the natural plant dynamics is disregarded and rigid robot designs without resonance behavior are considered. An extension to the classical CPG approach which applies to compliantly actuated systems is given by the so-called adaptive frequency oscillators (AFO) [BI08]. The central control unit of the AFO is the Hopf oscillator [Hop42] of which the positional state can be the control input θ of the compliantly actuated system (4.1) and the indirectly actuated state of the plant $(q, \dot{q})$ can be superimposed to the dynamics of the Hopf oscillator as feedback. Since the steady-state solution of the Hopf oscillator represents a harmonic limit cycle, the closed-loop dynamics of a nonlinear, AFO controlled system suffers exactly from the theoretical problems as discussed in Sect. 4.1.2.

4.3. Main controller idea

This section derives a control principle to stabilize periodic motions for compliantly actuated systems of the form (4.1) inspired by human experiments. Despite the current theoretical difficulties discussed in Sect. 4.1, humans are able to stabilize periodic motions easily, even in the presence of strong nonlinearities. This can be easily verified by sim-

ple experiments, where a human induces oscillations into a rod (see, Fig. 4.2). Stable oscillations could be very easily achieved even for the case of large deflections (i. e., in the presence of strong nonlinearities). The human does not need a long training phase to do so. This demonstrates the ability of humans to control periodic motions of nonlinear compliantly actuated systems. From these observations it is hypothesized that:

- The motor control of humans is able to stabilize periodic motions even in the presence of strong nonlinearities.
- The underlying control law has a simple and very robust structure.

On the basis of experimental observations from strategies used by humans, a control principle will be derived that confirms these hypotheses.

Accessing and measuring control and feedback signals of humans during natural motions is difficult and largely unresolved [HSH+96]. Therefore, this problem is circumvented by using hardware in the loop simulations with human control. Using a force feedback device, a human operator can be coupled in the feedback control loop with either a robotic plant or a simulated system. The latter allows to adjust the system parameters arbitrarily as done in the following experiments.

As sketched in Fig. 4.3, the real time simulation of (4.1) was interconnected with a direct drive (torque controlled) motor with a handle mounted on the rotor. This motor acts as force feedback device. An optical encoder provides the angular position of the motor as control signal $\theta(t)$ for the simulated compliantly actuated system (4.1). The generalized elastic force $\psi(\phi) = -\partial U(\phi)/\partial\phi$ computed by the simulation is commanded to the current controller of the force feedback device and thereby provides feedback to the human operator. This setup allows to emulate arbitrary dynamical systems that are controlled by a single position input / force output, and interface them to a human operator.

In a series of experiments, the oscillatory behavior of the compliantly actuated system (4.1) has been analyzed. A nonlinear cubic spring (cf. (4.3)) was considered, where the ratio of linear and cubic spring constants was chosen as $k_{\mathrm{cub}}/k_{\mathrm{lin}} = 70$. To comply with the range of maximum torques of the force feedback device $\tau_{max} = \pm 1\,\mathrm{Nm}$, inertia, damping, and spring parameters were adjusted. The dynamical system (4.1) was integrated (forward Euler method, time steps 0.001 s) on the same real time computer on which the force feedback device was controlled. Additionally, the motion of the pendulum was visualized on a screen. Several skilled participants[1] were tested. To initialize the tests, subjects were instructed to grasp the handle of the force feedback device and to rest in a centered, initial position (cf. Fig. 4.3), while the integrator was reset. Then, subjects were asked to move the handle to induce oscillations. The goal was to excite and stabilize periodic motions.

The experimental results revealed that humans can easily excite and sustain periodic motions, even in the presence of strong nonlinearities. All subjects have been applying similar strategies which can be summarized by the following very simple principle:

When a certain spring deflection (torque) is detected, the human operator countered it by moving the motor (control signal) in the opposite direction of the link deflection and thereby inducing energy into the system. In the remainder of this chapter, this strategy is formalized in a control law and properties of the resulting closed-loop dynamics are analyzed in detail.

[1] Participants were involved in the experimental background.

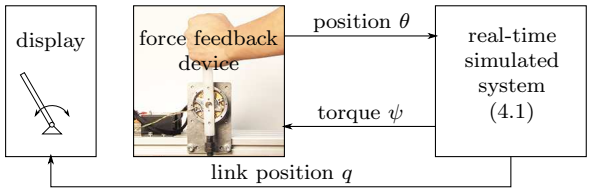

Figure 4.3.: Experimental setup to include a human in the control loop of a real-time simulated compliantly actuated system. Haptic feedback is provided by a force feedback device. Visual feedback is given by a display showing a real-time simulation of a robot.

4.4. Controller design

On the basis of observations made in Sect. 4.3, a switching based control law of the form

$$\theta(q(t),\theta_-) = \begin{cases} \hat{\theta} & \text{if} \quad q(t)-\theta_- < -\epsilon_\phi \\ 0 & \text{if} \quad |q(t)-\theta_-| < \epsilon_\phi \\ -\hat{\theta} & \text{if} \quad q(t)-\theta_- > \epsilon_\phi \end{cases} \tag{4.4}$$

is postulated. Herein, $\theta_- \in \{-\hat{\theta}, 0, \hat{\theta}\}$ denotes the state of the function $\theta(q(t),\theta_-)$ before the switching instance, i. e., $\theta(q(t),\theta_-)$ is piecewise continuous from the right in time t. The switching amplitude $\hat{\theta} > 0$ and the threshold value $\epsilon_\phi > 0$ are controller parameters. Depending on the ratio $\hat{\theta}/\epsilon_\phi$, two basic switching behaviors can be distinguished:

$$\hat{\theta} < 2\epsilon_\phi\,, \tag{4.5}$$

$$\hat{\theta} \geq 2\epsilon_\phi\,. \tag{4.6}$$

In case of (4.5), the function θ consists of three discrete states. The order of occurrence of these states is determined by the flow of the dynamics (4.1), being $(0, -\hat{\theta}, 0, \hat{\theta})$. In case of (4.6), the situation arises, where due to the switching, the condition for the next switching is fulfilled. Thereby, the function θ is defined such that the subsequent switching (corresponding to the new condition) occurs instantaneously. As a result, the switching function corresponding to parameters given by (4.6) can be expressed as

$$\theta(q(t),\theta_-) = \begin{cases} \hat{\theta} & \text{if} \quad q(t)-\theta_- < \epsilon_\phi \\ -\hat{\theta} & \text{if} \quad q(t)-\theta_- > -\epsilon_\phi \end{cases}\,. \tag{4.7}$$

Thereby, the switching function consists of two discrete states only, i. e., $\theta \in \{\hat{\theta}, -\hat{\theta}\}$.

Remark 4.1. *According to Propositon 4.1, the origin* $\{\phi := q - \theta = 0, \dot{q} = 0\}$ *of the dynamics* (4.1) *is globally asymptotically stable. Since additionally, in case of* (4.6)*, the potential energy right after the switching is at a higher level than the potential energy at the next switching condition, i. e.,* $U(2\hat{\theta} - \epsilon_\psi) > U(\epsilon_\psi)$ *or* $U(-2\hat{\theta} + \epsilon_\psi) > U(-\epsilon_\psi)$*, reaching the switching conditions is always guaranteed (Lemma 4.1). However, in case of* (4.5)*, situations arise, where the potential energy right after the switching is at a lower level than the potential energy at the next switching condition, i. e.,* $U(\hat{\theta} - \epsilon_\phi) < U(\epsilon_\phi)$ *or* $U(-\hat{\theta}+\epsilon_\phi) < U(-\epsilon_\phi)$ *such that reaching the switching conditions is not always guaranteed.*

Since the goal is to generate a stable limit cycle, the following analysis will focus on the controller (4.7) such that the following assumption is satisfied:

Assumption 4.3. *The switching parameters $\hat{\theta}$ and ϵ_ϕ are in the set*

$$(\hat{\theta}, \epsilon_\phi) \in \{(\hat{\theta}, \epsilon_\phi) \in \mathbb{R}_{\geq 0} \times \mathbb{R}_{\geq 0} \,|\, \hat{\theta} \geq 2\epsilon_\phi\}\,.$$

4.5. Hybrid dynamical system

The continuous dynamics (4.1) under the discontinuous control law (4.7) can be considered as an *autonomous-impulse hybrid system*. By expressing it in the framework of *general hybrid dynamical systems* [BBM98] it takes the form:

$$\mathcal{H} = [\Sigma, \mathcal{A}, \boldsymbol{g}]\ . \tag{4.8}$$

The dynamical system is represented by

$$\Sigma = [\mathcal{X}, \boldsymbol{f}]\,, \tag{4.9}$$

where by selecting as states $x_1 = q - \theta$ and $x_2 = \dot{q}$, the *continuous state space* is given by

$$\begin{aligned}
\mathcal{X} &= \mathcal{X}_1 \cup \mathcal{X}_2 \cup \mathcal{X}_3 \cup \mathcal{X}_4\,,\\
\mathcal{X}_1 &= \left\{\boldsymbol{x} \in \mathbb{R}^2 \,|\, x_1 \geq 2\hat{\theta} - \epsilon_\phi, x_2 \geq 0\right\}\,,\\
\mathcal{X}_2 &= \left\{\boldsymbol{x} \in \mathbb{R}^2 \,|\, x_1 \geq \epsilon_\phi, x_2 \leq 0\right\}\,,\\
\mathcal{X}_3 &= \left\{\boldsymbol{x} \in \mathbb{R}^2 \,|\, x_1 \leq -\left(2\hat{\theta} - \epsilon_\phi\right), x_2 \leq 0\right\}\,,\\
\mathcal{X}_4 &= \left\{\boldsymbol{x} \in \mathbb{R}^2 \,|\, x_1 \leq -\epsilon_\phi, x_2 \geq 0\right\}\,,
\end{aligned} \tag{4.10}$$

and the *continuous dynamics* is given by

$$\dot{\boldsymbol{x}} = \boldsymbol{f}(\boldsymbol{x}) = \begin{bmatrix} x_2 \\ -\frac{1}{M}\left(d(x_1, x_2) + \frac{\partial U(x_1)}{\partial x_1}\right) \end{bmatrix}\,, \quad \boldsymbol{x} \in \mathcal{X}\,. \tag{4.11}$$

When the state $\boldsymbol{x}$ of the continuous dynamics reaches the *autonomous jump set*

$$\begin{aligned}
\mathcal{A} &= \mathcal{A}_1 \cup \mathcal{A}_2\,,\\
\mathcal{A}_1 &= \left\{\boldsymbol{x} \in \mathbb{R}^2 \,|\, x_1 = \epsilon_\phi, x_2 \leq 0\right\}\,,\\
\mathcal{A}_2 &= \left\{\boldsymbol{x} \in \mathbb{R}^2 \,|\, x_1 = -\epsilon_\phi, x_2 \geq 0\right\}
\end{aligned} \tag{4.12}$$

the state is reset according to the *autonomous jump transition map*

$$\boldsymbol{x}_+ = \boldsymbol{g}(\boldsymbol{x}) = \begin{pmatrix} -\mathrm{sign}(x_1)\left|2\hat{\theta} - \epsilon_\phi\right| \\ x_2 \end{pmatrix}\,, \quad \boldsymbol{x} \in \mathcal{A}\,. \tag{4.13}$$

The qualitative behavior of the hybrid dynamical system $\mathcal{H}$ (4.8)–(4.13) in the state-plane is shown in Fig. 4.4. By starting with an initial state $\boldsymbol{x}_0 \in \mathcal{X}$, the solution $\boldsymbol{x}(\boldsymbol{x}_0, t)$ flows continuously according to $\dot{\boldsymbol{x}} = \boldsymbol{f}(\boldsymbol{x})$ until it (possibly) reaches the jump set $\mathcal{A}$. If $\boldsymbol{x} \in \mathcal{A}$, the state jumps to $\boldsymbol{x}_+ = \boldsymbol{g}(\boldsymbol{x})$ and then the solution continuously flows further with the reseted "initial condition" $\boldsymbol{x}_+ \in \mathcal{X}_0$, where

$$\mathcal{X}_0 = \boldsymbol{g}(\mathcal{A})\,, \tag{4.14}$$

denotes the jump destination set.

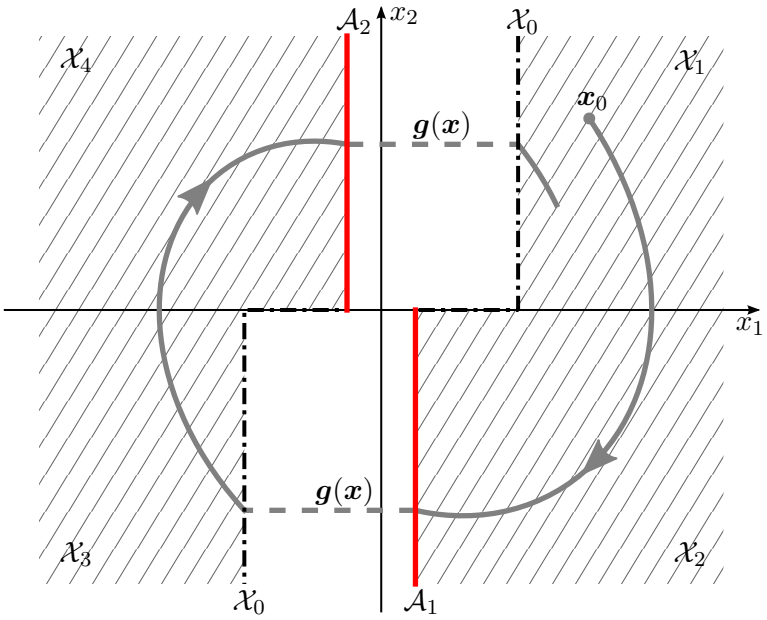

Figure 4.4.: Graphical representation of the hybrid dynamical system $\mathcal{H}$ (4.8)–(4.13) in the state-plane.

4.6. Hybrid closed orbits

Nontrivial closed orbits of continuous dynamical systems $\dot{\boldsymbol{x}} = \boldsymbol{f}(\boldsymbol{x})$ with $\boldsymbol{f}(\boldsymbol{0}) = \boldsymbol{0}$ correspond to solutions $\boldsymbol{x}(t) \in \mathbb{R}^n/\{\boldsymbol{0}\}$, where there exists a $T > 0$ for all $t \in \mathbb{R}_{\geq 0}$ such that $\boldsymbol{x}(t+T) = \boldsymbol{x}(t)$ (see, e. g., [Str94, p. 146]). This definition can be extended to the case of hybrid dynamical systems of the form (4.8):

Definition 4.1. *Nontrivial hybrid closed orbits correspond to complete solutions (comprising continuous and discrete portions) $\boldsymbol{x}(t) \in \mathbb{R}^n/\{\boldsymbol{0}\}$ of the hybrid dynamical system $\mathcal{H} = [\Sigma, \mathcal{A}, \boldsymbol{g}]$, where there exists a $T > 0$ for all $t \in \mathbb{R}_{\geq 0}$ such that $\boldsymbol{x}(t+T) = \boldsymbol{x}(t)$.*

This section proves the existence and uniqueness of such a solution for the particular hybrid system (4.8)–(4.13).

Theorem 4.1. *Given is the hybrid dynamical system* (4.8)–(4.13) *under Assumption 4.1, 4.2, and 4.3. There exists an unique, non-constant closed orbit according to Definition 4.1.*

The proof of this theorem, but also the convergence statement provided in the next section, are based on the following two lemmas:

Lemma 4.1. *The solutions $\boldsymbol{x}(t)$ of the continuous dynamics* (4.11) *under Assumption 4.1, 4.2, and 4.3 are such that for any initial state $\boldsymbol{x}_0 \in \mathcal{X}$, the state $\boldsymbol{x}$ reaches the jump set $\mathcal{A}$.*

Proof of Lemma 4.1. On the basis of Proposition 4.1 it will be shown that any solution of (4.11) which starts with initial conditions $\boldsymbol{x}_0 \in \mathcal{X}$ cannot flow to somewhere else than to the jump set $\mathcal{A}$.

First, it will be shown that any solution starting with initial state $\boldsymbol{x}_0 \in \mathcal{X}_1$ flows to $\mathcal{X}_2$. Then, it will be shown that any solution starting with initial state $\boldsymbol{x}_0 \in \mathcal{X}_2$ converges

to the jump set $\mathcal{A}_1$ (cf. Fig. 4.4). To this end, consider possible flowing directions at a point $\boldsymbol{x} \in \mathcal{X}_1$. Since $\boldsymbol{x} \in \mathcal{X}_1$ implies $x_1 > 0$ and $x_2 \geq 0$, but $x_1 > 0$ and $x_2 \geq 0$ only if $\dot{x}_1 = f_1(\boldsymbol{x}) = x_2 \geq 0$ and $\dot{x}_2 = f_2(\boldsymbol{x}) = -\frac{1}{M}(d(x_1, x_2) + \partial U(x_1)/\partial x_1) < 0$—where the latter inequality holds by virtue of Assumption 4.2 and 4.1 (i. e., $d(x_1, x_2) \geq 0 \iff x_2 \geq 0, \forall x_1 \in \mathbb{R}$ and $\partial U(x_1)/\partial x_1 > 0 \iff x_1 > 0$)—any trajectory $\boldsymbol{x}(t) \in \mathcal{X}_1$ of (4.11) can flow only in the non-negative x_1-direction and in the strictly negative x_2-direction (since $\dot{x}_1 \geq 0$ and $\dot{x}_2 < 0$). Additionally, according to Proposition 4.1, the origin $\boldsymbol{x} = \mathbf{0}$ of the system (4.11) is globally asymptotically stable. This implies that the distance to the origin measured by the Hamiltonian

$$H(\boldsymbol{x}) = T(x_2) + U(x_1) \tag{4.15}$$

of (4.11), where $T(x_2) = \frac{1}{2}Mx_2^2$, is non-increasing. Therefore, any solution starting with initial conditions $\boldsymbol{x}_0 \in \mathcal{X}_1$ flows to $\mathcal{X}_2$. Then, consider all solutions starting with initial conditions $\boldsymbol{x}_0 \in \mathcal{X}_2$. Since $\boldsymbol{x} \in \mathcal{X}_2$ is equivalent to $x_2 \leq 0$, but $x_2 \leq 0$ only if $\dot{x}_1 = f_1(\boldsymbol{x}) = x_2 \leq 0$, any trajectory $\boldsymbol{x}(t) \in \mathcal{X}_2$ of (4.11) can flow only in the non-positive x_1-direction. Furthermore, global asymptotic stability of the origin implies that the system cannot remain somewhere else than at the origin itself. But for any $\boldsymbol{x} \in \mathcal{A}_1$, the distance to the origin is greater than zero, i. e., $H(\boldsymbol{x} \in \mathcal{A}_1) > H(\mathbf{0}) = 0$. Therefore, any solution starting with initial conditions $\boldsymbol{x}_0 \in \mathcal{X}_2$ reaches $\mathcal{A}_1$, when it is approaching the origin. Finally, it should be noted:

Remark 4.2. *The hybrid dynamical system* (4.8)–(4.13) *possesses the central symmetries,* $\mathcal{X}_3 = -\mathcal{X}_1$, $\mathcal{X}_4 = -\mathcal{X}_2$, $\boldsymbol{f}(-\boldsymbol{x}) = -\boldsymbol{f}(\boldsymbol{x})$, $\mathcal{A}_2 = -\mathcal{A}_1$, *and* $\boldsymbol{g}(-\boldsymbol{x}) = -\boldsymbol{g}(\boldsymbol{x})$.

This is a direct consequence of Assumption 4.1, 4.2, and the symmetry of the switching function (4.7). Therefore, the above result holds also for the continuous flow sets $\mathcal{X}_3$ and $\mathcal{X}_4$, respectively.

As a result, any solution of the continuous dynamics (4.11) starting with initial conditions $\boldsymbol{x}_0 \in \mathcal{X}$ reaches the jump set $\mathcal{A}$. This completes the prove. □

Lemma 4.1 guarantees that complete solutions of the hybrid system (4.8)–(4.13) starting with initial conditions $\boldsymbol{x}_0 \in \mathcal{X}$ are continued forever. This property in combination with Remark 4.2 allows to reduce the analysis to one-half of the oscillation cycle.

The idea of the proof of Theorem 4.1 is based on the balance of energies. A particularly important part of the proof is based on the energy exchange during the continuous portion of the hybrid trajectory.

Definition 4.2. *Let*

$$H(\boldsymbol{x}_0) = T(\boldsymbol{x}_0) + U(\boldsymbol{x}_0) = T(\boldsymbol{x}(\boldsymbol{x}_0, t_0)) + U(\boldsymbol{x}(\boldsymbol{x}_0, t_0)), \quad \forall \boldsymbol{x}_0 \in \mathcal{X}_0$$

be the Hamiltonian comprising the kinetic and potential energy of the continuous dynamics (4.11) *right after the jump, where* $t_0 \in \mathbb{R}_{\geq 0}$ *denotes the initial time of the continuous trajectory and let*

$$H(\boldsymbol{x}_-) = T(\boldsymbol{x}_-) + U(\boldsymbol{x}_-) = T(\boldsymbol{x}(\boldsymbol{x}_0, t_1)) + U(\boldsymbol{x}(\boldsymbol{x}_0, t_1)), \quad \forall \boldsymbol{x}_- \in \mathcal{A}$$

be the Hamiltonian at the end of the same continuous trajectory, where $t_1 > t_0$ *denotes the terminal time of the continuous trajectory (i. e., the time-instance right before the next jump).*

Lemma 4.2. *The unsigned energy* $\mu : \mathbb{R}_{\geq 0} \to \mathbb{R}_{\geq 0}$*,*

$$\mu(|x_{0,2}|) := -\left(H(\boldsymbol{x}_-) - H(\boldsymbol{x}_0)\right) = -\int_{t_0}^{t_1} \dot{H}(\boldsymbol{x}(t))\mathrm{d}t = \int_{t_0}^{t_1} d(x_1(t), x_2(t))x_2(t)\mathrm{d}t\,, \quad (4.16)$$

dissipated along continuous trajectories as defined by Definition 4.2 of the dynamical system (4.9) *under Assumption 4.1, 4.2, and 4.3 is a function of the initial velocity* $|x_{0,2}|$ *which is:*

(i) continuous,

(ii) strictly monotonously increasing.

Proof. The statements (i) and (ii) will be proven in the order as stated in the lemma.

In order to show continuity, it is recognized that μ can be expressed as the difference of the Hamiltonians $H(\boldsymbol{x}_0) - H(\boldsymbol{x}_-)$ of the continuous dynamics (4.11). The Hamiltonian $H(\boldsymbol{x}) = T(x_2) + U(x_1)$ is continuous in its arguments, since $T(x_2) = \frac{1}{2}Mx_2^2$ and $U(x_1)$ is continuous in x_2 and x_1 (cf. Assumption 4.1), respectively. Therefore, $H(\boldsymbol{x}_0)$ is continuous in $|x_{0,2}|$. The term $H(\boldsymbol{x}_-)$ depends on the solution $\boldsymbol{x}_- = \boldsymbol{x}(\boldsymbol{x}_0, t_1)$ (cf. Definition 4.2) of the dynamical system (4.9), which in turn depends on the initial condition $\boldsymbol{x}_0$. Since due to Assumption 4.1 and 4.2, the continuous dynamics (4.11) is continuously differentiable in $\boldsymbol{x}$ which implies that $\boldsymbol{f}(\boldsymbol{x})$ is also locally Lipschitz continuous in $\boldsymbol{x}$, solutions $\boldsymbol{x}(\boldsymbol{x}_0, t)$ are continuous in $\boldsymbol{x}_0$ [Kha02, Theorem 3.5, p. 97]. Therefore, the function μ is continuous in its argument $|x_{0,2}|$, which proves statement (i).

Strict monotonicity of μ can be shown by comparing the energy dissipated along two continuous trajectories $\boldsymbol{x}'(t)$ and $\boldsymbol{x}''(t)$ with initial conditions $\boldsymbol{x}_0', \boldsymbol{x}_0'' \in \boldsymbol{g}(\mathcal{A}_2)$ such that $0 \leq x_{0,2}' < x_{0,2}''$, which both evolve from the jump destination set $\boldsymbol{g}(\mathcal{A}_2)$ to the next jump set $\mathcal{A}_1$, and showing that for any $x_{0,2}' < x_{0,2}''$,

$$\int_{t_0'}^{t_1'} d(x_1'(t), x_2'(t))x_2'(t)\mathrm{d}t < \int_{t_0''}^{t_1''} d(x_1''(t), x_2''(t))x_2''(t)\mathrm{d}t \quad (4.17)$$

holds. In order to validate that the above inequality is satisfied, the integrands of (4.17) could have been compared at equal time instances of the trajectories. However, since the durations of both trajectories are in general not equal, i. e., $t_1' - t_0' \neq t_1'' - t_0''$, it is advantageous to eliminate the explicit time dependency of the dissipated power integral (4.16) by the change of integration variables $x_2\mathrm{d}t = \mathrm{d}x_1$ (as proposed in the author's previous work [LAS14b]) which yields

$$\int_{t_0}^{t_1} d(x_1(t), x_2(t))x_2(t)\mathrm{d}t = \int_{2\hat{\theta}-\epsilon_\phi}^{x_1^\star} d(x_1, x_2(x_1))\mathrm{d}x_1 + \int_{x_1^\star}^{\epsilon_\phi} d(x_1, x_2(x_1))\mathrm{d}x_1\,. \quad (4.18)$$

The first integral corresponds to the energy dissipated along the trajectory starting at the jump destination set position $2\hat{\theta} - \epsilon_\phi$ and evolving to the x_1-intercept denoted by $x_1^\star$, i. e., evolving between the borders of the portion $\mathcal{X}_1$ and $\mathcal{X}_2$ of the continuous state space. The second integral corresponds to the energy dissipated along the trajectory starting at $x_1^\star$ and evolving to the next jump set position ϵ_ϕ, i. e., evolving in $\mathcal{X}_2$. The above separation of integrals regarding $\mathcal{X}_1$ and $\mathcal{X}_2$ is always possible, since any trajectory starting in the jump destination set $\boldsymbol{g}(\mathcal{A}_2)$ reaches the next jump set $\mathcal{A}_1$ by virtue of Lemma 4.1. Therefore, the

change of integration variables (4.18) can be applied to the integrals of inequality (4.17) such that (4.17) takes the form

$$\begin{aligned}&\int_{2\hat{\theta}-\epsilon_\phi}^{x_1^{\star\prime}} d(x_1, x_2'(x_1))\mathrm{d}x_1 + \int_{x_1^{\star\prime}}^{\epsilon_\phi} d(x_1, x_2'(x_1))\mathrm{d}x_1 \\ &< \int_{2\hat{\theta}-\epsilon_\phi}^{x_1^{\star\prime\prime}} d(x_1, x_2''(x_1))\mathrm{d}x_1 + \int_{x_1^{\star\prime\prime}}^{\epsilon_\phi} d(x_1, x_2''(x_1))\mathrm{d}x_1\,, \end{aligned} \tag{4.19}$$

where $x_1^{\star\prime}$ and $x_1^{\star\prime\prime}$ represent the x_1-intercepts of the images of $\boldsymbol{x}'(t)$ and $\boldsymbol{x}''(t)$, respectively. As shown in the continuity proof above, the dynamics (4.11) is Lipschitz continuous and therefore solutions of (4.11) are uniquely determined by its initial conditions [Kha02, Theorem 3.2, p. 93]. From uniqueness it follows in turn that

$$x_1^{\star\prime} < x_1^{\star\prime\prime}\,, \tag{4.20}$$

$$x_2'(x_1) < x_2''(x_1)\,, \quad \forall x_1 \in [2\hat{\theta} - \epsilon_\phi; x_1^{\star\prime}] \text{ and } \boldsymbol{x} \in \mathcal{X}_1\,, \tag{4.21}$$

$$x_2''(x_1) \geq 0\,, \quad \forall x_1 \in [x_1^{\star\prime}; x_1^{\star\prime\prime}] \text{ and } \boldsymbol{x} \in \mathcal{X}_1\,, \tag{4.22}$$

$$x_2''(x_1) \leq 0\,, \quad \forall x_1 \in [x_1^{\star\prime\prime}; x_1^{\star\prime}] \text{ and } \boldsymbol{x} \in \mathcal{X}_2\,, \tag{4.23}$$

$$x_2''(x_1) < x_2'(x_1)\,, \quad \forall x_1 \in [x_1^{\star\prime}; \epsilon_\phi] \text{ and } \boldsymbol{x} \in \mathcal{X}_2\,. \tag{4.24}$$

(Intuitively speaking, the image of $\boldsymbol{x}'(t)$ represents the "inner half-orbit" of the image of $\boldsymbol{x}''(t)$.) According to (4.20), each of the integrals on the right hand side of (4.19) can be further separated in two parts:

$$\int_{2\hat{\theta}-\epsilon_\phi}^{x_1^{\star\prime\prime}} d(x_1, x_2''(x_1))\mathrm{d}x_1 = \int_{2\hat{\theta}-\epsilon_\phi}^{x_1^{\star\prime}} d(x_1, x_2''(x_1))\mathrm{d}x_1 + \int_{x_1^{\star\prime}}^{x_1^{\star\prime\prime}} d(x_1, x_2''(x_1))\mathrm{d}x_1\,, \tag{4.25}$$

$$\int_{x_1^{\star\prime\prime}}^{\epsilon_\phi} d(x_1, x_2''(x_1))\mathrm{d}x_1 = \int_{x_1^{\star\prime\prime}}^{x_1^{\star\prime}} d(x_1, x_2''(x_1))\mathrm{d}x_1 + \int_{x_1^{\star\prime}}^{\epsilon_\phi} d(x_1, x_2''(x_1))\mathrm{d}x_1\,. \tag{4.26}$$

Then, since the generalized dissipative force $d(x_1, x_2)$ is strictly monotonously increasing in x_2 (Assumption 4.2), the relations (4.21)–(4.24) imply that

$$\int_{2\hat{\theta}-\epsilon_\phi}^{x_1^{\star\prime}} d(x_1, x_2'(x_1))\mathrm{d}x_1 < \int_{2\hat{\theta}-\epsilon_\phi}^{x_1^{\star\prime}} d(x_1, x_2''(x_1))\mathrm{d}x_1\,, \tag{4.27}$$

$$\int_{x_1^{\star\prime}}^{x_1^{\star\prime\prime}} d(x_1, x_2''(x_1))\mathrm{d}x_1 > 0\,, \tag{4.28}$$

$$\int_{x_1^{\star\prime\prime}}^{x_1^{\star\prime}} d(x_1, x_2''(x_1))\mathrm{d}x_1 > 0\,, \tag{4.29}$$

$$\int_{x_1^{\star\prime}}^{\epsilon_\phi} d(x_1, x_2'(x_1))\mathrm{d}x_1 < \int_{x_1^{\star\prime}}^{\epsilon_\phi} d(x_1, x_2''(x_1))\mathrm{d}x_1\,, \tag{4.30}$$

from which taking (4.25) and (4.26) into account it follows that the assumption of (4.19) and consequently also (4.17) is satisfied. It can be concluded that the energy dissipated along the continuous portion of the trajectory flowing between the borders of $\mathcal{X}_1 \cup \mathcal{X}_2$ is a strictly monotonously increasing function of the initial velocity $x_{0,2}$. Due to the central symmetry of the hybrid system (4.8)–(4.13) (cf. Remark 4.2) an analogous result can be obtained for trajectories flowing between the borders of $\mathcal{X}_3 \cup \mathcal{X}_4$. It can be concluded that the energy dissipated along any trajectory starting in $\mathcal{X}_0$ and flowing to $\mathcal{A}$ is a strictly monotonously increasing function of the initial velocity $|x_{0,2}|$, which validates statement (ii). □

Remark 4.3. *Unboundedness of the dissipation function $\mu(|x_{0,2}|)$ can be achieved, if the Assumptions 4.1 and 4.2 are strengthened such that $d(\phi,\dot{q})\dot{q} \geq d_{\min}\dot{q}^2$, for all $\phi \in \mathbb{R}$ and $\dot{q}(t)^2 \geq \dot{q}(0)^2 \exp(-\alpha t)$ for all $t \geq 0$, where $d_{\min}, \alpha > 0$ are constants. That is,*

$$\int_0^\delta d(\phi,\dot{q})\dot{q}\mathrm{d}t \geq d_{\min}\int_0^\delta \dot{q}^2\mathrm{d}t \geq d_{\min}\dot{q}(0)^2\int_0^\delta \exp(-\alpha t)\mathrm{d}t = d_{\min}\dot{q}(0)^2\frac{1-\exp(-\alpha\delta)}{\alpha}\,,$$

from which it follows that

$$\lim_{|\dot{q}(0)|\to\infty}\int_0^\delta d(\phi,\dot{q})\dot{q}\mathrm{d}t = \infty\,, \quad \forall\delta > 0\,.$$

Since the continuous dynamics (4.11) *is locally Lipschitz, there exists a finite $\delta > 0$ (i. e., the solution of* (4.11) *is continuous in time) such that it can be concluded that $\mu(|x_{0,2}|)$ is unbounded in its argument.*[2]

Proof of Theorem 4.1. In the following, it will be shown that the hybrid system (4.8)–(4.13) has a unique solution of which the image in the state-plane is a hybrid closed orbit.

Consider therefore the total energy exchange of half an oscillation cycle, e. g., consider the total energy exchange of a hybrid trajectory starting in the jump set $\boldsymbol{x}_- \in \mathcal{A}_2$, reseting to the jump destination set $\boldsymbol{x}_0 \in \boldsymbol{g}(\mathcal{A}_2)$ and then flowing continuously to the next jump set $\boldsymbol{x}(\boldsymbol{x}_0, t_1) \in \mathcal{A}_1$ (cf. Fig. 4.4):

$$\Delta H = U(\boldsymbol{x}_0) - U(\boldsymbol{x}_-) + U(\boldsymbol{x}(\boldsymbol{x}_0,t_1)) - U(\boldsymbol{x}_0) + T(\boldsymbol{x}(\boldsymbol{x}_0,t_1)) - T(\boldsymbol{x}_0)\,. \tag{4.31}$$

Remark 4.4. *The jump set $\{\boldsymbol{x} \in \mathcal{A} \,|\, x_2 \neq 0\}$ and the jump destination set $\{\boldsymbol{x} \in \mathcal{X}_0 \,|\, x_2 \neq 0\}$ represent both one-dimensional submanifolds of the continuous state space $\mathcal{X} \subset \mathbb{R}^2$ with (local) coordinate $x_2 \in \mathbb{R}/\{\mathbf{0}\}$ defined by the constraints $x_1 = -\mathrm{sign}(x_2)\epsilon_\phi$ and $x_1 = \mathrm{sign}(x_2)(2\hat{\theta} - \epsilon_\phi)$ according to Definition 2.16 of Sect. 2.4, respectively.*

From the above constraints it follows that the jump sets $\mathcal{A}_1, \mathcal{A}_2$ and consequently the jump destination sets $\boldsymbol{g}(\mathcal{A}_1), \boldsymbol{g}(\mathcal{A}_2)$ are defined such that $x_1 = \text{const.}$ in each set, i. e., $\boldsymbol{x} \in \mathcal{A}_1 \implies x_1 = \epsilon_\phi$, $\boldsymbol{x} \in \mathcal{A}_2 \implies x_1 = -\epsilon_\phi$, $\boldsymbol{x} \in \boldsymbol{g}(\mathcal{A}_1) \implies x_1 = -(2\hat{\theta} - \epsilon_\phi)$, and $\boldsymbol{x} \in \boldsymbol{g}(\mathcal{A}_2) \implies x_1 = 2\hat{\theta} - \epsilon_\phi$. Accordingly, (4.31) can be expressed as

$$\Delta H = U(2\hat{\theta} - \epsilon_\phi) - U(-\epsilon_\phi) + U(\epsilon_\phi) - U(2\hat{\theta} - \epsilon_\phi) + T(\boldsymbol{x}(\boldsymbol{x}_0,t_1)) - T(\boldsymbol{x}_0)\,, \tag{4.32}$$

where the first two differences on the right-hand side are constant. The first difference $U(2\hat{\theta} - \epsilon_\phi) - U(-\epsilon_\phi)$ represents exactly the energy injected by the jump and the second difference $U(\epsilon_\phi) - U(2\hat{\theta} - \epsilon_\phi)$ represents the potential energy exchange of the continuous trajectory (flowing from the initial set $\mathcal{X}_0$ to the jump set $\mathcal{A}$). Since the hybrid system (4.8)–(4.13) is symmetric (cf. Remark 4.2) and in particular, the potential function U is even in its argument (cf. Assumption 4.1), it follows that

$$\Delta U := U(2\hat{\theta} - \epsilon_\phi) - U(-\epsilon_\phi) = -\Big(U(\epsilon_\phi) - U(2\hat{\theta} - \epsilon_\phi)\Big) = c\,, \tag{4.33}$$

where c is a positive constant. This reduces the total energy exchange (4.31) to

$$\Delta H = T(\boldsymbol{x}(\boldsymbol{x}_0,t_1)) - T(\boldsymbol{x}_0)\,. \tag{4.34}$$

[2]The author would like to thank Cosimo Della Santina for discussions and ideas which lead to this statement.

Therefore, by virtue of Lemma 4.1 and the central symmetry (cf. Remark 4.2), the existence and uniqueness of a hybrid closed orbit can be proven, by showing that there exists a unique initial condition $\boldsymbol{x}_0 \in \mathcal{X}_0$ such that $\Delta H = 0$ or equivalently by showing that:

$$(\exists! \boldsymbol{x}_0 \in \mathcal{X}_0)\,[T(\boldsymbol{x}(\boldsymbol{x}_0, t_1)) = T(\boldsymbol{x}_0)]\ . \tag{4.35}$$

By substituting (4.33) in (4.32) it can be seen that condition (4.35) implies that the amount of energy c injected by the jump has to equal the amount of energy dissipated along the continuous portion of the trajectory, i. e.,

$$-\int_{t_0}^{t_1} \dot{H}(t)\mathrm{d}t = \int_{t_0}^{t_1} d(x_1(t), x_2(t))x_2(t)\mathrm{d}t = c\,, \tag{4.36}$$

where $\dot{H}$ represents the derivative of the Hamiltonian H which corresponds to the continuous dynamics (4.11) as introduced by (4.15). The problem of proving condition (4.35) reduces to showing that there exists a unique initial state $\boldsymbol{x}_0 \in \mathcal{X}_0$ such that the amount of energy dissipated during the continuous portion of the trajectory equals the constant c. In particular, since according to Remark 4.4, the set $\mathcal{X}_0$ represents a one-dimensional manifold in a sense that for all $\boldsymbol{x} \in \mathcal{X}_0$, $x_1 = \mathrm{sign}(x_2)(2\hat{\theta} - \epsilon_\phi)$ is determined by x_2, only an initial velocity $|x_{0,2}|$ needs to be found. Furthermore, since from Lemma 4.2 it is known that the dissipated energy in (4.36) is a continuous and strictly monotonously increasing[3] function of the initial velocity $|x_{2,0}|$, it can be concluded that for certain controller parameters $\hat{\theta} > 0$ and $\epsilon_\phi > 0$ (satisfying Assumption 4.3) there exists a unique initial state $\boldsymbol{x}_0 \in \mathcal{X}_0$ such that $\Delta H = 0$, which validates condition (4.35).

Remark 4.5. *In the limit case* $|x_{2,0}| = 0$, $\mu(0) = H(\boldsymbol{x}_0) - H(\boldsymbol{x}(\boldsymbol{x}_0, t_1) = c(\hat{\theta}, \epsilon_\phi) - T(x_2(\boldsymbol{x}_0, t_1)) \leq c(\hat{\theta}, \epsilon_\phi) = \text{const.}$ *since* $T(x_2(\boldsymbol{x}_0, t_1)) > 0$ *for all* $x_2 \neq 0$. *From this it follows that for any controller parameters* $\hat{\theta} > 0$ *and* $\epsilon_\phi > 0$ *satisfying Assumption 4.3, there exists an unique initial velocity* $|x_{2,0}|$ *such that condition* (4.35) *holds.*

Therefore, it can be finally concluded that given any controller parameters $\hat{\theta} > 0$ and $\epsilon_\phi > 0$ satisfying Assumption 4.3, there exists an unique hybrid closed orbit for the system (4.8)–(4.13). □

Remark 4.6 (Poincaré-Bendixson theorem)**.** *The initial state* $\boldsymbol{x}_0^{\mathrm{s}}$ *which satisfies condition* (4.35) *defines two closed, bounded regions* $\mathcal{R}_1 = \{\boldsymbol{x} \in \mathcal{X}_1 \cup \mathcal{X}_2 \,|\, H(\boldsymbol{x}) \leq H(\boldsymbol{x}_0^{\mathrm{s}})\}$ *and* $\mathcal{R}_2 = \{\boldsymbol{x} \in \mathcal{X}_3 \cup \mathcal{X}_4 \,|\, H(\boldsymbol{x}) \leq H(-\boldsymbol{x}_0^{\mathrm{s}})\}$ *consisting of nonsingular points of the continuous dynamics* (4.11) *such that some positive half-paths* $\mathcal{P}_1$ *and* $\mathcal{P}_2$ *of the hybrid system* (4.8)–(4.13) *lie within* $\mathcal{R}_1$ *and* $\mathcal{R}_2$*, respectively. Additionally,* $\mathcal{R}_1$ *and* $\mathcal{R}_2$ *do not contain equilibrium points. If the bounded regions* $\mathcal{R}_1$ *and* $\mathcal{R}_2$ *were "connected" such that the positive half-paths* $\mathcal{P}_1$ *and* $\mathcal{P}_2$ *can be considered as a single, positive half-path* $\mathcal{P}$*, then* $\mathcal{P}$ *is itself a closed phase path according to the Poincaré-Bendixson theorem [JS07, Theorem 11.1, p. 383].*

Due to this remark, the above result may be regarded as an extension of the well-known Poincaré-Bendixson theorem for continuous planar dynamics to the case of reset-induced, hybrid dynamical systems.

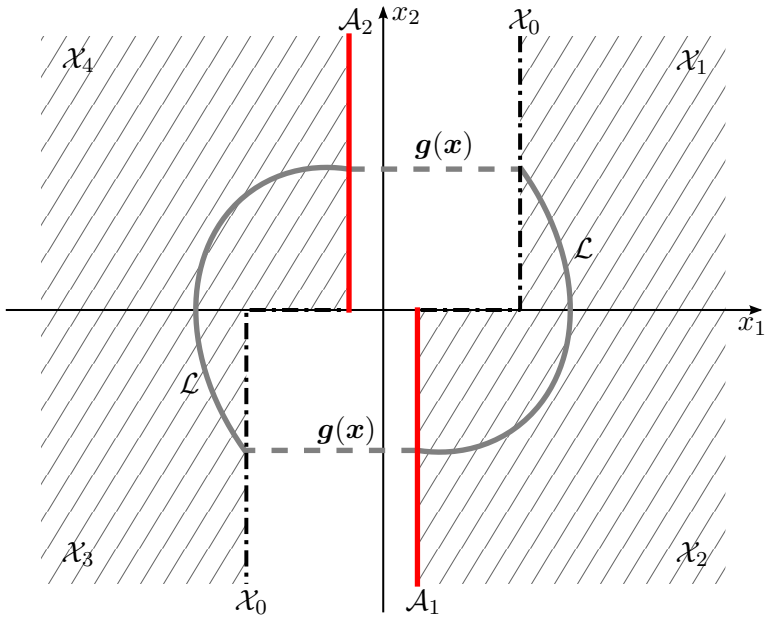

Figure 4.5.: Periodic orbit of the hybrid dynamical system (4.8)–(4.13).

4.7. Hybrid limit cycles

This section derives a stability statement for the hybrid dynamical system (4.8)–(4.13). Consider the hybrid closed orbit represented by the set

$$\mathcal{L} = \{\boldsymbol{x}(\boldsymbol{x}_0, t) \in \mathcal{X} \,|\, t \in \mathbb{R}_{\geq 0}, H(\boldsymbol{x}_0) - H(\boldsymbol{x}_-) = c, \boldsymbol{x}_0 \in \mathcal{X}_0, \boldsymbol{x}_- \in \mathcal{A}\} \,, \tag{4.37}$$

where $H(\boldsymbol{x}_0)$ and $H(\boldsymbol{x}_-)$ denote the Hamiltonian right after the jump and right before the next reset, respectively (cf. Definition 4.2). An example of (4.37) is shown in Fig. 4.5. The existence and uniqueness of $\mathcal{L}$ is implied by Theorem 4.1. In the following, the convergence properties of the system (4.8)–(4.13) w. r. t. $\mathcal{L}$ will be analyzed.

Convergence w. r. t. $\mathcal{L}$ is a set convergence problem, which cannot be directly treated by the concept of Lyapunov stability for equilibrium points. In contrast to asymptotic stability w. r. t. a point, it needs to be shown that the image of any trajectory (of the system (4.8)–(4.13)) converges to the set $\mathcal{L}$. A convergence statement for trajectories is given by the so-called *contraction analysis* introduced by *Lohmiller and Slotine* [LS98]. The convergence statement of the following theorem builds upon the idea of contraction analysis by extending its concepts to the case of hybrid trajectories, where the corresponding continuous Euler-Lagrange dynamics are planar[4]. The main differences of classical and "hybrid" contraction analysis and the definition of the latter are provided in advance of the theorem.

Remark 4.7. *Classical contraction analysis considers a virtual displacement of neighboring trajectories*[5]*, i. e., it considers the infinitesimal difference of trajectories measured at fixed time. Contraction is concluded in the region, where the squared length of the*

[3]The idea of monotonicity of the dissipated energy has also been recognized in [BFDLZ16].
[4]By planar it is meant that the dynamics consist of two states, i. e., $\boldsymbol{x} \in \mathbb{R}^2$
[5]Trajectories are neighboring if their images are contained in a contraction region, which is usually defined by an open ball [LS98].

virtual displacement is strictly decreasing [LS98]. Since the continuous portions of hybrid trajectories are in general not of equal duration, a comparison at fixed time would fail. Therefore, the proposed "hybrid" contraction analysis considers as displacement the distance of neighboring trajectories measured at fixed position x_1.

This motivates the following definition of *hybrid contraction* for planar Hamiltonian dynamics which implies convergence:

Definition 4.3. *Let the jump destination set $\mathcal{X}_0 \subset \mathcal{X}$ and the jump set $\mathcal{A} \subset \mathcal{X}$ be one-dimensional submanifolds of the continuous state space $\mathcal{X}$ defined such that $\boldsymbol{x} \in \mathcal{X}_0 \iff x_1 = \text{const.}$ for all $\text{sign}(x_2) = \text{const.}$ and $\boldsymbol{x} \in \mathcal{A} \iff x_1 = \text{const.}$ for all $\text{sign}(x_2) = \text{const.}$ hold, respectively. Let $\boldsymbol{x}'(t) \in \mathcal{X}$ and $\boldsymbol{x}''(t) \in \mathcal{X}$ be neighboring trajectories (i. e., the images of both trajectories are contained either in $\mathcal{X}_1 \cup \mathcal{X}_2$ or $\mathcal{X}_3 \cup \mathcal{X}_4$) of the same continuous dynamics with Hamiltonian $H(\boldsymbol{x})$ which evolve from $\boldsymbol{x}'(\boldsymbol{x}'_0, t'_0), \boldsymbol{x}''(\boldsymbol{x}''_0, t''_0) \in \mathcal{X}_0$ to $\boldsymbol{x}'(\boldsymbol{x}'_0, t'_1), \boldsymbol{x}''(\boldsymbol{x}''_0, t''_1) \in \mathcal{A}$. Let the signed distance of $\boldsymbol{x}''(t)$ w. r. t. $\boldsymbol{x}'(t)$ in the jump destination set $\mathcal{X}_0$ and in the next jump set $\mathcal{A}$ be measured by the difference of corresponding Hamiltonians $\Delta H_+ = H(\boldsymbol{x}''_0) - H(\boldsymbol{x}'_0)$ and $\Delta H_- = H(\boldsymbol{x}''(\boldsymbol{x}''_0, t''_1)) - H(\boldsymbol{x}'(\boldsymbol{x}'_0, t'_1))$, respectively. Then, the trajectories are said to be contracting if for any initial velocity $x'_{0,2} \neq x''_{0,2}$*

$$|\Delta H_-| < |\Delta H_+| \tag{4.38}$$

holds.

Theorem 4.2. *The image of any trajectory of the hybrid dynamical system* (4.8)–(4.13) *under Assumption 4.1 and 4.2 starting with initial condition $\boldsymbol{x}_0 \in \mathcal{X}$ will contract w. r. t. the hybrid closed orbit $\mathcal{L}$ defined by* (4.37)*, according to Definition 4.3 and thus converge to $\mathcal{L}$.*

Proof. In order to show that the images of all trajectories of the complete system (4.8)–(4.13) starting with initial state $\boldsymbol{x}_0 \in \mathcal{X}_0$ converge to $\mathcal{L}$, it will be shown that the images of their continuous portions converge to $\mathcal{L}$.

Lemma 4.1 implies that any trajectory starting with initial state in the continuous state space, i. e., $\boldsymbol{x}_0 \in \mathcal{X}$, reaches the jump set $\mathcal{A}$ such that the complete solution of the hybrid system (4.8)–(4.13) is continued forever. Therefore, it can be assumed without loss of generality that all continuous trajectories start in the jump destination set $\mathcal{X}_0$, i. e., $\boldsymbol{x}(\boldsymbol{x}_0, t_0) = \boldsymbol{x}_0 \in \mathcal{X}_0$, and end in the next jump set $\mathcal{A}$, i. e., $\boldsymbol{x}(\boldsymbol{x}_0, t_1) \in \mathcal{A}$, where $t_1 > t_0 \geq 0$ are defined as in Definition 4.2. The above problem reduces to showing that the images of these trajectories converge to $\mathcal{L}$ as the system evolves from $\mathcal{X}_0$ to $\mathcal{A}$ and therefore enables considering the convergence argument introduced by Definition 4.3.

Consider the trajectory corresponding to the hybrid closed orbit $\boldsymbol{x}^{\text{n}}(t) \in \mathcal{L}$ as nominal trajectory. Consider further two neighboring trajectories $\underline{\boldsymbol{x}}(t) \in \mathcal{X}$ and $\overline{\boldsymbol{x}}(t) \in \mathcal{X}$ for which $|\underline{x}_{0,2}| < |x^{\text{n}}_{0,2}|$ and $|\overline{x}_{0,2}| > |x^{\text{n}}_{0,2}|$ hold, respectively. (Intuitively speaking, the images of $\underline{\boldsymbol{x}}(t)$ and $\overline{\boldsymbol{x}}(t)$ correspond to the "inner" and "outer" paths of $\mathcal{L}$, respectively.) In the following, each of the neighboring trajectories $\underline{\boldsymbol{x}}(t)$ and $\overline{\boldsymbol{x}}(t)$ are compared to the nominal trajectory $\boldsymbol{x}^{\text{n}}(t)$ by testing condition (4.38) of Definition 4.3, separately.

Let $\Delta\underline{H}_+ = H(\underline{\boldsymbol{x}}_0) - H(\boldsymbol{x}^{\text{n}}_0)$ and $\Delta\underline{H}_- = H(\underline{\boldsymbol{x}}(\underline{\boldsymbol{x}}_0, \underline{t}_1)) - H(\boldsymbol{x}^{\text{n}}(\boldsymbol{x}^{\text{n}}_0, t^{\text{n}}_1))$ represent the signed distance of $\underline{\boldsymbol{x}}(t)$ w. r. t. $\boldsymbol{x}^{\text{n}}(t)$ in the jump destination set $\mathcal{X}_0$ and in the next jump set $\mathcal{A}$, respectively (cf. Definition 4.3). Since $\boldsymbol{x}_0 \in \mathcal{X}_0 \iff x_{0,1} = \text{const.}$ for all $\text{sign}(x_{0,2}) = \text{const.}$ and $\boldsymbol{x} \in \mathcal{A} \iff x_1 = \text{const.}$ for all $\text{sign}(x_2) = \text{const.}$, $U(\underline{\boldsymbol{x}}_0) = U(\boldsymbol{x}^{\text{n}}_0)$ and

$U(\underline{\boldsymbol{x}}(\underline{\boldsymbol{x}}_0, \underline{t}_1)) = U(\boldsymbol{x}^{\mathrm{n}}(\boldsymbol{x}_0^{\mathrm{n}}, t_1^{\mathrm{n}}))$ hold for the potential energy. Since $|\underline{x}_{0,2}| < |x_{0,2}^{\mathrm{n}}|$ and due to uniqueness of solutions of continuous dynamics, $T(\underline{\boldsymbol{x}}_0) < T(\boldsymbol{x}_0^{\mathrm{n}})$ and $T(\underline{\boldsymbol{x}}(\underline{\boldsymbol{x}}_0, \underline{t}_1)) < T(\boldsymbol{x}^{\mathrm{n}}(\boldsymbol{x}_0^{\mathrm{n}}, t_1^{\mathrm{n}}))$ hold for the kinetic energy. This implies that $\Delta\underline{H}_+ < 0$ and $\Delta\underline{H}_- < 0$. Therefore, in this case, the condition for contraction (4.38) of Definition 4.3, $|\Delta\underline{H}_-| < |\Delta\underline{H}_+|$, takes the form:

$$\begin{aligned} \Delta\underline{H}_+ &< \Delta\underline{H}_- \\ H(\underline{\boldsymbol{x}}_0) - H(\boldsymbol{x}_0^{\mathrm{n}}) &< H(\underline{\boldsymbol{x}}(\underline{\boldsymbol{x}}_0, \underline{t}_1)) - H(\boldsymbol{x}^{\mathrm{n}}(\boldsymbol{x}_0^{\mathrm{n}}, t_1^{\mathrm{n}})) \\ H(\underline{\boldsymbol{x}}_0) - H(\underline{\boldsymbol{x}}(\underline{\boldsymbol{x}}_0, \underline{t}_1)) &< H(\boldsymbol{x}_0^{\mathrm{n}}) - H(\boldsymbol{x}^{\mathrm{n}}(\boldsymbol{x}_0^{\mathrm{n}}, t_1^{\mathrm{n}})) \\ -\int_{\underline{t}_0}^{\underline{t}_1} \dot{H}(\underline{\boldsymbol{x}}(t))\mathrm{d}t &< -\int_{t_0^{\mathrm{n}}}^{t_1^{\mathrm{n}}} \dot{H}(\boldsymbol{x}^{\mathrm{n}}(t))\mathrm{d}t\,. \end{aligned} \tag{4.39}$$

The last inequality represents the relation of the amount of energy dissipated along the continuous trajectories $\underline{\boldsymbol{x}}(t)$ and $\boldsymbol{x}^{\mathrm{n}}(t)$, where $|\underline{x}_{0,2}| < |x_{0,2}^{\mathrm{n}}|$ holds. Since from Lemma 4.2 it is known that the energy dissipated along the continuous trajectories of the system (4.8)–(4.13) (evolving from $\mathcal{X}_0$ to $\mathcal{A}$) is a strictly monotonously increasing function of the initial velocity $|x_{0,2}|$, inequality (4.39) holds true. It can be concluded that the trajectories $\underline{\boldsymbol{x}}(t)$ and $\boldsymbol{x}^{\mathrm{n}}(t)$ satisfy condition (4.38) and are therefore contracting according to Definition 4.3.

Let $\Delta\overline{H}_+ = H(\overline{\boldsymbol{x}}_0) - H(\boldsymbol{x}_0^{\mathrm{n}})$ and $\Delta\overline{H}_- = H(\overline{\boldsymbol{x}}(\overline{\boldsymbol{x}}_0, \overline{t}_1)) - H(\boldsymbol{x}^{\mathrm{n}}(\boldsymbol{x}_0^{\mathrm{n}}, t_1^{\mathrm{n}}))$ represent the signed distance of $\overline{\boldsymbol{x}}(t)$ w. r. t. $\boldsymbol{x}^{\mathrm{n}}(t)$ in the jump destination set $\mathcal{X}_0$ and in the next jump set $\mathcal{A}$, respectively (cf. Definition 4.3). Since also in this case $\boldsymbol{x}_0 \in \mathcal{X}_0 \iff x_{0,1} = \text{const.}$ for all $\mathrm{sign}(x_{0,2}) = \text{const.}$ and $\boldsymbol{x} \in \mathcal{A} \iff x_1 = \text{const.}$ for all $\mathrm{sign}(x_2) = \text{const.}$, $U(\overline{\boldsymbol{x}}_0) = U(\boldsymbol{x}_0^{\mathrm{n}})$ and $U(\overline{\boldsymbol{x}}(\overline{\boldsymbol{x}}_0, \overline{t}_1)) = U(\boldsymbol{x}^{\mathrm{n}}(\boldsymbol{x}_0^{\mathrm{n}}, t_1^{\mathrm{n}}))$ hold for the potential energy. Since $|\overline{x}_{0,2}| > |x_{0,2}^{\mathrm{n}}|$ and due to uniqueness of solutions of continuous dynamics, $T(\overline{\boldsymbol{x}}_0) > T(\boldsymbol{x}_0^{\mathrm{n}})$ and $T(\overline{\boldsymbol{x}}(\overline{\boldsymbol{x}}_0, \overline{t}_1)) > T(\boldsymbol{x}^{\mathrm{n}}(\boldsymbol{x}_0^{\mathrm{n}}, t_1^{\mathrm{n}}))$ hold for the kinetic energy. This implies that $\Delta\overline{H}_+ > 0$ and $\Delta\overline{H}_- > 0$. Therefore, in this case, the condition for contraction (4.38) of Definition 4.3, $|\Delta\overline{H}_-| < |\Delta\overline{H}_+|$, takes the form:

$$\begin{aligned} \Delta\overline{H}_+ &> \Delta\overline{H}_- \\ H(\overline{\boldsymbol{x}}_0) - H(\boldsymbol{x}_0^{\mathrm{n}}) &> H(\overline{\boldsymbol{x}}(\overline{\boldsymbol{x}}_0, \overline{t}_1)) - H(\boldsymbol{x}^{\mathrm{n}}(\boldsymbol{x}_0^{\mathrm{n}}, t_1^{\mathrm{n}})) \\ H(\boldsymbol{x}^{\mathrm{n}}(\boldsymbol{x}_0^{\mathrm{n}}, t_1^{\mathrm{n}})) - H(\boldsymbol{x}_0^{\mathrm{n}}) &> H(\overline{\boldsymbol{x}}(\overline{\boldsymbol{x}}_0, \overline{t}_1)) - H(\overline{\boldsymbol{x}}_0) \\ -\int_{t_0^{\mathrm{n}}}^{t_1^{\mathrm{n}}} \dot{H}(\boldsymbol{x}^{\mathrm{n}}(t))\mathrm{d}t &> -\int_{\overline{t}_0}^{\overline{t}_1} \dot{H}(\overline{\boldsymbol{x}}(t))\mathrm{d}t\,. \end{aligned} \tag{4.40}$$

The last inequality represents the relation of the amount of energy dissipated along the continuous trajectories $\overline{\boldsymbol{x}}(t)$ and $\boldsymbol{x}^{\mathrm{n}}(t)$, where $|\overline{x}_{0,2}| > |x_{0,2}^{\mathrm{n}}|$ holds. Due to the strict monotonicity of the dissipated energy (cf. Lemma 4.2) also (4.40) holds true. It can be concluded that the trajectories $\overline{\boldsymbol{x}}(t)$ and $\boldsymbol{x}^{\mathrm{n}}(t)$ satisfy condition (4.38) and are therefore contracting according to Definition 4.3.

The above considered cases imply that the initial velocity $|x_{0,2}| \neq |x_{0,2}^{\mathrm{n}}|$ is arbitrary. As a result it can be concluded that the image of any neighboring trajectory $\boldsymbol{x}(t)$ of the hybrid system (4.8)–(4.13) converges to the hybrid closed orbit $\mathcal{L}$. □

Remark 4.8. *Since the images of complete neighboring trajectories which converge to the hybrid closed orbit, are not closed, the hybrid closed orbit itself is the only isolated path of the system. Therefore, according to the definition of [Str94, Chapt. 7, pp. 196], the hybrid closed orbit is said to be a limit cycle. Since the image of any neighboring trajectory of the hybrid dynamical system* (4.8)–(4.13) *spirals into the hybrid closed orbit, the limit cycle is said to be globally attractive.*

4.8. Summary

This chapter proposes a switching based control principle (4.7) which generates an unique and globally attractive limit cycle in planar, compliantly actuated mechanical systems of the form (4.1). The controller is solely based on measurements of the state at position level, i. e., it requires only the value of the deflection of the elastic element and no differentiation of measured signals, and it requires no parameter-knowledge of a model of the plant to compute the feedback. Since additionally the control principle is such that it switches based on a non-zero threshold value, the controller is robust against sensor-noise and ideally robust against model-parameter uncertainties. This is in contrast to limit cycle controller based on the Van der Pol oscillator, which need to feedback the full state of the plant, and require at least the model-knowledge of the dissipative and elastic element to compute the controller output.

The argumentation in the proof of Theorem 4.1 reveals that the proposed controller solely inputs energy into the compliantly actuated system. In particular, the amount of energy inputed by the controller equals exactly the amount of energy dissipated along the trajectory of the limit cycle. Assuming that the energy transfer from the actuator to the elastic element is associated with substantial losses in both directions (i. e., when the actuator performs work on the elastic element and vice versa), which is the case when, e. g., gear boxes are present, then, the control principle is energy efficient in a sense that it injects the minimum amount of energy into the plant which is required to sustain the limit cycle. This stands in marked contrast to implementations based on the Van der Pol oscillator, where the actuator performs either positive or negative work on the elasticity depending on whether the state of the system is inside or outside of the limit cycle, respectively. A particularly interesting feature of the proposed controller is given by the fact that under certain switching parameter assumption, the resulting control maximizes the energy of the limit cycle for given constant energy input. This can be validated by following a similar argumentation as for the optimal control results of [ÖH13] or the analysis in [SLOAS17].

It can be concluded that from a point of view of robustness and energy efficiency, the proposed switching based limit cycle control represents an advantageous alternative to controller implementations based on the Van der Pol oscillator principle.

A further contribution of this chapter is given by the stability analysis of which the main results are summarized in Theorem 4.1 and 4.2. A main difference of the existence and convergence statements of these theorems compared to ordinary analysis tools as given, e. g., by Lyapunov's stability methods for equilibrium points, results from the property of the closed-loop dynamics (4.1), (4.7) to be a hybrid dynamical system. Thereby, the proof of existence of a unique hybrid closed orbit and the corresponding convergence statement may be regarded as extensions of the well-known Poincaré-Bendixson theorem and Lohmiller's and Slotine's contraction analysis [LS98] to hybrid settings. As such, from the author's point of view, the hybrid stability analysis represents a valuable contribution to the theory of nonlinear systems for itself.

CHAPTER 5

Oscilioulation Modes

The natural or free motion of a mechanical system is the time evolution of configurations, which occurs, when the system state is displaced from its equilibrium. If the mechanical system is conservative, and if its Lagrangian comprises kinetic as well as potential energy, then the natural motions can be oscillatory. The probably simplest example of such a system, which displays natural oscillatory motions, is given by the mass-spring system. Its natural motions are even periodic, i. e., the *same* set of configurations (mass positions) is retraced repeatedly. Therefore, the image of the trajectory in the phase-space is (homeomorphic to) a circle (Fig. 5.1a). By adding a damper in parallel to the spring, natural motions of the resulting mass-spring-damper system can be still oscillatory but not periodic. That is, solely *subsets* of configurations are retraced repeatedly, and the image of the trajectory in the phase-space spirals to the origin (Fig. 5.1b). It can be easily verified that in case of periodic motions, the two-dimensional (2-D) state on the orbit is determined by a single parameter, e. g., the inscribed angle. In contrast, to describe the 2-D state of a general oscillation (with varying amplitude), two parameters are required, e. g., polar angle and radius, although the corresponding second-order differential equation is scalar too. The importance of this distinction becomes evident when turning to *multi-dimensional*, natural oscillatory motions, as can be displayed by the compliantly actuated multibody systems of interest, where the actuators are hold at constant positions. Periodic motions of such a multi-degrees-of-freedom (DOF) system are still governed by a single second-order equation, since the complete state evolves on a 1-D circle, which can be parametrized by a single parameter. This circle is embedded in a 2-D surface, i. e., a 2-D submanifold of the state space (Fig. 5.1c). Now generalizing the definition of general oscillatory motions from the scalar to the multi-dimensional case reveals, that the system configuration evolves on a 1-D curve, i. e., a 1-D submanifold of the configuration space. Since for general oscillatory motions, the amplitude of the oscillation on this curve is allowed to vary, an additional condition is required to determine the complete state by a single parameter. This condition is given by the differentiability of the 1-D submanifold (cf. tangent-vectors in Fig. 5.1d), which provides the directional relation between configuration and velocity such that the oscillatory motion can be described by a single, scalar, second-order equation. In summary, periodic motions can be described on 2-D submanifolds of the state space or under certain conditions (Theorem 5.3) on 1-D, differentiable submanifolds of

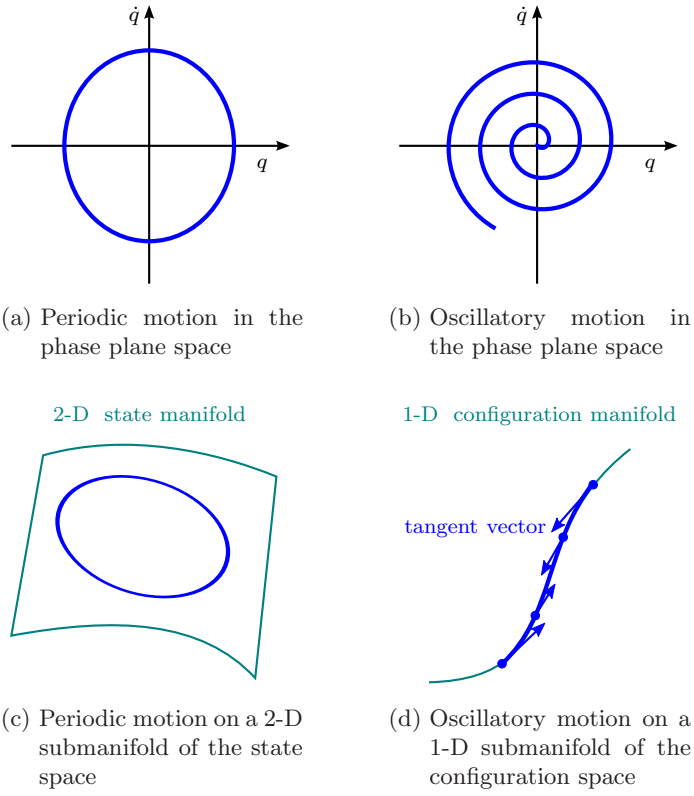

(a) Periodic motion in the phase plane space

(b) Oscillatory motion in the phase plane space

(c) Periodic motion on a 2-D submanifold of the state space

(d) Oscillatory motion on a 1-D submanifold of the configuration space

Figure 5.1.: Definition of oscillatory and periodic motions on modal manifolds.

the configuration space, while general oscillatory motions require the latter. Thus, the goal of analyzing and exploiting the natural oscillatory behavior of compliantly actuated multibody systems, motivates the introduction of the concept of *oscillation modes*, which *are said to be invariant, 1-D, differentiable submanifolds of the configuration space.*

In the literature [Ros66], [Ran71], [Ran74], [CVS90], [SP93], the problems of natural oscillatory and periodic motions are both treated by the concept of so-called *normal modes*. This reduction of dynamics originates in the analysis of periodic solutions of nonlinear but conservative mass-spring systems [Ros66], [Ran71], [Ran74], [CVS90]. The corresponding dynamics takes only velocity independent forces into account, i. e., the mass matrix is constant and no dissipative forces are present. Therefore, corresponding periodic solutions (if they exist) can be parametrized by 1-manifolds. Although [Ran74] and [CVS90] present explicit parameterizations for two-DOF systems of constant inertia but nonlinear and coupled springs, the dynamics of nonlinear, elastic multibody systems has not been considered so far. The general definition of normal modes [SP93] parametrizes the motion in terms of a single coordinate-velocity pair (2-manifold). As such, this definition contains also the case, where, e. g., Coriolis/centrifugal terms appear. However, the procedure proposed in [SP93] involves solutions of nonlinear, coupled partial differential equations, of which obtaining explicit solutions is even more difficult than solving the original dynamics itself. Therefore, existing approaches focus on the approximation of normal modes, mainly for continuous mechanical systems such as in [SP94], [BPS95], [PPS02], which are rather circumstantial for the multibody problem at hand.

The goal of this chapter is to parameterize the natural, oscillatory motions of nonlinear,

elastic multibody systems by an 1-D submanifold of the configuration space for subclasses of systems which allow such parameterizations. In Sect. 5.1 a definition of such *oscillation modes* is derived, by first revisiting the well-known concept of eigenmodes for linear systems based upon its differential geometric implications (Sect. 5.1.1) and then transferring the gained insights to the nonlinear domain. This results in the notion of eigenmodes of nonlinear dynamics as proposed in Sect. 5.1.2 [LFAS17]. Although the concept of so-called *modal lines* has already been recognized in [CVS90], the definition of eigenmodes at hand is more general, since it allows to take dynamics into account, which contains configuration dependent inertias and damping forces. A general definition of nonlinear oscillation modes is proposed in Sect. 5.1.3. In comparison to normal modes [SP93], this definition seems to be restrictive, since it considers only motions which can be parameterized by 1-D, differentiable submanifold of the configuration space, rather than by 2-D submanifolds of the state space. However, as discussed above, this restriction becomes necessary as soon as general oscillations, e. g., with decaying amplitudes are considered. Sect. 5.2 proposes a methodology to embody desired eigenmodes, e. g., corresponding to a task, in the nonlinear dynamics of elastic multibody systems, by design. Thereby, the approach yields a practically relevant and realizable example, which serves as "ground truth" to investigate and classify periodic orbits as provided in Sect. 5.3 [LPAS14].

5.1. Definition

The following definitions of oscillation modes are concerned with natural dynamics, i. e., the behavior of compliantly actuated mechanical systems as introduced in Sect. 3.1.1, where their directly actuated degrees of freedom are hold at constant positions. Consider therefore the dynamics

$$\boldsymbol{M}(\boldsymbol{q})\ddot{\boldsymbol{q}} + \boldsymbol{b}(\boldsymbol{q}, \dot{\boldsymbol{q}}) = -\frac{\partial U(\boldsymbol{q})}{\partial \boldsymbol{q}}^T \tag{5.1}$$

which corresponds to the PD controlled, compliantly actuated system (3.50) under the singular perturbation assumption of Sect. 3.2.3. The solely formal differences of (5.1) w. r. t. (3.50) are: $\boldsymbol{\theta}_{\mathrm{des}}$ of (3.50) is chosen to be constant such that according to Definition 3.4 of Sect. 3.1.1,

$$\left.\frac{\partial U(\boldsymbol{q})}{\partial \boldsymbol{q}}\right|_{\boldsymbol{q}=\bar{\boldsymbol{q}}_0(\boldsymbol{\theta}_{\mathrm{des}})} = \boldsymbol{0}\,, \tag{5.2}$$

and the generalized Coriolis/centrifugal and damping forces are summarized in the bias term

$$\boldsymbol{b}(\boldsymbol{q}, \dot{\boldsymbol{q}}) = \boldsymbol{C}(\boldsymbol{q}, \dot{\boldsymbol{q}})\dot{\boldsymbol{q}} + \boldsymbol{d}(\boldsymbol{q}, \dot{\boldsymbol{q}})\,, \tag{5.3}$$

where the dependency on $\boldsymbol{\theta}_{\mathrm{des}}$ is omitted, since desired actuator positions $\boldsymbol{\theta}_{\mathrm{des}}$ are constants.

5.1.1. Eigenmodes of linear dynamics

The concept of eigenmodes of linear dynamics is well-known from linear oscillation and control theory. However, its physical and geometrical interpretation provides insights about the notion of oscillation modes in the nonlinear case.

To this end, consider the linearization of the dynamics (5.1)

$$\boldsymbol{M}(\boldsymbol{q}_0)\Delta\ddot{\boldsymbol{q}} = -\boldsymbol{K}(\boldsymbol{q}_0)\Delta\boldsymbol{q} \tag{5.4}$$

at the equilibrium position $\boldsymbol{q}_0 = \bar{\boldsymbol{q}}_0(\boldsymbol{\theta}_{\mathrm{des}})$ as defined by (5.2). The Hessian of the potential energy

$$\boldsymbol{K}(\boldsymbol{q}_0) = \left.\frac{\partial^2 U(\boldsymbol{q})}{\partial \boldsymbol{q}^2}\right|_{\boldsymbol{q}=\boldsymbol{q}_0} \tag{5.5}$$

is referred to as the stiffness at the equilibrium position $\boldsymbol{q}_0$, and the bias terms (5.3) are neglected in the first instance. The relevance of velocity dependent forces for eigenmodes will be discussed later.

To solve the system of linear, second-order differential equations (5.4), the complex (harmonic) ansatz $\Delta\boldsymbol{q}(t) = \boldsymbol{w}\hat{z}\exp(\jmath\omega t)$ with amplitude $\hat{z}$ and frequency ω gives rise to the generalized eigenvalue problem

$$\lambda\boldsymbol{M}(\boldsymbol{q}_0)\boldsymbol{w} = \boldsymbol{K}(\boldsymbol{q}_0)\boldsymbol{w} \tag{5.6}$$

$$\text{s.t. } \|\boldsymbol{w}\|^2 = 1\,. \tag{5.7}$$

Herein, the eigenvalue $\lambda = \omega^2$ represents the squared eigenfrequency of the oscillation corresponding to the eigenvector $\boldsymbol{w}$. Due to the normalization (5.7), where $\|\boldsymbol{w}\|^2$ represents the squared length of $\boldsymbol{w}$ measured w. r. t. to a certain metric $\boldsymbol{S}$ (cf. Definition 2.6 and 2.7 of Sect. 2.2.2), the eigenvector $\boldsymbol{w}$ determines only the direction of oscillation. In general, the generalized eigenvalue problem (5.6), (5.7) possesses n distinct solutions $\{\lambda_i, \boldsymbol{w}_i\}$ for $i = 1 \ldots n$, each comprising a (squared) oscillation frequency and direction, which are referred to as the *eigenmodes* of the linear dynamics (5.4).

The generalized eigenvalue equations (5.6) can be interpreted according to Newton's third law as balance of inertial and elastic forces, $\lambda\boldsymbol{M}\boldsymbol{w}z$ and $\boldsymbol{K}\boldsymbol{w}z$, respectively: Any displacement $z \in \mathbb{R}$ in the direction of an eigenvector $\boldsymbol{w}$, $\Delta\boldsymbol{q} = \boldsymbol{w}z$, leads to an elastic force which causes an acceleration of the system in same direction as the displacement, i. e., $\Delta\ddot{\boldsymbol{q}} = -\lambda\Delta\boldsymbol{q} = -\boldsymbol{M}^{-1}\boldsymbol{K}\Delta\boldsymbol{q}$. In particular, the resulting acceleration $\Delta\ddot{\boldsymbol{q}}$ is proportional to the displacement $\Delta\boldsymbol{q}$, where the constant of proportionality is λ. As such, any solution of the linear dynamics (5.4) starting with an initial displacement in the direction of $\boldsymbol{w}$, $\Delta\boldsymbol{q}(0) = \boldsymbol{w}z(0)$, evolves strictly along $\boldsymbol{w}$, since the system accelerates exclusively along $\boldsymbol{w}$.

A sufficient condition for the existence of eigenmodes of linear dynamics (5.4) follows from the following lemma taken from [HJ85, Theorem 7.6.6, p. 466]:

Lemma 5.1. *Given a $n \times n$, positive definite matrix $\boldsymbol{A}$ and a $n \times n$ symmetric matrix $\boldsymbol{B}$, then there exists a nonsingular matrix $\boldsymbol{W}$ such that the matrices $\boldsymbol{W}^T\boldsymbol{A}\boldsymbol{W}$ and $\boldsymbol{W}^T\boldsymbol{B}\boldsymbol{W}$ are both diagonal.*

By letting $\boldsymbol{A} \triangleq \boldsymbol{M}$ and $\boldsymbol{B} \triangleq \boldsymbol{K}$, this lemma implies that there exists n independent eigenvectors $\boldsymbol{W} = [\boldsymbol{w}_1 \ldots \boldsymbol{w}_n]$ and corresponding eigenvalues $\lambda_1 \ldots \lambda_n$ satisfying the generalized eigenvalue equations (5.6), since $\boldsymbol{M}$ is positive definite by definition (cf. Remark 2.2 of Sect. 2.2.2) and $\boldsymbol{K}$ is symmetric according to Schwarz's theorem on mixed partial derivatives.

Consider now also the linearization of the generalized velocity dependent bias terms (5.3),

$$\boldsymbol{D}(\boldsymbol{q}_0)\Delta\dot{\boldsymbol{q}} = \left.\frac{\partial \boldsymbol{d}(\boldsymbol{q}, \dot{\boldsymbol{q}})}{\partial \dot{\boldsymbol{q}}}\right|_{\boldsymbol{q}=\boldsymbol{q}_0, \dot{\boldsymbol{q}}=\boldsymbol{0}} \Delta\dot{\boldsymbol{q}}\,, \tag{5.8}$$

in the linear dynamics (5.4), which yields

$$\boldsymbol{M}(\boldsymbol{q}_0)\Delta\ddot{\boldsymbol{q}} = -\boldsymbol{K}(\boldsymbol{q}_0)\Delta\boldsymbol{q} - \boldsymbol{D}(\boldsymbol{q}_0)\Delta\dot{\boldsymbol{q}}\,. \tag{5.9}$$

Then, for certain matrices $\boldsymbol{D}(\boldsymbol{q}_0)$, any displacement $z \in \mathbb{R}$ and any velocity $\dot{z} \in \mathbb{R}$ in the direction of an eigenvector $\boldsymbol{w}$ (of (5.6)), $\Delta\boldsymbol{q} = \boldsymbol{w}z$ and $\Delta\dot{\boldsymbol{q}} = \boldsymbol{w}\dot{z}$, respectively, cause an acceleration of the system in equal direction as the displacement and velocity, i. e., $\Delta\ddot{\boldsymbol{q}} = \boldsymbol{w}\ddot{z} = -\boldsymbol{M}^{-1}\left(\boldsymbol{K}\Delta\boldsymbol{q} + \boldsymbol{D}\Delta\dot{\boldsymbol{q}}\right) = -\boldsymbol{M}^{-1}\left(\boldsymbol{K}\boldsymbol{w}z + \boldsymbol{D}\boldsymbol{w}\dot{z}\right)$, where $\ddot{z} \in \mathbb{R}$ represents the acceleration amplitude. Therefore, any solution of the linear damped dynamics (5.9) starting with initial states in the direction of $\boldsymbol{w}$, $\Delta\boldsymbol{q}(0) = \boldsymbol{w}z(0)$ and $\Delta\dot{\boldsymbol{q}}(0) = \boldsymbol{w}\dot{z}(0)$, evolves strictly along $\boldsymbol{w}$, since the system accelerates exclusively along $\boldsymbol{w}$.

A sufficient condition regarding the structure of the matrix $\boldsymbol{D}$ is a direct consequence of Lemma 5.1:

Corollary 5.1. *Given the matrices of Lemma 5.1 and a $n \times n$ matrix $\boldsymbol{D}$, then $\boldsymbol{W}^T\boldsymbol{D}\boldsymbol{W}$ is a diagonal matrix if $\boldsymbol{D} = c_1\boldsymbol{A} + c_2\boldsymbol{B}$, is a linear combination of $\boldsymbol{A}$ and $\boldsymbol{B}$.*

Proof. The proof follows directly from Lemma 5.1, i. e.,

$$\boldsymbol{W}^T\boldsymbol{D}\boldsymbol{W} = \boldsymbol{W}^T\left(c_1\boldsymbol{A} + c_2\boldsymbol{B}\right)\boldsymbol{W} = c_1\boldsymbol{W}^T\boldsymbol{A}\boldsymbol{W} + c_2\boldsymbol{W}^T\boldsymbol{B}\boldsymbol{W}\,.$$

□

The above interpretation reveals that eigenmodes of linear dynamics (5.9) are solutions which evolve on an 1-D submanifold of the n-dimensional configuration space. Thereby, Lemma 5.1 and Corollary 5.1 provides sufficient conditions for their existence.

Remark 5.1. *The linear dynamics of the form* (5.9) *features n eigenmodes, if there exists a nonsingular $n \times n$ matrix $\boldsymbol{W}$ such that the i-th scalar differential equation of* (5.9) *under the change of coordinates $\boldsymbol{z} = \boldsymbol{W}^{-1}\Delta\boldsymbol{q}$,*

$$\ddot{z}_i = h_i(z_i, \dot{z}_i)\,, \tag{5.10}$$

where

$$\boldsymbol{h}(\boldsymbol{z}, \dot{\boldsymbol{z}}) = -\left(\boldsymbol{W}^T\boldsymbol{M}\boldsymbol{W}\right)^{-1}\left(\boldsymbol{W}^T\boldsymbol{K}\boldsymbol{W}\boldsymbol{z} + \boldsymbol{W}^T\boldsymbol{D}\boldsymbol{W}\dot{\boldsymbol{z}}\right)\,, \tag{5.11}$$

depends exclusively on z_i and $\dot{z}_i$ for each $i = 1 \ldots n$.

Although, the concept of eigenmodes of linear dynamics is well-known from linear oscillation and control theory, its geometrical interpretation provides substantial insights relevant for the definition of oscillation modes in the nonlinear case.

5.1.2. Eigenmodes of nonlinear dynamics

The geometrical interpretation of the generalized eigenvalue problem provided in the previous section allows to contribute a novel, intuitive extension of the concept of eigenmodes for general nonlinear dynamics of the form (5.1). In the following definition, the configuration manifold is assumed to be Euclidean space (i. e., $\boldsymbol{q} \in \mathbb{R}^n$ with identity metric).

Definition 5.1. *Let $\boldsymbol{q}_0$ be the equilibrium configuration of the system* (5.1) *and let $\boldsymbol{w}$ be the components of a constant vector of Euclidean space (i. e., $\boldsymbol{w} \in \mathbb{R}^n$). Let further $\Delta\boldsymbol{q} = \boldsymbol{q} - \boldsymbol{q}_0 = \boldsymbol{w}z$ and $\dot{\boldsymbol{q}} = \boldsymbol{w}\dot{z}$ be a displacement and a generalized velocity of amplitudes $z \in \mathbb{R}$ and $\dot{z} \in \mathbb{R}$ along $\boldsymbol{w}$, respectively. Then, $\boldsymbol{w} = \text{const.}$ is an eigenvector of the nonlinear dynamics* (5.1)*, if for any $z \in \mathbb{R}$ and $\dot{z} \in \mathbb{R}$ there exists a scalar $\ddot{z} = \ddot{z}(z, \dot{z}) \in \mathbb{R}$ (which represents the amplitude of acceleration along $\boldsymbol{w}$, i. e., $\ddot{\boldsymbol{q}} = \boldsymbol{w}\ddot{z}$) such that*

$$\boldsymbol{M}(\boldsymbol{q}_0 + \boldsymbol{w}z)\boldsymbol{w}\ddot{z} = -\boldsymbol{b}(\boldsymbol{q}_0 + \boldsymbol{w}z, \boldsymbol{w}\dot{z}) - \left.\frac{\partial U(\boldsymbol{q})}{\partial \boldsymbol{q}}\right|^T_{\boldsymbol{q}=\boldsymbol{q}_0+\boldsymbol{w}z} \tag{5.12}$$

is satisfied.

An eigenvector $\boldsymbol{w}$ according to Definition 5.1 together with a metric $\boldsymbol{S}$ such that $\|\boldsymbol{w}\|^2 = 1$ (cf. Definition 2.7 of Sect. 2.2.2) defines a linear transformation of the form $\Delta\boldsymbol{q} = \boldsymbol{q} - \boldsymbol{q}_0 = \boldsymbol{w}z$ and $\dot{\boldsymbol{q}} = \boldsymbol{w}\dot{z}$, where $z \in \mathbb{R}$ and $\dot{z} \in \mathbb{R}$ are referred to as modal coordinate and velocity, respectively. The set of all motions of the nonlinear dynamics (5.1), which can be parameterized by z and $\dot{z}$, exclusively, is referred to as an *eigenmode* of (5.1). By recalling the concept of invariant sets for dynamical systems (e. g., known from Lyapunov's stability theory [SL91, Definition 3.9, p. 68], a condition for the existence of eigenmodes can be formulated as follows.

Theorem 5.1. *Let $(\boldsymbol{q}, \dot{\boldsymbol{q}}) \in (\subseteq \mathbb{R}^n) \times \mathbb{R}^n$ be the state of the nonlinear dynamics* (5.1) *with equilibrium position $\boldsymbol{q}_0$ and let $\boldsymbol{w} \in \mathbb{R}^n$ be a constant vector. Let further $\bar{\boldsymbol{W}} = \ker\left(\boldsymbol{w}^T\right)$ be a $n \times (n-1)$ matrix of rank $n-1$ such that $\bar{\boldsymbol{W}}^T\boldsymbol{w} = \boldsymbol{0}$. If $\boldsymbol{w}$ satisfies condition* (5.12) *of Definition 5.1, then, the tangent bundle $\mathcal{TW}$ of the subset of configurations*

$$\mathcal{W} := \left\{\boldsymbol{q} \in \subseteq \mathbb{R}^n \,|\, \bar{\boldsymbol{W}}^T(\boldsymbol{q} - \boldsymbol{q}_0) = \boldsymbol{0}\right\} \tag{5.13}$$

represents an invariant set of the nonlinear dynamics (5.1)*. (The subset $\mathcal{W}$ is referred to as an eigenmode of* (5.1)*).*

Note that since the constraints at velocity level are related to the constraints at position level by differentiation w. r. t. to the independent variable of time, eigenmodes represent 1-D, differentiable submanifolds of the configuration space $\subseteq \mathbb{R}^n$.

Proof. Consider the dynamics (5.1) with equilibrium position $\boldsymbol{q}_0$. Assume that the system starts at an initial position $\boldsymbol{q}(0) = \boldsymbol{q}_0 + \boldsymbol{w}z(0)$ at rest, i. e., $\dot{\boldsymbol{q}}(0) = \boldsymbol{0}$. The initial displacement $\boldsymbol{w}z(0)$ w. r. t. the equilibrium position $\boldsymbol{q}_0$ causes a potential force which implies an acceleration

$$\ddot{\boldsymbol{q}} = -\boldsymbol{M}(\boldsymbol{q}_0 + \boldsymbol{w}z(0))^{-1} \left.\frac{\partial U(\boldsymbol{q})}{\partial \boldsymbol{q}}\right|^T_{\boldsymbol{q}=\boldsymbol{q}_0+\boldsymbol{w}z(0)}$$

according to (5.1). Since $\boldsymbol{w}$ is an eigenvector of (5.1), condition (5.12) of Definition 5.1 implies an initial acceleration along $\boldsymbol{w}$, i. e., $\ddot{\boldsymbol{q}} = \boldsymbol{w}\ddot{z}(0)$ such that the state of the system evolves along $\boldsymbol{w}$, i. e., $\boldsymbol{q}(t) = \boldsymbol{q}_0 + \boldsymbol{w}z(t)$ and $\dot{\boldsymbol{q}}(t) = \boldsymbol{w}\dot{z}(t)$. Since for any displacement $\boldsymbol{q}(t) - \boldsymbol{q}_0 = \boldsymbol{w}z(t)$ and for any velocity $\dot{\boldsymbol{q}}(t) = \boldsymbol{w}\dot{z}(t)$ condition (5.12) implies an acceleration along $\boldsymbol{w}$, i. e., $\ddot{\boldsymbol{q}}(t) = \boldsymbol{w}\ddot{z}(t)$ for all $t > 0$, all solutions of the dynamics (5.1) starting with initial conditions $\boldsymbol{q}(0) = \boldsymbol{q}_0 + \boldsymbol{w}z(0)$ and $\dot{\boldsymbol{q}}(0) = \boldsymbol{0}$ are such that the state $(\boldsymbol{q}, \dot{\boldsymbol{q}})$ remains in the set $\mathcal{TW}$ defined by (5.13) for all future time $t > 0$. By virtue of condition (5.12), this result holds also in case of nonzero initial velocities $\dot{\boldsymbol{q}}(0) = \boldsymbol{w}\dot{z}(0) \neq \boldsymbol{0}$. Therefore, it can be concluded that the set $\mathcal{TW}$ (defined by the eigenmode $\mathcal{W}$ of the nonlinear dynamics (5.1)) is an invariant set of the dynamical system (5.1). □

The $n-1$ holonomic, linear constraints $\bar{\boldsymbol{W}}^T(\boldsymbol{q}-\boldsymbol{q}_0)=\boldsymbol{0}$ in (5.13) define a 1-D submanifold of the configuration space $\mathbb{R}^n$ (cf. Definition 2.16 of Sect. 2.4). Thereby, this 1-manifold defines together with its tangent spaces a 2-D invariant set of states corresponding to the nonlinear dynamics (5.1). As will be justified immediately, it is not necessary that the $n-1$ constraints, defining such an invariant 1-manifold, are linear. In general, the $n-1$ constraints, defining the 2-D, invariant subset $\mathcal{T}W$ of $(\subseteq \mathbb{R}^n)\times\mathbb{R}^n$ can be nonlinear, which leads to the concept of general *oscillation modes*.

5.1.3. A general definition

The idea of general oscillation modes can already be explained by the concept of eigenvectors of nonlinear dynamics as proposed above:

Consider n linearly independent vectors $\boldsymbol{w}_i$ for $i=1\ldots n$ such that the matrix $\boldsymbol{W}=[\boldsymbol{w}_1\ldots\boldsymbol{w}_n]$ is nonsingular. Suppose that the j-th column of $\boldsymbol{W}$ for $j\in\{1,\ldots,n\}$, $\boldsymbol{w}_j$ is an eigenvector of the nonlinear dynamics (5.1) according to Definition 5.1. The matrix $\boldsymbol{W}$ defines a linear coordinate transformation of the form $\boldsymbol{q}-\boldsymbol{q}_0=\boldsymbol{W}\boldsymbol{z}$ such that the dynamics (5.1) under this change of coordinates can be expressed as

$$\ddot{\boldsymbol{z}}=\boldsymbol{h}(\boldsymbol{z},\dot{\boldsymbol{z}})=-\left[\boldsymbol{W}^T\boldsymbol{M}(\boldsymbol{z})\boldsymbol{W}\right]^{-1}\left[\boldsymbol{W}^T\boldsymbol{b}(\boldsymbol{z},\dot{\boldsymbol{z}})+\frac{\partial U(\boldsymbol{z})}{\partial \boldsymbol{z}}^T\right]. \tag{5.14}$$

Since $\boldsymbol{w}_j$ is an eigenvector of the dynamics (5.1), Theorem 5.1 implies that the tangent bundle $\mathcal{TW}_j$ of the subset of configurations

$$\mathcal{W}_j=\left\{\boldsymbol{q}\in\mathbb{R}^n \,|\, \boldsymbol{w}_i^\dagger(\boldsymbol{q}-\boldsymbol{q}_0)=0, \forall i\in\{1\ldots n\}/\{j\}\right\} \tag{5.15}$$

where

$$\begin{bmatrix}\boldsymbol{w}_1^\dagger\\ \vdots\\ \boldsymbol{w}_n^\dagger\end{bmatrix}:=\begin{bmatrix}\boldsymbol{w}_1 & \ldots & \boldsymbol{w}_n\end{bmatrix}^{-1},$$

is an invariant set of (5.1), which can be completely parameterized by the modal coordinate and velocity, $z_j\in\mathbb{R}$ and $\dot{z}_j\in\mathbb{R}$, respectively. The property that z_j and $\dot{z}_j$ parametrizes all coordinates and velocities in the invariant set $\mathcal{TW}_j$, respectively, implies in turn that if $z_i=\dot{z}_i=0$ for all $i\in\{1\ldots n\}/\{j\}$, then,

$$\ddot{z}_i=h_i(\boldsymbol{z},\dot{\boldsymbol{z}})=0$$

for all $i\in\{1\ldots n\}/\{j\}$ and for all $z_j,\dot{z}_j\in\mathbb{R}$, and obviously, the dynamics in $\mathcal{TW}_j$

$$\ddot{z}_j=h_j(z_j,\dot{z}_j)$$

depends exclusively on the corresponding modal coordinate and velocity, z_j and $\dot{z}_j$, respectively.

It is worth mentioning that in case $z_i\neq 0$ and $\dot{z}_i\neq 0$, the modal acceleration $\ddot{z}_j$ depends in general on the complete state $(\boldsymbol{z},\dot{\boldsymbol{z}})$, i. e., $\ddot{z}_j=h_j(\boldsymbol{z},\dot{\boldsymbol{z}})$. This stands in marked contrast to eigenmodes of linear dynamics as investigated in Sect. 5.1.1, where the dynamics of each eigenmode is completely decoupled in a sense that the acceleration of each mode depends only on its own state, independently of whether the system state evolves in the

corresponding invariant set or not. The linear constraints defining invariant sets $\mathcal{TW}_j$ to be regular planes of $(\subseteq \mathbb{R}^n) \times \mathbb{R}^n$ make the concept of eigenmodes, although of nonlinear dynamics, still a particular case, since the images of trajectories of nonlinear dynamics are in general also nonlinear. Note further that the configuration space needs not to be the Euclidean space $\subseteq \mathbb{R}^n$. These considerations motivate a more general concept of *oscillation modes*:

Definition 5.2. *Consider the system of second-order dynamics*

$$\ddot{\boldsymbol{q}} = \boldsymbol{g}(\boldsymbol{q}, \dot{\boldsymbol{q}}) \tag{5.16}$$

with (local) configuration coordinates $\boldsymbol{q} \in \subseteq \mathbb{R}^n$*, velocities* $\dot{\boldsymbol{q}} \in \mathbb{R}^n$*, respectively, and a unique equilibrium point at the origin such that* $\boldsymbol{g}(\boldsymbol{q}, \dot{\boldsymbol{q}}) = \boldsymbol{0} \iff \boldsymbol{q} = \dot{\boldsymbol{q}} = \boldsymbol{0}$*. Let*

$$\boldsymbol{z} = \boldsymbol{z}(\boldsymbol{q}) \in \subseteq \mathbb{R}^n \tag{5.17}$$

be a diffeomorphism such that the inverse $\boldsymbol{J}(\boldsymbol{q})^{-1}$ *of the Jacobian matrix* $\boldsymbol{J}(\boldsymbol{q}) = \partial \boldsymbol{z}(\boldsymbol{q})/\partial \boldsymbol{q}$ *keeps bounded from above, i. e.,* $\sup_{\boldsymbol{q} \in \subseteq \mathbb{R}^n} \left\| \boldsymbol{J}(\boldsymbol{q})^{-1} \right\| < \infty$*. If the dynamics* (5.16) *under the change of coordinates,*

$$\ddot{\boldsymbol{z}} = \boldsymbol{h}(\boldsymbol{z}, \dot{\boldsymbol{z}}) = \boldsymbol{J}(\boldsymbol{z})^{-1} \boldsymbol{g}(\boldsymbol{z}, \dot{\boldsymbol{z}}) \tag{5.18}$$

features the property that there exists an $j \in \{1, \ldots, n\}$ *and constants* c_i *such that if* $z_i = c_i$ *and* $\dot{z}_i = 0$*,*

$$h_i(\boldsymbol{z}, \dot{\boldsymbol{z}}) = 0\,, \tag{5.19}$$

for all $i \in \{1, \ldots, n\}/\{j\}$ *and for all* $z_j \in \subseteq \mathbb{R}$ $\dot{z}_j \in \mathbb{R}$*, then the following holds true:*

The 1-D, differentiable submanifold of the configuration space with local coordinates $\boldsymbol{q} \in \subseteq \mathbb{R}^n$*,*

$$\mathcal{Z}_j := \{\boldsymbol{q} \in (\subseteq \mathbb{R}^n) \,|\, z_i(\boldsymbol{q}) - c_i = 0, \forall i \in \{1, \ldots, n\}/\{j\}\}\,, \tag{5.20}$$

defines a 2-D, invariant subset $\mathcal{T}\mathcal{Z}_j$ *of the state space* $(\subseteq \mathbb{R}^n) \times \mathbb{R}^n$*, which is said to be an oscillation mode of the nonlinear dynamics* (5.16)*.*

By applying this definition to the dynamics of the compliantly actuated system at hand (5.1), particular insights regarding the structure of the change of coordinates (5.17) can be gained:

Theorem 5.2. *Consider the dynamics* (5.1) *under the change of coordinates* (5.17)*:*

$$\ddot{\boldsymbol{z}} = \boldsymbol{h}(\boldsymbol{z}, \dot{\boldsymbol{z}}) = -\bar{\boldsymbol{M}}(\boldsymbol{z})^{-1} \left[\bar{\boldsymbol{b}}(\boldsymbol{z}, \dot{\boldsymbol{z}}) + \frac{\partial U(\boldsymbol{z})}{\partial \boldsymbol{z}}^T \right]\,, \tag{5.21}$$

where $\bar{\boldsymbol{M}}(\boldsymbol{z}) = \boldsymbol{J}(\boldsymbol{q})^{-T} \boldsymbol{M}(\boldsymbol{q}) \boldsymbol{J}(\boldsymbol{q})^{-1}$*,* $\bar{\boldsymbol{b}}(\boldsymbol{z}, \dot{\boldsymbol{z}}) = \boldsymbol{J}(\boldsymbol{q})^{-T} \left[\boldsymbol{b}(\boldsymbol{q}, \dot{\boldsymbol{q}}) - \boldsymbol{M}(\boldsymbol{q}) \boldsymbol{J}(\boldsymbol{q})^{-1} \dot{\boldsymbol{J}}(\boldsymbol{q}) \dot{\boldsymbol{q}} \right]$*, and* $\partial U(\boldsymbol{z})/\partial \boldsymbol{z} = (\partial U(\boldsymbol{q}(\boldsymbol{z}))/\partial \boldsymbol{q}) \partial \boldsymbol{q}(\boldsymbol{z})/\partial \boldsymbol{z}$*.*[1] *Then, this dynamics satisfies condition* (5.19) *of Definition 5.2, if for all*

$$(\boldsymbol{z}, \dot{\boldsymbol{z}}) \in \mathcal{T}\bar{\mathcal{Z}}_j := \{(\boldsymbol{z}, \dot{\boldsymbol{z}}) \in (\subseteq \mathbb{R}^n)\mathbb{R}^n \,|\, z_i = c_i, \dot{z}_i = 0, \forall i \in \{1, \ldots, n\}/\{j\}\}\,,$$

all the following statements are true:

[1] Since $\boldsymbol{z}(\boldsymbol{q})$ is a diffeomorphism, $\boldsymbol{q}$ and $\dot{\boldsymbol{q}}$, or $\boldsymbol{z}$ and $\dot{\boldsymbol{z}}$ can be considered as equivalent representations of the dependencies, respectively.

1. *Let $\bar{M}_{ij}$ be the component in the i-th row and j-th column of the matrix $\bar{\boldsymbol{M}}$, then, $\bar{M}_{ij} = 0$ for all $i \in \{1, \dots, n\}/\{j\}$.*
2. *Let $\bar{b}_i$ be the i-th component of the co-vector $\bar{\boldsymbol{b}}$, then, $\bar{b}_i = 0$ for all $i \in \{1, \dots, n\}/\{j\}$.*
3. *Let $\partial U/\partial z_i$ be the i-th component of the co-vector $\partial U/\partial \boldsymbol{z}$, then, $\partial U/\partial z_i = 0$ for all $i \in \{1, \dots, n\}/\{j\}$.*

Proof. In the following, sufficiency of the statements 1–3 will be proven. Moreover, arguments for their necessity will be discussed. Since the theorem hypothesizes only sufficiency, the latter should be regarded merely as a conjecture. In the following argumentation, the index set $\mathcal{I} := \{1, \dots, n\}/\{j\}$ will be used extensively.

Consider the terms $\boldsymbol{h}^1 = \bar{\boldsymbol{M}}^{-1}\bar{\boldsymbol{b}}$ and $\boldsymbol{h}^2 = \bar{\boldsymbol{M}}^{-1}(\partial U/\partial \boldsymbol{z})^T$. The term $\boldsymbol{h}^1(\boldsymbol{z}, \dot{\boldsymbol{z}})$ depends on $\boldsymbol{z}$ and $\dot{\boldsymbol{z}}$, and the term $\boldsymbol{h}^2(\boldsymbol{z})$ depends solely on $\boldsymbol{z}$. Since both terms appear as sum in (5.21), but $\mathcal{Z}_j$ is a differentiable 1-manifold, condition (5.19) is satisfied if and only if $h_i^1 = 0$ and $h_i^2 = 0$ for all $i \in \mathcal{I}$, independently.

Suppose that statement 2 and 3 are true and assume further that $\bar{b}_j \neq 0$ and $\partial U/\partial z_j \neq 0$ (which are valid assumptions for $(\boldsymbol{z}, \dot{\boldsymbol{z}}) \in \mathcal{T}\bar{\mathcal{Z}}_j$). Then, statement 1 is sufficient, if $h_i^1 = 0$ and $h_i^2 = 0$ for all $i \in \mathcal{I}$. This can be shown by direct calculations, i. e., $h_k^1 = \bar{M}_{kl}^{-1}\bar{b}_l = 0$, since $\bar{b}_l = 0$ for all $l \in \mathcal{I}$ and $\bar{M}_{kl}^{-1} = 0$ for $l = j$ and for all $k \in \mathcal{I}$ by virtue of statement 1 to be true. The proof for h_i^2 works analogously by replacing above $\bar{b}_l$ by $\partial U/\partial z_l$. Necessity can be shown by contradiction: suppose that $h_r^1 = 0$ for $\bar{b}_j \neq 0$ (which is a valid assumption for $(\boldsymbol{z}, \dot{\boldsymbol{z}}) \in \mathcal{T}\bar{\mathcal{Z}}_j$). Suppose further that for an arbitrary $r \in \mathcal{I}$, $\bar{M}_{rj}^{-1} \neq 0$. Then, $\bar{M}_{rj}^{-1} \neq 0$ and $\bar{b}_j \neq 0$ is equivalent to $h_r^1 = \bar{M}_{rl}^{-1}\bar{b}_l \neq 0$, which contradicts the original assumption. Since $r \in \mathcal{I}$ is arbitrary, the above assumption leads to a contradiction for any $r \in \mathcal{I}$. Furthermore, it is recognized that $\bar{M}_{kk} > 0$ for all $k = 1 \dots n$, which results from the fact that $\boldsymbol{M}(\boldsymbol{q})$ is positive definite and $\boldsymbol{z}(\boldsymbol{q})$ is a diffeomorphism. Therefore, by hypothesis of statement 2 and 3 to be true, $h_i^1 = 0$ and $h_i^2 = 0$ are satisfied for all $i \in \mathcal{I}$ if and only if statement 1 is true. This proofs also sufficiency of statement 2 and 3. It remains to show that for $h_i^1 = 0$ and $h_i^2 = 0$ for all $i \in \mathcal{I}$, it is necessary that statement 1, 2, and 3 simultaneously hold true. To this end, consider the case where statement 1 is not satisfied, i. e., there exists an $r \in \mathcal{I}$ for which $\bar{M}_{rj}^{-1} \neq 0$. Suppose further that $\bar{b}_r \neq 0$. Note that since $\bar{\boldsymbol{b}}$ is bilinear in $\dot{\boldsymbol{z}}$, $\bar{b}_r \neq 0$ implies that $\bar{b}_r$ depends on $\dot{z}_j$ which is assumed to be non-zero and varying (for $(\boldsymbol{z}, \dot{\boldsymbol{z}}) \in \mathcal{T}\bar{\mathcal{Z}}_j$). A necessary condition for $h_r = h_r^1 + h_r^2 = 0$ is that $\bar{M}_{rj}^{-1}\bar{b}_j + \bar{M}_{rr}^{-1}\bar{b}_r = 0$ for all $(z_j, \dot{z}_j) \in (\subseteq \mathbb{R}) \times \mathbb{R}$. This is equivalent to $\bar{M}_{rj}^{-1}/\bar{M}_{rr}^{-1} = -\bar{b}_r/\bar{b}_j$ for independently varying z_j and $\dot{z}_j$. From $\bar{\boldsymbol{b}} = \bar{\boldsymbol{C}}\dot{\boldsymbol{z}}$ and from $\dot{\bar{\boldsymbol{M}}} = \bar{\boldsymbol{C}} + \bar{\boldsymbol{C}}^T$ (Definition 2.15 and Proposition 2.1), it follows that $\bar{b}_r \neq 0$ implies $\bar{M}_{rj}^{-1} \neq \text{const.}$. It might become evident that $\bar{M}_{rj}^{-1}/\bar{M}_{rr}^{-1} = -\bar{b}_r/\bar{b}_j$ cannot be always satisfied for independently varying z_j and $\dot{z}_j$. □

Theorem 5.2 reveals that the main difficulty of proving the existence of oscillation modes is finding a diffeomorphism, which satisfies all its conditions. However, it can be easily verified that Theorem 5.1 represents a particular case of Theorem 5.2, where the corresponding change of coordinates is linear. The following section proposes a novel methodology, which enables to embody even desired eigenmodes in nonlinear dynamics of the form (5.1), as will be also verified by practically relevant and realizable examples.

5.2. Embodiment in nonlinear dynamics

The concept of oscillation modes forms the basis for periodic motions in nonlinear systems of second-order dynamics, e. g., of the form (5.1). However, the shape of such invariant submanifolds generally differs from the desired shape of paths of a given task. In the following, a method is proposed which tackles this problem by exploiting the degrees of freedom in the mechanical design of compliantly actuated systems such that oscillation modes are imposed to match the desired modes of a given task. Thereby, the general goal can be formulated as follows:

Problem 5.1. *Consider the task coordinates $\boldsymbol{x} \in\subseteq \mathbb{R}^n$, which are related to the configuration variables $\boldsymbol{q} \in\subseteq \mathbb{R}^n$ by the generally nonlinear change of coordinates $\boldsymbol{x} = \boldsymbol{x}(\boldsymbol{q})$. Assume that the terms of the dynamics* (5.1) *depend additionally on N design parameters $\boldsymbol{\zeta} \in \mathbb{R}^N$ such as kinematics, inertial, and elastic parameters. The problem is finding parameters $\boldsymbol{\zeta}$ such that the oscillation modes of the dynamics* (5.1)*,*

$$\mathcal{Z}_j = \{\boldsymbol{q} \subseteq\in \mathbb{R}^n \,|\, x_i(\boldsymbol{q}) - c_i = 0, \forall i \in \{1, \ldots, n\}/\{j\}\} \tag{5.22}$$

match to desired modes $\mathcal{Z}_j^{\mathrm{des}}$ of a given task.

This formulation reveals that solving the general problem of oscillation mode matching implies equivalent properties of the task and modal coordinate transformations, $\boldsymbol{x}(\boldsymbol{q})$ and $\boldsymbol{z}(\boldsymbol{q})$ (cf. Definition 5.2), respectively. As can be seen from Theorem 5.2, finding a diffeomorphism $\boldsymbol{z}(\boldsymbol{q})$ represents already a highly nonlinear and challenging process for itself. However, finding a change of coordinates $\boldsymbol{z}(\boldsymbol{q})$ with equivalent "differential" properties as $\boldsymbol{x}(\boldsymbol{q})$ is even harder. By utilizing the concept of eigenmodes for nonlinear dynamics as introduced in Sect. 5.1.2, the Problem 5.1 can be drastically simplified, since solely a linear transformation needs to be found, where, e. g., statement 1 of Theorem 5.2 holds true by definition.

Problem 5.2. *Consider the dynamics* (5.1)*. Assume that the terms of* (5.1) *depend additionally on N design parameters $\boldsymbol{\zeta} \in \mathbb{R}^N$. Then, given desired eigenvectors of the task $\boldsymbol{w}_j^{\mathrm{des}}$ for $j \in \mathcal{J} \subseteq \{1, \ldots, n\}$, find parameters $\hat{\boldsymbol{\zeta}}$ satisfying certain physical and design constraints for which $\boldsymbol{w}_j(\hat{\boldsymbol{\zeta}})$ are eigenvectors according to Definition 5.1 and $\boldsymbol{w}_j(\hat{\boldsymbol{\zeta}}) \rightarrow \boldsymbol{w}_j^{\mathrm{des}}$, for all $j \in \mathcal{J} \subseteq \{1, \ldots, n\}$.*

The proposed methodology to solve this problem is referred to as *modal dynamics matching.*

5.2.1. Modal dynamics matching methodology

There are two main remaining aspects which make it still difficult to solve the Problem 5.2: (i) due to the generally nonlinear transformation $\boldsymbol{x} = \boldsymbol{f}(\boldsymbol{q})$ between configuration and task coordinates, the direction of desired eigenvectors $\boldsymbol{w}_j^{\mathrm{des}}$ expressed in the tangent space of the configuration manifold is not a priori known. (ii) For a general nonlinear dynamics (5.1), the condition (5.19) of Definition 5.1 is highly nonlinear in the displacement $\boldsymbol{w}_j z_j$. Therefore, seeking a solution to Problem 5.2, the following algorithmic steps are proposed:

1. Transform the entire problem under a change of coordinates $\boldsymbol{x} = \boldsymbol{f}(\boldsymbol{q})$ to the task-space. Then, the i-th row of the j-th desired eigenvector $\bar{w}_{i,j}^{\mathrm{des}} = 1$ if $i = j$ and $\bar{w}_{i,j}^{\mathrm{des}} = 0$ otherwise. Therefore, the j-th desired eigenvector is align with the j-th task-velocity component $\dot{x}_j$.

2. Solve the problem

$$\arg\min_{\boldsymbol{\zeta}_1} \sum_{i=1}^{N_\mathrm{q}} \sum_{j\in\mathcal{J}} \frac{1}{2} \left\| \bar{\boldsymbol{w}}_j(\boldsymbol{q}_i, \boldsymbol{\zeta}_1) - \bar{\boldsymbol{w}}_i^{\mathrm{des}} \right\|^2 \tag{5.23}$$

corresponding to the linearized dynamics (5.4) (expressed in task-coordinates $\boldsymbol{x}$) for a subset $\boldsymbol{\zeta}_1 \subset \boldsymbol{\zeta}$ of N_1 design parameters. This problem is subject to a generalized eigenvalue problem of the form (5.6), (5.7). It is evaluated at relevant configurations $\boldsymbol{q}_i \in \mathcal{Q} = \{\boldsymbol{q}_1, \ldots, \boldsymbol{q}_{N_\mathrm{q}}\}$ of the task. Note that this problem can be further simplified by recalling that the potential $U(\boldsymbol{q}) = U_\mathrm{g}(\boldsymbol{q}) + U_\mathrm{e}(\boldsymbol{q})$ comprises the gravitational and elastic potential, respectively. Then, problem (5.23) can be solved only for the Hessian of the elastic potential $\boldsymbol{K}(\boldsymbol{q}) = \partial^2 U_\mathrm{e}/\partial \boldsymbol{q}^2$, while the gravity force $\partial U_\mathrm{g}/\partial \boldsymbol{q}$ is treated as bias term in the next algorithmic step.

3. To remove the remaining coupling terms (omitted due to the linearization), substitute the parameters $\hat{\boldsymbol{\zeta}}_1$ solving problem (5.23) in (5.6), (5.7) (expressed in configuration-coordinates $\boldsymbol{q}$) to obtain the linear transformation $\boldsymbol{q} = \boldsymbol{W}\boldsymbol{z}$, where $\boldsymbol{W} = \begin{bmatrix}\boldsymbol{w}_1 \ldots \boldsymbol{w}_n\end{bmatrix}$. Then, consider this change of coordinates in Definition 5.2 in order to satisfy statement 3 of Theorem 5.2 by determining the remaining design parameters $\boldsymbol{\zeta}_2$.

An algorithm to solve step 2) is provided in Appendix A.2.1.

5.2.2. Modal dynamics matching example

The following example aims at validating that task-relevant eigenmodes exist and can be embodied in the nonlinear dynamics of an elastic multibody system.

Model

Consider the model of a three-segment leg during stance phase which is assumed to be attached to a body (trunk) with translational degrees of freedoms in the plane (Fig. 5.2). The thigh is connected to the trunk by a rotational joint with coordinate q_1. The shank is hinged to the thigh with relative coordinate q_3. There is a pulley concentric with the hip joint with relative coordinate q_2 which couples to the knee joint such that $q_3 = \beta(q_2 - q_1)$, where β is a parameter.[2] The foot is hinged to the shank. Thereby, the relative angle of this ankle joint is measured between the foot and the shank and is denoted by q_4. The kinematic constraint $q_4 = -q_3$ keeps the foot segment parallel to the thigh and thereby implements a pantograph mechanism which is known from biomechanics literature [WHI+00]. The segment lengths of thigh, shank, foot, are denoted by l_1, l_2, l_3 and their inertial parameters (mass, center of mass position, and mass moment of inertia) are labeled as m_i, c_i, and I_i^c, for $i = 1, 2, 3$, respectively. The center of mass of each segment is assumed at $c_i = l_i/2$. A point contact is assumed which in the tree-segment case is located at the tip of the foot. This mechanism has also two kinematics degrees of freedom. The orientations of the thigh and of the pulley concentric to the hip joint relative to the trunk are considered as minimum set of coordinates $\boldsymbol{q} = (q_1, q_2) \in \mathbb{R}^2$, respectively. These degrees of freedom are assumed to be actuated via springs of which the generalized elastic force are derived from the potential $U_\mathrm{e}(\boldsymbol{q}) = U_\mathrm{e}(q_1) + \alpha U_\mathrm{e}(q_2)$, where, e. g., $U_\mathrm{e}(q_i) = k_\mathrm{lin} q_i^2/2 + k_\mathrm{cub} q_i^4/4$, with parameters of the elasticity $\alpha, k_\mathrm{lin} > 0$ and $k_\mathrm{cub} \geq 0$. The complete set of design parameters comprises: $\boldsymbol{\zeta} = (m_\mathrm{t}, m_1, m_2, m_3, l_1, l_2, l_3, I_1^\mathrm{c}, I_2^\mathrm{c}, I_3^\mathrm{c}, k_\mathrm{lin}, k_\mathrm{cub}, \alpha, \beta)$.

[2] If the kinematic constraint is implemented by pulleys and cables, then $\beta = r_\mathrm{hip}/r_\mathrm{knee}$ represents the ratio of radii of the hip and knee pulley, respectively.

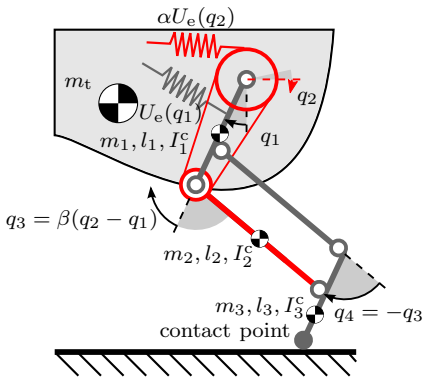

Figure 5.2.: Three-segment pantograph leg mechanism attached to a trunk with very high inertia.

Task-oriented coordinates

Typical tasks of segmented legs can be conveniently represented in polar coordinates, which are motivated by fundamental template dynamics models of legged locomotion such as the spring loaded inverted pendulum (SLIP). The SLIP model consists of a translational spring which connects the total body mass concentrated at the hip with the pivot point on the ground. This translational degree of freedom is commonly referred to as the leg axis. In some variants of the SLIP model, the orientation of the leg axis w. r. t. the ground can be (compliantly) actuated under the assumption of very high trunk inertia. The corresponding rotational degree of freedom is known to represent the leg or polar angle. Note that these task-oriented coordinates can be used to describe all gaits, where the contact between the foot and the ground can be geometrically modeled as a point. Therefore, the polar coordinates will form the basis for the modal leg design procedure presented in the following.

Design procedure

This example aims at validating the following two features of the eigenmode matching procedure:

1. The methodology enables to find design solutions which match to the desired task dynamics and simultaneously satisfy the implementation constraints such as non-zero link inertia.

2. Design degrees of freedom which are redundant for the eigenvector matching problem (5.23) can be exploited to achieve modal invariance for terms which are nonlinear even expressed in configuration coordinates $\boldsymbol{q}$ such as gravitational and elastic forces.

On the basis of the latter consideration, a subset of $N_1 = n(n-1) = 2$ design parameters needs to be chosen as optimization variables for the eigenvector matching procedure, while the remaining design parameters need to be fixed. Therefore, a geometric analysis reveals that the parameter assumption $l_2 = l_1 + l_3$ leads to the task-oriented (polar) coordinates

$$\boldsymbol{x} = \boldsymbol{x}(\boldsymbol{q}) = \begin{pmatrix} \left(1 - \frac{\beta}{2}\right) q_1 + \frac{\beta}{2} q_2 \\ (l_1 + l_3)\sqrt{2\left(1 + \cos\left(\beta\left(q_2 - q_1\right)\right)\right)} \end{pmatrix},$$

where the polar angle x_1 depends linearly on $\boldsymbol{q}$. Furthermore, the link lengths l_1 and l_3 can be selected, e. g., according to workspace considerations. The mass of the trunk m_t will not affect the eigenvectors and can be assumed to be constant. The remaining leg segment parameters m_i and I_i^c, for $i = 1, 2, 3$ influence only the gravity and inertial properties and k_lin, k_cub, and α only the elastic behavior of the system. According to the remark on algorithmic step 2 (cf. algorithm solving Problem 5.2), only the elastic potential U_e is considered for the eigenvector search. Since the matching procedure requires to decouple the modal inertial matrix (cf. statement 2 of Theorem 5.2) and needs to achieve the modal invariance property for the elastic dynamics (cf. statement 4 of Theorem 5.2), one parameter of each category needs to be selected as optimization variables, e. g., $\boldsymbol{\zeta}_1 = (I_1^\mathrm{c} + I_3^\mathrm{c}, \alpha)$ for the considered example, while the remaining parameters are fixed.

The case of linear elasticity: $k_\mathrm{cub} = 0$

The application of algorithm step 2 for solving Problem 5.2 reveals that constant eigenvectors which ideally match the desired ones can be found for a wide range of the fixed parameters $m_1, m_2, m_3, l_1, l_3, I_2^\mathrm{c}, k_\mathrm{lin}, \beta$. In particular, it results in implementable values of $I_1^\mathrm{c} + I_3^\mathrm{c} > 0$ and $\alpha > 0$. From inspection of the symbolic expressions[3] appearing in the eigenvector matching procedure, it can be seen that the family of design parameters

$$\begin{aligned} I_1^\mathrm{c} + I_3^\mathrm{c} =& \frac{3m_1 + m_2}{4} l_1^2 + \frac{2m_1 + m_2}{2} l_1 l_3 \\ & - \frac{3m_2 + m_3}{4} l_3^2 + I_2^\mathrm{c}\,, \end{aligned} \tag{5.24}$$

$$\alpha = \frac{\beta}{2 - \beta} \tag{5.25}$$

leads to globally matching, constant eigenvectors. Substituting the design parameters (5.24), (5.25) into the inertia and stiffness matrix expressed w. r. t. configuration variables $\boldsymbol{M}(\boldsymbol{q})$ and $\partial^2 U_\mathrm{e}(\boldsymbol{q})/\partial \boldsymbol{q}^2$, respectively, and using the result to solve the corresponding generalized eigenvalue problem, it can be seen that also the eigenvectors

$$\boldsymbol{W} = \begin{bmatrix} 1 & \frac{\beta}{\beta - 2} \\ 1 & 1 \end{bmatrix} \tag{5.26}$$

of the globally matching three-segment leg dynamics are constant. Note that this is the case, even though the inertial parameters are non-zero.

Remark 5.2. *Although under parameter conditions* (5.24) *and* (5.25)*, the generalized eigenvectors of* $\boldsymbol{M}(\boldsymbol{q})$ *and* $\partial^2 U_\mathrm{e}(\boldsymbol{q})/\partial \boldsymbol{q}^2$ *are constant for any* $\boldsymbol{q} \in \mathbb{R}^2$ *(cf.* (5.26)*), the eigenvalues of* (5.6)*,*

$$\begin{aligned} \lambda_1 &= \frac{k_\mathrm{lin}}{(2 - \beta)\left(\Theta_1 + \Theta_2 \cos\left(\beta\left(q_2 - q_1\right)\right)\right)}\,, \\ \lambda_2 &= \frac{k_\mathrm{lin}}{\beta\left(\Theta_1 - \Theta_2 \cos\left(\beta\left(q_2 - q_1\right)\right)\right)}\,, \end{aligned}$$

where $\Theta_1 > \Theta_2 > 0$ *are constants (defined in Appendix A.3), depend nonlinearly on the configuration* $q_3 = \beta\left(q_2 - q_1\right)$*.*

[3] This size of problems can still be treated with computer algebra software such as Maple

It can be concluded that the problem of (5.23) is solved accordingly.

Remark 5.3. *The application of algorithm step 3 (cf. algorithm solving Problem 5.2) to the gravitational bias term* $\bar{\boldsymbol{b}}_{\mathrm{g}}(\boldsymbol{z}) = (\partial U_{\mathrm{g}}(\boldsymbol{z})/\partial \boldsymbol{z})^T$ *reveals that for*

$$m_3 = \left(m_1 l_1 + m_2 \left(l_1 - l_3\right)\right)/l_3 \,, \tag{5.27}$$

$$\bar{\boldsymbol{b}}_{\mathrm{g}}(\boldsymbol{z}) = -\frac{\Theta_3}{l_1 + l_2} g_0 \begin{pmatrix} \sin\left(\frac{\beta(z_1 - z_2) - 2z_1}{\beta - 2}\right) + \sin\left(\frac{\beta(z_1 + z_2) - 2z_1}{\beta - 2}\right) \\ \frac{\beta}{\beta - 2}\left(\sin\left(\frac{\beta(z_1 + z_2) - 2z_1}{\beta - 2}\right) - \sin\left(\frac{\beta(z_1 - z_2) - 2z_1}{\beta - 2}\right)\right) \end{pmatrix}$$

such that $\bar{b}_{\mathrm{g},1}(\boldsymbol{z}) = 0$ *for all* $\boldsymbol{z} \in \{\boldsymbol{z} \in \mathbb{R}^2 \,|\, z_1 = 0\}$.

The above results motivate the following proposition of Theorem 5.2. Thereby, the considered components corresponding to the dynamics expressed in $\boldsymbol{q}$ coordinates (5.1), are provided in (A.7)–(A.10).

Proposition 5.1. *Let the matrix* $\boldsymbol{W}$ *of* (5.26) *define a linear transformation of the form* $\boldsymbol{z} = \boldsymbol{W}^{-1}\boldsymbol{q}$. *Then, the dynamics* (5.1) *with components* (A.7)–(A.10)*, features an oscillation mode with corresponding 2-D invariant subset of the state space,*

$$\mathcal{TZ}_2 := \left\{(\boldsymbol{q}, \dot{\boldsymbol{q}}) \in \mathbb{R}^4 \,|\, z_1(\boldsymbol{q}) = 0, \dot{z}_1(\dot{\boldsymbol{q}}) = 0\right\} \,, \tag{5.28}$$

according to Definition 5.2.

Proof. In order to prove this proposition, it will be shown that the statements of Theorem 5.2 hold true.

The inertia matrix (A.7) expressed in $\boldsymbol{z}$ coordinates,

$$\bar{\boldsymbol{M}}(\boldsymbol{z}) = \begin{bmatrix} 2\left(\Theta_1 + \Theta_2 \cos\left(\frac{2\beta}{\beta - 2} z_2\right)\right) & 0 \\ 0 & \frac{2\beta^2}{(\beta - 2)^2}\left(\Theta_1 - \Theta_2 \cos\left(\frac{2\beta}{\beta - 2} z_2\right)\right) \end{bmatrix} \tag{5.29}$$

is diagonal and therefore statement 1 is true, for any $\boldsymbol{z} \in \mathbb{R}^2$.

Let $\mathcal{T}\bar{\mathcal{Z}}_2 := \left\{(\boldsymbol{z}, \dot{\boldsymbol{z}}) \in \mathbb{R}^4 \,|\, z_1 = 0, \dot{z}_1 = 0\right\}$. Then, the Coriolis/centrifugal matrix (A.8) expressed in $\boldsymbol{z}$ coordinates takes form

$$\bar{\boldsymbol{C}}(\boldsymbol{z}, \dot{\boldsymbol{z}}) = \frac{2\Theta_2 \beta}{\beta - 2} \sin\left(\frac{2\beta}{\beta - 2} z_2\right) \begin{bmatrix} -\dot{z}_2 & -\dot{z}_1 \\ \dot{z}_1 & \frac{\beta^2}{(\beta - 2)^2} \dot{z}_2 \end{bmatrix} \tag{5.30}$$

such that

$$\bar{\boldsymbol{C}}(\boldsymbol{z}, \dot{\boldsymbol{z}})\dot{\boldsymbol{z}} = \frac{2\Theta_2 \beta}{\beta - 2} \sin\left(\frac{2\beta}{\beta - 2} z_2\right) \begin{pmatrix} 0 \\ \frac{\beta^2}{(\beta - 2)^2} \dot{z}_2^2 \end{pmatrix} \tag{5.31}$$

for any $(\boldsymbol{z}, \dot{\boldsymbol{z}}) \in \bar{\mathcal{Z}}_2$ and therefore statement 2 is true. The elastic force (A.10) expressed in $\boldsymbol{z}$ coordinates takes the form

$$\frac{\partial U_{\mathrm{e}}(\boldsymbol{z})}{\partial \boldsymbol{z}}^T = \begin{pmatrix} \frac{2k_{\mathrm{lin}}}{2 - \beta} z_1 \\ \frac{2\beta k_{\mathrm{lin}}}{(2 - \beta)^2} z_2 \end{pmatrix} \,, \tag{5.32}$$

where it can be seen that for any $z_2 \in \mathbb{R}$, $\partial U_{\mathrm{e}}(\boldsymbol{z})/\partial z_1 = 0$, if and only if $z_1 = 0$. Then, together with the result of Remark 5.3 it can be finally concluded that statement 3 is also true.

Therefore, all conditions of Theorem 5.2 are satisfied such that $\mathcal{TZ}_2$ represents an invariant set for the dynamics (5.1) with components (A.7)–(A.10). □

The case of nonlinear elasticity: $k_{\mathrm{cub}} > 0$**,** $\beta = 1$

A particular case of constant eigenvectors of the three segment leg with nonlinear (cubic) elasticities is given if the kinematic coupling parameter β is chosen unity, i. e., $\beta = 1$. It is found that the elastic force expressed in $\boldsymbol{z}$ coordinates features the following modal invariance properties (cf. statement 3 of Theorem 5.2):

$$\left.\frac{\partial U_{\mathrm{e}}(\boldsymbol{z})}{\partial \boldsymbol{z}}^T\right|_{\forall z_1 \in \mathbb{R}, z_2 = 0} = \begin{pmatrix} 2\left(k_{\mathrm{lin}} z_1 + k_{\mathrm{cub}} z_1^3\right) \\ 0 \end{pmatrix},$$

$$\left.\frac{\partial U_{\mathrm{e}}(\boldsymbol{z})}{\partial \boldsymbol{z}}^T\right|_{z_1 = 0, \forall z_2 \in \mathbb{R}} = \begin{pmatrix} 0 \\ 2\left(k_{\mathrm{lin}} z_2 + k_{\mathrm{cub}} z_2^3\right) \end{pmatrix},$$

This result provides evidence for the existence of oscillation modes in the dynamics of elastic multibody systems even with nonlinear elasticities.

This practically relevant example validates that using the methodology of modal dynamics matching, an elastic multibody system can be found of which the dynamics consists of oscillation modes, which match to a certain task. Thereby, the obtained design parameters are implementable as, e. g., the inertial parameters of bodies can be chosen to be non-zero. This example constitutes one of the first proofs of existence of invariant oscillation modes in practically implementable, nonlinear, elastic multibody systems. As such, this example forms the basis of investigations of periodic orbits provided in the next section.

5.3. Classification of periodic orbits

In the conservative case, the definitions proposed in Sect. 5.1 reveal that the existence of oscillation modes implies also the presence of periodic orbits which correspond to centres (cf. [JS07, Theorem 11.3, p. 390]). In the dissipative case, oscillation modes ensure the existence of limit cycles (cf. Theorem 4.1 and 4.2 of Chapt. 4) (under appropriate energy regulation control). Thereby, the following central question about periodic orbits arises: *Are oscillation modes necessary for the existence or excitability of periodic orbits?*

A general oscillation mode is defined by an 1-D, differentiable submanifold of the n-D configuration space. Considering also the associated tangent spaces, the invariant set of states corresponding to an oscillation mode is fully determined by its 1-manifold. An implication of this definition allows to define a criterion based upon it can be excluded that a periodic orbit evolves in an oscillation mode, without relying on an explicit description of the corresponding 1-manifold:

Theorem 5.3. *If the image of a trajectory of configuration variables is neither homeomorphic to a circle, an open interval, a closed interval, nor to an half-open interval, this motion corresponds not to an oscillation mode.*

Note that the essential statement is that an oscillation mode can only be either a line (without self-intersection) or a circle.

Proof. According to Definition 5.2, an oscillation mode is said to be an 1-D, differentiable submanifold of the n-D configuration space, i. e., an oscillation mode is defined by $n-1$ holonomic constraints of the n configuration variables. Since any submanifold is itself a manifold [Fra03, p. 18], it has to be shown that any 1-manifold is either a circle, an open interval, an closed interval, or an half-open interval, or is homeomorphic to one of them. But this follows exactly from the classification theorem [Gal87]. □

If a periodic orbit satisfies any assumption of Theorem 5.3, the method of elimination reveals that the orbit can be at most a 2-D submanifold of the $2n$-D state space, e. g., defined by $2n-2$ non-holonomic constraints of the $2n$ state variables. These considerations motivate the classification of periodic orbits which will be investigated as given in Table 5.1:

	linear	nonlinear
holonomic (one-manifold)	Sect. 5.3.2	Sect. 5.3.3
non-holonomic (two-manifold)		Sect. 5.3.4

Table 5.1.: Classification of periodic orbits

5.3.1. Excitation of periodic orbits

Consider the dynamics of the form

$$\boldsymbol{M}(\boldsymbol{q})\ddot{\boldsymbol{q}} + \boldsymbol{b}(\boldsymbol{q}, \dot{\boldsymbol{q}}) = -\frac{\partial U(\boldsymbol{\theta}, \boldsymbol{q})}{\partial \boldsymbol{q}}^T \tag{5.33}$$

which corresponds to (5.1) with the only difference that $\boldsymbol{\theta} := \boldsymbol{\theta}_{\text{des}}$ is considered as control input such that for a given $\boldsymbol{\theta}$ the equilibrium position is $\boldsymbol{q} = \bar{\boldsymbol{q}}(\boldsymbol{\theta})$ according to Definition 3.4 of Sect. 3.1.1. The system (5.33) is non-conservative in a sense that the dissipative term $\boldsymbol{d}(\boldsymbol{q}, \dot{\boldsymbol{q}})$ defined in (5.3) satisfies $\boldsymbol{d}(\boldsymbol{q}, \dot{\boldsymbol{q}}) \neq \boldsymbol{0}$ for all $\dot{\boldsymbol{q}} \neq \boldsymbol{0}$. For $\boldsymbol{\theta} = \text{const.}$, the equilibrium point $\{\boldsymbol{q} = \bar{\boldsymbol{q}}(\boldsymbol{\theta}), \dot{\boldsymbol{q}} = \boldsymbol{0}\}$ of (5.33) is globally asymptotically stable (cf. Proposition 3.2 in combination with the singular perturbation assumption of Sect. 3.2.3) such that any trajectory of the system (5.33) is not closed, since for any initial condition the state converges to the equilibrium point. Therefore, to obtain a closed orbit, energy needs to be injected periodically (cf. the approach of Chapt. 4). The method proposed in the following, aims at indicating periodic motions in non-conservative dynamics of the form (5.33). The only assumption made about a possible periodic orbit is as follows:

Assumption 5.1. *Let $\boldsymbol{\theta}^0$ be a constant control input. Then, a displacement $\Delta\boldsymbol{\theta} = \boldsymbol{\theta} - \boldsymbol{\theta}^0 = \boldsymbol{w}\Delta\theta_{\text{w}}$ along a generalized eigenvector $\boldsymbol{w}$ of the linearization of the dynamics* (5.33) *at the equilibrium position $\boldsymbol{q} = \bar{\boldsymbol{q}}(\boldsymbol{\theta}^0)$ (cf.* (5.4) *and* (5.6)–(5.7)*) with amplitude $\Delta\theta_{\text{w}} \in \mathbb{R}$, accelerates the system* (5.33) *such that its state moves "mainly" on a periodic orbit of the corresponding conservative system.*

As such, persistent excitation of possible periodic motions can be achieved by a switching-based control law of the form (cf. Sect. 4.4)

$$\boldsymbol{\theta} = \boldsymbol{\theta}^0 + \boldsymbol{w} \begin{cases} \hat{\theta}_{\text{w}} & \text{if} \quad \frac{\partial U(\boldsymbol{\theta}^-, \boldsymbol{q})}{\partial \boldsymbol{q}}\boldsymbol{w} < -\epsilon_{\text{w}} \\ 0 & \text{if} \quad \left|\frac{\partial U(\boldsymbol{\theta}^-, \boldsymbol{q})}{\partial \boldsymbol{q}}\boldsymbol{w}\right| \leq \epsilon_{\text{w}} \\ -\hat{\theta}_{\text{w}} & \text{if} \quad \frac{\partial U(\boldsymbol{\theta}^-, \boldsymbol{q})}{\partial \boldsymbol{q}}\boldsymbol{w} > \epsilon_{\text{w}} \end{cases}, \tag{5.34}$$

where $\boldsymbol{\theta}^-$ represents the controller state before the switching, and $1 \gg \epsilon_{\text{w}} > 0$ and $\hat{\theta}_{\text{w}} > 0$ are threshold and switching amplitude constants, respectively. Note that in the limit case $\epsilon_{\text{w}} = 0$, the controller would switch exactly at positions, where $(\partial U(\boldsymbol{\theta}, \boldsymbol{q})/\partial \boldsymbol{q})\boldsymbol{w} = 0$. However, at these positions, the sign of the switching function (5.34) is not determined and therefore it is required to chose the threshold ϵ_{w} unequal but close to zero.

5.3.2. Periodic orbits in eigenmodes

In Assumption 5.1, the auxiliary term "mainly" has been utilized, which seems to be rather imprecise. The reason for that statement is to avoid any assumption about the existence of oscillation modes. In contrast, if the dynamics (5.33) consists of an eigenvector according to Definition 5.1, then, Assumption 5.1 can be reformulated as a corollary of Theorem 5.1.

Corollary 5.2. *Consider the dynamics* (5.33) *with potential energy* $U(\boldsymbol{\theta}, \boldsymbol{q}) = U_{\mathrm{g}}(\boldsymbol{q}) + U_{\mathrm{e}}(\boldsymbol{q} - \boldsymbol{\theta})$. *Assume that there exists a* $\boldsymbol{\theta}^0$ *such that* $\boldsymbol{w}$ *is an eigenvector of* (5.33) *according to Definition 5.1. Then, for any initial state in the invariant set*

$$\mathcal{TW} := \left\{ (\boldsymbol{q}, \dot{\boldsymbol{q}}) \in (\subseteq \mathbb{R}^n) \times \mathbb{R}^n \,|\, \bar{\boldsymbol{W}}^T \left(\boldsymbol{q} - \bar{\boldsymbol{q}}(\boldsymbol{\theta}^0) \right) = \boldsymbol{0}, \bar{\boldsymbol{W}}^T \dot{\boldsymbol{q}} = \boldsymbol{0} \right\} \tag{5.35}$$

as defined by (5.13), *i. e.,* $(\boldsymbol{q}(0), \dot{\boldsymbol{q}}(0)) \in \mathcal{TW}$, *the control input* (5.34) *excites the system such that resulting motions remain in* $\mathcal{TW}$ *for all future time, i. e.,* $(\boldsymbol{q}(t), \dot{\boldsymbol{q}}(t)) \in \mathcal{TW}$ *for all* $t > 0$.

Proof. For any displacement along $\boldsymbol{w}$ with amplitude $z \in \mathbb{R}$, $\Delta\boldsymbol{q} = \boldsymbol{q} - \bar{\boldsymbol{q}}(\boldsymbol{\theta}^0) = \boldsymbol{w}z$, there exists an acceleration amplitude $\ddot{z} \in \mathbb{R}$ such that $\ddot{\boldsymbol{q}} = \boldsymbol{w}\ddot{z}$ according to Definition 5.1. But this implies that for any displacement of the control input along $\boldsymbol{w}$ with amplitude $\hat{\theta}_{\mathrm{w}} \in \mathbb{R}$, $\Delta\boldsymbol{\theta} = \boldsymbol{\theta} - \boldsymbol{\theta}^0 = \boldsymbol{w}\hat{\theta}_{\mathrm{w}}$, there exists also an acceleration amplitude $\ddot{z} \in \mathbb{R}$ such that $\ddot{\boldsymbol{q}} = \boldsymbol{w}\ddot{z}$, since $U_{\mathrm{e}}(\boldsymbol{q} - \boldsymbol{\theta})$. Therefore, the assumptions of Corollary 5.2 are proven based upon a direct consequence of Theorem 5.1. □

An example of a dynamics satisfying the conditions of Corollary 5.2 is given by the compliantly actuated system (5.33) with components (A.7)–(A.10) provided in the Appendix A.3. Considering a damping term, e. g., of the form

$$\boldsymbol{d}(\boldsymbol{q}, \dot{\boldsymbol{q}}) = \begin{pmatrix} d_0 \dot{q}_1 \\ \frac{\beta}{\beta - 2} d_0 \dot{q}_2 \end{pmatrix} \tag{5.36}$$

with constant $d_0 > 0$, this dynamics consists of an eigenvector $\boldsymbol{w} = \begin{pmatrix} \beta/(\beta - 2) & 1 \end{pmatrix}^T$ according to Definition 5.1 for a wide range of model-parameters as exemplary provided in Table 5.2. In particular, combining the result of Corollary 5.2 with a straightforward extension[4] of Theorem 4.2, it can be shown that one can always excites a limit cycle along the mode of a dissipative dynamics.

5.3.3. Periodic orbits in nonlinear oscillation modes

The following analysis investigates the effect of damping on the excitability of periodic orbits in cases, where linear displacements according to the switching law (5.34) lead to incompatible accelerations regarding oscillation modes. This is the case, e. g., when only a nonlinear representation of the oscillation mode is known.

[4]The extension requires to consider a configuration depend, scalar inertia which does not conceptually change the proof, since it increases only the number of continuous dynamical subsystems which need to be considered.

Construction of a nonlinear oscillation mode

So far, only eigenmodes could be identified from practical examples. However, for the basic understanding of nonlinear oscillations, it is crucial to know, if also nonlinear modes can exist for real systems, and if the modal excitation approach, as proposed in Sect. 5.3.1, applies also for this general case. The first part of this question, namely the existence of nonlinear modes, is validated by constructing the following simple example. Consider the dynamics (5.33) with components (A.7)–(A.10) which consists of an eigenvector $\boldsymbol{w} = \begin{pmatrix}\beta/(\beta-2) & 1\end{pmatrix}^T$ according to Definition 5.1. Consider further the kernel of $\boldsymbol{w}^T$, $\bar{\boldsymbol{W}} = \ker\left(\boldsymbol{w}^T\right) = \begin{pmatrix}1 & 1\end{pmatrix}^T$ which defines the 2-D, invariant subset of the state space $\mathbb{R}^4$,

$$\mathcal{TW} := \left\{(\boldsymbol{q}, \dot{\boldsymbol{q}}) \in \mathbb{R}^4 \,|\, q_1 - \bar{q}_1(\boldsymbol{\theta}) + q_2 - \bar{q}_2(\boldsymbol{\theta}) = 0, \dot{q}_1 + \dot{q}_2 = 0\right\} , \tag{5.37}$$

corresponding to the eigenmode defined by $\boldsymbol{w}$. The 1-D curve representing an eigenmode expressed in terms of the configuration variables $\boldsymbol{q}$ is by definition a straight line. In the considered case, the parametric representation takes the form

$$\boldsymbol{q}_{\mathrm{w}}(\boldsymbol{\theta}, z) = \begin{pmatrix}\bar{q}_1(\boldsymbol{\theta}) + \frac{\beta}{\beta-2} z \\ \bar{q}_2(\boldsymbol{\theta}) + z\end{pmatrix} , \tag{5.38}$$

where $z \in \mathbb{R}$ denotes the parameter of the manifold. If one would, however, have taken a different set of coordinates to describe the dynamical system, e. g.,

$$\boldsymbol{x} = \boldsymbol{x}(\boldsymbol{q}) = \begin{pmatrix}(q_1)^3 \\ q_2\end{pmatrix} , \tag{5.39}$$

the mode would have a nonlinear shape

$$\boldsymbol{x}_{\mathrm{w}}(\boldsymbol{\theta}, z) = \boldsymbol{x}(\bar{\boldsymbol{q}}(\boldsymbol{\theta}) + \boldsymbol{w}z) = \begin{pmatrix}\left(\bar{q}_1(\boldsymbol{\theta}) + \frac{\beta}{\beta-2} z\right)^3 \\ \bar{q}_2(\boldsymbol{\theta}) + z\end{pmatrix} , \tag{5.40}$$

in these coordinates. Note that eigenmodes of nonlinear dynamics are defined w. r. t. an equilibrium configuration which in case of compliantly actuated systems (5.33) depends on the control input $\boldsymbol{\theta}$, i. e., $\boldsymbol{q}_0 = \bar{\boldsymbol{q}}(\boldsymbol{\theta})$ (cf. Corollary 5.2). Therefore, also the considered manifold representing the eigenmode (5.38) under the nonlinear change of coordinates (5.39) depends on $\boldsymbol{\theta}$, but is known and exists for any $\boldsymbol{\theta}$ for which $\boldsymbol{w}$ is an eigenvector of the corresponding dynamics.

Influence of damping on the excitability of periodic orbits

The following simulations investigate the influence of damping on the excitability of periodic orbits in oscillation modes, where only a nonlinear representation is assumed to be known. In order to relate the dissipative properties of the oscillation mode and the remaining, transverse dynamics[5], viscous damping of the form

$$\boldsymbol{d}(\boldsymbol{q}_0, \dot{\boldsymbol{q}}) = \boldsymbol{W}_{\mathrm{M}}^{-T} \begin{bmatrix}2\xi_1\sqrt{\lambda_1(\boldsymbol{q}_0)} & 0 \\ 0 & 2\xi_2\sqrt{\lambda_2(\boldsymbol{q}_0)}\end{bmatrix} \boldsymbol{W}_{\mathrm{M}}^{-1} \tag{5.41}$$

[5]The portion of the dynamics which can be expressed in terms of coordinates representing the holonomic constraints, is referred to as transverse dynamics, cf., e. g., the definition in [SFG10].

reflected inertia	Θ_1	$0.006771\,\mathrm{kgm}^2$
reflected inertia	Θ_2	$0.006250\,\mathrm{kgm}^2$
gravitational constant	g_0	$0\,\mathrm{m/s}^2$
pulley ratio	β	1
linear spring constant	k_{lin}	$1.75\,\mathrm{Nm/rad}$
cubic spring constant	k_{cub}	$0.25\,\mathrm{Nm/rad}^3$

Table 5.2.: Inertial and elastic parameters of dynamics (5.33) with components (A.7)–(A.10) featuring an eigenmode considered in simulation.

can be considered. The matrix $\boldsymbol{W}_{\mathrm{M}}$ of generalized eigenvectors of $\partial^2 U/\partial \boldsymbol{q}^2(\boldsymbol{q} = \boldsymbol{q}_0)$ and $\boldsymbol{M}(\boldsymbol{q}_0)$ is normalized w. r. t. $\boldsymbol{M}(\boldsymbol{q}_0)$, i. e., $\boldsymbol{W}_{\mathrm{M}}^T \boldsymbol{M}(\boldsymbol{q}_0)\boldsymbol{W}_{\mathrm{M}} = \boldsymbol{I}$ such that $\xi_1 \in [0;1]$ and $\xi_2 \in [0;1]$ represent normalized damping factors corresponding to the transverse and eigenmode dynamics, respectively. It is expected that for high damping of the transverse and low damping of the eigenmode dynamics, periodic motions can be achieved which evolve largely in the oscillation mode, although its shape is nonlinear. This hypothesis is tested in simulations, where $\xi_2 = 0.1$ is fixed, while ξ_1 is varied accordingly, i. e., $(\xi_1/\xi_2) \in \{1, 5, 10\}$: In detail, the simulation model comprises the dynamics ((5.33) with (A.7)–(A.10), (5.41), the model-parameters provided in Table 5.2), and the switching law (5.34), all expressed under the change of coordinates (5.39). For all simulations, the switching threshold and amplitude are selected $\epsilon_{\mathrm{w}} = 0.001\,\mathrm{Nm}$ and $\hat{\theta}_{\mathrm{w}} = 1.25\,\mathrm{rad}$, respectively, and the initial control input $\bar{\boldsymbol{\theta}}^0 = \boldsymbol{x}(\boldsymbol{q}_0 = \bar{\boldsymbol{q}}(\boldsymbol{\theta}^0))$, configuration $\boldsymbol{x}_0 = \boldsymbol{x}(\boldsymbol{q}_0 = \bar{\boldsymbol{q}}(\boldsymbol{\theta}^0))$, and velocity $\dot{\boldsymbol{x}}_0 = \bar{\boldsymbol{w}}1\,\mathrm{rad/s}$, with $\bar{\boldsymbol{w}} = \partial \boldsymbol{x}(\boldsymbol{q})/\partial \boldsymbol{q}(\bar{\boldsymbol{q}}(\boldsymbol{\theta}^0))\boldsymbol{w}$, are chosen depending on $\boldsymbol{\theta}^0 = (-1, 1)\frac{70\pi}{180}\,\mathrm{rad}$ such that during simulation, the Jacobian matrix $\partial \boldsymbol{x}(\boldsymbol{q})/\partial \boldsymbol{q}$ becomes expectedly not singular.

Fig. 5.3 depicts the motion of the last four simulated oscillation cycles in (a) the phase planes $x_1(t)$ vs. $\dot{x}_1(t)$ and $x_2(t)$ vs. $\dot{x}_2(t)$ and (b) the configuration plane $x_1(t)$ vs. $x_2(t)$:

- The images of trajectories, as shown in (a), represent isolated paths, even though four oscillation cycles are plotted. This clearly indicates the *excitation* of *periodic orbits*, for all damping settings $(\xi_1/\xi_2) \in \{1, 5, 10\}$.

- By *increasing the damping of the transversal dynamics*, the *periodic motion approaches* the nonlinearly appearing *oscillation mode* (cf. (b)). In particular, when the damping of the transversal dynamics is ten-times higher than of the oscillation mode, i. e., $\xi_1/\xi_2 = 10$, then, the configuration variables move mainly in that 1-D submanifold. This finding is further supported by the observation that the distance of the actual w. r. t. the theoretical switching position decreases, when the damping of the transversal dynamics increases.

- When the damping of eigenmode and transversal dynamics is equal and low, i. e., $\xi_2 = \xi_1 = 0.1$, the image of the trajectory in the configuration plane intersects itself (cf. (b)). Since a self-intersecting curve is neither homeomorphic to a circle, an open interval, a closed interval, nor to a half-open interval, it cannot represent an 1-manifold. By virtue of Theorem 5.3, this in turn reveals that in case of low damping of the transversal dynamics, a periodic orbit results, but it is not contained in an oscillation mode according to Definition 5.2.

The above result reveals that, as soon as all modal conditions are fulfilled, a straightforward way to excite a nonlinear mode is to transform to the coordinates given by inverting

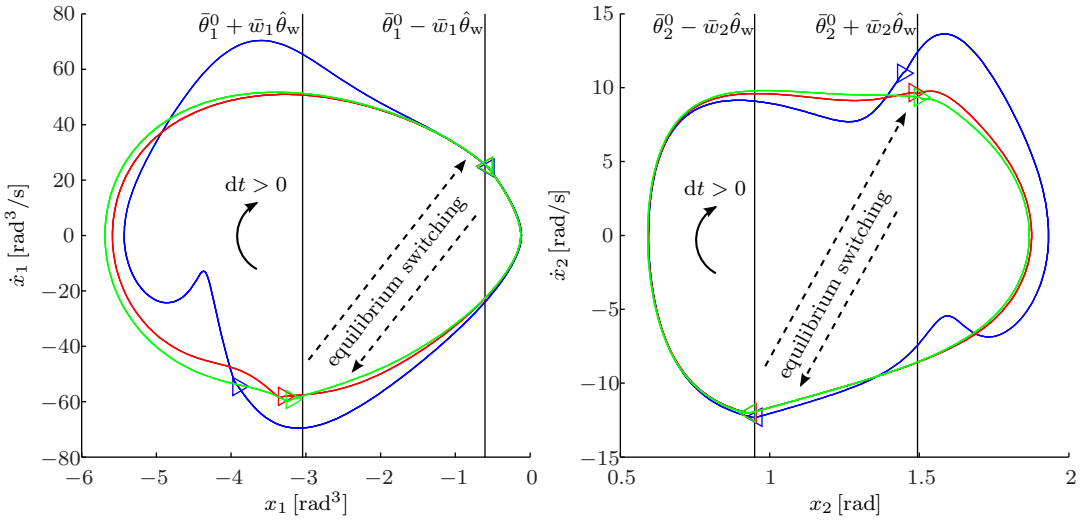

(a) Phaseplots

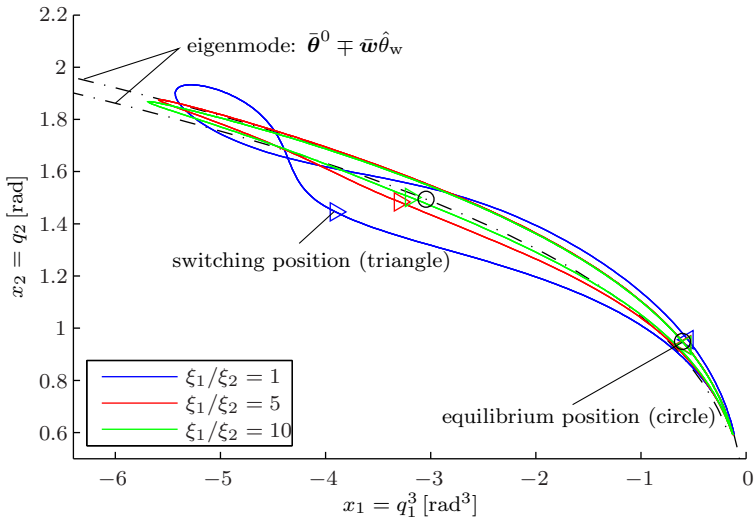

(b) Motion w. r. t. manifold of oscillation mode

Figure 5.3.: Effect of damping on the excitation of periodic motions in nonlinear oscillation modes by means of a linear displacement $\bar{\boldsymbol{\theta}} = \bar{\boldsymbol{\theta}}^0 \pm \bar{\boldsymbol{w}}\hat{\theta}_\mathrm{w}$. Triangle-markers denote actual switching points. For increased damping of the transversal dynamics, the actual switching position approaches the theoretical one.

mass	m_1	$0.5\,\mathrm{kg}$
mass	m_2	$0.5\,\mathrm{kg}$
link length	l	$0.1\,\mathrm{m}$
linear spring constant	k_{lin}	$2.0\,\mathrm{Nm/rad}$
cubic spring constant	k_{cub}	$0.25\,\mathrm{Nm/rad}^3$

Table 5.3.: Inertial and elastic parameters of the double pendulum example considered in simulation.

the modal function such that the nonlinear mode appears as a straight line. This way, an exact solution is obtained to excite and sustain oscillations evolving in the mode of the system.

5.3.4. Non-holonomic periodic orbits

The example of the previous section reveals that due to the presence of damping, periodic motions of the compliantly actuated systems (5.33) can be excited by means of the nonrestrictive, linearization based Assumption 5.1. In particular, the corresponding simulation results give rise to seek for conceptually different periodic orbits which evolve not in holonomic oscillation modes.

Consider, e. g., the dynamics of elastic, planar double pendulums. The relative angle of the first link w. r. t. to an inertial frame and the relative angle of the second link w. r. t. the first link are measured by the configuration variables q_1 and q_2, respectively. When all configuration variables are zero, i. e., $\boldsymbol{q} = \boldsymbol{0}$, both links are aligned. The lengths of all links are assumed to be equally l and its masses m_1, m_2 are assumed to be concentrated at half the link-lengths. In all joints cubic springs with equilibrium positions θ_i and equal spring constants $k_{\mathrm{lin}}, k_{\mathrm{cub}} > 0$ are considered such that the potential energy takes the form $U(\boldsymbol{q} - \boldsymbol{\theta}) = \sum_{i=1}^{2} \frac{1}{2} k_{\mathrm{lin}} (q_i - \theta_i)^2 + \frac{1}{4} k_{\mathrm{cub}} (q_i - \theta_i)^4$. Linear, viscous damping of the form $d\dot{q}_i$ is assumed, where $d \geq 0$. Therefore, the dynamics consists of the structure of (5.33). In the following simulations, the inertial and elastic parameters given in Table 5.3 are considered.

Centres

The example of Sect. 5.3.3 revealed that the exact excitation of non-conservative oscillation dynamics (based on displacements) requires explicit knowledge of oscillation modes. Since for the elastic double pendulum dynamics at hand, even their existence is not yet ensured, it is obvious to investigate periodic motions in form of centres first: Centres are defined for autonomous phase-planar systems (i. e., for a second-order dynamics). A centre is a stable equilibrium point surrounded in its immediate neighborhood by closed paths [JS07, p. 10]. From this definition it becomes evident, that a centre corresponds to a level-set of the total energy, which implies that the system is conservative, i. e., $d = 0$. Therefore, the energy level is fully determined by the initial state. In order to avoid assumptions on the shape of centres so far as it is possible, an initial state needs to be chosen, where the dynamics behaves locally like in a linear mode. Considering the equilibrium position of the springs $\boldsymbol{\theta} = \boldsymbol{0}$ implying $\bar{\boldsymbol{q}}(\boldsymbol{\theta}) = \boldsymbol{0}$, the initial configuration $\boldsymbol{q}(0) = \boldsymbol{0}$ is such that for any velocity $\dot{\boldsymbol{q}} \in \mathbb{R}^2$, the Coriolis/centrifugal matrix vanishes identically, i. e., $\boldsymbol{C}(\boldsymbol{0}, \dot{\boldsymbol{q}}) = \boldsymbol{0}$, and the system is in steady motion, i. e., $\ddot{\boldsymbol{q}} = \boldsymbol{0}$, since the potential force is also zero, i. e., $\partial U / \partial \boldsymbol{q}(\boldsymbol{q} = \boldsymbol{0}) = \boldsymbol{0}$. Furthermore, at $\boldsymbol{q} = \boldsymbol{0}$, the Hessian matrix of the potential energy

does not depend on the spring deflection $\boldsymbol{q} - \boldsymbol{\theta}$, i. e., $\partial^2 U / \partial \boldsymbol{q}^2(\boldsymbol{q} = \boldsymbol{0}) = \mathrm{diag}((k_{\mathrm{lin}}, k_{\mathrm{lin}}))$. This suggests to chose the initial velocity along one of the generalized eigenvectors $\boldsymbol{w}_i$, for $i = 1, 2$, of $\partial^2 U / \partial \boldsymbol{q}^2(\boldsymbol{q} = \boldsymbol{0})$ and $\boldsymbol{M}(\boldsymbol{q} = \boldsymbol{0})$ (cf. (5.6)–(5.7)), i. e., $\dot{\boldsymbol{q}}(0) = \boldsymbol{w}_i v_0$ with $v_0 \in \mathbb{R}$.

Fig. 5.4 shows the results of simulations which investigate the existence and structure of centres for different initial velocity amplitudes $v_0 \in \mathbb{R}$ along the first eigenvector $\boldsymbol{w}_1(\boldsymbol{q} = \boldsymbol{0})$ (corresponding to the lower eigenvalue $\lambda_1(\boldsymbol{q} = \boldsymbol{0}) < \lambda_2(\boldsymbol{q} = \boldsymbol{0})$). In order to indicate periodicity, ten oscillation cycles are plotted for each initial velocity amplitude v_0:

- Whilst taking into account that numerical integration is subject to noise, the considered elastic pendulum dynamics displays periodic orbits for initial velocity amplitudes $v_0 \in \{5, 20\}\,\mathrm{rad/s}$ as depicted in (a). For remaining velocity amplitudes $v_0 \in \{10, 15, 17, 19, 21\}\,\mathrm{rad/s}$, the motion is quasi-periodic in a sense that images of state-trajectories evolve in error-bands. This is even the case for values of v_0 close to but not exactly $20\,\mathrm{rad/s}$ (which corresponds to a periodic orbit).

- The motion of configuration variables $q_1(t)$ vs. $q_2(t)$ evolves approximately on 1-D curves, but their shape differs for different initial velocity amplitudes v_0 (cf. (b)). Due to this *non-holonomic behavior, these periodic orbits cannot be described by differentiable 1-manifolds.*

In contrast, as shown in Fig. 5.5, taking again into account that numerical integration is subject to noise, the elastic double pendulum dynamics displays periodic orbits for any of the considered initial velocity amplitudes $v_0 \in \{15, 30, 45, 60\}$ along the second eigenvector $\boldsymbol{w}_2(\boldsymbol{q} = \boldsymbol{0})$ (cf. (a)). In particular, the motion of the configuration variables $q_1(t)$ vs. $q_2(t)$ evolves on the same straight line, even though the initial velocity amplitude v_0 is varied (cf. (b)). This strongly indicates the existence of an eigenvector according to Definition 5.1, although an analytic expression could not be found yet. Furthermore, as illustrated in (c), the shape of this (possible) oscillation mode, expressed w. r. t. Cartesian coordinates describing the position of the pendulum tip, can approximately be represented by the even parabola function $x_2 = a_2 x_1^2 - a_0$. Such a shape can be exploited for the control of elastic, legged systems as presented in Sect. 6.4.

Non-conservative periodic orbits

The example of Sect. 5.3.3 revealed that viscous damping has a stabilizing effect on periodic motions. This result together with the evidence of periodic and quasi-periodic orbits with even non-holonomic structure gained above, motivates the investigation of the elastic double pendulum dynamics in the non-conservative case.

Consider again the elastic pendulum dynamics with parameters as given in Table 5.3, but where in contrast to the previous example the damping constant is chosen to be $d = 0.05\,\mathrm{Nms/rad}$. The resulting dissipation can be counter-acted by the excitation control (5.34).

Fig. 5.6 shows the results of simulations investigating the excitability of periodic motions for different switching amplitudes $\hat{\theta}_{\mathrm{w}} \in \{0.5, 0.75, 1.0\}\,\mathrm{rad}$ along the first eigenvector $\boldsymbol{w}_1(\boldsymbol{q} = \boldsymbol{0})$. The phaseplots, $q_1(t)$ vs. $\dot{q}_1(t)$ and $q_2(t)$ vs. $\dot{q}_2(t)$, of the last seven (simulated) oscillation cycles as depicted in (a), reveal that the elastic double pendulum dynamics can be excited with different switching amplitudes $\hat{\theta}_{\mathrm{w}}$ to display periodic orbits. However, the motion of configuration variables $q_1(t)$ vs. $q_2(t)$ evolves on curves, which at least for the greatest switching amplitude $\hat{\theta}_{\mathrm{w}}$ are homeomorphic neither to a circle nor to an interval

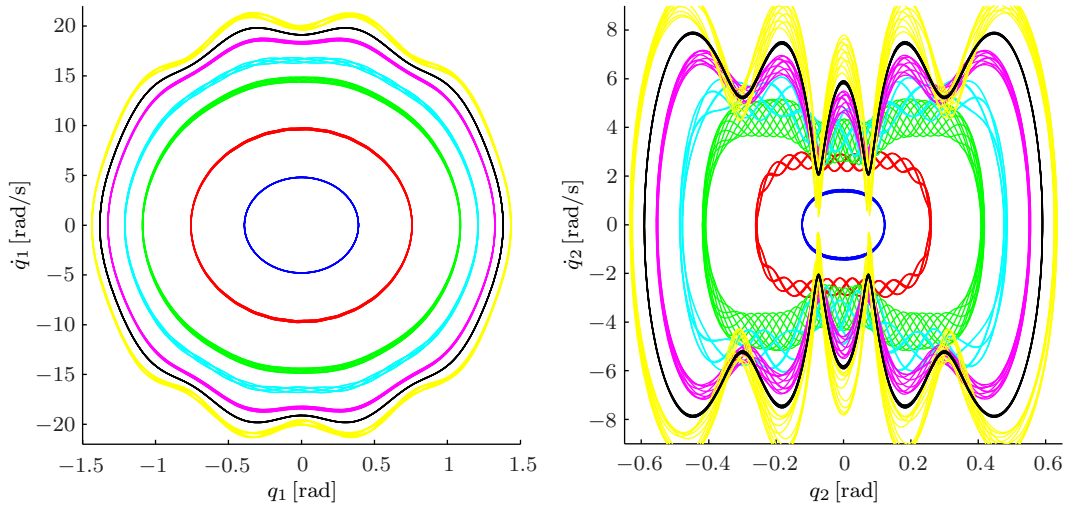

(a) Phaseplot expressed w. r. t. configuration coordinates. Periodic and quasi-periodic orbits (within an error band) can be observed.

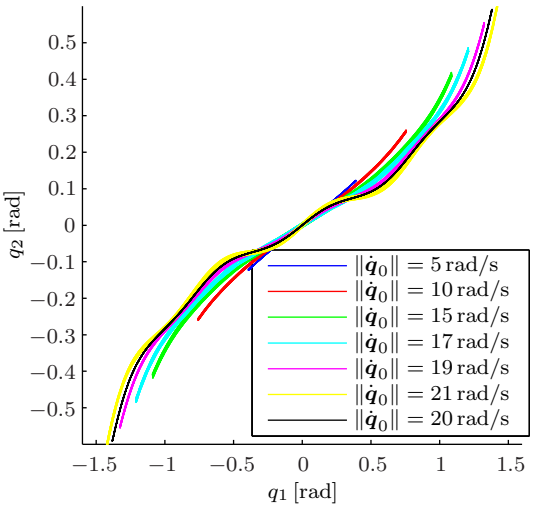

(b) Motion of configuration variables. It can be seen that the shape of paths depends on the initial velocity. This indicates non-holonomic constraints of the underlaying mode.

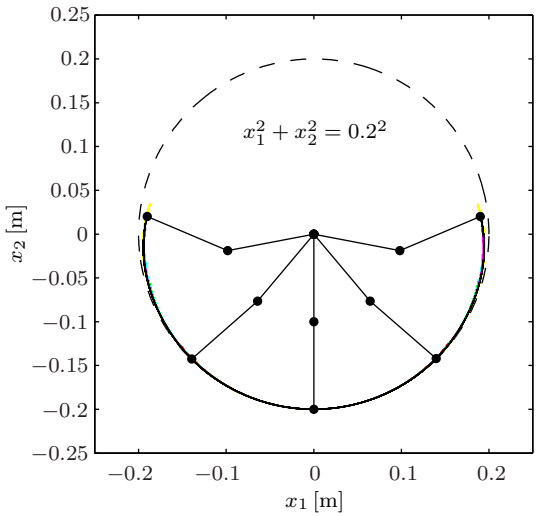

(c) Cartesian motion of the double pendulum

Figure 5.4.: Centres of the elastic double pendulum for different initial conditions along the *first eigenvector* of the linearized dynamics at equilibrium position $\bar{\boldsymbol{q}} = \boldsymbol{0}$. For each initial velocity, ten oscillation cycles are shown.

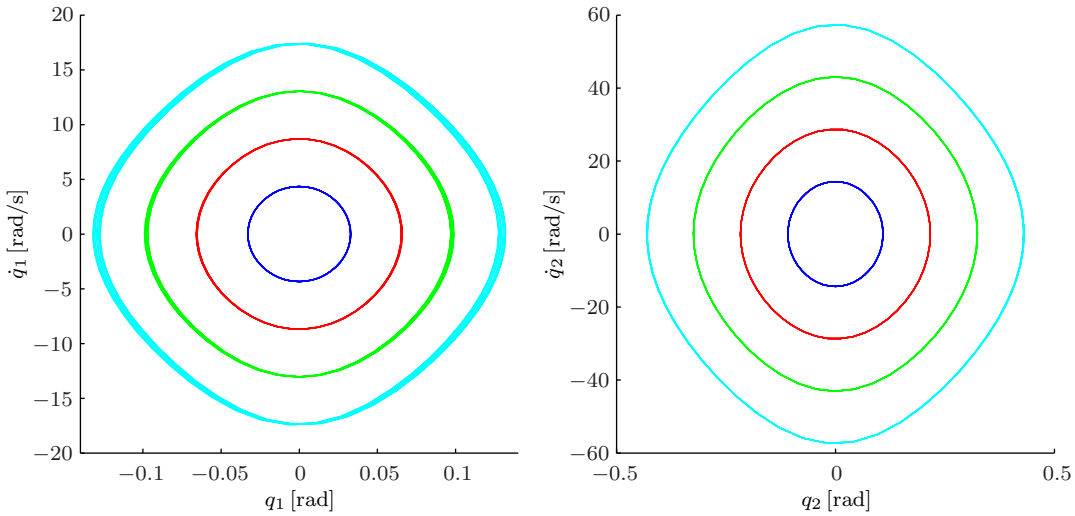

(a) Phaseplot expressed w. r. t. configuration coordinates. Periodic orbits can be observed.

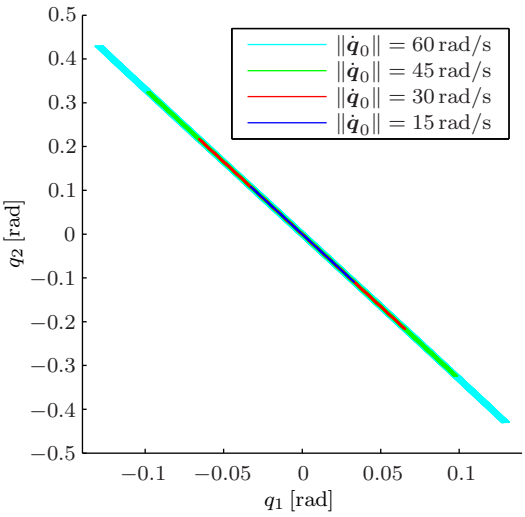

(b) Motion of configuration variables. The paths are all on the same straight line. This indicates the exsistence of an eigenmode.

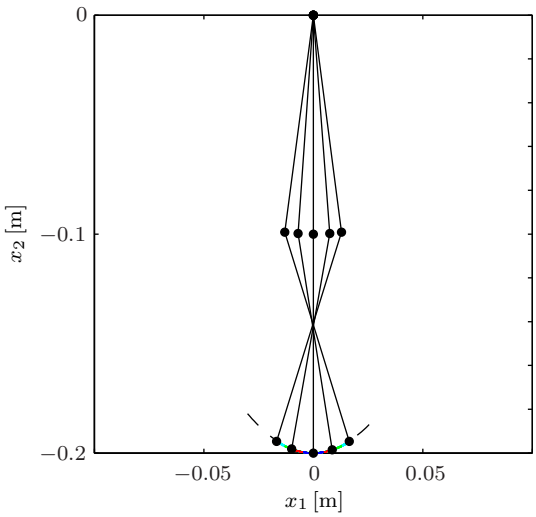

(c) Cartesian motion of the double pendulum

Figure 5.5.: Centres of the elastic double pendulum for different initial conditions along the *second eigenvector* of the linearized dynamics at equilibrium position $\bar{\boldsymbol{q}} = \boldsymbol{0}$. For each initial velocity, ten oscillation cycles are shown.

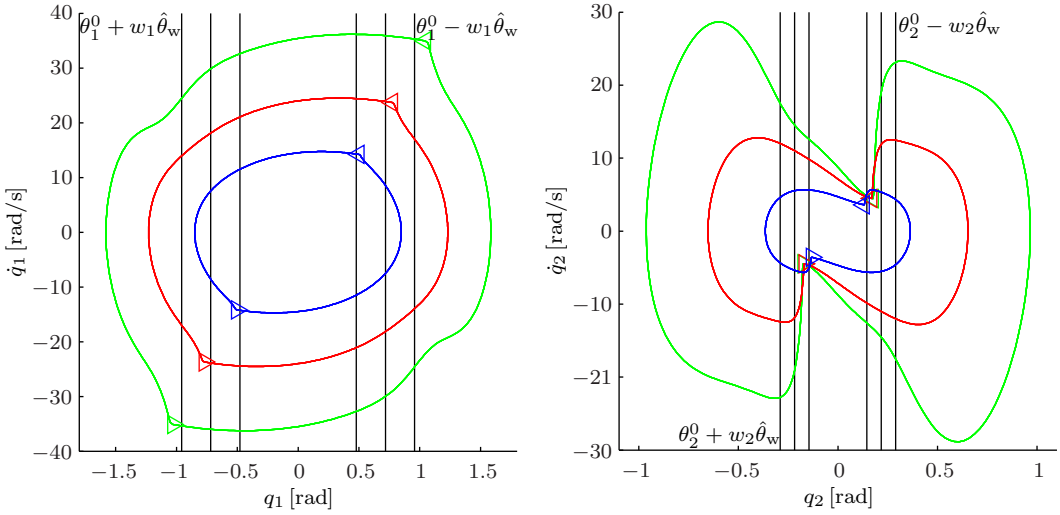

(a) Phaseplot expressed w. r. t. configuration coordinates. Periodic motions are excited for all switching amplitudes. This agrees with the observations of humans exciting a rod, which motivateted the switching-based limit cycle control proposed in Chapt. 4.

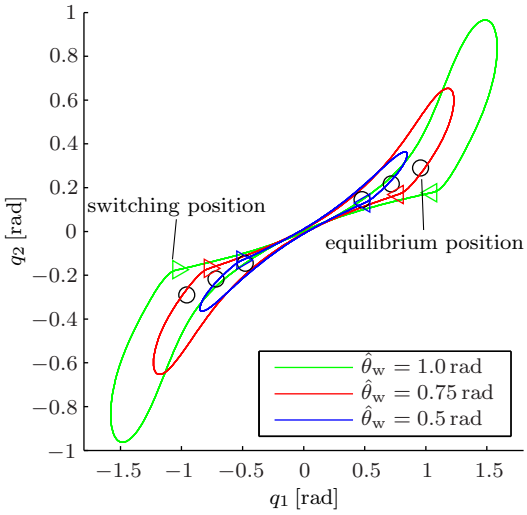

(b) Motion of configuration variables

Figure 5.6.: Periodic orbits of the elastic double pendulum excited along the *first eigenvector* of the linearized dynamics at equilibrium position $\bar{\boldsymbol{q}} = \mathbf{0}$ using the switching law (5.34). For each switching amplitude, seven oscillation cycles are shown.

(cf. (b)) such that according to Theorem 5.3, these motions corresponds not to oscillation modes.

In contrast, as shown in Fig. 5.7, the elastic pendulum dynamics displays periodic orbits for any switching amplitude $\hat{\theta}_{\mathrm{w}} \in \{0.5, 0.75, 1.0\}\,\mathrm{rad}$ along the second eigenvector $\boldsymbol{w}_2(\boldsymbol{q} = \boldsymbol{0})$ (cf. (a)). In particular, the motion of configuration variables $q_1(t)$ vs. $q_2(t)$ evolves on curves which are either homeomorphic to (half-open) intervals considering half oscillation cycles between switching positions or homeomorphic to circles considering complete oscillation cycles (cf. (b)) such that corresponding periodic orbits can be parametrized by 1-manifolds. This again strongly indicates the existence of an eigenvector of the elastic double pendulum dynamics according to Definition 5.1.

Remark 5.4. *Simulations of elastic n-pendulum dynamics with $n > 2$ reveal that if damping is present, excitations along eigenvectors corresponding not to the lowest eigenvalue (at equilibrium position) result in periodic orbits which can be parametrized by one-dimensional, differentiable manifolds.*

5.4. Summary

This chapter investigates the existence and excitability of oscillatory and periodic motions in the natural dynamics of compliantly actuated systems. The initial conjecture about the existence of natural, configuration-recurrent oscillations motivates a novel definition of oscillation modes, which is based upon 1-D, differentiable submanifolds of the configuration space. Thereby, the concept of eigenmodes of nonlinear dynamics has been proposed as a particular, linear class of oscillation modes. Although, the existence of so-called modal lines has been shown to exist in a class of systems consisting of constant masses but nonlinear elasticities before [CVS90], the proposed method of modal dynamics matching yields practically relevant and realizable examples of nonlinear, elastic multibody systems consisting of eigenmodes, which include also Coriolis/centrifugal effects.

The classification of periodic orbits of elastic mutlibody systems reveals that cases exist which cannot be described by the concept of oscillation modes. In particular, it has been shown by simulation that the elastic double pendulum dynamics displays centres with even a non-holonomic structure on the one hand. This is in accordance with topological results stating that every dynamical system having a closed configuration space displays a periodic motion [Fra03, Sect. 10.2d]. However, the comparison of the excitability of periodic orbits by linear displacements (as proposed in Chapt. 4) reveals that exact excitations of natural motions rely on the existence and knowledge of oscillation modes on the other hand. Although, the necessity of oscillation modes for the existence of periodic motions remains an open research topic so far, the examples at hand already validate the importance of this concept for energetically efficient robotic applications.

In Chapt. 4, a switching-based limit cycle controller and a corresponding convergence analysis have been derived for a second-order system. Since in oscillation modes, the dynamics of elastic multibody systems reduce to exactly this type of second-order dynamics, the control and convergence analysis of Chapt. 4 can directly be applied.

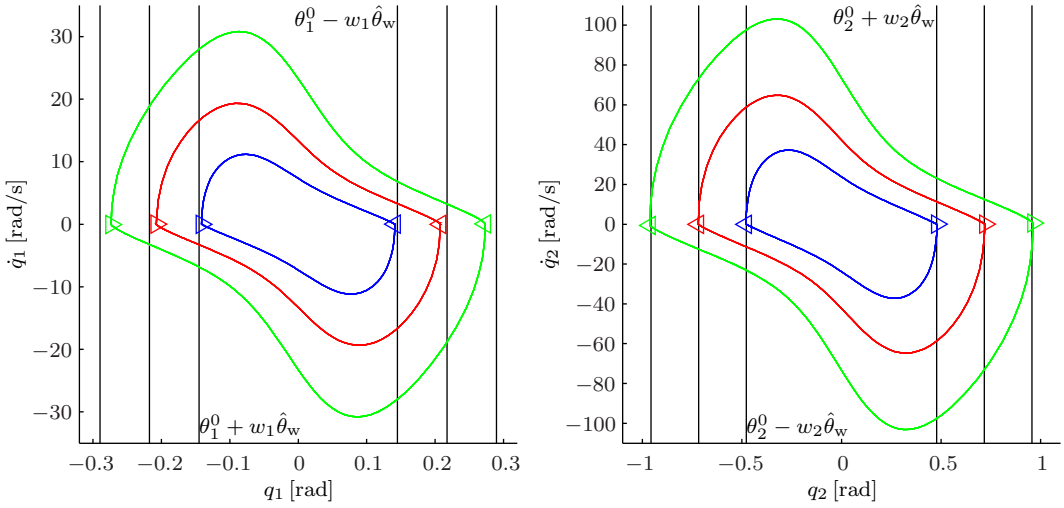

(a) Phaseplot expressed w. r. t. configuration coordinates

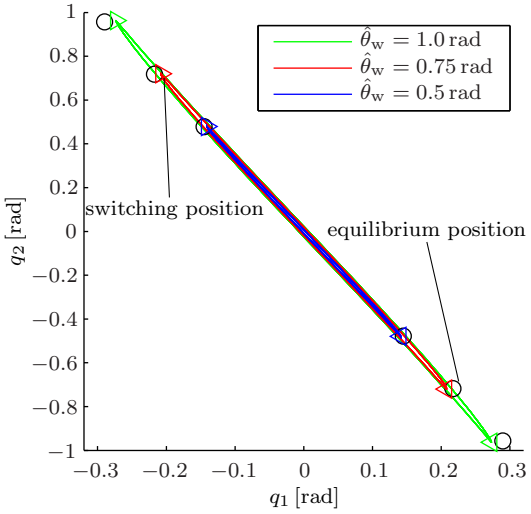

(b) Motion of configuration variables

Figure 5.7.: Periodic orbits of the elastic double pendulum excited along the *second eigenvector* of the linearized dynamics at equilibrium position $\bar{\boldsymbol{q}} = \mathbf{0}$ using the switching law (5.34). For each switching amplitude, seven oscillation cycles are shown.

CHAPTER 6

Modal Control

Compliantly actuated multibody systems feature the property of converting between kinetic and (elastic) potential energy back and forth. The compliance in the power-train allows joint motion even when the actuators do not move. In that case, the elastic elements perform the movement. If the system is controlled properly, the intrinsic, generally oscillatory behavior of the plant, can be exploited particularly in highly dynamical explosive or periodic motion tasks. Since in compliantly actuated systems, the power input to links is routed via the springs, a common wisdom of the mechanical design is to achieve as few friction as possible. This however entails the tendencies of the nonlinear dynamical system to display "chaotic" or impractical (w. r. t. a given task) natural motions, which make the control a challenging task. In the previous chapter, a theory has been introduced which enables to analyze and to alter the natural oscillatory behavior of such plants. The aim of this chapter is to address the problem of controlling multi-DOF compliantly actuated systems to perform a certain oscillatory or periodic task, while exploiting the natural dynamics behavior of the plant which can be described by its oscillation modes.

Explosive multi-joint motions of compliantly actuated robotic arms, such as throwing of a ball, have typically been achieved by numerical optimal control approaches [BHV11], [BPH$^+$12], [HHAS12], [BPH$^+$13]. These methods are mainly applied to systems with only two joints involved in the motion, as computational costs and the number of local minima explode with the number of degrees of freedom.

The natural oscillatory dynamics of compliantly actuated systems can be especially exploited in intrinsically periodic tasks of robotic arms such as hammering and pick-and-place, or in legged systems by tasks such as walking, jumping, and running. In particular for such motions, the power of the links is not limited by the power of the actuators, since the energy can be input cyclically in sequential portions into the plant. However, a major difficulty of controlling *multi-DOF* periodic motions in such systems is given by the fact that even if a Hamiltonian dynamics is achieved, e. g., by regulating the total energy to a constant level [GOAS13], the existence of a periodic orbit is not guaranteed. This means, e. g., when the total energy of a system is a quadratic form, then the only thing one can say about solutions is that they evolve on an paraboloid of one dimension less than the state space. In contrast, if the Hamiltonian dynamics of interest is *planar* (i. e., the state space is 2-D), then the volume of constant energy has the shape of a (planar) ellipse, which

necessarily also represents a periodic solution of the system. From these considerations it becomes clear that by guaranteeing the state of a compliantly actuated system to evolve in a 2-D manifold accomplishes a sufficient condition for the existence of periodic motions.

In the past, numerous methods have been developed to achieve invariant and even attractive 2-D manifolds in the state space of mechanical systems by control [GAP01], [CEU02], [WGK03], [DS03], [GOAS13]. The pioneering work of *Grizzle et al.* [GAP01] and its further development proposed in [CEU02] are based upon the concept of zero dynamics (ZD) control [Isi95]. The central idea is to generate a lower-dimensional, attractive subset (which is called zero manifold) in which the analysis of periodic solutions is drastically simplified. These methods are introduced in the context of bipedal locomotion control. By incorporating also the effect of impacts, which typically occur for dynamic gaits, the notion of hybrid zero dynamics (HZD) is introduced in [WGK03]. In particular, the approaches presented in [GAP01], [CEU02], [WGK03] apply to rigid-body control systems with a degree of under-actuation[1] of one. A common property of ZD and HZD methods is that stable periodic orbits are designed based on a Poincaré map approach, of which a comprehensive explanation is provided in [WGC+07]. The numerical, simulation based search for controls which generate periodic solutions is avoided by the methods presented in [DS03] and [GOAS13]. *Duindam and Stramigioli* propose a controller which achieves asymptotic convergence w. r. t. a desired curve in the configuration space of fully actuated rigid-body systems. Considering the same class of plants, a control method to achieve an attractive 1-D manifold of the configuration space is based on a semi-definite Lyapunov function approach [GOAS13]. Although the HZD and Lyapunov function based methods generalize to the compliantly actuated system case, as shown in [SPG13] and [GO16], respectively, the natural oscillatory behavior of the plant is not explicitly taken into account.

Further related approaches to generate coordinated, periodic motions of robotic multibody systems especially with plant-inherent elasticities in the joints are based upon adaptive frequency oscillators (AFO) [BI08], periodic motion tracking and simultaneous stiffness adaptation [UGK14], or inter-limb synchronization control [FvdSS14]. The method of AFOs presented in [BI08] exploits the concept of central pattern generators (CPG) [Ijs01]. Although the CPG considered in [BI08] adapt to an inherent frequency of the plant, the distribution of amplitudes, which are commanded to the joint actuators, needs to be manually tuned. Therefore, the resulting periodic excitation corresponds not necessarily to an oscillation mode of the plant. The control approach proposed in [FvdSS14] applies to systems composed of variable stiffness joints. A synchronization of periodic motions of different joints is achieved by considering their stiffnesses as control input.

In this chapter, control methods are proposed which induce oscillatory or periodic motions, and additionally exploit the natural oscillatory dynamics of the compliantly actuated systems to a large extent. Thereby, a major design goal is to replace the dynamic shaping based invariant manifolds, as outlined above, by plant inherent oscillation modes as introduced in Chapt. 5. Since oscillation modes are particular properties of elastic multibody systems (which need to be embodied in the mechanical design) on the one hand, but a general purpose robotic system needs to be versatile on the other hand, four different control concepts are proposed, which exploit the natural dynamics of compliantly actuated systems to different extent: In Sect. 6.1 the method of *modal globalization* is proposed [LGP+13a]. It considers the natural oscillatory dynamics locally, and designs

[1] The degree of under-actuation is the difference in the number of degrees of freedom and independent, scaler control inputs.

the control input such that they become valid globally. *Modal shaping*, as introduced in Sect. 6.2, exploits the concepts of Cartesian impedance control [OASK+04], [ASOH04], [Ott08] to design an 1-D submanifold in which the configuration variables are controlled to evolve [LGDAS14]. In that constraints manifold, the intrinsic oscillatory dynamics of the plant is maintained. In Sect. 6.3, the concept of *modal adaptation* is proposed [LGP+13b]. This method offers the capability to control periodic motions in inherent oscillation modes with at most the knowledge about the elastic and gravity model of the plant. Finally, in Sect. 6.4 a control concept is introduced, which exploits the nonlinearity of the elastic multibody system to match the direction of local eigenvectors to a given task [LAS16].

6.1. Modal globalization

Oscillation modes are intrinsic properties of the natural dynamics of compliantly actuated systems. Therefore, their existence and particularly their global validity are in general not guaranteed. The method of *modal globalization* control aims at high energetic efficiency in the generation of motion, although oscillation modes are not existent or known. Thereby, the idea is to consider the motion in the vicinity of an equilibrium point, where the prevalence of oscillation modes is guaranteed at least locally (cf. Sect. 5.1.1), and controlling the plant such that corresponding invariance properties become valid globally.

6.1.1. Controller design

Consider the dynamics

$$\boldsymbol{M}(\boldsymbol{q})\ddot{\boldsymbol{q}} + \boldsymbol{C}(\boldsymbol{q},\dot{\boldsymbol{q}})\dot{\boldsymbol{q}} + \frac{\partial U(\boldsymbol{\theta},\boldsymbol{q})}{\partial \boldsymbol{q}}^T = \boldsymbol{0}\,, \tag{6.1}$$

which corresponds to the conservative, indirectly actuated state dynamics of the compliantly actuated system as introduced by (3.27) in Sect. 3.1.1. In order not to presume any stabilizing effect on (excitable) periodic motions (cf. Sect. 5.3), dissipative forces are not considered in the dynamics (6.1).

Let $\boldsymbol{\theta} = \boldsymbol{\theta}^0 = \text{const.}$ such that $\boldsymbol{q}_0 = \bar{\boldsymbol{q}}(\boldsymbol{\theta}^0)$ (Definition 3.4) represent the equilibrium position of interest. Then, the generalized eigenvectors $\boldsymbol{W}(\boldsymbol{q}_0) = \big[\boldsymbol{w}_1(\boldsymbol{q}_0), \ldots, \boldsymbol{w}_n(\boldsymbol{q}_0)\big]$ of the local stiffness and inertia matrix $\boldsymbol{K}(\boldsymbol{q}_0) = \frac{\partial^2 U(\boldsymbol{q})}{\partial \boldsymbol{q}^2}\Big|_{\boldsymbol{q}=\boldsymbol{q}_0}$ and $\boldsymbol{M}(\boldsymbol{q}_0)$, respectively, define invariant directions of oscillation in the vicinity of $\boldsymbol{q}_0$ (cf. Sect. 5.1.1). A dynamics which preserves the modal invariance properties of the linearization, but which is structurally much closer to the original dynamics (6.1), can be obtained by considering a change of coordinates of the form

$$\Delta\boldsymbol{q} = \boldsymbol{q} - \boldsymbol{q}_0 = \boldsymbol{W}(\boldsymbol{q})\boldsymbol{z}\,, \tag{6.2}$$

where $\boldsymbol{z} \in \mathbb{R}^n$. This coordinate transformation is based on solutions of the generalized eigenvalue problem (5.6)–(5.7) (defined in Sect. 5.1.1), $\{\lambda_i(\boldsymbol{q}), \boldsymbol{w}_i(\boldsymbol{q})\}$ for $i = 1 \ldots n$, evaluated at the current configuration $\boldsymbol{q}$ such that the desired closed-loop dynamics can be expresses as

$$\ddot{z}_i + 2\xi_i\sqrt{\lambda_i(\boldsymbol{q})}\dot{z}_i + \lambda_i(\boldsymbol{q})z_i = 0\,, \quad \forall i = 1 \ldots n\,. \tag{6.3}$$

The eigenvectors $\boldsymbol{W}(\boldsymbol{q}) = \big[\boldsymbol{w}_1(\boldsymbol{q}), \ldots, \boldsymbol{w}_n(\boldsymbol{q})\big]$ underlying this modal dynamics are normalized such that $\boldsymbol{W}(\boldsymbol{q})^T\boldsymbol{M}(\boldsymbol{q})\boldsymbol{W}(\boldsymbol{q}) = \boldsymbol{I}$ and consequently $\boldsymbol{W}(\boldsymbol{q})^T\boldsymbol{K}(\boldsymbol{q})\boldsymbol{W}(\boldsymbol{q}) = \text{diag}\,(\lambda_i(\boldsymbol{q}))$.

To influence the convergence properties of each of the modal dynamics (6.3) separately, a modal damping term of the form

$$\boldsymbol{D}(\boldsymbol{q})\dot{\boldsymbol{q}} = \boldsymbol{W}(\boldsymbol{q})^{-T}\mathrm{diag}\left(2\xi_i\sqrt{\lambda_i(\boldsymbol{q})}\right)\boldsymbol{W}(\boldsymbol{q})^{-1}\dot{\boldsymbol{q}} \tag{6.4}$$

is assumed to be assigned by control. Thereby, the normalized damping factors $\xi_i \in [0;1]$ can, e. g., be chosen low or zero for a desired mode and high for all other modes. This way,model uncertainties and disturbances can be handled by control.

The control law can be derived by transforming the plant dynamics (6.1) under the change of coordinates (6.2) and comparing the result with the desired modal dynamics (6.3). This yields,

$$-\frac{\partial U(\boldsymbol{\theta},\boldsymbol{q})}{\partial \boldsymbol{q}}^T = -\boldsymbol{D}(\boldsymbol{q})\dot{\boldsymbol{q}} - \boldsymbol{K}(\boldsymbol{q})\Delta\boldsymbol{q} + \boldsymbol{W}(\boldsymbol{q})^{-T}\tilde{\boldsymbol{C}}(\boldsymbol{q},\dot{\boldsymbol{q}})\dot{\boldsymbol{z}} + \boldsymbol{\gamma}(\boldsymbol{q},\dot{\boldsymbol{q}},\ddot{\boldsymbol{q}})\,, \tag{6.5}$$

where the terms

$$\begin{aligned}\boldsymbol{W}(\boldsymbol{q})^{-T}\tilde{\boldsymbol{C}}(\boldsymbol{q},\dot{\boldsymbol{q}})\dot{\boldsymbol{z}} + \boldsymbol{\gamma}(\boldsymbol{q},\dot{\boldsymbol{q}},\ddot{\boldsymbol{q}}) \\ = \boldsymbol{C}(\boldsymbol{q},\dot{\boldsymbol{q}})\dot{\boldsymbol{q}} + 2\boldsymbol{M}(\boldsymbol{q})\dot{\boldsymbol{W}}(\boldsymbol{q})\dot{\boldsymbol{z}} + \left(\boldsymbol{M}(\boldsymbol{q})\ddot{\boldsymbol{W}}(\boldsymbol{q}) + \boldsymbol{D}(\boldsymbol{q})\dot{\boldsymbol{W}}(\boldsymbol{q})\right)\boldsymbol{z}\end{aligned} \tag{6.6}$$

are responsible for the modal globalization process.

Assumption 6.1. *The matrix $\boldsymbol{K}(\boldsymbol{q})$ is assumed to be bounded from above such that together with the positive definiteness of $\boldsymbol{K}(\boldsymbol{q})$ and $\boldsymbol{M}(\boldsymbol{q})$, the corresponding eigenvalues are bounded from below and above by positive constants $\lambda_{i,\min} > 0$ and $\lambda_{i,\max} > \lambda_{i,\min}$, respectively, i. e.,*

$$\inf_{\boldsymbol{q}\in\mathbb{R}^n} \lambda_i\left(\boldsymbol{K}(\boldsymbol{q}),\boldsymbol{M}(\boldsymbol{q})\right) > \lambda_{i,\min} \tag{6.7}$$

$$\sup_{\boldsymbol{q}\in\mathbb{R}^n} \lambda_i\left(\boldsymbol{K}(\boldsymbol{q}),\boldsymbol{M}(\boldsymbol{q})\right) < \lambda_{i,\max} \tag{6.8}$$

for all $i = 1 \ldots n$.

This assumption forms the precondition for the exponential stability proof proposed in the next section. An alternative control law, which avoids the boundedness condition on $\boldsymbol{K}(\boldsymbol{q})$ but still achieves globally valid oscillation modes, allows currently to proof only asymptotic stability:

Remark 6.1. *The control law*

$$-\frac{\partial U(\boldsymbol{\theta},\boldsymbol{q})}{\partial \boldsymbol{q}}^T = -\boldsymbol{D}(\boldsymbol{q})\dot{\boldsymbol{q}} - \boldsymbol{K}(\boldsymbol{q})\Delta\boldsymbol{q} + \boldsymbol{W}(\boldsymbol{q})^{-T}\left(\tilde{\boldsymbol{C}}(\boldsymbol{q},\dot{\boldsymbol{q}}) - \mathrm{diag}\left(\tilde{C}_{ii}(\boldsymbol{q},\dot{\boldsymbol{q}})\right)\right)\dot{\boldsymbol{z}} + \boldsymbol{\gamma}(\boldsymbol{q},\dot{\boldsymbol{q}},\ddot{\boldsymbol{q}}) \tag{6.9}$$

leads to the closed-loop dynamics

$$\frac{1}{\lambda_i(\boldsymbol{q})}\ddot{z}_i - \frac{\dot{\lambda}_i(\boldsymbol{q})}{2\lambda_i(\boldsymbol{q})^2}\dot{z}_i + \frac{2\xi_i}{\sqrt{\lambda_i(\boldsymbol{q})}}\dot{z}_i + z_i = 0\,. \tag{6.10}$$

For $\xi_i > 0$, asymptotic stability of the equilibrium point $\boldsymbol{z} = \dot{\boldsymbol{z}} = \boldsymbol{0}$ can be easily proven by a candidate Lyapunov function of the form $V(\boldsymbol{z},\dot{\boldsymbol{z}}) = \sum_{i=1}^{n}\frac{1}{2}\left(\frac{1}{\lambda_i}\dot{z}_i^2 + z_i^2\right)$ analogously to the proof of Proposition 4.1 provided in Appendix A.1.

6.1.2. Exponential stability

The proof of exponential stability is based upon a particular class of strict Lyapunov functions with constant Hessians.

Theorem 6.1. *Consider the dynamics*

$$\ddot{z} + 2\xi\sqrt{\lambda(t)}\dot{z} + \lambda(t)z = 0\,, \tag{6.11}$$

where $\xi \in (0;1]$ *is constant and* $\lambda \in (\lambda_{\min};\lambda_{\max})$ *is bounded by strictly positive constants* $\lambda_{\min} < \lambda_{\max}$. *If for a given* $\xi \in (0;1]$,

$$\frac{\lambda_{\max}}{\lambda_{\min}} \leq \left(\frac{\xi^2+1+\xi\sqrt{\xi^2+1}}{\xi^2+1-\xi\sqrt{\xi^2+1}}\right)^2 \tag{6.12}$$

is satisfied, then the origin $\boldsymbol{x} = (z,\dot{z}) = \mathbf{0}$ *of the dynamics* (6.11) *is globally exponentially stable, uniformly in time* t.

Proof. The origin $\boldsymbol{x} = \mathbf{0}$ of the system (6.11) is exponentially stable, if there exists a continuously differentiable function $V : \mathbb{R}_{\geq 0} \times \mathbb{R}^2 \to \mathbb{R}$ such that

$$a_1\|\boldsymbol{x}\|^2 \leq V(t,\boldsymbol{x}) \leq a_2\|\boldsymbol{x}\|^2 \tag{6.13}$$

$$\dot{V}(t,\boldsymbol{x}) \leq -a_3\|\boldsymbol{x}\|^2 \tag{6.14}$$

for all $t \geq 0$ and for all $\boldsymbol{x} \in \mathbb{R}^2$, where a_1, a_2 and a_3 are positive constants [Kha02, Theorem 4.10, p. 154].

Condition (6.13) can be validated by considering a candidate Lyapunov function of the form

$$V(\boldsymbol{x}) = \frac{1}{2}\boldsymbol{x}^T\begin{bmatrix} c_2 & c_1/2 \\ c_1/2 & 1 \end{bmatrix}\boldsymbol{x}\,. \tag{6.15}$$

Herein, c_1 and c_2 are constants satisfying

$$c_2 > c_1^2/4 \tag{6.16}$$

such that $V(\boldsymbol{x}) > 0$ for all $\boldsymbol{x} \neq \mathbf{0}$. The Hessian of $V(\boldsymbol{x})$, $\partial^2 V(\boldsymbol{x})/\partial\boldsymbol{x}^2$, is constant and positive definite (by definition (6.16)) such that condition (6.13) is satisfied by selecting $a_1 = \min_{i\in\{1,2\}} \lambda_i\left(\partial^2 V(\boldsymbol{x})/\partial\boldsymbol{x}^2\right) > 0$ and $a_2 = \max_{i\in\{1,2\}} \lambda_i\left(\partial^2 V(\boldsymbol{x})/\partial\boldsymbol{x}^2\right) \geq a_1$.

The derivative of $V(\boldsymbol{x})$ along the solution of (6.11),

$$\dot{V}(t,\boldsymbol{x}) = -\frac{1}{2}\boldsymbol{x}^T\boldsymbol{H}(\lambda(t))\boldsymbol{x}\,, \tag{6.17}$$

where

$$\boldsymbol{H}(\lambda(t)) = \begin{bmatrix} c_1\lambda(t) & \lambda(t) + c_1\xi\sqrt{\lambda(t)} - c_2 \\ \text{sym.} & 4\xi\sqrt{\lambda(t)} - c_1 \end{bmatrix}, \tag{6.18}$$

satisfies condition (6.14), if the matrix $\boldsymbol{H}(\lambda(t))$ is positive definite for all $\lambda \in [\lambda_{\min};\lambda_{\max}]$. This in turn is the case if and only if the leading principal minors of $\boldsymbol{H}$ are strict positive, i. e.,

$$c_1\lambda > 0\,, \tag{6.19}$$

$$\det\left(\boldsymbol{H}(\lambda)\right) > 0 \tag{6.20}$$

for all $\lambda \in (\lambda_{\min}; \lambda_{\max})$. Condition (6.19) can be satisfied for any $c_1 > 0$, since λ is strictly positive. It remains to show that there exists $c_1, c_2 > 0$ for which in addition to (6.16), also condition (6.20) holds for all $\lambda \in (\lambda_{\min}; \lambda_{\max})$.

The determinant of condition (6.20) represents a polynomial of degree of 2:

$$p(\lambda) = -\lambda^2 + 2\xi c_1 \lambda^{\frac{3}{2}} + \left[2c_2 - \left(1 + \xi^2\right) c_1^2\right] \lambda + 2\xi c_1 c_2 \lambda^{\frac{1}{2}} - c_2^2 \,. \tag{6.21}$$

Since the coefficient of the term of highest degree is negative and the degree of the polynomial is even, it follows that $\lim\limits_{\lambda\to\infty} p(\lambda) = \lim\limits_{\lambda\to-\infty} p(\lambda) = -\infty$. It can be verified by direct calculation that $p(\lambda)$ has at most two real roots

$$\lambda_{\max\,/\,\min} = \frac{\left(\xi c_1 + \beta \pm \sqrt{\left[\left(\xi^2 - 1\right) c_1 + 2\xi\beta\right] c_1}\right)^2}{4} \,, \tag{6.22}$$

where $\beta := 4c_2 - c_1^2 > 0$ according to condition (6.16). If the radicand $\left[\left(\xi^2 - 1\right) c_1 + 2\xi\beta\right] c_1$ is nonnegative, then the polynomial (6.21) has exactly two (positive) real roots implying that $p(\lambda) = \det\left(\boldsymbol{H}(\lambda)\right) > 0$ for all $\lambda \in (\lambda_{\min}; \lambda_{\max})$. It remains to validate condition (6.12). To this end, define

$$\alpha(c_1, \beta) = \frac{\lambda_{\max}}{\lambda_{\min}} = \frac{\left(\xi c_1 + \beta + \sqrt{\left[\left(\xi^2 - 1\right) c_1 + 2\xi\beta\right] c_1}\right)^2}{\left(\xi c_1 + \beta - \sqrt{\left[\left(\xi^2 - 1\right) c_1 + 2\xi\beta\right] c_1}\right)^2} \tag{6.23}$$

according to (6.22). By differentiation it can be seen that

$$\begin{pmatrix} \frac{\partial\alpha(c_1,\beta)}{\partial c_1} \\ \frac{\partial\alpha(c_1,\beta)}{\partial\beta} \end{pmatrix} = \boldsymbol{0} \iff c_1 = \xi\beta \,. \tag{6.24}$$

By substituting this result in (6.23), it turns out that[2]

$$\alpha_{\max} = \frac{\lambda_{\max}}{\lambda_{\min}} = \left(\frac{\xi^2 + 1 + \xi\sqrt{\xi^2 + 1}}{\xi^2 + 1 - \xi\sqrt{\xi^2 + 1}}\right)^2 \tag{6.25}$$

is only a function of ξ. This validates condition (6.12) of the theorem.

Remark 6.2. *One of the bounds on λ,*

$$\lambda_{\max\,/\,\min} = \frac{\beta^2 \left(\xi^2 + 1 \pm \xi\sqrt{\xi^2 + 1}\right)^2}{4} \tag{6.26}$$

can be chosen independently of the ratio of eigenvalue bounds $\alpha_{\max}$ defined in (6.25)*.*

The matrix $\boldsymbol{H}(\lambda(t))$ is positive definite for all $\lambda \in (\lambda_{\min}; \lambda_{\max})$, $\dot{V}(t, \boldsymbol{x}) < 0$ for all $\boldsymbol{x} \neq \boldsymbol{0}$ and for all $t \in \mathbb{R}_{\geq 0}$. Thus, condition (6.14) can be satisfied by selecting

$$a_3 = \inf_{\lambda\in(\lambda_{\min};\lambda_{\max})} \left[\min_{i\in\{1,2\}} \lambda_i\left(\boldsymbol{H}(\lambda)\right)\right] > 0 \,.$$

Since conditions (6.13) and (6.14) hold also for $\|\boldsymbol{x}\| \to \infty$, the origin $\boldsymbol{x} = \boldsymbol{0}$ of the system (6.11) is globally exponentially stable. □

[2] By considering the Hessian of $\alpha(c_1, \beta)$ it can be seen that the extremum $c_1 = \xi\beta$ is a maximum.

Proposition 6.1. *Given are $\xi_i \in (0;1]$ for $i = 1 \dots n$. If in addition to Assumption 6.1,*

$$\frac{\lambda_{i,\max}}{\lambda_{i,\min}} \leq \left(\frac{\xi_i^2 + 1 + \xi_i \sqrt{\xi_i^2 + 1}}{\xi_i^2 + 1 - \xi_i \sqrt{\xi_i^2 + 1}} \right)^2 \tag{6.27}$$

holds for all $i = 1 \dots n$, then the origin $\boldsymbol{z} = \dot{\boldsymbol{z}} = \boldsymbol{0}$ of the system (6.3) is globally exponentially stable.

Proof. By replacing the dependency of λ_i on the configuration variables $\boldsymbol{q}$ by time t, i. e., $\lambda_i(\boldsymbol{q}) = \lambda_i(t)$, Theorem 6.1 can be applied to the i-th subsystem in (6.3), separately. □

6.1.3. Energy based limit cycle generation

In this section, a method is presented to generate a limit cycle along a globalized mode of the system (6.1). The controller regulates the energy corresponding to the considered mode to a desired level, similar to what was done in [GOAS13]. The approach can be regarded as an alternative to the method proposed in Sect. 4.4.

Consider the dynamics of the k-th globalized mode in the form of Remark 6.1,

$$\frac{1}{\lambda_k(t)} \ddot{z}_k - \frac{\dot{\lambda}_k(t)}{2\lambda_k(t)^2} \dot{z}_k + \frac{2\xi_k}{\sqrt{\lambda_k(t)}} \dot{z}_k + z_k = 0 \,, \tag{6.28}$$

where the dependency of λ_k on the configuration variables $\boldsymbol{q}$ is replaced by time t, i. e., $\lambda_k(\boldsymbol{q}) = \lambda_k(t)$. (The remaining $n-1$ subsystems can also be considered in the form of (6.3).) The goal is to find a (nonlinear) damping coefficient ξ_k such that the Hamiltonian of the k-th mode

$$H(t, z_k, \dot{z}_k) = \frac{1}{2\lambda_k(t)} \dot{z}_k^2 + \frac{1}{2} z_k^2 \,, \tag{6.29}$$

regulates to the constant desired value $H_{\mathrm{des}} > 0$. From the derivative of $H(t, z_k, \dot{z}_k)$ along the solution of (6.28),

$$\dot{H}(t, z_k, \dot{z}_k) = -\frac{2\xi_k}{\sqrt{\lambda_k(t)}} \dot{z}_k^2 \,, \tag{6.30}$$

it can be seen that this is achieved if

$$\xi_k = \frac{\sqrt{\lambda_k(t)}}{2} k_{\mathrm{H}} \tilde{H}(t, z_k, \dot{z}_k) \,, \tag{6.31}$$

where $k_{\mathrm{H}} > 0$ represents a controller gain and $\tilde{H}(t, z_k, \dot{z}_k) = H(t, z_k, \dot{z}_k) - H_{\mathrm{des}}$.

Theorem 6.2. *The system (6.28) and (6.31) displays an asymptotically stable limit cycle*

$$\mathcal{L} = \left\{ (z_k, \dot{z}_k) \in \mathbb{R}^2 \,|\, H(t, z_k, \dot{z}_k) = H_{\mathrm{des}} \right\} .$$

Proof. Consider the continuously differentiable function

$$V(t, z_k, \dot{z}_k) = \frac{1}{2} \tilde{H}(t, z_k, \dot{z}_k)^2 \tag{6.32}$$

as candidate Lyapunov function satisfying $V(t, z_k, \dot{z}_k) = 0$ only if $(z_k, \dot{z}_k) \in \mathcal{L}$ and $\dot{V}(t, z_k, \dot{z}_k) = -k_{\mathrm{H}} \tilde{H}(t, z_k, \dot{z}_k)^2 \dot{z}_k^2 \leq 0$ for all $t \in \mathbb{R}_{\geq 0}$ and for all $(z_k, \dot{z}_k) \in \mathbb{R}^2$. Since, additionally, $V(t, z_k, \dot{z}_k)$ is bounded from below and above by positive definite functions

$$S_1(z_k, \dot{z}_k) = \frac{1}{2} \left(\frac{1}{2\lambda_{k,\max}} \dot{z}_k^2 + \frac{1}{2} z_k^2 - H_{\mathrm{des}} \right)^2 ,$$
$$S_2(z_k, \dot{z}_k) = \frac{1}{2} \left(\frac{1}{2\lambda_{k,\min}} \dot{z}_k^2 + \frac{1}{2} z_k^2 - H_{\mathrm{des}} \right)^2 ,$$

on $\mathbb{R}^2$, respectively, i. e.,

$$S_1(z_k, \dot{z}_k) \leq V(t, z_k, \dot{z}_k) \leq S_2(z_k, \dot{z}_k) \,,$$

(where $\lambda_{k,\min}$ and $\lambda_{k,\max}$ exist by Assumption 6.1,) $\mathcal{L}$ is uniformly stable according to [Kha02, Theorem 4.8, p. 151].

To prove attractiveness of $\mathcal{L}$, Barbalat's lemma (see, e. g., [SL91, Lemma 4.3, p. 125]) can be applied: It has already been shown that $V(t, z_k, \dot{z}_k)$ is bounded from below and that $\dot{V}(t, z_k, \dot{z}_k)$ is negative semi-definite. It remains to show that $\dot{V}(t, z_k, \dot{z}_k)$ is uniformly continuous in time t. This can be done by showing that

$$\ddot{V}(t, z_k, \dot{z}_k) = -2k_{\mathrm{H}} \tilde{H}(t, z_k, \dot{z}_k)^2 \dot{z}_k \left(k_{\mathrm{H}} + \ddot{z}_k\right)$$

is bounded, which is the case since (6.28) and (6.31) is stable. Therefore, it follows that

$$\lim_{t \to \infty} \dot{V}(t, z_k, \dot{z}_k) = 0 \,. \tag{6.33}$$

Let $\mathcal{B}_\epsilon(\mathcal{L})$ be a neighborhood of $\mathcal{L}$ such that $\{z_k = 0, \dot{z}_k = 0\} \notin \mathcal{B}_\epsilon(\mathcal{L})$. Since, $\mathcal{L}$ is stable, initial conditions can be always chosen such that the solution remains in $\mathcal{B}_\epsilon(\mathcal{L})$. Moreover, (6.33) implies that either $\dot{z}_k \to 0$ or $H(t, z_k, \dot{z}_k) \to H_{\mathrm{des}}$ as $t \to \infty$. But since the system cannot converge to $\{z_k \neq 0, \dot{z}_k = 0\}$ and $\{z_k = 0, \dot{z}_k = 0\} \notin \mathcal{B}_\epsilon(\mathcal{L})$, it can be concluded that the solution must converge to $\mathcal{L}$. □

6.2. Modal shaping

To achieve high performance and efficiency, oscillation modes corresponding to the dynamics of certain tasks can be embodied into a compliantly actuated system. However, there might be also other (less important) tasks a robotic system should be able to perform, whose dynamics cannot be (simultaneously) embodied into the plant. For that purpose, a method is required which achieves the dynamics behavior of these additional tasks by control. This shaping of dynamics to increase the versatility of the compliantly actuated system implies losses of performance and efficiency. The proposed method of modal shaping aims at minimizing the control effort and the corresponding energetic losses by exploiting the intrinsic oscillator behavior of the plant for motion generation in the shaped mode. The basic idea of modal shaping is to constrain the motion of the configuration variables to an 1-D submanifold corresponding to the desired task by control, but consider the intrinsic oscillatory behavior of the compliantly actuated system for motion generation in this mode.

The approach is introduced for so-called floating base systems, where not all of the indirectly actuated degrees of freedom are statically controllable (cf. Sect. 3.1.1). However, the case of so-called fixed base systems (where all of the indirectly actuated degrees of freedom are statically controllable) is trivially contained.

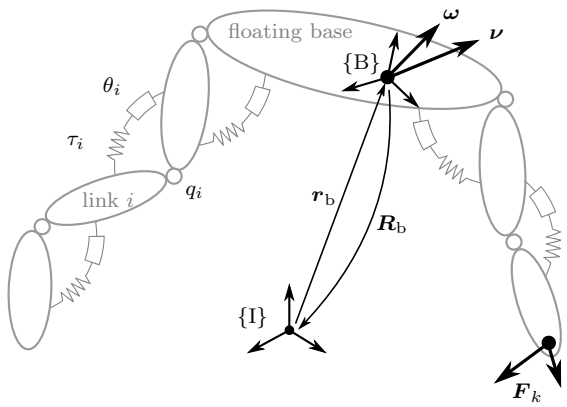

Figure 6.1.: Kinematic description of compliantly actuated free-floating base systems

6.2.1. Compliantly actuated free-floating base system

Consider the kinematic structure of a floating base system, which can be defined as shown in Fig. 6.1. The (absolute) position and orientation of the base link frame {B} with respect to an inertial frame {I} can be described by $\boldsymbol{r}_\mathrm{b} \in \mathbb{R}^3$ and $\boldsymbol{R}_\mathrm{b} \in SO(3)$, respectively, and the configuration of the kinematic chains attached to the base link can be represented by so-called joint coordinates $\boldsymbol{q} \in \mathbb{R}^n$, where n denotes the number of indirectly actuated, statically controllable degrees of freedom. The generalized velocity of the complete system $\boldsymbol{v} = \begin{bmatrix}\boldsymbol{\omega}^T & \dot{\boldsymbol{r}}_\mathrm{b}^T & \dot{\boldsymbol{q}}^T\end{bmatrix}^T$ comprises the angular and translational velocity of the base link, $\boldsymbol{\omega} \in \mathbb{R}^3$ and $\dot{\boldsymbol{r}}_\mathrm{b} \in \mathbb{R}^3$, respectively, and the joint velocity $\dot{\boldsymbol{q}} \in \mathbb{R}^n$. The dynamics of the floating base system can be expressed in the form

$$\boldsymbol{M}(\boldsymbol{R}_\mathrm{b}, \boldsymbol{q})\dot{\boldsymbol{v}} + \boldsymbol{b}(\boldsymbol{R}_\mathrm{b}, \boldsymbol{q}, \boldsymbol{v}) + \begin{pmatrix} \boldsymbol{0} \\ \boldsymbol{d}(\dot{\boldsymbol{q}}) + \frac{\partial U_\mathrm{e}(\boldsymbol{\theta}, \boldsymbol{q})}{\partial \boldsymbol{q}}^T \end{pmatrix} = \sum_k \boldsymbol{J}_k(\boldsymbol{q})^T \boldsymbol{F}_k \,, \tag{6.34}$$

where $\boldsymbol{M}(\boldsymbol{R}_\mathrm{b}, \boldsymbol{q})$ denotes the symmetric and positive definite $(n+6)\times(n+6)$ inertia matrix, $\boldsymbol{b}(\boldsymbol{R}_\mathrm{b}, \boldsymbol{q}, \boldsymbol{v}) \in \mathbb{R}^{(6+n)}$ represents the generalized bias forces containing Coriolis/centrifugal and gravity effects, and $\boldsymbol{d}(\dot{\boldsymbol{q}}) \in \mathbb{R}^n$ are generalized dissipative forces satisfying $\boldsymbol{d}(\dot{\boldsymbol{q}})^T\dot{\boldsymbol{q}} > 0$ for all $\dot{\boldsymbol{q}} \neq \boldsymbol{0}$. The term on the right hand side of (6.34) includes contact wrenches $\boldsymbol{F}_k \in \mathbb{R}^6$ acting at contact points k, with corresponding Jacobian matrices $\boldsymbol{J}_k(\boldsymbol{q})$. The last n equations of (6.34) are assumed to be in the singular perturbation form of Sect. 3.2.3 such that the actuator coordinates $\boldsymbol{\theta} \in \mathbb{R}^n$ represent the control input. In particular, the elastic potential $U_\mathrm{e}(\boldsymbol{\theta}, \boldsymbol{q})$ satisfies Assumption 3.2 and 3.3 such that there exists a diffeomorphism $\bar{\boldsymbol{q}}_\mathrm{e} : \mathbb{R}^n \to \mathbb{R}^n$ satisfying

$$\left.\frac{\partial U_\mathrm{e}(\boldsymbol{\theta}, \boldsymbol{q})}{\partial \boldsymbol{q}}\right|_{\boldsymbol{q}=\bar{\boldsymbol{q}}_\mathrm{e}(\boldsymbol{\theta})} = \boldsymbol{0} \,, \quad \forall \boldsymbol{\theta} \in \mathbb{R}^n \,,$$

analogously to Definition 3.4 of Sect. 3.1.1. Additionally, Assumption 3.3 ensures that given any $\boldsymbol{q} \in \mathbb{R}^n$,

$$\boldsymbol{\tau} = -\frac{\partial U_\mathrm{e}(\boldsymbol{\theta}, \boldsymbol{q})}{\partial \boldsymbol{q}}^T \tag{6.35}$$

can be uniquely solved for $\boldsymbol{\theta} = \boldsymbol{\theta}(\boldsymbol{\tau}, \boldsymbol{q})$. Thus, $\boldsymbol{\theta}$ and $\boldsymbol{\tau} \in \mathbb{R}^n$ can be considered as equivalent control inputs.

6.2.2. 1-D task manifold

Consider as an intermediate step the coordinates $\boldsymbol{x} \in \mathbb{R}^m$, with $m \leq n$, defined by the mapping

$$\boldsymbol{x}(\boldsymbol{q}, \bar{\boldsymbol{q}}_\mathrm{e}(\boldsymbol{\theta}_0)) : \mathbb{R}^n \times \mathbb{R}^n \to \mathbb{R}^m \,. \tag{6.36}$$

These coordinates are assumed to be defined such that they describe the task. Since the goal is to achieve a certain elastic behavior, it is advantageous to define this coordinates w. r. t. an equilibrium configuration $\bar{\boldsymbol{q}}_\mathrm{e}(\boldsymbol{\theta}_0) = \text{const.}$ such that $\boldsymbol{q} = \bar{\boldsymbol{q}}_\mathrm{e}(\boldsymbol{\theta}_0)$ implies $\boldsymbol{x} = \boldsymbol{0}$. Then, the mapping

$$\boldsymbol{\phi}(\boldsymbol{x}) : \mathbb{R}^m \to \mathbb{R}^{m-1} \tag{6.37}$$

with full rank Jacobian matrix $\boldsymbol{J}_\upphi(\boldsymbol{x}) = \partial\boldsymbol{\phi}(\boldsymbol{x})/\partial\boldsymbol{x}$ such that $\boldsymbol{\phi}(\boldsymbol{x}) = \boldsymbol{0}$ defines an 1-D submanifold of the task-space $\mathbb{R}^m$,

$$\mathcal{Z} := \{\boldsymbol{x} \in \mathbb{R}^m \,|\, \boldsymbol{\phi}(\boldsymbol{x}) = \boldsymbol{0}\} \,. \tag{6.38}$$

Remark 6.3. *A natural choice of task-coordinates for legged floating base systems is given by* $\boldsymbol{x}(\boldsymbol{q}) := \boldsymbol{r}_\mathrm{BC}(\boldsymbol{q}) - \boldsymbol{r}_\mathrm{BC}(\bar{\boldsymbol{q}}_\mathrm{e}(\boldsymbol{\theta}_0))$*, where* $\boldsymbol{r}_\mathrm{BC}(\boldsymbol{q}) : \mathbb{R}^n \to \mathbb{R}^3$ *represents the position of the total center of mass (COM) of the floating base system w. r. t. the body-fixed frame of the base link* $\{\mathrm{B}\}$*. In that case, the 1-manifold defined by* (6.38) *represents an 1-D curve along which the displacement of the COM is constraint to evolve.*

The elastic force acting in the co-tangent spaces of the 1-manifold defined by (6.38) can be derived from the elastic potential $U_\mathrm{e}(\boldsymbol{\theta}_0, \boldsymbol{q}) = U_\mathrm{e}(\boldsymbol{\theta}_0, \boldsymbol{q}(\boldsymbol{x}(\boldsymbol{\phi})))$ by considering the (elastic) forces in the constraint direction first:

$$\boldsymbol{\tau}_\upphi = -\left[\frac{\partial U_\mathrm{e}(\boldsymbol{\theta}_0, \boldsymbol{q}(\boldsymbol{x}(\boldsymbol{\phi})))}{\partial \boldsymbol{q}} \frac{\partial \boldsymbol{q}}{\partial \boldsymbol{x}} \frac{\partial \boldsymbol{x}}{\partial \boldsymbol{\phi}}\right]^T = -\frac{\partial \boldsymbol{x}}{\partial \boldsymbol{\phi}}^T \frac{\partial \boldsymbol{q}}{\partial \boldsymbol{x}}^T \frac{\partial U_\mathrm{e}(\boldsymbol{\theta}_0, \boldsymbol{q})}{\partial \boldsymbol{q}}^T \,. \tag{6.39}$$

The last factor on the most right hand side of this equation equals the generalized elastic force expressed in configuration coordinates as defined by (6.35). It can be seen that this force is successively transformed to task and constraint coordinates by the transposed of the Jacobian matrices $\partial\boldsymbol{q}/\partial\boldsymbol{x} \in \mathbb{R}^{n\times m}$ and $\partial\boldsymbol{x}/\partial\boldsymbol{\phi} \in \mathbb{R}^{m\times(m-1)}$ corresponding to the inverse of the mappings (6.36) and (6.37), respectively. In order to resolve the redundancy in the problem of successive transformation of forces to lower-dimensional subspaces as appearing in (6.39), the Jacobian matrices of the mappings (6.36) and (6.37) can be augmented to become invertible [PCY99], i. e.,

$$\begin{pmatrix} \mathrm{d}\boldsymbol{x} \\ \mathrm{d}\boldsymbol{n}_\mathrm{x} \end{pmatrix} = \boldsymbol{J}_\mathrm{x}^\mathrm{aug} \mathrm{d}\boldsymbol{q} \,, \quad \boldsymbol{J}_\mathrm{x}^\mathrm{aug} = \begin{pmatrix} \boldsymbol{J}_\mathrm{x} \\ \boldsymbol{J}_{\mathrm{n}_\mathrm{x}} \end{pmatrix} \in \mathbb{R}^{n\times n} \,, \tag{6.40}$$

$$\begin{pmatrix} \mathrm{d}\boldsymbol{\phi} \\ \mathrm{d}\boldsymbol{n}_\upphi \end{pmatrix} = \boldsymbol{J}_\upphi^\mathrm{aug} \mathrm{d}\boldsymbol{x} \,, \quad \boldsymbol{J}_\upphi^\mathrm{aug} = \begin{pmatrix} \boldsymbol{J}_\upphi \\ \boldsymbol{J}_{\mathrm{n}_\upphi} \end{pmatrix} \in \mathbb{R}^{m\times m} \,. \tag{6.41}$$

The inversion of these augmented Jacobian matrices (which is required to evaluate (6.39)) can be simplified by considering the following lemma, which is proven in [Ott08, Sect. A.5].

Lemma 6.1. *Let*

$$\boldsymbol{J}^\mathrm{aug} = \begin{pmatrix} \boldsymbol{J} \\ \boldsymbol{J}_\mathrm{n} \end{pmatrix} \tag{6.42}$$

be a $n \times n$ matrix, where $\boldsymbol{J} \in \mathbb{R}^{m \times n}$ with $m < n$ is of rank m. If the $(n-m) \times n$ matrix $\boldsymbol{J}_{\mathrm{n}}$ is chosen as

$$\boldsymbol{J}_{\mathrm{n}} = \left(\boldsymbol{Z}\boldsymbol{S}\boldsymbol{Z}^T\right)^{-1} \boldsymbol{Z}\boldsymbol{S}\,,$$

where the nullspace base matrix $\boldsymbol{Z}$ of rank $n-m$ satisfies $\boldsymbol{J}\boldsymbol{Z}^T = \boldsymbol{0}$ and the $n \times n$ matrix $\boldsymbol{S}$ represents a positive definite metric, then, the inverse of (6.42) *can be written in the form*

$$(\boldsymbol{J}^{\mathrm{aug}})^{-1} = \left[\boldsymbol{S}^{-1}\boldsymbol{J}^T \left(\boldsymbol{J}\boldsymbol{S}^{-1}\boldsymbol{J}^T\right)^{-1} \quad \boldsymbol{Z}^T\right] .$$

Applying this lemma to the matrices in (6.40) and (6.41) yields the Jacobian matrices required in (6.39),

$$\frac{\partial \boldsymbol{q}}{\partial \boldsymbol{x}} = \boldsymbol{S}_{\mathrm{x}}^{-1}\boldsymbol{J}_{\mathrm{x}}^T \left(\boldsymbol{J}_{\mathrm{x}}\boldsymbol{S}_{\mathrm{x}}^{-1}\boldsymbol{J}_{\mathrm{x}}^T\right)^{-1} , \tag{6.43}$$

$$\frac{\partial \boldsymbol{x}}{\partial \boldsymbol{\phi}} = \boldsymbol{S}_{\phi}^{-1}\boldsymbol{J}_{\phi}^T \left(\boldsymbol{J}_{\phi}\boldsymbol{S}_{\phi}^{-1}\boldsymbol{J}_{\phi}^T\right)^{-1} . \tag{6.44}$$

Additionally, these inversions yield also expressions for the portions of the elastic potential forces in the nullspaces of the task and constraint co-tangent spaces,

$$\boldsymbol{\tau}_{\mathrm{n_x}} = -\boldsymbol{Z}_{\mathrm{x}} \frac{\partial U_{\mathrm{e}}(\boldsymbol{\theta}_0, \boldsymbol{q})}{\partial \boldsymbol{q}}^T \tag{6.45}$$

and

$$\tau_{\mathrm{z}} = -\boldsymbol{Z}_{\phi} \frac{\partial \boldsymbol{q}}{\partial \boldsymbol{x}}^T \frac{\partial U_{\mathrm{e}}(\boldsymbol{\theta}_0, \boldsymbol{q})}{\partial \boldsymbol{q}}^T , \tag{6.46}$$

respectively. In particular, $\boldsymbol{\tau}_{\mathrm{z}}$ represents exactly the portion of the elastic potential force in the co-tangent spaces of the desired 1-manifold defined by (6.38).

6.2.3. Controller design

The controller at task-coordinate level comprises the two terms

$$\boldsymbol{\tau}_{\mathrm{x}} = \boldsymbol{J}_{\phi}^T \boldsymbol{\tau}_{\phi}^{\mathrm{des}} + \boldsymbol{J}_{\mathrm{n}_{\phi}}^T \tau_{\mathrm{z}}^{\mathrm{des}} . \tag{6.47}$$

The first term of (6.47),

$$\boldsymbol{\tau}_{\phi}^{\mathrm{des}} = -\boldsymbol{D}_{\phi}\dot{\boldsymbol{\phi}} - \boldsymbol{K}_{\phi}\boldsymbol{\phi}\,, \tag{6.48}$$

with $\boldsymbol{D}_{\phi}$ and $\boldsymbol{K}_{\phi}$ being $(m-1) \times (m-1)$ symmetric and positive definite gain matrices, implements the attractiveness of the desired 1-manifold. In other words, the controller term (6.48) forces the motion of the task-coordinates $\boldsymbol{x}$ to approach the 1-D submanifold $\mathcal{Z}$ defined by (6.38). The second term of (6.47) can be exploited to implement a limit cycle in the 1-manifold $\mathcal{Z}$, e. g., using the switching based control strategy of Sect. 4.4,

$$\tau_{\mathrm{z}}^{\mathrm{des}} = \tau_{\mathrm{z}} + \Delta\tau_{\mathrm{z}}(\tau_{\mathrm{z}})\,, \tag{6.49}$$

where τ_z is defined by (6.46) and

$$\Delta\tau_\mathrm{z}(\tau_\mathrm{z}) = \begin{cases} +\hat{\tau}_\mathrm{z} & \text{if} \quad \tau_\mathrm{z} > \epsilon_{\tau_\mathrm{z}} \\ 0 & \text{if} \quad |\tau_\mathrm{z}| < \epsilon_{\tau_\mathrm{z}} \\ -\hat{\tau}_\mathrm{z} & \text{if} \quad \tau_\mathrm{z} < -\epsilon_{\tau_\mathrm{z}} \end{cases} \tag{6.50}$$

represents the switching function. Herein, $\epsilon_{\tau_\mathrm{z}} > 0$ and $\hat{\tau}_\mathrm{z} > 0$ denote the constant switching threshold and amplitude, respectively. Note that, without this limit cycle controller, i. e., $\tau_\mathrm{z}^\mathrm{des} = \tau_\mathrm{z}$, only the portion of the elastic potential force in the co-tangent spaces of the desired 1-manifold (6.46) would be implemented. This in turn would lead to an exclusive, intrinsic elastic behavior for motions of the compliantly actuated system in that submanifold.

In case of redundancy of the configuration-space w. r. t. to the task-space, i. e., $m < n$, the task controller (6.47) determines the control input $\boldsymbol{\tau}$ of the plant (6.34) with (6.35) only up to $n - m$ dimensions. In other words, there exists infinite actuator configurations $\boldsymbol{\theta}$ which implement the generalized force of the task $\boldsymbol{\tau}_\mathrm{x}$.

Resolving redundancy solely by nullspace projection

The redundancy in the implementation of the task controller (6.47) in the control input $\boldsymbol{\tau}$ can be resolved by projecting the intrinsic, generalized elastic potential force $\partial U_\mathrm{e}(\boldsymbol{\theta}_0, \boldsymbol{q})/\partial \boldsymbol{q}$ into the co-tangent space of the nullspace of the task, i. e.,

$$\boldsymbol{\tau} = \boldsymbol{J}_\mathrm{x}^T \boldsymbol{\tau}_\mathrm{x} - \boldsymbol{J}_\mathrm{n_x}^T \boldsymbol{Z}_\mathrm{x} \frac{\partial U_\mathrm{e}(\boldsymbol{\theta}_0, \boldsymbol{q})}{\partial \boldsymbol{q}}^T , \tag{6.51}$$

cf. (6.40) and (6.45). This implementation preserves the equilibrium configuration $\bar{\boldsymbol{q}}_\mathrm{e}(\boldsymbol{\theta}_0)$ as far as $\partial U_\mathrm{e}(\boldsymbol{\theta}_0, \boldsymbol{q})/\partial \boldsymbol{q}$ generates no force interfering with the task control (6.47).

If the constraint is exactly satisfied, i. e., $\boldsymbol{\phi}(\boldsymbol{x}) = \dot{\boldsymbol{\phi}}(\boldsymbol{x}) = \boldsymbol{0}$, and if additionally the limit cycle controller is not active, i. e., $\Delta\tau_\mathrm{z}(\tau_\mathrm{z}) = 0$, then, $\boldsymbol{\tau} = -\partial U_\mathrm{e}(\boldsymbol{\theta}_0, \boldsymbol{q})/\partial \boldsymbol{q}$ such that the constant actuator configuration $\boldsymbol{\theta} = \boldsymbol{\theta}_0$ implements the control input (6.51). This is in accordance with the initial goal of minimizing the effort of modal shaping control. Moreover, it is worth mentioning that the controller (6.51) requires no knowledge of the contact state of the floating base system (6.34). While this might be an advantage from a robustness point of view on the one hand, it does not allow to incorporate conditions on the contact forces such as friction cone constraints on the other hand. This motivates the alternative implementation proposed in the following.

Resolving redundancy by optimal contact force distribution

An alternative approach to implement the task control (6.47) in the control input $\boldsymbol{\tau}$ is to distribute the contact forces of the floating base system (6.34) via optimization. Consider therefore a stacked vector of contact forces

$$\boldsymbol{f}_\mathrm{c} = \begin{pmatrix} \boldsymbol{f}_1 \\ \vdots \\ \boldsymbol{f}_{n_\mathrm{c}} \end{pmatrix} \in \mathbb{R}^{3n_\mathrm{c}} , \tag{6.52}$$

where n_c is the number of contact points.[3] The contact forces are related to the control input $\boldsymbol{\tau}$ by the mapping

$$\boldsymbol{\tau} = \boldsymbol{J}_\mathrm{c}(\boldsymbol{R}_\mathrm{b}, \boldsymbol{q})^T \boldsymbol{f}_\mathrm{c}\,, \tag{6.53}$$

where $\boldsymbol{J}_\mathrm{c}(\boldsymbol{R}_\mathrm{b}, \boldsymbol{q}) = \frac{\partial \boldsymbol{r}_\mathrm{c}(\boldsymbol{q})}{\partial \boldsymbol{q}}$ represents the Jacobian matrix of the mapping $\boldsymbol{r}_\mathrm{c}(\boldsymbol{q}) : \mathbb{R}^n \to \mathbb{R}^{3n_\mathrm{c}}$ relating the configuration variables $\boldsymbol{q}$ to the absolute positions of the contact points $\boldsymbol{r}_\mathrm{c}$. Using the relation (6.53), the problem of finding a control input $\boldsymbol{\tau}$ transforms into the problem of distributing the contact forces $\boldsymbol{f}_c$ such that they implement the task control (6.47) subject to certain constraints on the contact forces itself. This can be achieved by minimizing, e. g., a quadratic cost function of the form

$$E(\boldsymbol{f}_c) = \alpha_1 \left\| \boldsymbol{J}_\mathrm{c}^T \boldsymbol{f}_\mathrm{c} - \boldsymbol{J}_\mathrm{x}^T \boldsymbol{\tau}_\mathrm{x} \right\|^2 + \alpha_2 \left\| \boldsymbol{J}_\mathrm{c}^T \boldsymbol{f}_\mathrm{c} - \boldsymbol{J}_{\mathrm{n_x}}^T \boldsymbol{\tau}_{\mathrm{n_x}} \right\|^2 + \alpha_3 \left\| \boldsymbol{f}_\mathrm{c} \right\|^2 , \tag{6.54}$$

where the first term aims at implementing the task control (6.47), the second term aims at preserving the equilibrium configuration $\bar{\boldsymbol{q}}_\mathrm{e}(\boldsymbol{\theta}_0)$, and the third term performs a regulation, with weighting constants $\alpha_1 \gg \alpha_2 \gg \alpha_3 > 0$. Considering unilateral and Coulomb friction constraints, i. e.,

$$\boldsymbol{f}_i \in \mathcal{F}_i := \left\{ \boldsymbol{f}_i \in \mathbb{R}^3 \,|\, \sqrt{f_{i_\mathrm{x}}^2 + f_{i_\mathrm{y}}^2} \leq \mu f_{i_\mathrm{z}}, f_{i_\mathrm{z}} \geq 0 \right\} , \tag{6.55}$$

where $\mu \geq 0$ denotes the Coulomb friction coefficient,[4] the optimization problem

$$\min E(\boldsymbol{f}_\mathrm{c}) \quad \text{s.t.} \quad \boldsymbol{f}_i \in \mathcal{F}_i\,, \quad \forall i \in \{1, \ldots, n_\mathrm{c}\} \tag{6.56}$$

can be solved to determine $\boldsymbol{f}_c$ which using (6.53) yields the control input $\boldsymbol{\tau}$.

Note that if the Coulomb friction constraints (6.55) and the regulation term of the cost function (6.54) are removed, i. e., $\boldsymbol{f}_\mathrm{c} \in \mathbb{R}^{3n_\mathrm{c}}$ and $\alpha_3 = 0$, then, the control law (6.51) is obtained.

6.3. Modal adaptation

The existence of oscillation modes forms the basis for configuration recurrent (oscillatory) or periodic motions. By exploiting such natural oscillation dynamics, the energetic efficiency and performance (for a given input power) can be maximized. This can be achieved by controlling the compliantly actuated system in one of its oscillation modes. However, any control in a mode requires the knowledge of its geometric shape. Since, oscillation modes are intrinsic dynamics properties of the plant, this knowledge cannot be a priori assumed. Even if oscillation modes are embodied in the (mechanical) design (e. g., by applying the methodology proposed in Sect. 5.2), model uncertainties need to be taken into account. In robotic systems, model uncertainties might also be caused by picking a load, or due to changing and (partially) unknown, environmental contact conditions. Therefore, the method of *modal adaptation* control aims at identifying the geometric shape of an oscillation mode. The basic idea is to excite an oscillation by injecting (potential) energy (cf. Sect. 4.4) along an initial guess of the oscillation mode, and then, improve the

[3] Note that the contact forces $\boldsymbol{f}_i$ are geometrically related to the contact wrenches $\boldsymbol{F}_k$ as introduced in (6.34).

[4] Using a polyhedral approximation of the friction cone, the constraint (6.55) can be expressed in linear form.

estimate by adapting to the resulting natural motion. By presuming the attractiveness of oscillation modes given by damping effects (as validated in Sect. 5.3.3), which are present in any physical system, it can be expected that the motion as well as the estimate of the geometric shape converges successively to the oscillation mode.

6.3.1. Control input on oscillation mode

Consider the dynamics of the compliantly actuated system (5.33) investigated also in Sect. 5.3.1, i. e.,

$$\ddot{\boldsymbol{q}} = \boldsymbol{g}(\boldsymbol{q}, \dot{\boldsymbol{q}}, \boldsymbol{\theta}) = -\boldsymbol{M}(\boldsymbol{q})^{-1} \left[\boldsymbol{b}(\boldsymbol{q}, \dot{\boldsymbol{q}}) + \frac{\partial U(\boldsymbol{\theta}, \boldsymbol{q})}{\partial \boldsymbol{q}}^T \right] . \tag{6.57}$$

The configuration $\boldsymbol{q} \in \mathbb{R}^n$ is assumed to be statically controllable via the control input $\boldsymbol{\theta} \in \mathbb{R}^n$, i. e., the potential function $U(\boldsymbol{\theta}, \boldsymbol{q})$ satisfies Assumption 3.5 and 3.6 of Sect. 3.1.1.

Assume there exists a control input $\boldsymbol{\theta} = \boldsymbol{\theta}_0 = \text{const.}$ for which the dynamics (6.57) features an oscillation mode $\mathcal{Z} \subset \mathbb{R}^n$, i. e., an invariant, 1-D submanifold of the configuration space $\mathbb{R}^n$ such that once the state $(\boldsymbol{q}, \dot{\boldsymbol{q}})$ is in $\mathcal{TZ}$, it remains there for all future time (cf. Definition 5.2 of Sect. 5.1.3). Let the oscillation mode $\mathcal{Z}$ be embedded as an 1-manifold $\mathcal{S} \subseteq \mathbb{R}$, such that the generally nonlinear, differentiable mapping,

$$F : \mathcal{Z} \to \mathcal{S} , \tag{6.58}$$

yields an 1-D parametrization $s = F(\boldsymbol{q})$ of $\mathcal{Z}$. Then, the induced scalar dynamics

$$\ddot{s} = \frac{\partial}{\partial \boldsymbol{q}} \left(\frac{\partial F(\boldsymbol{q})}{\partial \boldsymbol{q}} \dot{\boldsymbol{q}} \right) \dot{\boldsymbol{q}} + \frac{\partial F(\boldsymbol{q})}{\partial \boldsymbol{q}} \boldsymbol{g}(\boldsymbol{q}, \dot{\boldsymbol{q}}, \boldsymbol{\theta}_0) \tag{6.59}$$

is equivalent to the original dynamical system (6.57) for all $(\boldsymbol{q}, \dot{\boldsymbol{q}}) \in \mathcal{TZ}$, since F is a diffeomorphism of $\mathcal{Z}$ onto $\mathcal{S}$.

Remark 6.4. *The exact knowledge of F provides an explicit,* scalar*, second-order differential equation as given by* (6.59)*. Therefore, finding F solves the problem of reducing the dimensionality of the original dynamics* (6.57) *from n-D to 1-D as treated in [KM94].*

The above derivation reveals how to reduce the n-D natural dynamics of the compliantly actuated system, i. e., (6.57) with $\boldsymbol{\theta} = \boldsymbol{\theta}_0$, to the 1-D dynamics of its oscillation mode. However, in order to exploit this intrinsic dynamical behavior by control, it needs to be investigated whether $\mathcal{Z}$ remains an invariant submanifold when the control input $\boldsymbol{\theta}$ is changed w. r. t. $\boldsymbol{\theta}_0$, i. e., $\boldsymbol{\theta} \neq \boldsymbol{\theta}_0$, and if there exists an 1-D *modal control manifold* for which selecting the control input $\boldsymbol{\theta}$ in the subset $\mathcal{Z}$, still represents an oscillation mode of the compliantly actuated system (6.57). Therefore, recall that the potential function $U(\boldsymbol{\theta}, \boldsymbol{q})$ satisfies Assumption 3.5 and 3.6 of Sect. 3.1.1. This implies the existence of a diffeomorphism $\bar{\boldsymbol{q}}(\boldsymbol{\theta}) : \mathbb{R}^n \to \mathbb{R}^n$ (cf. Definition 3.4 and Proposition 3.1 of Sect. 3.1.1) such that given any $\boldsymbol{\theta} \in \mathbb{R}^n$,

$$\left. \frac{\partial U(\boldsymbol{\theta}, \boldsymbol{q})}{\partial \boldsymbol{q}} \right|_{\boldsymbol{q} = \bar{\boldsymbol{q}}(\boldsymbol{\theta})} = \boldsymbol{0} . \tag{6.60}$$

In particular, condition (6.60) defines the equilibrium configuration of the system (6.57) $\bar{\boldsymbol{q}}(\boldsymbol{\theta})$ in terms of the control input $\boldsymbol{\theta}$. Since, the oscillation mode $\mathcal{Z}$ is defined w. r. t. an equilibrium configuration, it is advantageous to determine also the corresponding modal control manifold in terms of $\bar{\boldsymbol{q}}(\boldsymbol{\theta})$.

Definition 6.1. *Let $\mathcal{Z}$ be an oscillation mode of the compliantly actuated system* (6.57)*, satisfying Assumption 3.5 and 3.6 defined w. r. t. a constant control input $\boldsymbol{\theta} = \boldsymbol{\theta}_0 = \bar{\boldsymbol{q}}^{-1}(\boldsymbol{q}_0)$ according to Definition 5.2. Then, the set $\mathcal{C} := \bar{\boldsymbol{q}}^{-1}(\mathcal{Z})$ is said to be a modal control manifold corresponding to $\mathcal{Z}$, if for any (other) $\boldsymbol{\theta} \in \mathcal{C}$, the subset $\mathcal{Z}$ remains an oscillation mode of the controlled system* (6.57)*.*

From Definition 6.1, it becomes evident that controlling the system (6.57) in its oscillation mode $\mathcal{Z}$ requires the inverse mapping of F,

$$\boldsymbol{G} : \mathcal{S} \to \mathcal{Z} \,, \tag{6.61}$$

of which the existence is ensured, since F is a diffeomorphism. Assuming that the compliantly actuated system (6.57) features in addition to $\mathcal{Z}$ also a modal control manifold $\mathcal{C}$ (according to Definition 6.1), the modally controlled dynamics on $\mathcal{S}$ can be expressed by

$$\ddot{s} = \frac{\partial}{\partial \boldsymbol{q}} \left(\frac{\partial F}{\partial \boldsymbol{q}} \frac{\partial \boldsymbol{G}}{\partial s} \dot{s} \right) \frac{\partial \boldsymbol{G}}{\partial s} \dot{s} + \frac{\partial F}{\partial \boldsymbol{q}} \boldsymbol{g} \left(\boldsymbol{G}(s), \frac{\partial \boldsymbol{G}}{\partial s} \dot{s}, \bar{\boldsymbol{q}}^{-1}(\boldsymbol{G}(\bar{s}^{\mathrm{des}})) \right) \,, \tag{6.62}$$

where $\bar{s}^{\mathrm{des}} \in \mathcal{S}$ represents the control input, which by hypothesis of Definition 6.1 is "compatible" with the oscillation mode $\mathcal{Z}$. Thereby, the corresponding control input $\boldsymbol{\theta}$ (of the original system (6.57)) is given by composing the inverse mappings $\boldsymbol{G}$ and $\bar{\boldsymbol{q}}^{-1}$, i. e.,

$$\boldsymbol{\theta} = \left(\bar{\boldsymbol{q}}^{-1} \circ \boldsymbol{G} \right) (\bar{s}^{\mathrm{des}}) \in \mathcal{C} \,. \tag{6.63}$$

Note that the property of the compliantly actuated system (6.57) to feature an oscillation mode $\mathcal{Z}$ implies not necessarily the existence of a corresponding modal control manifold $\mathcal{C}$. The existence of $\mathcal{C}$ represents an additional "symmetry" assumption imposed on the potential function $U(\boldsymbol{\theta}, \boldsymbol{q})$.

Assumption 6.2. *The potential function $U(\boldsymbol{\theta}, \boldsymbol{q})$ is symmetric w. r. t. the oscillation mode $\mathcal{Z}$ in a sense that given any constant modal configuration $s \in \mathcal{S}/\{\bar{s}_0\}$, where $\boldsymbol{\theta}_0 = \bar{\boldsymbol{q}}^{-1}(\boldsymbol{G}(\bar{s}_0))$ denotes the constant control input for which $\mathcal{Z}$ is defined, the potential force satisfies*

$$\frac{\left. \frac{\partial U(\bar{\boldsymbol{q}}^{-1}(\boldsymbol{G}(\bar{s})), \boldsymbol{q})}{\partial \boldsymbol{q}} \right|_{\boldsymbol{q}=\boldsymbol{G}(s)}^{T}}{\left\| \left. \frac{\partial U(\bar{\boldsymbol{q}}^{-1}(\boldsymbol{G}(\bar{s})), \boldsymbol{q})}{\partial \boldsymbol{q}} \right|_{\boldsymbol{q}=\boldsymbol{G}(s)}^{T} \right\|} = \text{const.} \,, \tag{6.64}$$

for all $\bar{s} \in \mathcal{S}/\{\bar{s}_0\}$.

The above assumption enables to change the static equilibrium within the oscillation mode. This property is constituted by potential functions, where the elastic and gravitational part satisfy the modal condition independently (cf. Theorem 5.2 and Corollary 5.2).

6.3.2. Adaptation of oscillation modes

In the following, it is assumed that the mappings (6.58) and (6.61) (required to control the system (6.57) in $\mathcal{Z}$) are not (exactly) known. In that case, a basis function approach can be considered to approximate (6.58) and (6.61) as shown in [Kra91].[5] Without going into

[5] In [Cyb89] it has been shown that the superposision of nonlinearly parametrized sigmoidal functions can approximate any nonlinear function up to an arbitrary precision [Kra91].

details of function approximation theory, it is assumed that the mappings (6.58) and (6.61) are determined by a generally large number n_ζ of parameters $\boldsymbol{\zeta} \in \mathbb{R}^{n_\zeta}$, i. e., $s \approx F(\boldsymbol{q}, \boldsymbol{\zeta})$ and $\boldsymbol{q} \approx \boldsymbol{G}(s, \boldsymbol{\zeta})$. Based on this assumption, one can consider the projection point of the configuration $\boldsymbol{q}$ into the embedded 1-manifold corresponding to the parameters $\boldsymbol{\zeta}$,

$$\hat{\boldsymbol{q}} = (\boldsymbol{G} \circ F)(\boldsymbol{q}, \boldsymbol{\zeta})\,. \tag{6.65}$$

Then, given a series of observations $\boldsymbol{q}(r)$ in the time interval $r \in [0; t]$ and assuming that the parameters $\boldsymbol{\zeta}(t)$ are constant during the observations $[0; t]$, the problem of estimating $\boldsymbol{\zeta}(t)$ can be formulated as minimizing the average of the squared distance between $\boldsymbol{q}(r)$ and its projection point $\hat{\boldsymbol{q}}(r)$ over the observation interval $[0; t]$, i. e.,

$$\hat{\boldsymbol{\zeta}}(t) = \min_{\boldsymbol{\zeta}(t)} J(\boldsymbol{\zeta}(t))\,, \tag{6.66}$$

where

$$J(\boldsymbol{\zeta}(t)) = \frac{1}{t} \int_0^t \left\| \boldsymbol{q}(r) - (\boldsymbol{G} \circ F)(\boldsymbol{q}(r), \boldsymbol{\zeta}(t)) \right\|^2 \mathrm{d}r\,. \tag{6.67}$$

This problem can be solved by means of common methods of numerical optimization. In particular, these techniques can be applied recursively, e. g., by implementing an extended Kalman filter approach [ACPS07]. However, the basis functions which approximate the mappings (6.58) and (6.61) with sufficient accuracy depend in general nonlinearly on their parameters. Therefore, the accurate adaptation of general oscillation modes entails the common difficulties of nonlinear programming such as finding the global minimum of (6.67). Note that estimating an exact representation of the oscillation mode implies that the functional (6.67) vanishes identically.

The problem of modal adaptation simplifies drastically, if the (nonlinear) compliantly actuated system (6.57) features an eigenvector according to Definition 5.1 of Sect. 5.1.

6.3.3. Adaptation of eigenmodes

Consider the compliantly actuated system (6.57). Assume that there exists a control input $\boldsymbol{\theta} = \boldsymbol{\theta}_0 = \text{const.}$ for which this system features an eigenvector $\boldsymbol{w}$ according to Definition 5.1 of Sect. 5.1.2. The constant vector $\boldsymbol{w}$ defines an eigenmode $\mathcal{W} \subset \mathbb{R}^n$, which according to Theorem 5.1 of Sect. 5.1.2 represents an invariant, 1-D submanifold of the configuration space $\mathbb{R}^n$. In particular, the 1-D embedding $F : \mathcal{W} \to \mathcal{S}$ of the submanifold $\mathcal{W}$ parametrizes a straight line. Therefore, F and also its inverse mapping $\boldsymbol{G} : \mathcal{S} \to \mathcal{W}$ is linear, i. e.,

$$\boldsymbol{q} = \boldsymbol{G}(s) = \boldsymbol{w}s + \bar{\boldsymbol{q}}(\boldsymbol{\theta}_0)\,, \tag{6.68}$$

where $\bar{\boldsymbol{q}}(\boldsymbol{\theta}_0)$ satisfies the static equilibrium condition (6.60). To derive the linear embedding F, consider the $n \times (n-1)$ matrix $\bar{\boldsymbol{W}} = \ker\left(\boldsymbol{w}^T\right) = \text{const.}$ of rank $n-1$ satisfying $\bar{\boldsymbol{W}}^T \boldsymbol{w} = \boldsymbol{0}$ (cf. Theorem 5.1 of Sect. 5.1.2). Additionally, assume (without loss of generality) that the matrix $\bar{\boldsymbol{W}}$ is chosen such that the augmented $n \times n$ matrix $\boldsymbol{W} = \begin{bmatrix} \boldsymbol{w} & \bar{\boldsymbol{W}} \end{bmatrix}$ is orthogonal, i. e., $\boldsymbol{W}^{-1} = \boldsymbol{W}^T$. Then, F can be expressed as

$$s = F(\boldsymbol{q}) = \boldsymbol{w}^T \left[\boldsymbol{q} - \bar{\boldsymbol{q}}(\boldsymbol{\theta}_0)\right]\,. \tag{6.69}$$

From (6.68) and (6.69), it becomes clear that if the compliantly actuated system (6.57) features also a modal control manifold $\mathcal{C} = \bar{\boldsymbol{q}}^{-1}(\mathcal{W})$ according to Definition 6.1, then the

knowledge of the (constant) eigenvector $\boldsymbol{w}$ enables to control the system in its embedded 1-manifold $\mathcal{S}$.

In the following, the case is considered where the eigenvector $\boldsymbol{w}$ is not (exactly) known. Therefore, an algorithm is derived which enables to adapt the eigenvector $\boldsymbol{w}$, and consequently also the mappings (6.68) and (6.69), based on observations of displacements $\tilde{\boldsymbol{q}}(k) = \boldsymbol{q}(k) - \bar{\boldsymbol{q}}(\boldsymbol{\theta}_0)$ at discrete time $k \in \mathbb{N}$.

Let $\boldsymbol{w}(k-1)$ be an initial estimate of the eigenvector such that using (6.68) and (6.69), the projection point of the displacement $\tilde{\boldsymbol{q}}(k)$ on the estimate of the embedded eigenmode $\mathcal{S}$ is given by

$$\hat{\tilde{\boldsymbol{q}}}(k) = \boldsymbol{w}(k-1)s(k) \tag{6.70}$$

where

$$s(k) = \boldsymbol{w}(k-1)^T \tilde{\boldsymbol{q}}(k)\,. \tag{6.71}$$

Consider an observation interval $[1;k]$ wherein the estimated eigenvector $\boldsymbol{w}(k)$ is assumed to be held constant. Then, the problem of estimating $\boldsymbol{w}(k)$ can be formulated as finding a $\boldsymbol{w}(k)$ which minimizes the average of the squared distance between the observed displacement $\tilde{\boldsymbol{q}}(j)$ and its projection point $\hat{\tilde{\boldsymbol{q}}}(j)$ over the observation interval $j \in [1;k]$, i. e.,

$$\hat{\boldsymbol{w}}(k) = \min_{\boldsymbol{w}(k)} J(\boldsymbol{w}(k))\,, \tag{6.72}$$

where

$$J(\boldsymbol{w}(k)) = \frac{1}{k}\sum_{j=1}^{k} \|\tilde{\boldsymbol{q}}(j) - \boldsymbol{w}(k)s(j)\|^2_{\boldsymbol{S}(j)} \tag{6.73}$$

and the $n \times n$ matrix $\boldsymbol{S}(j)$ represents a time-varying, symmetric, and positive definite metric.[6]

The problem (6.72) and (6.73) is well-known as principal component analysis (PCA). Thereby, the estimate $\hat{\boldsymbol{w}}(k)$ represents the principal vector corresponding to the leading singular value of the matrix of observations $\tilde{\boldsymbol{Q}}(k) = \begin{bmatrix}\tilde{\boldsymbol{q}}(1) & \dots & \tilde{\boldsymbol{q}}(k)\end{bmatrix}^T \in \mathbb{R}^{k\times n}$ [BH89]. In [OBL00], a solution to the adaptation problem is proposed, which is based on a standard recursive least-squares (RLS) procedure. A possible alternative implementation can be obtained by considering a Kalman filter (KF) based approach, as shown, e. g., in [ACPS07]. However, the RLS based method leads to the most simplest and computationally cheapest realization of recursive PCA. Therefore, it will be considered for modal adaptation. Note that the contribution of this thesis is to link the method of recursive PCA with the problem of controlling nonlinear, compliantly actuated systems in its eigenmodes. Due to the tantamount importance of modal adaptation for the control of nonlinear elastic multibody systems, a brief derivation will be provided in the following, although the details have already been described, e. g., in [ACPS07].

Let $\boldsymbol{w}(0) = \text{const.}$ be an initial guess of the eigenvector and let $\boldsymbol{w}(j-1) = \boldsymbol{w}(0)$ such that in (6.73), $s(j) = \boldsymbol{w}(0)^T\tilde{\boldsymbol{q}}(j)$, for $j = 1 \dots k$. Then,

$$\frac{\partial J(\boldsymbol{w}(k))}{\partial \boldsymbol{w}(k)} = \boldsymbol{0} \iff \hat{\boldsymbol{w}}(k) = \frac{\tilde{\boldsymbol{Q}}(k)^T\boldsymbol{s}(k)}{\boldsymbol{s}(k)^T\boldsymbol{s}(k)}\,, \tag{6.74}$$

[6] The metric can be chosen $\boldsymbol{S}(j) = \gamma^{k-j}\boldsymbol{I}$, where $\gamma \in (0;1]$ is a constant forgetting factor, which takes the non-stationary environment into account. For simplicity, here, γ is chosen unity without loss of generality.

where $\boldsymbol{s}(k) = \begin{bmatrix} s(1) & \dots & s(k) \end{bmatrix}^T \in \mathbb{R}^{k\times 1}$, solves the problem (6.72) and (6.73) in a sense of least-squares. Now, assume that at time k, a new observation $\tilde{\boldsymbol{q}}(k)$ becomes available such that $\tilde{\boldsymbol{Q}}(k)$ and $\boldsymbol{s}(k)$ can be partitioned in

$$\tilde{\boldsymbol{Q}}(k) = \begin{pmatrix} \tilde{\boldsymbol{Q}}(k-1) \\ \tilde{\boldsymbol{q}}(k)^T \end{pmatrix} \tag{6.75}$$

and

$$\boldsymbol{s}(k) = \begin{pmatrix} \boldsymbol{s}(k-1) \\ s(k) \end{pmatrix}, \tag{6.76}$$

respectively. Then, considering this partitioning in (6.74), it follows that

$$\hat{\boldsymbol{w}}(k) = \frac{\tilde{\boldsymbol{Q}}(k-1)^T \boldsymbol{s}(k-1) + \tilde{\boldsymbol{q}}(k)s(k)}{\boldsymbol{s}(k)^T \boldsymbol{s}(k)} \tag{6.77}$$

$$= \frac{\tilde{\boldsymbol{w}}(k-1) + \tilde{\boldsymbol{q}}(k)s(k)}{\|\tilde{\boldsymbol{w}}(k)\|} \tag{6.78}$$

$$= \beta(k)\hat{\boldsymbol{w}}(k-1) + \alpha(k)\tilde{\boldsymbol{q}}(k)s(k)\,, \tag{6.79}$$

where in the second step, the property $\|\hat{\boldsymbol{w}}(k)\| = 1$ is taken into account (i. e., $\hat{\boldsymbol{w}}(k) = \tilde{\boldsymbol{w}}(k)/\|\tilde{\boldsymbol{w}}(k)\|$), and in the last step, the substitutions $\alpha(k) = \left(\boldsymbol{s}(k)^T \boldsymbol{s}(k)\right)^{-1}$ and $\beta(k) = \left(\boldsymbol{s}(k-1)^T \boldsymbol{s}(k-1)\right)\alpha(k)$ are performed. By choosing $\beta(k) = 1 - \alpha(k)s(k)^2$ in (6.79), the simple principal component analyzer, which is known as *Oja's rule* [Oja82], i. e.,

$$\hat{\boldsymbol{w}}(k) = \hat{\boldsymbol{w}}(k-1) + \alpha(k)s(k)\left[\tilde{\boldsymbol{q}}(k) - s(k)\hat{\boldsymbol{w}}(k-1)\right], \tag{6.80}$$

is obtained.

Remark 6.5. *By selecting $\alpha(t) \propto 1/t$, the time continuous counterpart of Oja's rule* (6.80) *is given by*

$$\frac{\mathrm{d}}{\mathrm{d}t}\hat{\boldsymbol{w}}(t) = \boldsymbol{R}(t)\hat{\boldsymbol{w}}(t) - \left(\hat{\boldsymbol{w}}(t)^T \boldsymbol{R}(t)\hat{\boldsymbol{w}}(t)\right)\hat{\boldsymbol{w}}(t)\,, \tag{6.81}$$

where $\boldsymbol{R}(t) = \int_0^t \tilde{\boldsymbol{q}}(r)\tilde{\boldsymbol{q}}(r)^T \mathrm{d}r$.

Theorem 6.3. *[Oja82] If the $n \times n$ matrix $\boldsymbol{R}(t)$ is at least positive semi-definite, and if the largest eigenvalue of $\boldsymbol{R}(t)$ has multiplicity one, then, the normalized eigenvector $\boldsymbol{r}$ corresponding to the largest eigenvalue of $\boldsymbol{R}(\infty)$ represents an asymptotically stable equilibrium point of the dynamical system* (6.81)*. That is, if $\hat{\boldsymbol{w}}(0)^T\boldsymbol{r} > 0$ or $\hat{\boldsymbol{w}}(0)^T\boldsymbol{r} < 0$, then $\hat{\boldsymbol{w}}(t)$ converges to $\boldsymbol{r}$ or $-\boldsymbol{r}$ as $t \to \infty$, respectively.*

6.3.4. Modally adaptive periodic motion control

In the following, the concepts of modal adaptation and switching based limit cycle control (Sect. 4.4) are combined.

Oscillation modes

Consider the compliantly actuated system (6.57). Assume that the system features an oscillation mode $\mathcal{Z}$ and a corresponding modal control manifold $\mathcal{C} = \bar{\boldsymbol{q}}^{-1}(\mathcal{Z})$ according to Definition 5.2 and 6.1, respectively. Then, defining the control input of the system (6.57) by (6.63), i. e.,

$$\boldsymbol{\theta} = \bar{\boldsymbol{q}}^{-1}\left(\boldsymbol{G}\left(\bar{s}^{\mathrm{des}}, \hat{\boldsymbol{\zeta}}\right)\right), \tag{6.82}$$

$$\bar{s}^{\mathrm{des}}(s(t), \bar{s}_{-}^{\mathrm{des}}) = \bar{s}_0 + \begin{cases} +\hat{\bar{s}} & \text{if} \quad s(t) - \bar{s}_{-}^{\mathrm{des}} < -\epsilon_{\phi_{\mathrm{s}}} \\ 0 & \text{if} \quad \left|s(t) - \bar{s}_{-}^{\mathrm{des}}\right| < \epsilon_{\phi_{\mathrm{s}}} \\ -\hat{\bar{s}} & \text{if} \quad s(t) - \bar{s}_{-}^{\mathrm{des}} > \epsilon_{\phi_{\mathrm{s}}} \end{cases}, \tag{6.83}$$

implements the switching based control (4.4) of Sect. 4.4 on the embedded 1-manifold $\mathcal{S}$. In (6.83), $\bar{s}_{-}^{\mathrm{des}}$ represents the state of the switching function $\bar{s}^{\mathrm{des}}(s(t), \bar{s}_{-}^{\mathrm{des}})$ before the switching instance, and $\hat{\bar{s}} > 0$ and $\epsilon_{\phi_{\mathrm{s}}} > 0$ are switching amplitude and threshold, respectively. The dependency of the inverse mapping $\boldsymbol{G}(\cdot, \hat{\boldsymbol{\zeta}})$ on $\hat{\boldsymbol{\zeta}}$ indicates that the controller (6.82) and (6.83) is based on an estimate of $\mathcal{S}$. Therefore, by presuming a certain attractiveness of the oscillation mode $\mathcal{Z}$,[7] the switching control (6.82) and (6.83) can be combined with an algorithm which adapts to $\hat{\boldsymbol{\zeta}}$ by minimizing the cost function as introduced in (6.73). This enables not only the generation of periodic motions, but also offers the capability of identifying oscillation modes.

Eigenmodes

The problem of modally adaptive periodic motion control simplifies, if the oscillation mode $\mathcal{Z}$ represents an eigenmode $\mathcal{W}$ according to Definition 5.1 and Theorem 5.1, i. e., $\mathcal{Z} = \mathcal{W}$. If the compliantly actuated system (6.57) features an eigenmode $\mathcal{W}$ and a corresponding modal control manifold $\mathcal{C} = \bar{\boldsymbol{q}}^{-1}(\mathcal{W})$ according to Definition 6.1, the control (6.82) and (6.83) reduces to

$$\boldsymbol{\theta} = \bar{\boldsymbol{q}}^{-1}\left(\bar{\boldsymbol{q}}(\boldsymbol{\theta}_0) + \hat{\boldsymbol{w}}(t)\bar{s}^{\mathrm{des}}\right), \tag{6.84}$$

$$\bar{s}^{\mathrm{des}}(s(t), \bar{s}_{-}^{\mathrm{des}}) = \begin{cases} +\hat{\bar{s}} & \text{if} \quad s(t) - \bar{s}_{-}^{\mathrm{des}} < -\epsilon_{\phi_{\mathrm{s}}} \\ 0 & \text{if} \quad \left|s(t) - \bar{s}_{-}^{\mathrm{des}}\right| < \epsilon_{\phi_{\mathrm{s}}} \\ -\hat{\bar{s}} & \text{if} \quad s(t) - \bar{s}_{-}^{\mathrm{des}} > \epsilon_{\phi_{\mathrm{s}}} \end{cases}, \tag{6.85}$$

where the initial control input $\boldsymbol{\theta}_0 = \text{const.}$ is assumed to satisfy $\boldsymbol{\theta}_0 \in \mathcal{C}$. The control (6.84) and (6.85) depends on the mappings (6.69) and (6.68), which implement the limit cycle control (4.4) of Sect. 4.4 on the embedded 1-manifold $\mathcal{S}$ corresponding to the eigenmode $\mathcal{W}$. Since, these mappings are linear and fully determined by the constant eigenvector $\boldsymbol{w}$, Oja's rule (6.80) represents a simple but effective algorithm to adapt the eigenmode $\mathcal{W}$.

Remark 6.6. *By virtue of Remark 6.5, the difference equation* (6.80) *can be approximated by the differential equation* (6.81)*, or* (6.80) *can be directly replaced by* (6.81)*, if a continuous-time frame work can be assumed. If the correlation matrix* $\boldsymbol{R}(t)$ *is at least positive semi-definite and the largest eigenvalue of* $\boldsymbol{R}(t)$ *has multiplicity one, Theorem 6.3*

[7] Local attractiveness of $\mathcal{Z}$ is a result of damping inherent any physical plant, cf. Sect. 5.3.3.

ensures that (6.81) *features an asymptotically stable fixed-point* $\boldsymbol{r}$ *representing the normalized eigenvector corresponding to the largest eigenvalue of* $\boldsymbol{R}(\infty)$*. Therefore, assuming a certain attractiveness of the eigenmode* $\mathcal{W}$ *and initializing* $\hat{\boldsymbol{w}}$ *in the corresponding region of attraction, it can be expected that the control* (6.84) *and* (6.85) *excites a motion* $\tilde{\boldsymbol{q}}(t)$ *with (unique) maximum variance in the direction of* $\boldsymbol{w}$*. This implies not only that the conditions on the eigenvalues of* $\boldsymbol{R}(t)$ *are satisfied, but also gives rise to* $\boldsymbol{r} \approx \boldsymbol{w}$*. As a result,* $\hat{\boldsymbol{w}}$ *converges to* $\boldsymbol{w}$ *as* $t \to \infty$ *such that the* n*-D dynamical system* (6.57) *collapses to the scalar dynamics* (6.62)*. However, this in turn would allow to conclude the existence of an asymptotically stable limit cycle according to Theorem 4.1 and 4.2.*

Remark 6.7. *The modally adaptive periodic motion control* (6.84)*,* (6.85) *and* (6.80) *requires the knowledge of the mapping* $\bar{\boldsymbol{q}}(\boldsymbol{\theta})$ *and its inverse, which can be computed based on a model of the potential energy* $U(\boldsymbol{\theta}, \boldsymbol{q})$*. However, for a practically important subclass of compliantly actuated systems* (6.57)*, the approximation* $\bar{\boldsymbol{q}}(\boldsymbol{\theta}) \approx \boldsymbol{\theta}$ *suffices to generate a periodic motion in* $\mathcal{W}$*. This subclass contains the cases, where the potential energy can be separated in* $U(\boldsymbol{\theta}, \boldsymbol{q}) = U_{\mathrm{g}}(\boldsymbol{q}) + U_{\mathrm{e}}(\boldsymbol{q} - \boldsymbol{\theta})$*, and each of the terms* $\frac{\partial U_{\mathrm{g}}(\boldsymbol{q})}{\partial \boldsymbol{q}}$ *and* $\frac{\partial U_{\mathrm{e}}(\boldsymbol{q}-\boldsymbol{\theta})}{\partial \boldsymbol{q}}$ *satisfies the eigenvector condition of Definition 5.1, independently. For such systems, the control* (6.84)*,* (6.85) *and* (6.80) *uses no model-parameter knowledge to compute the feedback. In any case, the controller depends only on measurements at position level, i. e.,* $\boldsymbol{q}(t)$*, and no (numerical) derivatives of measured signals are required. Therefore, the control method is very robust against model uncertainties and sensor noise.*

6.4. Modal matching

Oscillation modes (as defined in Sect. 5.1) are 1-D, invariant submanifolds, which describe the natural, oscillatory behavior of n-D elastic multibody dynamics w. r. t. an equilibrium configuration. While, the solutions of n-D, linear spring mass systems can always be decomposed in terms of n eigenmodes (independently of the equilibrium configuration), the number of oscillation modes which a nonlinear, compliantly actuated system may feature is not necessarily determined by its dimensionality n. This is as the inertial properties of such systems depend nonlinearly on the configuration, and even the static equilibrium conditions are nonlinear. The proposed method of *modal matching* control aims at exploiting the additional "degree of freedom" resulting due to these nonlinearities in order to match and control the natural oscillatory behavior of compliantly actuated systems w. r. t. a given task. The concept of modal matching is based on the idea of controlling the local eigenvectors rather than considering globally valid oscillation modes. On this basis, the modal matching methodology introduces an algorithm to find equilibrium configurations for which a local eigenvector matches to the desired direction of the task. Additionally, a corresponding differential mapping is proposed, which enables to continuously control the direction of these local eigenmodes. The approach is predestined to control the oscillatory behavior during the stance phase of highly dynamical gaits. Therefore, the matching algorithm and continuous control methods are derived based upon the general model of compliantly actuated, legged, free floating base systems, which are subject to contact constraints. This trivially contains also the case of compliantly actuated, fixed-base systems.

6.4.1. Task dynamics formulation via constraints

Consider the compliantly actuated, free floating base system, which can be partitioned in the form

$$\boldsymbol{M}(\boldsymbol{x}_\mathrm{b},\boldsymbol{q})\begin{pmatrix}\frac{\mathrm{D}\dot{\boldsymbol{x}}_\mathrm{b}}{\mathrm{D}t}\\ \frac{\mathrm{D}\dot{\boldsymbol{q}}}{\mathrm{D}t}\end{pmatrix}+\begin{pmatrix}\frac{\partial U(\boldsymbol{\theta},\boldsymbol{x}_\mathrm{b},\boldsymbol{q})}{\partial \boldsymbol{x}_\mathrm{b}}^T\\ \frac{\partial U(\boldsymbol{\theta},\boldsymbol{x}_\mathrm{b},\boldsymbol{q})}{\partial \boldsymbol{q}}^T\end{pmatrix}=\boldsymbol{0}\,. \tag{6.86}$$

The system (6.86) is defined on an affinely connected Riemannian space with metric tensor

$$\boldsymbol{M}(\boldsymbol{x}_\mathrm{b},\boldsymbol{q})=\begin{bmatrix}\boldsymbol{M}_\mathrm{bb}(\boldsymbol{x}_\mathrm{b},\boldsymbol{q}) & \boldsymbol{M}_\mathrm{bq}(\boldsymbol{x}_\mathrm{b},\boldsymbol{q})\\ \boldsymbol{M}_\mathrm{bq}(\boldsymbol{x}_\mathrm{b},\boldsymbol{q})^T & \boldsymbol{M}_\mathrm{qq}(\boldsymbol{x}_\mathrm{b},\boldsymbol{q})\end{bmatrix} \tag{6.87}$$

and corresponding Riemannian connection according to Definition 2.7 and 2.13. Its global coordinates comprise the base and statically controllable configuration variables, $\boldsymbol{x}_\mathrm{b}\in\mathbb{R}^{n_\mathrm{b}}$ and $\boldsymbol{q}\in\mathbb{R}^n$, respectively, for which $n_\mathrm{b}\leq n$ is assumed. In particular, the base coordinates $\boldsymbol{x}_\mathrm{b}$ are assumed to be selected such that they represent the desired task. The potential function $U(\boldsymbol{\theta},\boldsymbol{x}_\mathrm{b},\boldsymbol{q})=U_\mathrm{g}(\boldsymbol{x}_\mathrm{b},\boldsymbol{q})+U_\mathrm{e}(\boldsymbol{\theta},\boldsymbol{q})$ consists of the gravity potential $U_\mathrm{g}(\boldsymbol{x}_\mathrm{b},\boldsymbol{q})$ and the elastic potential $U_\mathrm{e}(\boldsymbol{\theta},\boldsymbol{q})$. Additionally, $U(\boldsymbol{\theta},\boldsymbol{x}_\mathrm{b},\boldsymbol{q})$ satisfies Assumptions 3.5 and 3.6 in a sense that for any $\boldsymbol{x}_\mathrm{b}\in\mathbb{R}^{n_\mathrm{b}}$, $\boldsymbol{q}$ is statically controllable via the control input $\boldsymbol{\theta}\in\mathbb{R}^n$.

The proposed formulation of the task dynamics is based upon physical constraints. Consider therefore the mapping $\boldsymbol{\phi}:\mathbb{R}^{n_\mathrm{b}}\times\mathbb{R}^{n-n_\mathrm{b}}\times\mathbb{R}^n\to\mathbb{R}^n$ satisfying

$$\boldsymbol{\phi}(\boldsymbol{x}_\mathrm{b},\boldsymbol{l},\boldsymbol{q})=\boldsymbol{0} \tag{6.88}$$

Remark 6.8. *In case of legged systems, the functions $\boldsymbol{\phi}$ comprise contact points corresponding to legs in stance, but may contain also configurations of legs in swing.*

The additional coordinates $\boldsymbol{l}\in\mathbb{R}^{n-n_\mathrm{b}}$ are introduced to explicitly resolve the problem of over-actuation. They have to be chosen such that $n-n_\mathrm{b}$ constraints are "relaxed".

Remark 6.9. *A natural choice of $\boldsymbol{l}$ for legged systems is given by the relative distance between contact points corresponding to different legs in stance.*

Assumption 6.3. *The $n\times n$ Jacobian matrices $\frac{\partial\boldsymbol{\phi}(\boldsymbol{x}_\mathrm{b},\boldsymbol{l},\boldsymbol{q})}{\partial\boldsymbol{q}}$ and $\left[\frac{\partial\boldsymbol{\phi}(\boldsymbol{x}_\mathrm{b},\boldsymbol{l},\boldsymbol{q})}{\partial\boldsymbol{x}_\mathrm{b}}\quad\frac{\partial\boldsymbol{\phi}(\boldsymbol{x}_\mathrm{b},\boldsymbol{l},\boldsymbol{q})}{\partial\boldsymbol{l}}\right]$ of the constraint mapping $\boldsymbol{\phi}(\boldsymbol{x}_\mathrm{b},\boldsymbol{l},\boldsymbol{q})$ are invertible for all $\boldsymbol{q}\in\mathbb{R}^n$ and $(\boldsymbol{x}_\mathrm{b},\boldsymbol{l})\in\mathcal{X}$, where $\mathcal{X}\subset\mathbb{R}^n$.*

Based on this assumption, the task dynamics can be derived by introducing the Lagrange multipliers $\boldsymbol{\lambda}\in\mathbb{R}^n$, which incorporate the constraints (6.88) in (6.86) (cf. Sect. 2.4), i. e.,

$$\left[\boldsymbol{M}_\mathrm{bb}\boldsymbol{M}_\mathrm{bq}\right]\begin{pmatrix}\frac{\mathrm{D}\dot{\boldsymbol{x}}_\mathrm{b}}{\mathrm{D}t}\\ \frac{\mathrm{D}\dot{\boldsymbol{q}}}{\mathrm{D}t}\end{pmatrix}+\frac{\partial U(\boldsymbol{\theta},\boldsymbol{x}_\mathrm{b},\boldsymbol{q})}{\partial\boldsymbol{x}_\mathrm{b}}^T=\left(\frac{\partial\boldsymbol{\phi}(\boldsymbol{x}_\mathrm{b},\boldsymbol{l},\boldsymbol{q})}{\partial\boldsymbol{x}_\mathrm{b}}\right)^T\boldsymbol{\lambda}\,, \tag{6.89}$$

$$\boldsymbol{0}=\left(\frac{\partial\boldsymbol{\phi}(\boldsymbol{x}_\mathrm{b},\boldsymbol{l},\boldsymbol{q})}{\partial\boldsymbol{l}}\right)^T\boldsymbol{\lambda}\,, \tag{6.90}$$

$$\left[\boldsymbol{M}_\mathrm{bq}^T\boldsymbol{M}_\mathrm{qq}\right]\begin{pmatrix}\frac{\mathrm{D}\dot{\boldsymbol{x}}_\mathrm{b}}{\mathrm{D}t}\\ \frac{\mathrm{D}\dot{\boldsymbol{q}}}{\mathrm{D}t}\end{pmatrix}+\frac{\partial U(\boldsymbol{\theta},\boldsymbol{x}_\mathrm{b},\boldsymbol{q})}{\partial\boldsymbol{q}}^T=\left(\frac{\partial\boldsymbol{\phi}(\boldsymbol{x}_\mathrm{b},\boldsymbol{l},\boldsymbol{q})}{\partial\boldsymbol{q}}\right)^T\boldsymbol{\lambda}\,. \tag{6.91}$$

The Lagrange multipliers $\boldsymbol{\lambda}$ in (6.89)–(6.91) can be eliminated by substituting (6.91) in (6.89) and (6.90), which yields,

$$\left(\left[\boldsymbol{M}_{\mathrm{bb}}\boldsymbol{M}_{\mathrm{bq}}\right] + \boldsymbol{\Phi}_{\mathrm{qb}}^{T}\left[\boldsymbol{M}_{\mathrm{bq}}^{T}\boldsymbol{M}_{\mathrm{qq}}\right]\right)\begin{pmatrix}\frac{\mathrm{D}\dot{\boldsymbol{x}}_{\mathrm{b}}}{\mathrm{D}t}\\ \frac{\mathrm{D}\dot{\boldsymbol{q}}}{\mathrm{D}t}\end{pmatrix} = -\frac{\partial U(\boldsymbol{\theta},\boldsymbol{x}_{\mathrm{b}},\boldsymbol{q})}{\partial \boldsymbol{x}_{\mathrm{b}}}^{T} - \boldsymbol{\Phi}_{\mathrm{qb}}^{T}\frac{\partial U(\boldsymbol{\theta},\boldsymbol{x}_{\mathrm{b}},\boldsymbol{q})}{\partial \boldsymbol{q}}^{T}, \tag{6.92}$$

$$\boldsymbol{\Phi}_{\mathrm{ql}}^{T}\left[\boldsymbol{M}_{\mathrm{bq}}^{T}\boldsymbol{M}_{\mathrm{qq}}\right]\begin{pmatrix}\frac{\mathrm{D}\dot{\boldsymbol{x}}_{\mathrm{b}}}{\mathrm{D}t}\\ \frac{\mathrm{D}\dot{\boldsymbol{q}}}{\mathrm{D}t}\end{pmatrix} = -\boldsymbol{\Phi}_{\mathrm{ql}}^{T}\frac{\partial U(\boldsymbol{\theta},\boldsymbol{x}_{\mathrm{b}},\boldsymbol{q})}{\partial \boldsymbol{q}}^{T}. \tag{6.93}$$

The transposed of the Jacobian matrices,

$$\boldsymbol{\Phi}_{\mathrm{qb}}(\boldsymbol{x}_{\mathrm{b}},\boldsymbol{l},\boldsymbol{q}) = -\left(\frac{\partial \boldsymbol{\phi}(\boldsymbol{x}_{\mathrm{b}},\boldsymbol{l},\boldsymbol{q})}{\partial \boldsymbol{q}}\right)^{-1}\left(\frac{\partial \boldsymbol{\phi}(\boldsymbol{x}_{\mathrm{b}},\boldsymbol{l},\boldsymbol{q})}{\partial \boldsymbol{x}_{\mathrm{b}}}\right), \tag{6.94}$$

$$\boldsymbol{\Phi}_{\mathrm{ql}}(\boldsymbol{x}_{\mathrm{b}},\boldsymbol{l},\boldsymbol{q}) = -\left(\frac{\partial \boldsymbol{\phi}(\boldsymbol{x}_{\mathrm{b}},\boldsymbol{l},\boldsymbol{q})}{\partial \boldsymbol{q}}\right)^{-1}\left(\frac{\partial \boldsymbol{\phi}(\boldsymbol{x}_{\mathrm{b}},\boldsymbol{l},\boldsymbol{q})}{\partial \boldsymbol{l}}\right), \tag{6.95}$$

transform (pull-back) not only forces (co-vectors) from $\boldsymbol{q}$ to $\boldsymbol{x}_{\mathrm{b}}$ and $\boldsymbol{l}$ coordinates, $\boldsymbol{\Phi}_{\mathrm{qb}}$ and $\boldsymbol{\Phi}_{\mathrm{ql}}$ map (push-forward) also the velocities (vectors) in the opposite direction, e. g., $\dot{\boldsymbol{x}}_{\mathrm{b}}$ and $\dot{\boldsymbol{l}}$ to $\dot{\boldsymbol{q}}$, respectively. Since the covariant time derivatives of vector fields are again vectors, they transform accordingly such that

$$\frac{\mathrm{D}\dot{\boldsymbol{q}}}{\mathrm{D}t} = \boldsymbol{\Phi}_{\mathrm{qb}}\frac{\mathrm{D}\dot{\boldsymbol{x}}_{\mathrm{b}}}{\mathrm{D}t}, \tag{6.96}$$

$$\frac{\mathrm{D}\dot{\boldsymbol{q}}}{\mathrm{D}t} = \boldsymbol{\Phi}_{\mathrm{ql}}\frac{\mathrm{D}\dot{\boldsymbol{l}}}{\mathrm{D}t} \tag{6.97}$$

hold. Therefore, the constrained dynamics (6.92) and (6.93) can be compactly expressed in terms of the "extended" task coordinates $\boldsymbol{x} = (\boldsymbol{x}_{\mathrm{b}}, \boldsymbol{l}) \in \mathcal{X}$, i. e.,

$$\bar{\boldsymbol{M}}(\boldsymbol{x},\boldsymbol{q})\frac{\mathrm{D}\dot{\boldsymbol{x}}}{\mathrm{D}t} = -\frac{\partial U(\boldsymbol{\theta},\boldsymbol{x}_{\mathrm{b}},\boldsymbol{q}(\boldsymbol{x}))}{\partial \boldsymbol{x}}^{T}, \tag{6.98}$$

where the constrained inertia matrix and potential force, which are required later, are given by

$$\bar{\boldsymbol{M}} = \begin{bmatrix}\boldsymbol{M}_{\mathrm{bb}} + \boldsymbol{M}_{\mathrm{bq}}\boldsymbol{\Phi}_{\mathrm{qb}} + \boldsymbol{\Phi}_{\mathrm{qb}}^{T}\boldsymbol{M}_{\mathrm{bq}}^{T} + \boldsymbol{\Phi}_{\mathrm{qb}}^{T}\boldsymbol{M}_{\mathrm{qq}}\boldsymbol{\Phi}_{\mathrm{qb}} & \boldsymbol{M}_{\mathrm{bq}}\boldsymbol{\Phi}_{\mathrm{ql}} + \boldsymbol{\Phi}_{\mathrm{qb}}^{T}\boldsymbol{M}_{\mathrm{qq}}\boldsymbol{\Phi}_{\mathrm{ql}}\\ \left(\boldsymbol{M}_{\mathrm{bq}}\boldsymbol{\Phi}_{\mathrm{ql}} + \boldsymbol{\Phi}_{\mathrm{qb}}^{T}\boldsymbol{M}_{\mathrm{qq}}\boldsymbol{\Phi}_{\mathrm{ql}}\right)^{T} & \boldsymbol{\Phi}_{\mathrm{ql}}^{T}\boldsymbol{M}_{\mathrm{qq}}\boldsymbol{\Phi}_{\mathrm{ql}}\end{bmatrix} \tag{6.99}$$

and

$$\frac{\partial U(\boldsymbol{\theta},\boldsymbol{x}_{\mathrm{b}},\boldsymbol{q}(\boldsymbol{x}))}{\partial \boldsymbol{x}}^{T} = \begin{pmatrix}\frac{\partial U(\boldsymbol{\theta},\boldsymbol{x}_{\mathrm{b}},\boldsymbol{q})}{\partial \boldsymbol{x}_{\mathrm{b}}}^{T} + \boldsymbol{\Phi}_{\mathrm{qb}}^{T}\frac{\partial U(\boldsymbol{\theta},\boldsymbol{x}_{\mathrm{b}},\boldsymbol{q})}{\partial \boldsymbol{q}}^{T}\\ \boldsymbol{\Phi}_{\mathrm{ql}}^{T}\frac{\partial U(\boldsymbol{\theta},\boldsymbol{x}_{\mathrm{b}},\boldsymbol{q})}{\partial \boldsymbol{q}}^{T}\end{pmatrix}, \tag{6.100}$$

respectively.

Remark 6.10. *The derivation of the constrained task dynamics formulation exploits the concept of covariant differentiation as introduced in Sect. 2.2.3. This leads to a very compact notation, as the Coriolis/centrifugal terms are "hidden" in the operator* D. *Considering, e. g., the affinely connected Riemannian manifold with metric tensor* $\bar{\boldsymbol{M}}(\boldsymbol{x})$*, then, the covariant differential of the vector field* $\dot{\boldsymbol{x}}(\boldsymbol{x})$ *can be expressed as*

$$\mathrm{D}\dot{x}^{j} = \mathrm{d}\dot{x}^{j} + \Gamma_{h}{}^{j}{}_{k}\dot{x}^{h}\mathrm{d}x^{k} = 0, \quad i,j,k = 1\ldots n,$$

where $\Gamma_{h}{}^{j}{}_{k}$ *denotes the Christoffel symbols of the second kind, which are associated with the metric tensor* $\bar{\boldsymbol{M}}(\boldsymbol{x})$ *(cf. Definition 2.10 and 2.13).*

According to Assumption 6.3, $\boldsymbol{q}$ and $\dot{\boldsymbol{q}}$ can always be expressed in terms of $\boldsymbol{x}$ and $\dot{\boldsymbol{x}}$ such that the dependencies of the components in (6.98) could have been replaced, respectively. However, since the modal matching algorithm proposed in the following section aims at including also solutions which not satisfy the constraints (6.88) identically, this replacement is not performed. Instead, the unconstrained coordinates $\boldsymbol{\chi} = (\boldsymbol{x}, \boldsymbol{q}) \in \mathbb{R}^{2n}$ are introduced.

6.4.2. Modal matching algorithm

In this section, an algorithm is derived which matches the local eigenvectors of constrained dynamics of the form (6.98) to a given task. Consider therefore the linearization of (6.98) w. r. t. to an equilibrium position $\bar{\boldsymbol{x}}(\bar{\boldsymbol{q}}(\boldsymbol{\theta}))$,

$$\bar{\boldsymbol{M}}(\bar{\boldsymbol{\chi}})\ddot{\boldsymbol{x}} + \bar{\boldsymbol{K}}(\bar{\boldsymbol{\chi}})\left[\boldsymbol{x} - \bar{\boldsymbol{x}}(\bar{\boldsymbol{q}}(\boldsymbol{\theta}))\right] = \boldsymbol{0}\,. \tag{6.101}$$

Herein, $\bar{\boldsymbol{K}}(\bar{\boldsymbol{\chi}}) = \partial^2 U(\boldsymbol{\theta}, \boldsymbol{x}_\mathrm{b}, \boldsymbol{q}(\boldsymbol{x})/\partial \boldsymbol{x}^2$ represents the local stiffness matrix at the point of linearization $\bar{\boldsymbol{\chi}} = (\bar{\boldsymbol{x}}(\bar{\boldsymbol{q}}), \bar{\boldsymbol{q}})$. The ordinary time derivative $\ddot{\boldsymbol{x}}$ of $\dot{\boldsymbol{x}}$ results due to the linearization of the covariant derivative $\mathrm{D}\dot{\boldsymbol{x}}/\mathrm{D}t$. Assuming algebraic and geometric multiplicity of one, the generalized eigenvalue problem corresponding to $\bar{\boldsymbol{K}}(\bar{\boldsymbol{\chi}})$ and $\bar{\boldsymbol{M}}(\bar{\boldsymbol{\chi}})$ (cf. (5.6) and (5.7)),

$$\lambda \bar{\boldsymbol{M}}(\bar{\boldsymbol{\chi}})\boldsymbol{w} = \bar{\boldsymbol{K}}(\bar{\boldsymbol{\chi}})\boldsymbol{w} \tag{6.102}$$

$$\text{s.t. } \|\boldsymbol{w}\|^2 = 1\,, \tag{6.103}$$

yields as solution n generalized eigenvectors $\boldsymbol{w}_i(\bar{\boldsymbol{\chi}}) \in \{\boldsymbol{w} \in \mathbb{R}^n \mid \|\boldsymbol{w}\|^2 = 1\}$, for $i = 1 \ldots n$. Based on $\boldsymbol{w}_i(\bar{\boldsymbol{\chi}})$, the problem of modal matching can be formulated as follows:

Problem 6.1. *Given is the desired eigenvector $\boldsymbol{w}_\mathrm{des}$ expressed w. r. t. the task coordinates $\boldsymbol{x}$. Let $\boldsymbol{w}(j)(\bar{\boldsymbol{\chi}})$ be the eigenvector which has minimum distance to the desired eigenvector $\boldsymbol{w}_\mathrm{des}$, i. e., $k = \min_{i\in[1;n]}\left(\|\boldsymbol{w}_i(\bar{\boldsymbol{\chi}}) - \boldsymbol{w}_\mathrm{des}\|\right)$. Then, the problem of modal matching can be formulated as finding an equilibrium configuration $\bar{\boldsymbol{\chi}}$ satisfying the constraints* (6.88) *for which $\boldsymbol{w}(j)(\bar{\boldsymbol{\chi}}) = \boldsymbol{w}_\mathrm{des}$.*

In the following, the algorithm which solves this problem is derived. Thereby, the simplified notation $\boldsymbol{w} := \boldsymbol{w}(j)$ is used.

Consider the differential mapping

$$\mathrm{d}\boldsymbol{w} = \frac{\partial \boldsymbol{w}(\bar{\boldsymbol{\chi}})}{\partial \bar{\boldsymbol{\chi}}}\mathrm{d}\bar{\boldsymbol{\chi}} \tag{6.104}$$

and approximate $\mathrm{d}\boldsymbol{w} \approx \boldsymbol{w}_\mathrm{des} - \boldsymbol{w}$ and $\mathrm{d}\bar{\boldsymbol{\chi}} \approx \bar{\boldsymbol{\chi}}(j+1) - \bar{\boldsymbol{\chi}}(j)$. Then, a recursion of the form

$$\bar{\boldsymbol{\chi}}(j+1) = \bar{\boldsymbol{\chi}}(j) + \left[\frac{\partial \boldsymbol{w}}{\partial \bar{\boldsymbol{\chi}}}(\bar{\boldsymbol{\chi}}(j))\right]^\dagger (\boldsymbol{w}_\mathrm{des} - \boldsymbol{w}) \tag{6.105}$$

can be considered to find a $\hat{\bar{\boldsymbol{\chi}}}$ which minimizes the error $\tilde{\boldsymbol{w}} = \boldsymbol{w}_\mathrm{des} - \boldsymbol{w}$. In (6.105), the operator $(\cdot)^\dagger$ denotes the generalized inverse of a matrix. This is required since the linear system of equations (6.104) is under-determined, i. e., $\partial \boldsymbol{w}/\partial \bar{\boldsymbol{\chi}}$ is a $n \times 2n$ matrix. In particular, the matrix $\partial \boldsymbol{w}/\partial \bar{\boldsymbol{\chi}}$ is of rank $n-1$, since the length of the eigenvector is identity (cf. condition (6.103)). This rank-deficiency can be resolved by introducing a mapping of the form $\boldsymbol{y}(\boldsymbol{w}) : \mathbb{R}^n \to \mathbb{R}^{n-1}$, where $\boldsymbol{y} = \boldsymbol{y}(\boldsymbol{w})$ is a representation of the direction of $\boldsymbol{w}$

(see, Appendix A.2.2). The differential of this mapping takes the form $\mathrm{d}\boldsymbol{y} = \frac{\partial \boldsymbol{y}(\boldsymbol{w})}{\partial \boldsymbol{w}}\mathrm{d}\boldsymbol{w}$. Applying the chain rule results in

$$\frac{\partial \boldsymbol{y}}{\partial \boldsymbol{w}}\mathrm{d}\boldsymbol{w} = \frac{\partial \boldsymbol{y}}{\partial \boldsymbol{w}}\frac{\partial \boldsymbol{w}}{\partial \bar{\boldsymbol{\chi}}}\mathrm{d}\bar{\boldsymbol{\chi}}\,, \tag{6.106}$$

where the $(n-1)\times 2n$ Jacobian matrix $(\partial \boldsymbol{y}/\partial \boldsymbol{w})(\partial \boldsymbol{w}/\partial \bar{\boldsymbol{\chi}})$ is of rank $n-1$. Note that the Jacobian matrix in (6.106) does not account for the constraints (6.88), which represent an implicit relation between $\bar{\boldsymbol{q}}$ and $\bar{\boldsymbol{x}}$. The constraints (6.88) can be incorporated differentially by

$$\begin{bmatrix} \frac{\partial \boldsymbol{y}}{\partial \boldsymbol{w}}\mathrm{d}\boldsymbol{w} \\ \boldsymbol{0} \end{bmatrix} = \boldsymbol{J}(\bar{\boldsymbol{\chi}})\mathrm{d}\bar{\boldsymbol{\chi}} \tag{6.107}$$

where

$$\boldsymbol{J}(\bar{\boldsymbol{\chi}}) = \begin{bmatrix} \frac{\partial \boldsymbol{y}}{\partial \boldsymbol{w}}\frac{\partial \boldsymbol{w}}{\partial \bar{\boldsymbol{\chi}}} \\ \frac{\partial \boldsymbol{\phi}}{\partial \bar{\boldsymbol{\chi}}} \end{bmatrix} \tag{6.108}$$

is now a $(2n-1)\times 2n$ matrix. Therefore, the linear system of equations (6.107) is still under-determined. The degree of freedom in the solution of (6.107) can be exploited to span an 1-D subspace.[8] In case of mode matching it represents the vector space where changes in the configuration $\mathrm{d}\bar{\boldsymbol{\chi}}$ do not vary the eigenvector $\boldsymbol{w}$. The remaining nullspace can be resolved by augmenting the Jacobian [PCY99]:

$$\boldsymbol{J}_{\mathrm{aug}} = \begin{pmatrix} \boldsymbol{J} \\ \boldsymbol{Z} \end{pmatrix}\,, \tag{6.109}$$

where the $1\times 2n$ matrix $\boldsymbol{Z}$ represents a basis spanning the nullspace of $\boldsymbol{J}$ such that $\boldsymbol{J}\boldsymbol{Z}^T = \boldsymbol{0}$. Finally, the mode matching algorithm can be compactly described by the following formula:

$$\bar{\boldsymbol{\chi}}(j+1) = \bar{\boldsymbol{\chi}}(j) + \gamma \boldsymbol{J}_{\mathrm{aug}}(\bar{\boldsymbol{\chi}}(j))^{-1} \begin{bmatrix} \frac{\partial \boldsymbol{y}}{\partial \boldsymbol{w}}\left(\boldsymbol{w}_{\mathrm{des}} - \boldsymbol{w}(j)(\bar{\boldsymbol{\chi}}(j))\right) \\ \boldsymbol{0}_{n\times 1} \\ \boldsymbol{Z}(\bar{\boldsymbol{\chi}}(j))\left(\bar{\boldsymbol{\chi}}_{\mathrm{des}} - \bar{\boldsymbol{\chi}}(j)\right) \end{bmatrix}\,. \tag{6.110}$$

Herein, $\bar{\boldsymbol{\chi}}_{\mathrm{des}}$ denotes the desired equilibrium configuration satisfying the constraints (6.88), i. e., $\boldsymbol{\phi}(\bar{\boldsymbol{\chi}}_{\mathrm{des}}) = \boldsymbol{0}$, and $\gamma > 0$ represents the step size of the iteration. Note that $\bar{\boldsymbol{\chi}}_{\mathrm{des}}$ is maintained with lower priority compared to achieving the desired eigenvector $\boldsymbol{w}_{\mathrm{des}}$ and keeping the constraints (6.88).

Remark 6.11. *The closed-form computation (i. e., avoiding finite differences) of the augmented Jacobian in* (6.110) *requires to compute the closed-form differentiation of the eigenvector $\boldsymbol{w}$ w. r. t. the optimization parameters $\bar{\boldsymbol{\chi}}$. This can be achieved using the procedure, which is provided in Appendix A.2.3.*

6.4.3. Local eigenvector control

The eigenvector Jacobian matrix $\partial \boldsymbol{w}/\partial \boldsymbol{\chi}$ constitutes a differential relation between the configuration $\boldsymbol{\chi}$ and the eigenvector $\boldsymbol{w}$. This relation can be exploited to continuously

[8] Note that there exist infinitely many possibilities to span the nullspace of $\boldsymbol{J}$.

control the eigenvector, e. g., by introducing a potential which stabilizes the direction $\boldsymbol{y}$ of the eigenvector $\boldsymbol{w}$ w. r. t. an equilibrium $\boldsymbol{y}_0$. In order to implement such a behavior, consider the elastic potential $U_\mathrm{e}(\boldsymbol{\theta}, \boldsymbol{q})$ and assume that $\boldsymbol{q} = \boldsymbol{q}(\boldsymbol{y})$. Then, analogously to (6.39), the elastic force on the manifold of the eigenvector direction $\boldsymbol{y}$ can be expressed as

$$\boldsymbol{\tau}_\mathrm{y} = -\left[\frac{\partial U_\mathrm{e}(\boldsymbol{\theta}, \boldsymbol{q}(\boldsymbol{y}))}{\partial \boldsymbol{q}} \frac{\partial \boldsymbol{q}}{\partial \boldsymbol{y}}\right]^T . \tag{6.111}$$

The $n \times (n-1)$ Jacobian matrix $\partial \boldsymbol{q}/\partial \boldsymbol{y}$ can be derived by substituting the differential of the constraints (6.88),

$$\mathrm{d}\boldsymbol{\phi} = \frac{\partial \boldsymbol{\phi}(\boldsymbol{x}, \boldsymbol{q})}{\partial \boldsymbol{x}} \mathrm{d}\boldsymbol{x} + \frac{\partial \boldsymbol{\phi}(\boldsymbol{x}, \boldsymbol{q})}{\partial \boldsymbol{q}} \mathrm{d}\boldsymbol{q} = \boldsymbol{0}\,, \tag{6.112}$$

in the expression of the differential of $\boldsymbol{y}$, i. e.,

$$\begin{aligned}
\mathrm{d}\boldsymbol{y} &= \frac{\partial \boldsymbol{y}(\boldsymbol{w})}{\partial \boldsymbol{w}} \left[\frac{\partial \boldsymbol{w}(\boldsymbol{x}, \boldsymbol{q})}{\partial \boldsymbol{x}} \mathrm{d}\boldsymbol{x} + \frac{\partial \boldsymbol{w}(\boldsymbol{x}, \boldsymbol{q})}{\partial \boldsymbol{q}} \mathrm{d}\boldsymbol{q}\right] && (6.113)\\
&= \frac{\partial \boldsymbol{y}(\boldsymbol{w})}{\partial \boldsymbol{w}} \left[\frac{\partial \boldsymbol{w}(\boldsymbol{x}, \boldsymbol{q})}{\partial \boldsymbol{q}} - \frac{\partial \boldsymbol{w}(\boldsymbol{x}, \boldsymbol{q})}{\partial \boldsymbol{x}} \left(\frac{\partial \boldsymbol{\phi}(\boldsymbol{x}, \boldsymbol{q})}{\partial \boldsymbol{x}}\right)^{-1} \frac{\partial \boldsymbol{\phi}(\boldsymbol{x}, \boldsymbol{q})}{\partial \boldsymbol{q}}\right] \mathrm{d}\boldsymbol{q} && (6.114)\\
&= \bar{\boldsymbol{J}}(\boldsymbol{q}) \mathrm{d}\boldsymbol{q}\,. && (6.115)
\end{aligned}$$

This yields the $(n-1) \times n$ Jacobian matrix $\bar{\boldsymbol{J}}(\boldsymbol{q}) = \partial \boldsymbol{y}/\partial \boldsymbol{q}$ of which the inverse is needed to compute $\boldsymbol{\tau}_\mathrm{y}$ in (6.111). Again, the 1-D nullspace can be resolved by augmenting $\bar{\boldsymbol{J}}$ by a $1 \times n$ matrix $\bar{\boldsymbol{Z}} \neq \boldsymbol{0}$ satisfying $\bar{\boldsymbol{J}} \bar{\boldsymbol{Z}}^T = \boldsymbol{0}$ such that

$$\bar{\boldsymbol{J}}_\mathrm{aug}(\boldsymbol{q}) = \begin{bmatrix} \bar{\boldsymbol{J}}(\boldsymbol{q}) \\ \bar{\boldsymbol{Z}}(\boldsymbol{q}) \end{bmatrix} \tag{6.116}$$

is invertible. Therefore, the elastic force on the manifold of the eigenvector direction $\boldsymbol{y}$ is given by

$$\begin{bmatrix} \boldsymbol{\tau}_\mathrm{y}(\boldsymbol{\theta}, \boldsymbol{q}) \\ \tau_\mathrm{w}(\boldsymbol{\theta}, \boldsymbol{q}) \end{bmatrix} = -\bar{\boldsymbol{J}}_\mathrm{aug}(\boldsymbol{q})^{-T} \frac{\partial U_\mathrm{e}(\boldsymbol{\theta}, \boldsymbol{q})}{\partial \boldsymbol{q}}^T , \tag{6.117}$$

where $\tau_\mathrm{w} \in \mathbb{R}$ represents the portion of the elastic force, which does not change the direction of the eigenvector $\boldsymbol{w}$. Then, given an equilibrium configuration $\boldsymbol{q}_0$ (which may be the result of the modal matching procedure of Sect. 6.4.2) and a desired eigenvector direction $\boldsymbol{y}_\mathrm{des}$, a positive definite potential of the form $U_\mathrm{y}(\boldsymbol{y} - \boldsymbol{y}_\mathrm{des}) : \mathbb{R}^{n-1} \to \mathbb{R}$ can be implemented by

$$\boldsymbol{\tau}(\boldsymbol{\theta}, \boldsymbol{q}) = -\frac{\partial U_\mathrm{e}(\boldsymbol{\theta}, \boldsymbol{q})}{\partial \boldsymbol{q}}^T = \bar{\boldsymbol{J}}_\mathrm{aug}(\boldsymbol{q})^T \begin{pmatrix} \boldsymbol{\tau}_\mathrm{y}^\mathrm{des}(\boldsymbol{y}) \\ \tau_\mathrm{w}(\bar{\boldsymbol{q}}^{-1}(\boldsymbol{q}_0), \boldsymbol{q}) \end{pmatrix} . \tag{6.118}$$

Thereby,

$$\boldsymbol{\tau}_\mathrm{y}^\mathrm{des}(\boldsymbol{y}) = -\frac{\partial U_\mathrm{y}(\boldsymbol{y} - \boldsymbol{y}_\mathrm{des})}{\partial \boldsymbol{y}}^T \tag{6.119}$$

represents the control of the eigenvector direction, and in particular, the force which does not affect the eigenvector direction,

$$\tau_\mathrm{w}(\bar{\boldsymbol{q}}^{-1}(\boldsymbol{q}_0), \boldsymbol{q}) = -\bar{\boldsymbol{Z}}(\boldsymbol{q}) \frac{\partial U_\mathrm{e}(\bar{\boldsymbol{q}}^{-1}(\boldsymbol{q}_0), \boldsymbol{q})}{\partial \boldsymbol{q}}^T , \tag{6.120}$$

is completely realized by the original elastic potential of the plant U_e.

6.5. Validation

In this section, the modal control approaches are validated in simulations and experiments on compliantly actuated robotic systems. In addition to the proof of concept, the particular focus lays on establishing the basic qualification of the proposed modal control methods for dynamic legged locomotion. The concepts of modal globalization and adaptation control as introduced in Sect. 6.1 and 6.3, respectively, are general methods which can be exploited to efficiently generate periodic motions in compliantly actuated robotic legs as well as arms. They are experimentally tested on the variable stiffness actuator (VSA) robotic arm, DLR Hand Arm System [GASB+11] also due to its availability. Furthermore, a comprehensive experimental verification including an optimality analysis of modal adaptation based control for a robotic leg with compliantly actuated joints is provided in [SLOAS17]. A key feature of modal shaping control (Sect. 6.2) is the resolution of (elastic) over-actuation (i. e., the number of statically controllable variables is greater than the number of degrees of freedom) which typically appears in multi-legged systems. Therefore, modal shaping control is validated on a compliantly actuated quadruped model in simulation. The modal matching algorithm and the derived local eigenvector control (Sect. 6.4) are predestined tools for jumping and running control in elastic, segmented legged systems. A proof of concept of modal matching based control is performed on a compliantly actuated, single leg model in simulation.

6.5.1. Experiments on the DLR Hand Arm System

The DLR Hand Arm System shown in Fig. 6.2 is a prototypical variable stiffness actuator (VSA) robotic system, which is comprehensively described in [GASB+11]. The arm (excluding the lower arm rotation and the wrist) consists of a 4 degrees of freedom kinematic chain (three orthogonal rotation axes in the shoulder, one for the elbow). Thereby, each joint is equipped with a VSA mechanism implemented as a main motor in series with a nonlinear spring and a much smaller motor to adjust the stiffness characteristic, where the positional coordinates are denoted by θ and σ, respectively (cf. Fig. 6.2b). The order of nonlinearity introduced due to the mechanically implemented floating spring joint [WH08] is depicted in Fig. 6.2c for several stiffness presets. In the case of the lowest preset $\sigma = 0$ the variation of the stiffness over the minimum and maximum spring deflection is about 1400%. Here, the stiffness presets of all joints are held to constant values during all experiments, i. e., $\boldsymbol{\sigma} = \text{const.}$ are regarded as parameters. The rigid body dynamics satisfies Assumption 3.8 and 3.9 such that the fully justified model

$$\boldsymbol{B}\ddot{\boldsymbol{\theta}} + \frac{\partial U_\mathrm{e}(\boldsymbol{q}-\boldsymbol{\theta})}{\partial \boldsymbol{\theta}}^T = \boldsymbol{u}\,, \tag{6.121}$$

$$\boldsymbol{M}(\boldsymbol{q})\ddot{\boldsymbol{q}} + \boldsymbol{C}(\boldsymbol{q},\dot{\boldsymbol{q}})\dot{\boldsymbol{q}} + \frac{\partial U_\mathrm{g}(\boldsymbol{q})}{\partial \boldsymbol{q}}^T + \frac{\partial U_\mathrm{e}(\boldsymbol{q}-\boldsymbol{\theta})}{\partial \boldsymbol{q}}^T = \boldsymbol{\tau}_\mathrm{ext}\,, \tag{6.122}$$

can be considered.[9]

[9] Dissipative forces are omitted in this model, since damping and friction in parallel to the elasticity and on the link-side are negligible by mechancal design. Furthermore, a friction compensation as proposed in [TASLH08] can be presumed on the motor side.

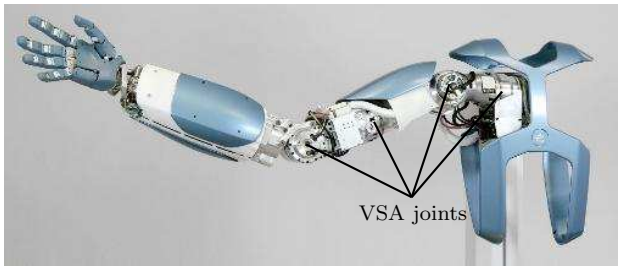

(a) The DLR Hand Arm System

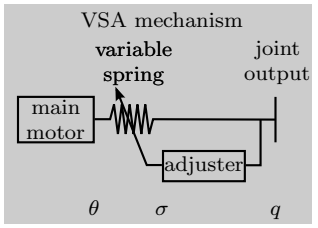

(b) VSA mechanism

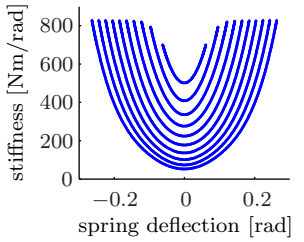

(c) Stiffness of the VSA mechanism

Figure 6.2.: Description of the arm of the DLR Hand Arm System. (a) highlights the VSA joints implemented as sketched in (b). (c) depicts the stiffness characteristic for adjuster positions $\sigma = \{0, 0.02, \ldots, 0.18\}$. Herein, the most outer curve corresponds to $\sigma = 0$.

Modal globalization based periodic motion control

The modal globalization based limit cycle controller (6.5) in combination with (6.31) has been tested in experiments on the DLR Hand Arm System. Since, (6.5) presumes the elastic torques,

$$\boldsymbol{\tau} = \boldsymbol{f}_{\mathrm{e}}(\boldsymbol{\theta} - \boldsymbol{q}) := -\frac{\partial U_{\mathrm{e}}(\boldsymbol{q} - \boldsymbol{\theta})}{\partial \boldsymbol{q}}^T = \frac{\partial U_{\mathrm{e}}(\boldsymbol{q} - \boldsymbol{\theta})}{\partial \boldsymbol{\theta}}^T \tag{6.123}$$

as control input, a decoupling based approach to track desired elastic torques $\boldsymbol{\tau}_{\mathrm{des}}$ has been considered.[10]

The controller is based upon the transformation of the motor dynamics (6.121) under the change of coordinates $\boldsymbol{\theta} = \boldsymbol{f}_{\mathrm{e}}^{-1}(\boldsymbol{\tau}) + \boldsymbol{q}$, which yields

$$\boldsymbol{B}\left[\frac{\partial \boldsymbol{f}_{\mathrm{e}}^{-1}(\boldsymbol{\tau})}{\partial \boldsymbol{\tau}}\ddot{\boldsymbol{\tau}} + \frac{\mathrm{d}}{\mathrm{d}t}\left(\frac{\partial \boldsymbol{f}_{\mathrm{e}}^{-1}(\boldsymbol{\tau})}{\partial \boldsymbol{\tau}}\right)\dot{\boldsymbol{\tau}}\right] + \boldsymbol{B}\ddot{\boldsymbol{q}} + \boldsymbol{\tau} = \boldsymbol{u}\,. \tag{6.124}$$

Selecting the control input in (6.121) as

$$\boldsymbol{u} = \boldsymbol{B}\ddot{\boldsymbol{q}} + \boldsymbol{B}\frac{\mathrm{d}}{\mathrm{d}t}\left(\frac{\partial \boldsymbol{f}_{\mathrm{e}}^{-1}(\boldsymbol{\tau})}{\partial \boldsymbol{\tau}}\right)\dot{\boldsymbol{\tau}} + \boldsymbol{\tau}_{\mathrm{des}} + \boldsymbol{B}\frac{\partial \boldsymbol{f}_{\mathrm{e}}^{-1}(\boldsymbol{\tau})}{\partial \boldsymbol{\tau}}\left(\ddot{\boldsymbol{\tau}}_{\mathrm{des}} - \boldsymbol{D}_{\tau}\dot{\tilde{\boldsymbol{\tau}}} - \boldsymbol{K}_{\tau}\tilde{\boldsymbol{\tau}}\right)\,, \tag{6.125}$$

leads to the decoupled error dynamics of the elastic torque,

$$\ddot{\tilde{\boldsymbol{\tau}}} + \boldsymbol{D}_{\tau}\dot{\tilde{\boldsymbol{\tau}}} + \left[\boldsymbol{K}_{\tau} + \left(\frac{\partial \boldsymbol{f}_{\mathrm{e}}^{-1}(\boldsymbol{\tau})}{\partial \boldsymbol{\tau}}\right)^{-1}\boldsymbol{B}^{-1}\right]\tilde{\boldsymbol{\tau}} = \boldsymbol{0}\,, \tag{6.126}$$

[10]The method is an extention of [OASKH03] to the case of nonlinear elasticities.

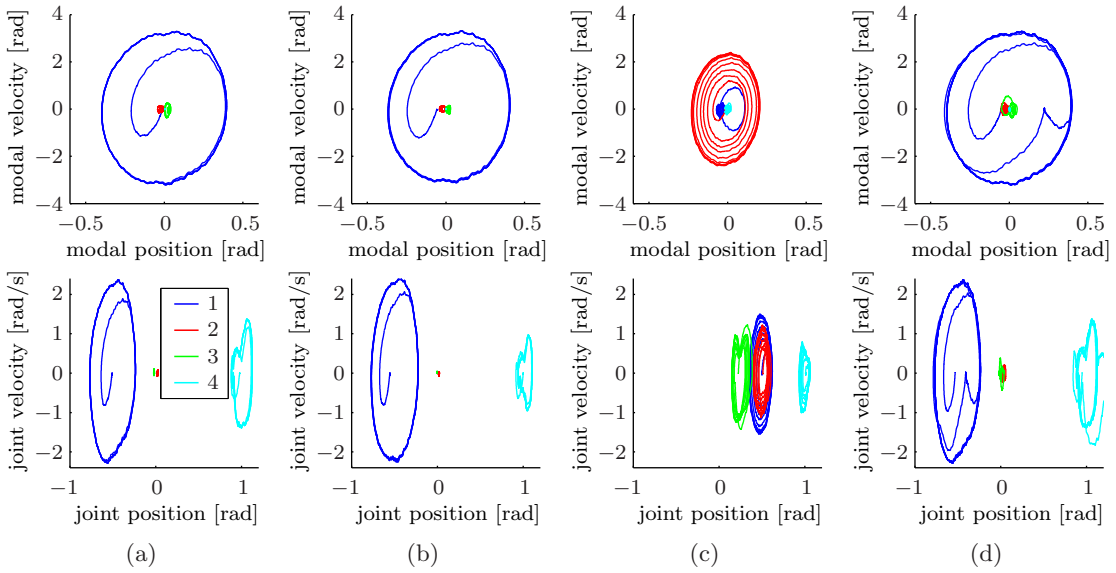

Figure 6.3.: Phase plots of modal (top) and joint (bottom) motion: (a) first mode, low VSA stiffness; (b) first mode, high VSA stiffness; (c) second mode; (d) external disturbance.

where $\tilde{\boldsymbol{\tau}} = \boldsymbol{\tau} - \boldsymbol{\tau}_{\text{des}}$ denotes the tracking error, and $\boldsymbol{K}_\tau$ and $\boldsymbol{D}_\tau$ are symmetric and positive definite controller gain matrices.

The modal globalization control (6.5) has been implemented by selecting $\boldsymbol{\tau}_{\text{des}}$ in (6.125) as

$$\boldsymbol{\tau}_{\text{des}} = \frac{\partial U_{\text{g}}(\boldsymbol{q})}{\partial \boldsymbol{q}}^T - \boldsymbol{D}(\boldsymbol{q})\dot{\boldsymbol{q}} - \boldsymbol{K}(\boldsymbol{q})\Delta\boldsymbol{q} + \boldsymbol{W}(\boldsymbol{q})^{-T}\tilde{\boldsymbol{C}}(\boldsymbol{q},\dot{\boldsymbol{q}})\dot{\boldsymbol{z}} + \boldsymbol{\gamma}(\boldsymbol{q},\dot{\boldsymbol{q}},\ddot{\boldsymbol{q}})\,, \tag{6.127}$$

where $\boldsymbol{D}(\boldsymbol{q})\dot{\boldsymbol{q}} = \boldsymbol{W}(\boldsymbol{q})^{-T}\text{diag}\left(2\xi_i\sqrt{\lambda_i(\boldsymbol{q})}\right)\boldsymbol{W}(\boldsymbol{q})^{-1}\dot{\boldsymbol{q}}$. For all experiments the desired stiffness has been set to $\boldsymbol{K} = \boldsymbol{I}_{4\times4}150.0\,\text{Nm/rad}$, and the modal damping factors have been chosen

$$\xi_k = \frac{\sqrt{\lambda_k(t)}}{2} k_{\text{H}} \left[\tilde{H}(t, z_k, \dot{z}_k) - \frac{\dot{\lambda}_k(t)}{2\lambda_k(t)^2}\right] \tag{6.128}$$

to generate a limit cycle on the k-th (globalized) mode according to (6.31) and $\xi_i = 1$ for the remaining modes, i. e., $i \in [1;4]/\{k\}$. The parameters of the torque tracking control (6.125) have been set to $\boldsymbol{K}_\tau = \text{diag}(10,5,5,5)\,1/t\{s\}^2$ and $\boldsymbol{D}_\tau = \text{diag}(2\xi_\tau\omega_{\tau,i})\,1/t\{s\}$, where $\xi_\tau = 1$ and $\boldsymbol{\omega}_\tau = (\boldsymbol{K}_\tau + \left(\partial \boldsymbol{f}_{\text{e}}^{-1}(\boldsymbol{\tau})/\partial/\boldsymbol{\tau}\right)^{-1}\boldsymbol{B}^{-1})^{1/2}$. To overcome the numerical computation of higher derivatives of measured signals, only the desired joint torque $\boldsymbol{\tau}_{\text{des}}$ and the first derivative $\dot{\boldsymbol{\tau}}_{\text{des}}$ had been considered in (6.125). The limit cycle control (6.128) has been applied either to the first or second mode. Thereby, the desired total energy has been set to $H_{\text{des}} = 0.08\,\text{J}$ or $H_{\text{des}} = 0.035\,\text{J}$, respectively, and the corresponding gain has been selected $k_V = 1.5$. In order to induce the limit cycle motion, the robotic arm has been manually pushed from one of the initial configurations: $\boldsymbol{q}_{\text{des}} = (-\pi/6, 0, 0, \pi/3)$ for the first and $\boldsymbol{q}_{\text{des}} = (\pi/6, \pi/6, \pi/12, \pi/3)$ for the second mode.

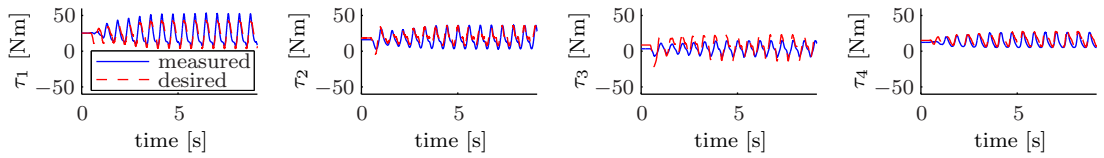

Figure 6.4.: Measured and desired elastic torque corresponding to the second mode motion depicted in Fig. 6.3c.

The experimentally recorded first mode motions for the stiffness presets $\boldsymbol{\sigma} = \boldsymbol{\sigma}_{\min}$ (low stiffness) and $\boldsymbol{\sigma} = 0.5\boldsymbol{\sigma}_{\max}$ (high stiffness) are shown in Fig. 6.3a and 6.3b. For both stiffness presets the modal motion is similar. This is as the desired dynamics is the same. In both cases, the motion of the first mode asymptotically approaches the limit cycle, while the motion of the remaining modes stays within a small region around the origin of the modal state space. The motion in terms of link positions involves mainly the first and fourth joint. Second mode motions are shown in Fig. 6.3c. This mode involves the motion of all joints. The corresponding tracking performance of the elastic torque controller is shown in Fig. 6.4. During the regulation phase (where the robot maintains in the initial configuration), a constant tracking error can be observed. This can be due to friction (not considered in the elastic torque tracking control). In order to reduce the tracking error during the high acceleration phases of the desired torque, the second time derivative $\ddot{\boldsymbol{\tau}}_{\text{des}}$ can be provided. Furthermore, the attractive behavior of the modal limit cycle is depicted in Fig. 6.3d. Thereby, the robotic arm has been externally disturbed by catching and releasing the wrist manually during motion. The motion converges back to the limit cycle in less than a half an oscillation cycle.

To verify the efficiency of the proposed approach, a performance measure based on power considerations is introduced. Consider the total power of the VSA robot dynamics (6.121), (6.122), and (6.123):

$$P_{\text{tot}} = \underbrace{\boldsymbol{\tau}_{\text{tot}}^T \dot{\boldsymbol{q}}}_{P_{\text{link}}} + \underbrace{\boldsymbol{u}^T \dot{\boldsymbol{\theta}}}_{P_{\text{motor}}} + \underbrace{\frac{\partial U_{\text{e}}(\boldsymbol{\theta}, \boldsymbol{q})}{\partial \boldsymbol{q}} \dot{\boldsymbol{q}}}_{P_{\text{stf}}} + P_{\text{dis}} \,. \tag{6.129}$$

Herein, P_{link} (where $\boldsymbol{\tau}_{\text{tot}} = \boldsymbol{\tau} + \boldsymbol{\tau}_{\text{ext}}$) and P_{motor} denote the power of the links and motors, respectively. The power transmitted via the springs is denoted by P_{stf} and P_{dis} represents the dissipated power. The generated motion is periodic. Since, the link variables $\boldsymbol{q}$ are statically controllable via the motor coordinates $\boldsymbol{\theta}$, also the input and output power is periodic. Additionally, the power flow w. r. t. the motors is subject to substantial losses in both directions. An efficiency measure which accounts for the periodicity and the losses of motor power can be defined as the ratio of root-mean-square (RMS) values of the input and output power, i. e.,

$$\eta_{\text{RMS}}(t) = \frac{\sqrt{\int_0^t P_{\text{link}}(r)^2 \mathrm{d}r}}{\sqrt{\int_0^t P_{\text{motor}}(r)^2 \mathrm{d}r}} \,. \tag{6.130}$$

The performance in case of low and high VSA stiffness presets is compared for equal desired modal limit cycle dynamics. Thereby, $\eta_{\text{RMS}}(t)$ has been evaluated for the experimental recordings corresponding to motions shown in Fig. 6.3a and Fig. 6.3b. The time evolutions

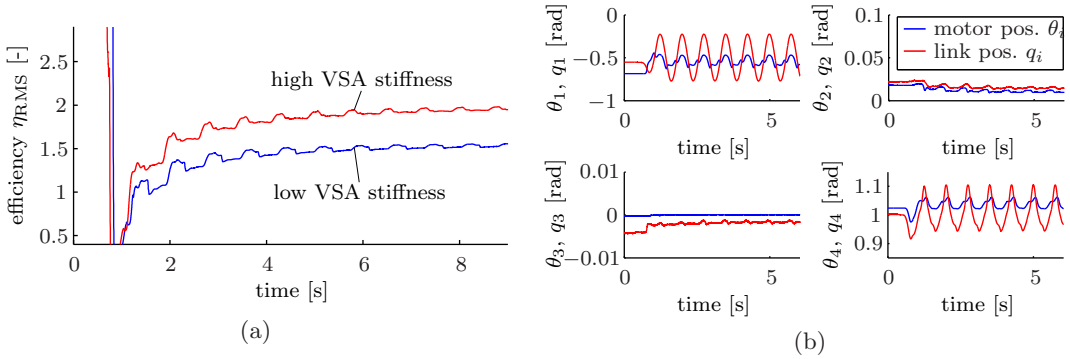

Figure 6.5.: Efficiency of modal globalization based control. (a) Comparison of the measures η_{RMS} for high and low VSA stiffness presets. (b) Link and motor position corresponding to the more efficient VSA stiffness preset.

of $\eta_{\mathrm{RMS,low}}(t)$ and $\eta_{\mathrm{RMS,high}}(t)$, which are plotted in Fig. 6.5a, are qualitatively similar for both cases and can be explained as follows. During the resting phase, the motor and link power is zero, and consequently the performance measures are meaningless. As the robot is externally disturbed $\eta_{\mathrm{RMS}} \gg 1$ due to the external power input. Then, the controller is active and the value undercuts $\eta_{\mathrm{RMS}} = 1$ before it approaches the stationary values of $\eta_{\mathrm{RMS,low}} \approx 1.8$ and $\eta_{\mathrm{RMS,high}} \approx 2.3$. In the stationary phase, the effective motor power is lower than the link power. The difference is provided by the elastic elements. Simply speaking, the motor performs less motion than the link as shown in Fig. 6.5b. In particular, matching the VSA stiffness to the desired dynamics leads to increasing efficiency. Therefore, it can be concluded that the modal globalization based limit cycle generation is efficient w. r. t. the power exchange.

Modally adaptive periodic motion control

The modally adaptive periodic motion control (6.80), (6.84), and (6.85) has been verified in experiments with the DLR Hand Arm System. Since, (6.84) defines the motor position $\boldsymbol{\theta}$ as control input, a PD controller of the form (cf. (3.31))

$$\boldsymbol{u} = -\boldsymbol{K}_{\mathrm{P}} \left(\boldsymbol{\theta} - \boldsymbol{\theta}_{\mathrm{des}} \right) - \boldsymbol{K}_{\mathrm{D}} \dot{\boldsymbol{\theta}} \tag{6.131}$$

is considered. For all experiments the controller gains are set to the maximally realizable values of $\boldsymbol{K}_{\mathrm{P}} = \boldsymbol{I}_{4\times4} 6000\,\mathrm{Nm/rad}$ and $\boldsymbol{K}_{\mathrm{D}} = \boldsymbol{I}_{4\times4} 250\,\mathrm{Nms/rad}$ such that the singular perturbation assumption of Sect. 3.2.3 is satisfied, i. e., $\boldsymbol{\theta} \approx \boldsymbol{\theta}_{\mathrm{des}}$. The switching function (6.85) is implemented based on feedback of the elastic torque (6.123) along $\boldsymbol{w}$:

$$\tau_{\mathrm{s}} = -\boldsymbol{w}^T \frac{\partial U_{\mathrm{e}}(\boldsymbol{q} - \boldsymbol{\theta})}{\partial \boldsymbol{q}}^T , \tag{6.132}$$

$$\theta_{\mathrm{s}}(\tau_{\mathrm{s}}(t)) = \begin{cases} +\hat{\theta}_{\mathrm{s}} & \text{if} \quad \tau_{\mathrm{s}}(t) > \epsilon_{\tau_{\mathrm{s}}} \\ 0 & \text{if} \quad |\tau_{\mathrm{s}}(t)| < \epsilon_{\tau_{\mathrm{s}}} \\ -\hat{\theta}_{\mathrm{s}} & \text{if} \quad \tau_{\mathrm{s}}(t) < -\epsilon_{\tau_{\mathrm{s}}} \end{cases} . \tag{6.133}$$

This implementation neglects the influence of gravity such that the control input (6.84) becomes

$$\boldsymbol{\theta} = \boldsymbol{\theta}_0 + \boldsymbol{w}\theta_\mathrm{s}\,. \tag{6.134}$$

In particular, it allows to propose a physical interpretation of the switching parameters $\epsilon_{\tau_\mathrm{s}} > 0$ and $\hat{\theta}_\mathrm{s} > 0$:

Remark 6.12. *Consider the case where τ_s crosses $-\epsilon_{\tau_\mathrm{s}}$ from above. Assume without loss of generality that $\boldsymbol{\theta}_0 = \mathbf{0}$. Then, the energy injected due to the switching is given by*

$$\Delta U_\mathrm{e} = U_\mathrm{e}(\boldsymbol{q} + \boldsymbol{w}\hat{\theta}_\mathrm{s}) - U_\mathrm{e}(\boldsymbol{q}) = \left.\frac{\partial U_\mathrm{e}(\boldsymbol{\phi})}{\partial \boldsymbol{\phi}}\right|_{\boldsymbol{\phi}=\boldsymbol{q}+c_1\boldsymbol{w}\hat{\theta}_\mathrm{s}} \boldsymbol{w}\hat{\theta}_\mathrm{s}\,, \tag{6.135}$$

with $\boldsymbol{q} \in \mathcal{A}$, where the jump set

$$\mathcal{A} := \left\{ \boldsymbol{q} \in \mathbb{R}^n \,|\, \frac{\partial U_\mathrm{e}(\boldsymbol{q})}{\partial \boldsymbol{q}}\boldsymbol{w} = \epsilon_{\tau_\mathrm{s}} \right\} \tag{6.136}$$

represents a $(n-1)$-D submanifold of the n-D configuration space. The latter equality in (6.135) *follows from the mean value theorem, where $c_1 \in [0;1]$. The difference of the elastic torque along $\boldsymbol{w}$ due to the switching can be expressed as*

$$\begin{aligned}
\Delta\tau_\mathrm{s} &= \frac{\partial U_\mathrm{e}(\boldsymbol{q} + \boldsymbol{w}\hat{\theta}_\mathrm{s})}{\partial \boldsymbol{q}}\boldsymbol{w} - \frac{\partial U_\mathrm{e}(\boldsymbol{q})}{\partial \boldsymbol{q}}\boldsymbol{w} && (6.137)\\
&= \frac{\partial U_\mathrm{e}(\boldsymbol{q} + \boldsymbol{w}\hat{\theta}_\mathrm{s})}{\partial \boldsymbol{q}}\boldsymbol{w} - \epsilon_{\tau_\mathrm{s}} && (6.138)\\
&= \boldsymbol{w}^T \left.\frac{\partial^2 U_\mathrm{e}(\boldsymbol{\phi})}{\partial \boldsymbol{\phi}^2}\right|_{\boldsymbol{\phi}=\boldsymbol{q}+c_2\boldsymbol{w}\hat{\boldsymbol{\theta}}_\mathrm{s}} \boldsymbol{w}\hat{\theta}_\mathrm{s}\,, && (6.139)
\end{aligned}$$

where equality (6.138) *exploits $\boldsymbol{q} \in \mathcal{A}$. In* (6.139)*, the mean value theorem with $c_2 \in [0;1]$ is applied again. By virtue of Assumption 3.2, the Hessian of the elastic potential (sometimes referred to as the local stiffness) $\partial^2 U_\mathrm{e}(\boldsymbol{\phi})/\partial\boldsymbol{\phi}^2$ keeps positively bounded away from zero and from above. Therefore, there exists constants $c_4 > c_3 > 0$ such that*

$$c_3 < \boldsymbol{w}^T \frac{\partial^2 U_\mathrm{e}(\boldsymbol{\phi})}{\partial \boldsymbol{\phi}^2}\boldsymbol{w} < c_4 \tag{6.140}$$

holds for all $\boldsymbol{\phi} \in \mathbb{R}^n$. However, this implies that

$$\max_{c_1\in[0;1]} \left(\left.\frac{\partial U_\mathrm{e}(\boldsymbol{\phi})}{\partial \boldsymbol{\phi}}\right|_{\boldsymbol{\phi}=\boldsymbol{q}+c_1\boldsymbol{w}\hat{\theta}_\mathrm{s}} \boldsymbol{w} \right) = \left.\frac{\partial U_\mathrm{e}(\boldsymbol{\phi})}{\partial \boldsymbol{\phi}}\right|_{\boldsymbol{\phi}=\boldsymbol{q}+\boldsymbol{w}\hat{\theta}_\mathrm{s}} \boldsymbol{w}\,, \tag{6.141}$$

which by substituting in (6.135)*, while taking* (6.139) *and* (6.140) *into account, yields the upper bound for the injected energy*

$$\Delta U_\mathrm{e} \leq \frac{\partial U_\mathrm{e}(\boldsymbol{q} + \boldsymbol{w}\hat{\theta}_\mathrm{s})}{\partial \boldsymbol{q}}\boldsymbol{w}\hat{\theta}_\mathrm{s} = \boldsymbol{w}^T \left.\frac{\partial^2 U_\mathrm{e}(\boldsymbol{\phi})}{\partial \boldsymbol{\phi}^2}\right|_{\boldsymbol{\phi}=\boldsymbol{q}+c_2\boldsymbol{w}\hat{\boldsymbol{\theta}}_\mathrm{s}} \boldsymbol{w}\hat{\theta}_\mathrm{s}^2 + \epsilon_{\tau_\mathrm{s}}\hat{\theta}_\mathrm{s} \leq c_4\hat{\theta}_\mathrm{s}^2 + \epsilon_{\tau_\mathrm{s}}\hat{\theta}_\mathrm{s}\,. \tag{6.142}$$

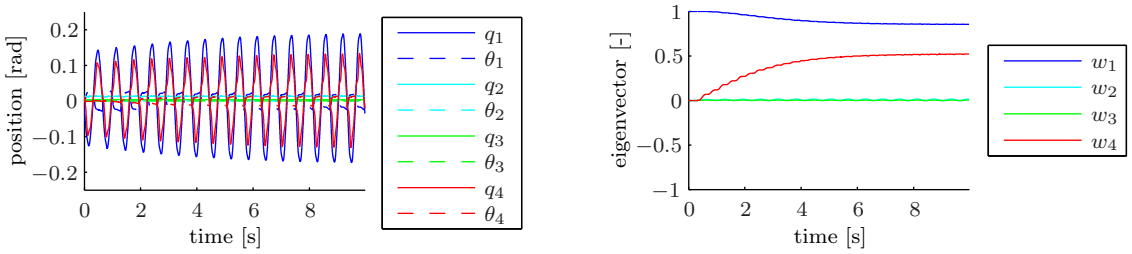

Figure 6.6.: Convergence of eigenvector adaptation: measured link position $\boldsymbol{q}(t)$ and motor position $\boldsymbol{\theta}(t)$ (left); instantenous eigenvector $\boldsymbol{w}(t)$ (right).

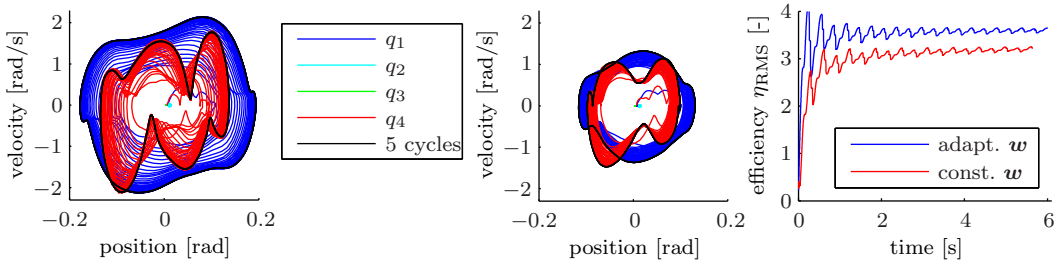

Figure 6.7.: Comparison of energy efficiency for the generation of periodic motions based on modally adapted and trivial excitations: (a) phase plot of joint motion for the modally adaptive control; (b) phase plot of joint motion for the trivial excitation; (c) evaluation of the efficiency measure η_{RMS} comparing both approaches.

In case of the DLR Hand Arm System at hand, the elastic potential is joint-wise decoupled and equal, i. e., $U_{\mathrm{e}}(\boldsymbol{q}-\boldsymbol{\theta}) = \sum_{i=1}^{4} U_{\mathrm{e,joint}}(q_i - \theta_i)$. Since, $\|\boldsymbol{w}\| = 1$ by definition, it follows that $c_4 = \max_{\phi\in\mathbb{R}} \left(\partial^2 U_{\mathrm{e,joint}}(\phi)/\partial\phi^2\right)$.[11]

The first experiment validates the convergence property of the eigenvector adaptation (6.80). Therefore, the (trivial) initial condition $\boldsymbol{w}(0) = \begin{bmatrix}1 & 0 & 0 & 0\end{bmatrix}^T$ is considered. Fig. 6.6 shows the measured motor position $\boldsymbol{\theta}(t)$, link position $\boldsymbol{q}(t)$, and the instantaneous output of the eigenvector adaption $\boldsymbol{w}(t)$. It can be clearly seen that the modal weights $\boldsymbol{w}(t)$ converge to $\boldsymbol{w} = \begin{bmatrix}0.85 & 0.00 & 0.00 & 0.52\end{bmatrix}^T$ within less than 5 s.

Further experiments with the DLR Hand Arm System compare the energy efficiency of #1 eigenvector adaptation based periodic motion control (6.80), (6.134), and (6.133), with #2 an excitation based on the constant, (trivial) weight $\boldsymbol{w}_0 = \begin{bmatrix}1 & 0 & 0 & 0\end{bmatrix}^T$. Note that the latter has been utilized in the empirical study of periodic motions in [LPAS14]. The threshold is set to $\epsilon_{\tau_{\mathrm{s}}} = 5.0\,\mathrm{Nm}$ for both experiments. The switching amplitudes are adjusted to $\hat{\theta}_{\mathrm{s}} = 0.03\,\mathrm{rad}$ and $\hat{\theta}_{\mathrm{s}} = 0.02\,\mathrm{rad}$ for experiment #1 and #2, respectively, such that the injected energy due to the switchings is approximately equal across the experiments (cf. Remark 6.12). Fig. 6.7a and 6.7b depict phase plots of joint motions for experiment #1 and #2, respectively. Although, the energies injected by control are

[11] A particular corrolary of Remark 6.12 is given if $U_{\mathrm{e}} = 1/2k(\boldsymbol{q}-\boldsymbol{\theta})^T(\boldsymbol{q}-\boldsymbol{\theta})$. Then, $\Delta U_{\mathrm{e}} = 1/2k\hat{\theta}_{\mathrm{s}}^2 + \epsilon_{\tau_{\mathrm{s}}}\hat{\theta}_{\mathrm{s}}$, as recognized in [SLOAS17].

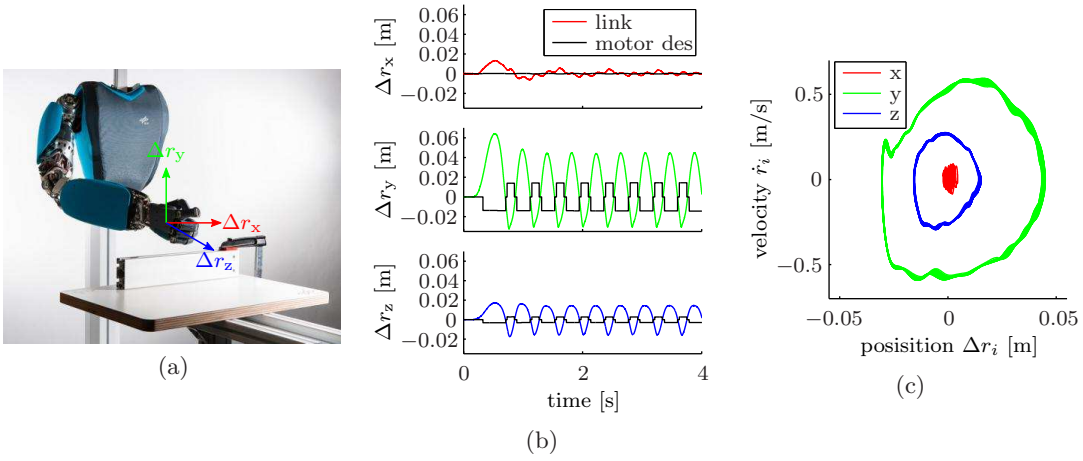

(a) (b) (c)

Figure 6.8.: Modally adaptive periodic motion control with disturbances of environmental contacts: (a) experimental setup; (b) commanded motor and resulting link motion expressed in Cartesian end-effector coordinates; (c) phase plot of Cartesian end-effector motion (quasi-periodic steady state).

approximately equal for both experiments, the oscillation amplitudes of the adaptive control are higher than for the trivial excitation. The increased efficiency of the adaptive control is further validated by evaluating the efficiency measure (6.130) for measurements of both experiments. Fig. 6.7c shows the results. It can be seen that the efficiency in case of the adaptive approach is higher than with the trivial excitation. Therefore, it can be concluded that the eigenvector adaptation based periodic motion generation increases the energy efficiency.

Finally, the ability of the control (6.80), (6.134), and (6.133) to stabilize periodic motions is validated, even when contacts with the environment occur. Therefore, the robotic arm is placed in an initial configuration as shown in Fig. 6.8a. The threshold ϵ_{τ_s} and the switching amplitude $\hat{\theta}_s$ are adjusted such that the end-effector gets in contact with the environment. To initially start the oscillations, the end-effector is manually deflected and released. In Fig. 6.8b, it can be seen that after the initial disturbance the motion in the x- and y-directions approaches a quasi-periodic steady state within less than three oscillation cycles. The phase plot of Cartesian end-effector displacements $\Delta\boldsymbol{r}$ vs. velocities $\dot{\boldsymbol{r}}$ is shown in Fig. 6.8c for the steady state phase of the oscillation. Herein, the impact can be observed, which is manifested by an abrupt change of the velocity in the (positive) y-direction. Fig. 6.8c further reveals that even in the presence of periodically occurring contacts, the controller stabilizes periodic motions within a small error band. From this experiment with the robotic arm, it can be conclude that the control approach might be also applicable for systems with compliantly actuated legs. Hereby, hopping, jumping, walking and running constitute periodic motions of oscillatory systems that are dominated by contact sequences.

6.5.2. Simulations of a compliantly actuated quadruped model

In the following, computer simulations of a compliantly actuated quadruped model are presented. They have the purpose to validate the applicability of modal control concepts

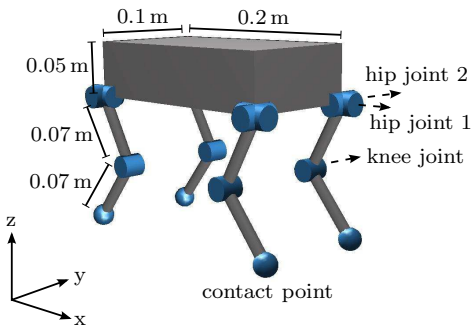

trunk mass	5.000 kg
trunk inertia x	0.0052 kgm^2
trunk inertia y	0.0177 kgm^2
trunk inertia z	0.0208 kgm^2
trunk COM	center of leg pivots
thigh/shank mass	0.100 kg
thigh/shank inertia	0.00004 kg
thigh/shank COM	center of segment

Figure 6.9.: Rigid body model of a compliantly actuated quadruped.

	hip 1	hip 2	knee
stiffness	8.0 Nm/rad	4.0 Nm/rad	4.0 Nm/rad
damping	0.16 Nms/rad	0.04 Nms/rad	0.04 Nms/rad

Table 6.1.: Visco-elastic parameters of the quadruped model shown in Fig. 6.9 considered for modal-shaping-based jumping.

to legged locomotion, but also aim at supporting the mechanical design of such robotic systems at an early stage of development. The considered quadruped model as shown in Fig 6.9 consists of four legs and a total number of $n = 12$ hinge joints (two perpendicular hinge joints in each hip and one in each knee). Each joint is actuated via a linear spring of the form $\tau_i = k_i\,(\theta_i - q_i)$, and linear, viscous friction of the form $d_i(\dot{q}_i) = d_i^0 \dot{q}_i$ acts link side. Ground contact points are considered at the tips of each leg. Thereby, a Coulomb friction constant of $\mu = 0.75$ is assumed for all contact points. The trunk is modeled as a free floating rigid body with the shape of cuboid, where the legs are attached to the lower rectangle. The forward dynamics is computed based on the articulated body algorithm [Fea08] and a point version of the compliant contact model [AF10]. The resulting ordinary differential equations are integrated in Matlab/Simulink® using a variable step solver.

Modal shaping based directed jumping control

The methodology of modal shaping can be utilized to implement directed jumping on multi-legged robotic systems. This is validated in simulations, where the control (6.47)–(6.50) is applied to the compliantly actuated quadruped model with parameters as listed in Table 6.1. Thereby, the position of the total center of mass (COM) w. r. t. the trunk is considered as task coordinates $\boldsymbol{x} = (x_\mathrm{x}, x_\mathrm{y}, x_\mathrm{z})$. To implement directed jumping motions, linear constraints of the form $\phi_1(\boldsymbol{x}) = c_1 x_\mathrm{x} + c_2 x_\mathrm{z} = 0$ and $\phi_2(\boldsymbol{x}) = c_3 x_\mathrm{y} + c_4 x_\mathrm{z} = 0$ can be considered. The corresponding 1-D submanifold represents a straight line passing through the origin. Herein, $\psi_1 = \mathrm{atan2}(c_1, c_2)$ and $\psi_2 = \mathrm{atan2}(c_3, c_4)$ represent the angles between the x-axis respectively y-axis and the line. The proportional and derivative gains of the constraint controller (6.48) are set to $\boldsymbol{K}_\phi = \mathrm{diag}(2,2)\,10^5\mathrm{N/m}$ and $\boldsymbol{D}_\phi = \mathrm{diag}(1,1)\,10^4\mathrm{Ns/m}$, respectively.[12] The parameters of switching control (6.50) are $\epsilon_{\tau_\mathrm{z}} =$

[12]Note that the high magnitude of the gains results due to the scaling of the COM coordinates. Loosely speaking, displacing the low-weight legs displaces the center of mass only marginally.

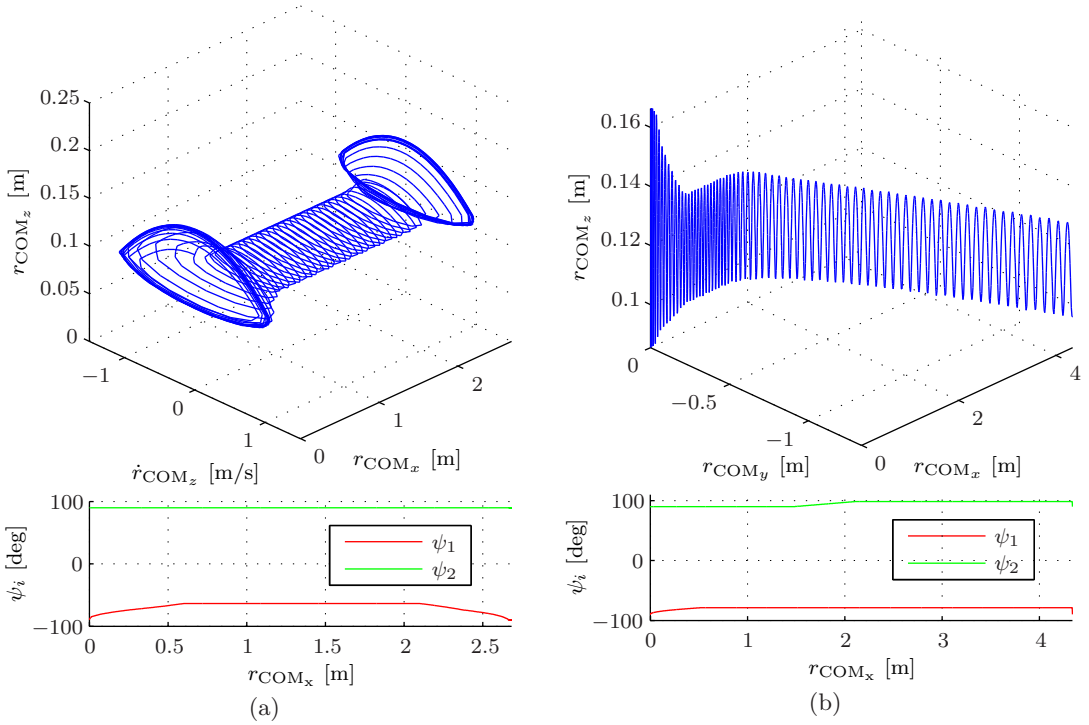

Figure 6.10.: Modal shaping based, directed quadrupedal jumping: absolute total COM motion (top); angles of linear constraints (bottom).

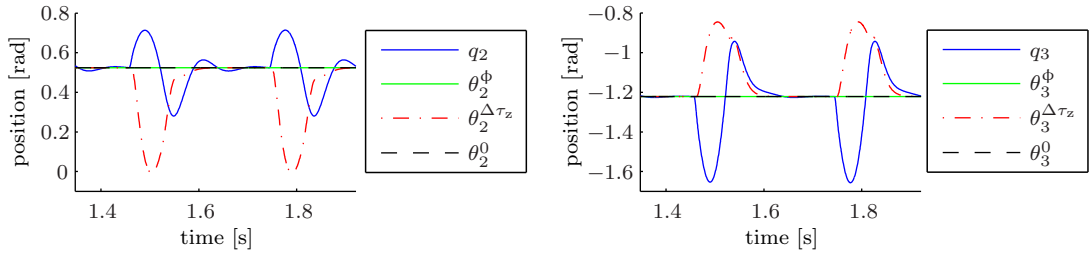

Figure 6.11.: Contributions of contraints and switching control to the actuator motion for vertical jumping: $\boldsymbol{\theta}^0 = \boldsymbol{K}^{-1}(\boldsymbol{J}_{\mathrm{x}}^T \boldsymbol{J}_{\mathrm{n}_\phi}^T \tau_{\mathrm{z}} - \boldsymbol{J}_{\mathrm{n}_{\mathrm{x}}}^T \boldsymbol{Z}_{\mathrm{x}} \frac{\partial U_{\mathrm{e}}(\boldsymbol{\theta}_0, \boldsymbol{q})}{\partial \boldsymbol{q}}^T) + \boldsymbol{q}$ (static); $\boldsymbol{\theta}^{\phi} = \boldsymbol{\theta}^0 + \boldsymbol{K}^{-1} \boldsymbol{J}_{\mathrm{x}}^T \boldsymbol{J}_{\phi}^T \boldsymbol{\tau}_{\phi}^{\mathrm{des}}$ (constraints); $\boldsymbol{\theta}^{\Delta\tau_{\mathrm{z}}} = \boldsymbol{\theta}^{\phi} + \boldsymbol{K}^{-1} \boldsymbol{J}_{\mathrm{x}}^T \boldsymbol{J}_{\mathrm{n}_\phi}^T \Delta\tau_{\mathrm{z}}$ (switching).

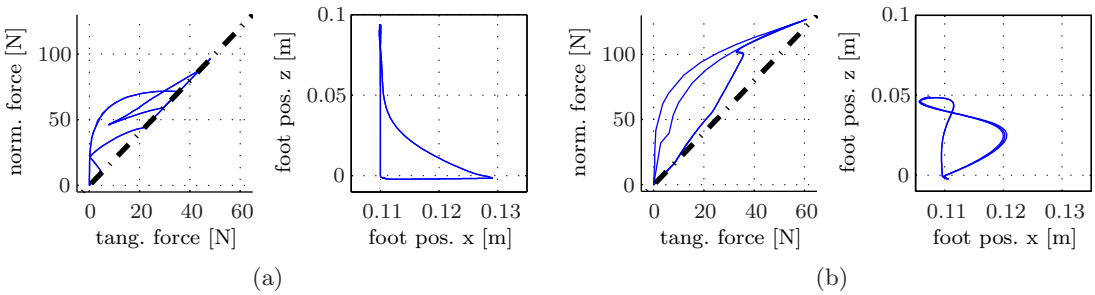

Figure 6.12.: Comparison of contact force and contact point motion for implementations of vertical jumping with (a) unconstrained contact forces (b) friction cone constraints.

	hip 1	hip 2	knee
stiffness	8.0 Nm/rad	4.0 Nm/rad	8.0 Nm/rad
damping	0.16 Nms/rad	0.04 Nms/rad	0.04 Nms/rad

Table 6.2.: Visco-elastic parameters of the quadruped model shown in Fig. 6.9 considered for modal-adaptation-based jumping.

500 N and $\hat{\tau}_z = 3500\,\text{N}$. Additionally, the output of the switching function (6.50) is filtered by means of a second order transfer function $\frac{\Delta\tau_z^{\text{out}}(r)}{\Delta\tau_z^{\text{in}}(r)} = \frac{1}{T_v^2 r^2 + 2T_v r + 1}$, where r denotes the Laplace variable, and the time constant is set to $T_v = 0.01\,\text{s}$.

The following simulations validate that modal shaping based jumping control can be implemented solely by the nullspace projections (6.51). The direction of the linearly constrained submanifold is varied in order to control the spatial direction of the jumping motion. Fig. 6.10a depicts a 3-D phase plot of the floating base motion and the direction of the line defined by the constraints. The phase plot shows the relation between the vertical velocity and position along the horizontal position of the total COM. The trunk motion of the quadruped approaches initially a periodic motion in the vertical direction, then evolves to a forward hopping motion and finally approaches the initial vertical motion again. Fig. 6.10b depicts the total COM position for 3-D jumping. The quadruped starts with a vertical jumping motion and then evolves to a forward and sideward movement. This demonstrates the capability of the proposed method to control the direction of the jumping motion. Additionally, Fig. 6.11 shows the contributions of the constraints and switching control to the realization of vertical jumping. It can be observed that the motion of the motors is dominated by the filtered output of the switching control (6.50). The contribution of the constraints controller to the control input is negligible. In that case, the submanifold line is vertical and the constraint is trivially satisfied. Therefore, this validates the basic design goal of modal shaping to change the intrinsic dynamics behavior of the plant to a minimal extent by control. Finally, the influence of implementing modal shaping control via contact force distribution (6.56) is evaluated for a vertical jumping motion. Thereby, a lower Coulomb friction constant of $\mu = 0.5$ is assumed. To reach the limit of friction cone constraints, also the parameters of the switching control (6.50) are increased to $\epsilon_{\tau_z} = 2000\,\text{N}$ and $\hat{\tau}_z = 5500\,\text{N}$. In Fig. 6.12, the normal vs. tangential contact force and the vertical vs. horizontal movement of the tip of one leg is compared to the implementation without contact force constraints. It can be seen that without the contact force distribution, the contact force reaches the limit of the friction cone and a horizontal movement of the tip of the leg occurs (sliding contact). This is avoided with the controller implementation via the contact force optimization (6.56).

Modal adaptation based vertical jumping

The performance of eigenvector adaptation based vertical jumping control is validated for the compliantly actuated quadruped model shown in Fig. 6.9 with visco-elastic parameters provided in Table 6.2. Thereby, the controller implementation (6.80), (6.84), and (6.85) is considered. The parameters of the switching controller are chosen $\epsilon_{\phi_s} = 0.2\,\text{rad}$ and $\hat{\hat{s}} = 1.0\,\text{rad}$. The initial weights of the adaptation controller are selected based on the

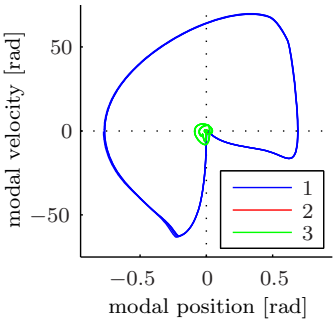

(a) Initial modal orbit.

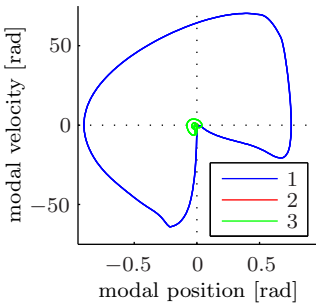

(b) Changed modal orbit.

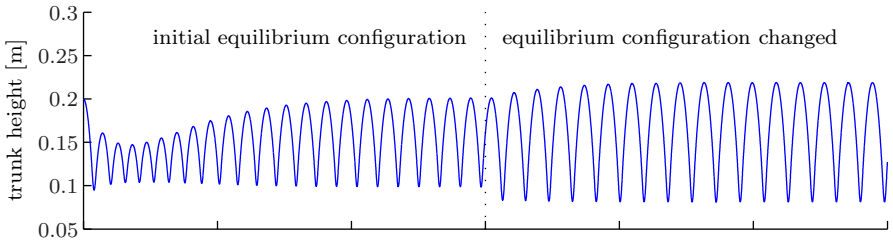

(c) Motion of trunk height.

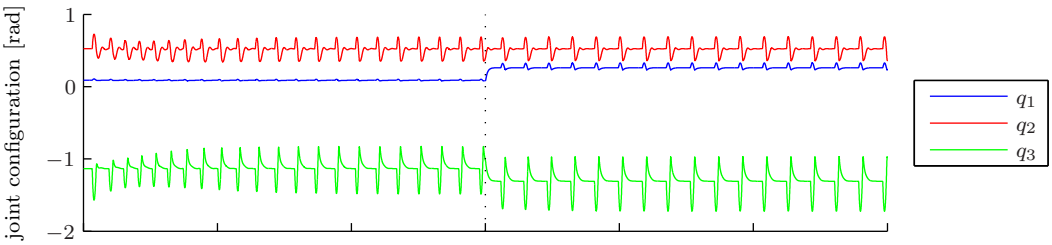

(d) Joint motion left foreleg.

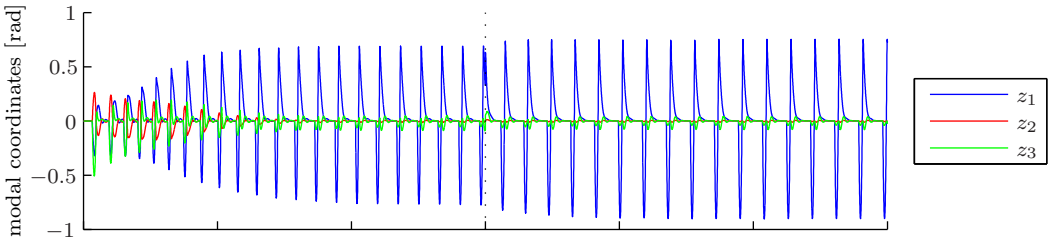

(e) Three leading modal coordinates.

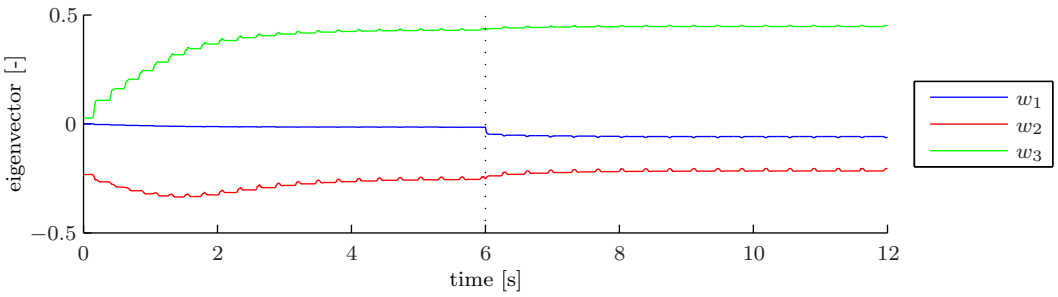

(f) First three components of the leading principal vector.

Figure 6.13.: Modally adaptive jumping control of a compliantly actuated quadruped.

	hip 1	hip 2	knee
	initial equilibrium configuration		
foreleg left (FL)	5 deg	30 deg	−65 deg
foreleg right (FR)	−5 deg	30 deg	−65 deg
hindleg left (HL)	5 deg	−30 deg	65 deg
hindleg right (HR)	−5 deg	−30 deg	65 deg
	changed equilibrium configuration		
foreleg left (FL)	15 deg	30 deg	−75 deg
foreleg right (FR)	−15 deg	30 deg	−75 deg
hindleg left (HL)	15 deg	−30 deg	75 deg
hindleg right (HR)	−15 deg	−30 deg	75 deg

Table 6.3.: Equilibrium configurations of the quadruped model shown in Fig. 6.9.

differential kinematic relations in the initial configuration provided in Table 6.3, i. e.,

$$\boldsymbol{w}_j(0) = \frac{\partial \boldsymbol{r}_j}{\partial \boldsymbol{q}_j}(\bar{\boldsymbol{q}}_j^0)^{-1} \begin{pmatrix} 0 \\ 0 \\ 1 \end{pmatrix} \left\| \frac{\partial \boldsymbol{r}_j}{\partial \boldsymbol{q}_j}(\bar{\boldsymbol{q}}_j^0)^{-1} \begin{pmatrix} 0 \\ 0 \\ 1 \end{pmatrix} \right\|^{-1},$$

where $\boldsymbol{r}_j \in \mathbb{R}^3$ denotes the position of the foot w. r. t. to pivot point of the j-th leg, for $j \in \{\mathrm{FL}, \mathrm{FR}, \mathrm{HL}, \mathrm{HR}\}$. Note that also here the approximation $\bar{\boldsymbol{q}}(\boldsymbol{\theta}) \approx \boldsymbol{\theta}$ is made.

A vertical jumping motion is simulated. To demonstrate the adaptation properties of the controller, the central equilibrium configuration is changed during the simulation experiment. This switching of controller parameters to values also given in Table 6.3 is performed at $t \approx 6\,\mathrm{s}$ (when all legs are lifted). The modal invariance properties are analyzed by considering a linear mapping $\boldsymbol{z} : \mathbb{R}^n \to \mathbb{R}^n$ based on the actually estimated vector $\boldsymbol{w}(t)$, i. e., $\boldsymbol{z} = \boldsymbol{W}^{-1}\left(\boldsymbol{q} - \bar{\boldsymbol{q}}^0\right)$, where the $n \times n$ matrix $\boldsymbol{W} = \left[\boldsymbol{w}(t) \quad \ker\left(\boldsymbol{w}(t)^T\right)\right]$ spans an orthogonal basis. Fig. 6.13a and 6.13b depict phase plots of modal motion corresponding to the first three modes. Thereby, Fig. 6.13a and 6.13b show the last four oscillation cycles before the change of controller parameters at $t = 6\,\mathrm{s}$ and at the end of simulation $t = 12\,\mathrm{s}$, respectively. It can be seen that for the initial as well as for the changed parameter setting, the motion of the system converges to a periodic orbit mainly in the first mode. The contributions in the second and third mode are negligible compared to the first mode motion (cf. also Fig. 6.13e). The evolution of the first three components of the eigenvector $\boldsymbol{w}(t)$ are depicted in Fig. 6.13f. The time-plots of the vertical trunk and joint motions (where the latter correspond to the left foreleg) are shown in Fig. 6.13c and Fig. 6.13d, respectively. It can be observed that the amplitude of the vertical trunk oscillation increases as the central equilibrium configuration is changed. This can be explained by the increased leg abduction (cf. motion of q_1 in Fig. 6.13d), which leads to an increased stiffness in the direction of the first mode such that the energy injected by switching control (6.85) is also increased. Note that except for the initial guess of the eigenvector $\boldsymbol{w}(0)$ (which is based only on a geometric model of the legs), the controller requires no model-parameter knowledge to adapt to periodic jumping motions. This, clearly demonstrates the advantageous adaptation properties of modally adaptive periodic motion control applied to compliantly actuated, multi-legged jumping systems.

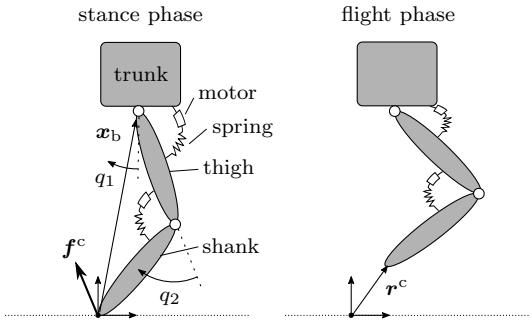

trunk mass	0.600 kg
thigh/shank length	0.080 m
thigh/shank mass	0.050 kg
thigh/shank inertia	0.00003 kg
thigh/shank COM	center of segment
hip stiffness	1.0 Nm/rad
knee stiffness	2.0 Nm/rad
hip damping	0.015 Nms/rad
knee damping	0.03 Nms/rad

Figure 6.14.: Model of compliantly actuated single leg system.

6.5.3. Modal matching based jumping control

The methodology of modal matching as proposed in Sect. 6.4 is predestined to control highly dynamical locomotion (such as jumping or running) in compliantly actuated legged systems. This is exemplary validated by a realization of forward jumping control in single leg. As shown in Fig. 6.14, the considered system consists of a base body which is free to translate in the sagittal plane and a two-segment leg with compliant actuation in the hip and knee joint. In more detail, the free floating dynamics has the structure of (6.86) with base and joint coordinates $\boldsymbol{x}_\mathrm{b} \in \mathbb{R}^2$ and $\boldsymbol{q} \in \mathbb{R}^2$, respectively. The elastic potential is assumed to be quadratic, i. e., $U_\mathrm{e}(\boldsymbol{q} - \boldsymbol{\theta}) = 1/2 \sum_{i=1}^{2} k_i (q_i - \theta_i)^2$, where $k_1 > 0$ and $k_2 > 0$ denote constant stiffness parameters, and $\boldsymbol{\theta} \in \mathbb{R}^2$ represents the control input. Additionally, linear, viscous friction of the form $d_i(\dot{q}_i) = d_i^0 \dot{q}_i$ for $i = 1, 2$ acts link side. Following the concept of virtual legs as proposed by *Raibert* in [Rai86], the presented single leg example can be straightforwardly extended to multi-legged systems by linking all legs which are simultaneously in stance.

Finite state machine

The jumping controller comprises a collection of feedback control actions, which are embedded in a finite state machine (FSM). Thereby, the transition between discrete states are triggered based on continuous state dependent events. As depicted in Fig. 6.15, the state machine has the following states:

- flight phase,
- stance phase,
- and push-off phase,

which also represent the phases of the controlled jumping motion. These phases are triggered by events which occur when the continuous system state hit the boundary of corresponding switching manifolds:

- The flight phase is triggerd by the takeoff event TO which occur when the normal component f_n^c of the contact force defined in Fig. 6.14 hits zero from above.
- The touchdown event TD triggers the stance phase when the foot hits the ground, i. e., when the distance between the contact point and the ground r_n^c (see, Fig. 6.14) hits zero from above.

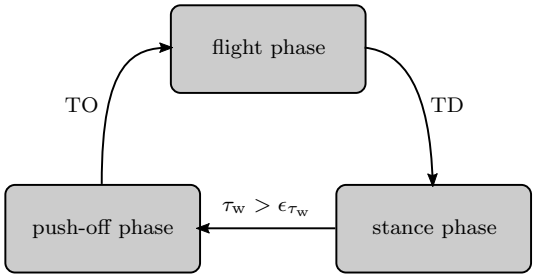

Figure 6.15.: Jumping control finite state machine.

- The elastic force $\tau_w \in \mathbb{R}$ defined in (6.111) initiates the push-off phase, when the threshold ϵ_{τ_w} is crossed from below.

Note that the above events incorporate continuous state feedback in the control. In the following, the control actions of the flight, stance, and push-off phase are derived. They lead to a continuing jumping cycle, as will be shown by a simulation presented after the controller derivation.

Foot placement during flight phase

In the first instance, the aim of the flight phase control is to reconfigure the leg such that after the touchdown, the trunk moves along the *desired* local eigenvector. The direction of the translational velocity of the base, i. e., $\alpha_{v,TD} = \text{angle}(\dot{\boldsymbol{x}}_b(TD))$ is assumed to be known a priori. Note that $\alpha_{v,TD}$ can be predicted based on the takeoff velocity angle $\alpha_{v,TO}$ by assuming a frictionless ballistic flight phase. In particular, $\alpha_{v,TO}$ can be predicted based on the joint velocity $\dot{\boldsymbol{q}}$ just before the takeoff by solving the time derivative of the contact constraints (6.88). Then given $\alpha_{v,TD}$, the touchdown configuration (foot placement) can be obtained based on the modal matching algorithm (6.110), where the desired local eigenvector is selected as $\boldsymbol{w}_{des} = \boldsymbol{w}_{des}(\alpha_{v,TD})$. In case of the two-segment leg example considered here, the degrees of freedom of the rigid-body system during the contact phase are $n = 2$. Therefore, the one-to-one correspondence $\boldsymbol{x}_b(\boldsymbol{q}) : \mathbb{R}^2 \to \mathbb{R}^2$ can be presumed. As a consequence, the direction coordinate of the eigenvector $y \in \mathbb{R}$ is scalar, and the augmented Jacobian of (6.110) simplifies to

$$\boldsymbol{J}_{aug}(\boldsymbol{q}) = \begin{bmatrix} \frac{\partial y(\boldsymbol{w})}{\partial \boldsymbol{w}} \frac{\partial \boldsymbol{w}(\boldsymbol{q})}{\partial \boldsymbol{q}} \\ \boldsymbol{Z}(\boldsymbol{q}) \end{bmatrix} \tag{6.143}$$

where the 1×2 matrix $\boldsymbol{Z}(\boldsymbol{q}) \neq \boldsymbol{0}$ satisfies $\frac{\partial y(\boldsymbol{w})}{\partial \boldsymbol{w}} \frac{\partial \boldsymbol{w}(\boldsymbol{q})}{\partial \boldsymbol{q}} \boldsymbol{Z}(\boldsymbol{q})^T = \boldsymbol{0}$. In particular, due to the low dimensionality of the eigenvector matching problem, the reduced recursion

$$\bar{\boldsymbol{q}}(j+1) = \bar{\boldsymbol{q}}(j) + \gamma \boldsymbol{J}_{aug}(\bar{\boldsymbol{q}}(j))^{-1} \begin{bmatrix} \frac{\partial y}{\partial \boldsymbol{w}} \left(\boldsymbol{w}_{des} - \boldsymbol{w}(\bar{\boldsymbol{q}}(j)) \right) \\ \boldsymbol{Z}(\boldsymbol{q}(j)) \left(\bar{\boldsymbol{q}}_{des} - \bar{\boldsymbol{q}}(j) \right) \end{bmatrix}$$

can be considered. Fig. 6.16a depicts an example simulation result of the mode matching procedure. In the shown case, the motion of the hip is largely along the desired eigenvector. Note that due to the mode matching procedure, the segmented leg behaves like a spring loaded telescopic leg as considered in the pogo-stick model of *Raibert* [Rai86] or the spring loaded inverted pendulum model [Bli89].

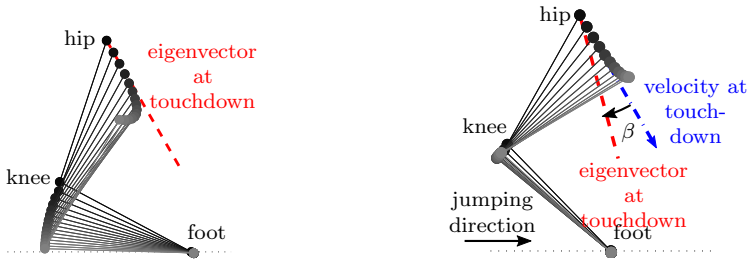

Figure 6.16.: Eigenvector matching based control actions: (a) touchdown velocity in eigenvector direction; (b) eigenvector direction deviates from touchdown velocity by modal angle of attack β.

For directed (forward) jumping motions, velocity angles at touchdown and takeoff can be assumed to display equal magnitude but opposite signs. Therefore, the instantaneous eigenvector needs to be tilted from the touchdown to the takeoff direction. This tilting can be naturally achieved by means of the eigenvector matching based reconfiguration. Therefore, the relative angle $\beta = y(\boldsymbol{q}_\mathrm{j}(\mathrm{TD})) - \alpha_{\mathrm{v,TD}}$ is introduced, which is referred to as angle of attack (see, Fig. 6.16b). The angle of attack β represents a control input which indirectly influences the tilting momentum. It can be utilized to control the horizontal jumping velocity. Since, the touchdown respectively takeoff angle, i. e., $\alpha_{\mathrm{v,TD}} = -\alpha_{\mathrm{v,TO}}$, is representatively for the locomotion velocity, it can be considered as control variable. In order to regulate $\alpha_{\mathrm{v,TO}}$, the repetitive control law

$$\beta(o+1) = \beta(o) - k_\alpha \left(\alpha_{\mathrm{v,TO}} - \alpha_{\mathrm{v,TO}}^{\mathrm{des}}\right)$$

is proposed. Herein, $k_\alpha > 0$ denotes an update gain, $\alpha_{\mathrm{v,TO}}^{\mathrm{des}}$ is the desired velocity angle at takeoff, and o represents the iteration variable of the o-th jumping cycle. Note that this concept generalizes also the foot placement algorithm of *Raibert* [Rai86] as introduced for a telescopic leg to the case of a two-segment leg.

Stance phase control

The stance phase is in charge of weight bearing and stabilizing the tilting of the instantaneous eigenvector. Both tasks can be realized by shaping the elastic potential according to the control law (6.118)–(6.120). By considering the equilibrium configuration $\boldsymbol{q}_0 = \bar{\boldsymbol{q}}(\mathrm{TD})$ resulting from the eigenvector matching procedure described above, the plant inherent elastic force

$$\tau_\mathrm{w}(\boldsymbol{\theta}_0 - \boldsymbol{q}) = -\boldsymbol{Z}(\boldsymbol{q}) \frac{\partial U_\mathrm{e}(\boldsymbol{q} - \boldsymbol{\theta}_0)}{\partial \boldsymbol{q}}^T \tag{6.144}$$

implements the task of weight bearing. Herein, the influence of gravity on the equilibrium configuration is neglected, i. e., $\boldsymbol{\theta}_0 \approx \boldsymbol{q}_0$. To achieve a stable transition from the direction of the eigenvector at touchdown to the direction at push-off, symmetry w. r. t. the vertical line is assumed, i. e., $y_\mathrm{des} = 0$. Considering further a quadratic potential $U_\mathrm{y}(y) = 1/2 k_\mathrm{y} y^2$

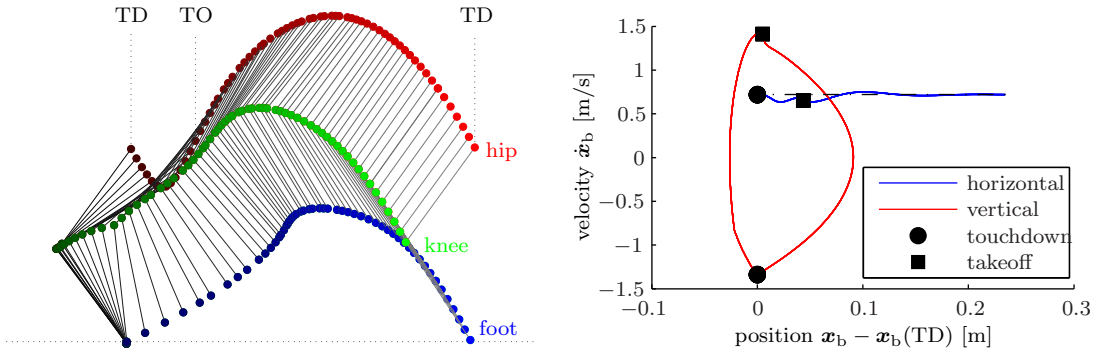

(a) (b)

Figure 6.17.: Motion of modal matching based jumping: (a) complete jumping cycle between two consecutive touchdown events; (b) phase plot of trunk motion (9 jumping cycles, positional state reset to zero at touchdown).

with constant stiffness $k_y > 0$, the entire control of the stance phase takes the form

$$\boldsymbol{\tau}^{\text{des}} = \boldsymbol{J}_{\text{aug}}(\boldsymbol{q})^T \begin{pmatrix} -k_y y \\ -\boldsymbol{Z}(\boldsymbol{q}) \frac{\partial U_e(\boldsymbol{q}-\boldsymbol{\theta}_0)}{\partial \boldsymbol{q}}^T \end{pmatrix}, \tag{6.145}$$

where $\boldsymbol{J}_{\text{aug}}$ and $\boldsymbol{Z}$ are defined in (6.143). This controller is implemented by selecting the input as

$$\boldsymbol{\theta} = \boldsymbol{\theta}_{\text{des}} = \boldsymbol{f}_e^{-1}(\boldsymbol{\tau}_{\text{des}}) + \boldsymbol{q}\,, \tag{6.146}$$

where $\boldsymbol{f}_e(\boldsymbol{\theta} - \boldsymbol{q}) := -(\partial U_e(\boldsymbol{q} - \boldsymbol{\theta})/\partial \boldsymbol{q})^T$.

Push-off initiation

The push-off phase is triggered when the elastic force $\tau_w(\boldsymbol{\theta}_0 - \boldsymbol{q})$ defined by (6.144) crosses the threshold $\epsilon_{\tau_w} > 0$ from below. This follows the concept of switching based limit cycle generation as proposed in Sect. 4.4. The control action of the push-off phase is a pure switching of the actuator position in the direction of the instantaneous eigenvector $\boldsymbol{w}(\boldsymbol{q}(\text{PO}))$, i. e.,

$$\boldsymbol{\theta} = \boldsymbol{\theta}_{\text{des}}(\text{PO}) + \frac{\left(\frac{\partial \boldsymbol{x}_b(\boldsymbol{q})}{\partial \boldsymbol{q}}\right)^{-1} \boldsymbol{w}(\boldsymbol{q}(\text{PO}))}{\left\| \left(\frac{\partial \boldsymbol{x}_b(\boldsymbol{q})}{\partial \boldsymbol{q}}\right)^{-1} \boldsymbol{w}(\boldsymbol{q}(\text{PO})) \right\|} \hat{\theta}_w\,. \tag{6.147}$$

Herein, $\hat{\theta}_w > 0$ is a constant switching amplitude, and $\boldsymbol{\theta}_{\text{des}}(\text{PO})$ represents the output of the stance phase controller (6.145) and (6.146) at time instance PO where the push-off phase is triggered. This control action is responsible for the energy input required to sustain the periodic jumping motion.

Simulation results

The concept of modal matching based jumping control is validated in simulation. Therefore, the forward dynamics of the closed-loop system, comprising the above described,

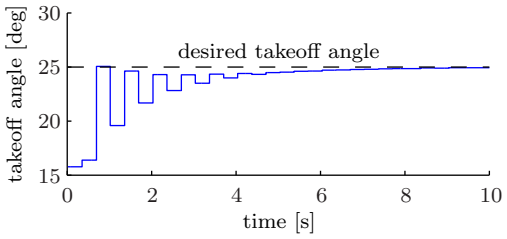

Figure 6.18.: Convergence behavior of the takeoff angle w. r. t. its desired value of 25 deg.

hybrid controller and the compliantly actuated, single leg system of Fig. 6.14, is integrated using a variable step solver of MATLAB/Simulink®.[13]

Fig. 6.17a shows a complete jumping cycle between two consecutive touchdown events in the steady-state phase of motion. Interestingly, during the stance phase, the hip moves approximately along a path with the shape of a parabola. The slope at takeoff and touchdown fits to the slope of the parabola corresponding to the ballistic flight phase. This gives rise to the conjecture that modal matching based jumping control implements a 1-D, hybrid manifold. In particular, this is achieved by merely shaping the elastic potential of the plant w. r. t. to the directional coordinates of the local eigenvector. Fig. 6.17b shows a phase plot of trunk motion, where the positional state is reset to zero at each touchdown, i. e., $\boldsymbol{x}_\mathrm{b} - \boldsymbol{x}_\mathrm{b}(\mathrm{TD})$ vs. $\dot{\boldsymbol{x}}_\mathrm{b}$. Nine complete jumping cycles are plotted. It can be observed that the horizontal velocity is almost constant. The average locomotion velocity is 0.68 m/s with a maximum deviation of 0.07m/s. This is already an indicator for efficient locomotion. Fig. 6.18 depicts the convergence behavior of the takeoff angle, which is a control variable of the repetitive low gain control. It can be observed that the controller is able to regulate the system to the desired value of 25 deg.

6.6. Summary

This chapter contributes several methodologies to exploit the natural oscillatory dynamics of compliantly actuated systems in the control. Since energy efficiency and task versatility are generally opposing aims, four different control approaches are proposed, which achieve either the former or latter goal to a larger extent.

The method of modal globalization control, as presented in Sect. 6.1 relies not on the existence of global oscillation modes. Therefore, this concept realizes decoupled, scalar oscillatory dynamics of any statically controllable compliantly actuated system. Since the plant inherent inertia and local stiffness matrix are maintained, energy efficiency in the generation of limit cycles can be gained. Additionally, a constructive controller design is provided which allows to prove exponential decay of oscillations in undesired modes.

The method, as introduced in Sect. 6.2, provides a tool to design a 1-D, attractive submanifold corresponding to a desired task. The task manifold may consist of any shape as long as the embedded curve is diffeomorphic to a circle or a line. The method is advantageous from view point of versatility in the realization of tasks. To implement the virtual constraints corresponding to the tasks in a real-hardware system, an appropriate torque interface at joint level needs to be provided. Although, this comes in general at the

[13] The forward dynamics of the rigid-body system is computed based on the articulated body algorithm [Fea08] and a point version of the compliant contact model [AF10].

price of efficiency, it has been shown by simulation that the approach contains the case of stabilizing an inherent oscillation mode of the plant.

One of the core contributions of this thesis is the concept of modally adaptive periodic motion control, as proposed in Sect. 6.3. It provides a method to successively excite periodic motions in an oscillation mode and simultaneously adapt to the corresponding embedding. This is achieved with at most the parameter-knowledge of a model of the plant inherent potential force. In particular, the adaption and excitation control requires only measurements of states at position level, i. e., differentiation of measured signals is avoided. Therefore, the method is very robust against model uncertainties and noise. This is validated in experiments on a variable stiffness robotic arm. In case of adaptive periodic motion control in an eigenmode of the nonlinear dynamical system, as defined in Sect. 5.1.2, ideas of a convergence proof are provided. A rigorous stability analysis may require to combine the hybrid system techniques considered in Chapt. 4 with the statistical methods utilized in [Oja82] to prove Theorem 6.3. As such, the complete proof opens a separate research topic for itself. A further scientifically interesting outcome of the method is the hypothesis that the modally adaptive periodic motion control is implemented in the neural circuits of biological systems, of which a first conceptual validation is provided in [SLAS16].

The method of modal matching, as introduced in Sect. 6.4 exploits the nonlinear dependency of the dynamics of compliantly actuated systems on the configuration to match the direction of local eigenvectors to a given task. Based on modal matching, an effective method proposed to control highly dynamic locomotion in compliantly actuated legs. This is validated by a simulation, where an almost constant forward movement (velocity) is achieved. The modal matching algorithm, which has been found in the course of the controller design, can also be utilized to find the equilibrium configurations corresponding to an oscillation mode.

The modal control concepts proposed in this chapter, provide a toolbox for natural dynamics based explosive and periodic motion control. The outcome of this chapter will be applied within the advanced control of compliantly actuated legged system treated in Chapt. 7.

CHAPTER 7

Application to Legged Locomotion

The tasks of legged locomotion such as walking, jumping, or running are intrinsically cyclic or even periodic (in the steady-state phase). Therefore, the concept of oscillation modes presented in Chapt. 5 and the corresponding methods of modal control, as introduced in Chapt. 6, are predestined to approach high performance and energetic efficiency in the execution of such tasks.

The benefits of springs in legged locomotion have been validated in the conceptual work of *Alexander* [Ale90]. The hypothesis that the high-dimensional, nonlinear dynamics of complex legged animals collapses to template models of strongly reduced order, like the spring loaded inverted pendulum (SLIP) model [Bli89] and extensions [SGGB02], [GSB06], [MRS08], [MLG$^+$10], [RBM$^+$10], is further supported by experimental results [FK99]. In particular, the authors of the review article [HFKG06] hypothesize that embodying these template models as invariant (and attracting) submanifolds (cf. oscillation modes, Chapt. 5) into the high order multibody dynamics of articulated legged systems is a key aspect of energy efficient and performant locomotion.

In this chapter, compliantly actuated legged robots are presented, which have such template models of locomotion embodied. The compliantly actuated quadruped *Bert*, which will be introduced in Sect. 7.1, features oscillation modes in which the dynamics behave like the fundamental SLIP model.[1] It is shown that these oscillation modes can be exploited to implement the gaits of pronking and trotting by computationally simple and robust modal control. Sect. 7.2 presents the compliantly actuated biped *C-Runner*. Under a certain selection of elasticities, the system features a quasi-static oscillation mode in which the scalar dynamics represents a complete dynamic walking stride. Furthermore, a bi-articular stiffness setting is proposed, which features an input and output decoupled elastic behavior in locomotion task-oriented coordinates. This can be exploited in bipedal running control.

[1] The SLIP has two kinematic degrees of freedoms. Therefore, the union of two 1-D invariant subsets is meant by the oscillation modes in which the configuration variables of the SLIP model evolve.

7.1. Quadrupedal locomotion

The fastest mammals on earth are quadrupeds.[2] As discussed in the introduction of this chapter, it is very likely that such a high performance is the result of a very optimized, system inherent locomotion dynamics. In the last decades, numerous quadrupedal robots have been developed, which are based upon hydraulic/pneumatic actuators [Rai85], [RBN+08], [STG+11], [SBB+15], electrically powered direct drives [SWC+13], [SWC+15] and compliantly actuated systems [STV+13], [HGB+12], [HGJ+16].[3] The quadruped reported in [Rai85] is composed of hydraulically/pneumatically powered telescopic legs, which closely resemble the dynamics of a spring-mass system. On the basis of such a system, in [Rai86], [Rai90], fundamental control principles of legged locomotion have been found and demonstrated to perform effectively in experiments. These findings are further augmented and successfully validated on systems, which exploit also the advantageous properties of segmented legs such as versatility regarding locomotion in uneven terrain [RBN+08], [GCH+13], [HGH+14], [GCH+14]. All the mentioned quadrupedal robots have demonstrated remarkable dynamic walking and running performance. Thereby, a common approach is to implement a certain interaction or virtual model behavior by joint torque control, while exploiting physical elasticities mainly to absorb high frequency external forces, which occur due to ground impacts of the feet. An exception is MIT's cheetah [SWC+13] with its electrical direct drives of low inertia and friction. As a result of electric energy storage capabilities and a very optimized power train, MIT's cheetah achieves already high energetic efficiency. However, the efficiency of storing energy in mechanical springs is potentially higher than electrical energy recuperation, therefore in this thesis, concepts are proposed to implement the dynamics of (quadrupedal) locomotion gaits in the mechanical design.

7.1.1. Bert: a compliantly actuated quadruped with modal legs

The purpose of building the compliantly actuated quadruped Bert is achieving a robotic system which has the fundamental dynamics of legged locomotion embodied in the mechanical design. The main difference of Bert compared to other quadrupedal robot designs reported so far (as outlined above) is the embodiment of SLIP dynamics in its articulated legs. The parameters yielding such a dynamical behavior can be found by applying the eigenmode embodiment procedure presented in Sect. 5.2. In order to meet the additional versatility requirements, i. e., preserving the capability of climbing over an obstacle or crawling through a rock crevice, a segmented leg design is considered.

Modal leg design

For the first proof of concept, the mechanically simplest mechanism of a two-segment leg is selected as structural model. In more detail, the model of a two-segment leg during stance is considered, as shown in Fig. 7.1a. The leg is assumed to be attached to the main body (trunk) with very high inertial properties such that its rotation can be neglected, i. e., the trunk has only the two translational degrees of freedom of the plane.[4] The thigh

[2] The cheetah can reach a peak velocity of 120 km/h and the antelope approaches a maximum speed of 88 km/h over a distance of 800 m.

[3] This is only a representative selection of quadrupedal robots.

[4] Note that this assumption holds especially for quadrupeds, where the fore- and hindlegs are configured symmetrically and the center of mass (COM) of the trunk is located at the center of pivot points of the legs.

is connected to the trunk by a rotational joint with coordinate q_1. The shank is hinged to the thigh with relative coordinate q_3. There is a pulley concentric with the hip joint with relative coordinate q_2 which couples to the knee joint such that $q_3 = q_2 - q_1$. A point-foot is considered which is constrained during stance phases to touch the ground such that the configuration of the system is determined by the minimum set of configuration coordinates $\boldsymbol{q} = (q_1, q_2) \in \mathbb{R}^2$. Assuming that each leg segment has equal length $a > 0$ and equal mass $m_\mathrm{l} > 0$ concentrated at the segment center, and assuming further that hip joint and pulley are actuated via linear springs with spring constants $k_1 > 0$ and $k_2 > 0$, the dynamics of the structural two-segment leg model can be expressed in the form

$$\boldsymbol{M}(\boldsymbol{q})\ddot{\boldsymbol{q}} + \boldsymbol{C}(\boldsymbol{q}, \dot{\boldsymbol{q}})\dot{\boldsymbol{q}} = -\frac{\partial U_\mathrm{g}(\boldsymbol{q})}{\partial \boldsymbol{q}}^T - \boldsymbol{K}\left(\boldsymbol{q} - \boldsymbol{\theta}\right) , \tag{7.1}$$

where the 2×2 inertia and stiffness matrices have the form

$$\boldsymbol{M}(\boldsymbol{q}) = a^2 \begin{bmatrix} m_\mathrm{t} + \frac{m_\mathrm{l}}{4} & \left(m_\mathrm{t} + \frac{m_\mathrm{l}}{2}\right)\cos\left(q_2 - q_1\right) \\ \text{sym.} & m_\mathrm{t} + \frac{5m_\mathrm{l}}{4} \end{bmatrix} \tag{7.2}$$

and

$$\boldsymbol{K} = \begin{bmatrix} k_1 & 0 \\ 0 & k_2 \end{bmatrix} , \tag{7.3}$$

respectively.

The goal is to match the dynamics, as described above, to the one of the SLIP model. Consider therefore the stance phase dynamics of the SLIP model expressed in polar coordinates,

$$\begin{aligned} m_\mathrm{C}\left\{\begin{bmatrix} x_2^2 & 0 \\ 0 & 1 \end{bmatrix}\begin{pmatrix} \ddot{x}_1 \\ \ddot{x}_2 \end{pmatrix} + x_2\begin{bmatrix} \dot{x}_2 & \dot{x}_1 \\ -\dot{x}_1 & 0 \end{bmatrix}\begin{pmatrix} \dot{x}_1 \\ \dot{x}_2 \end{pmatrix} + g_0\begin{pmatrix} -\sin(x_1)x_2 \\ \cos(x_1) \end{pmatrix}\right\} \\ = -\begin{pmatrix} 0 \\ \frac{\partial U_\mathrm{e}(x_2 - r_0)}{\partial x_2} \end{pmatrix} . \end{aligned} \tag{7.4}$$

As schematically sketched in Fig. 7.1b, $\boldsymbol{x} \in \mathbb{R} \times \mathbb{R}_{\geq 0}$ denotes the position of the mass m_C w. r. t. to the pivot point on the ground expressed in a polar coordinate system. Thereby, x_1 represents the polar angle and x_2 denotes the radius. Due to this choice of coordinates, the elastic potential $U_\mathrm{e}(x_2 - r_0)$ depends only on the displacement in the radial direction (w. r. t. to the rest length $r_0 > 0$). Note that the nonlinear SLIP dynamics features an eigenmode $\mathcal{W} := \{\boldsymbol{x} \in \mathbb{R} \times \mathbb{R}_{\geq 0} \,|\, x_1 = 0\}$ according to Definition 5.1.

To match the structural dynamics model of the two-segment leg (7.1)–(7.3) to the desired SLIP dynamics (7.4), (7.1)–(7.3) is transformed under the change of coordinates

$$\hat{\boldsymbol{x}} = \boldsymbol{f}(\boldsymbol{q}) = \begin{pmatrix} \frac{q_1 + q_2}{2} \\ a\sqrt{2\left(1 + \cos\left(q_2 - q_1\right)\right)} \end{pmatrix} . \tag{7.5}$$

Thereby, $\hat{\boldsymbol{x}} \in \mathbb{R} \times [0; 2a]$ denotes the position of the hip w. r. t. to the contact point in polar coordinates. Then, choosing as design parameters the mass of the legs m_l and the ratio of stiffness k_2/k_1, i. e., $\boldsymbol{\zeta}_1 = (m_\mathrm{l}, k_2/k_1)$, it is found that global matching of eigenvectors is achieved if $m_\mathrm{l} = 0$ and $k := k_1 = k_2$, i. e., $\hat{\boldsymbol{\zeta}}_1 = (0, 1)$. Substituting these design parameters

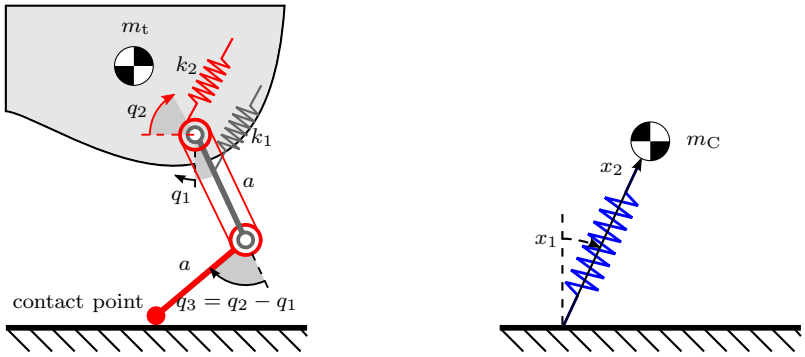

(a) (b)

Figure 7.1.: Matching the dynamics of a two-segment leg to the SLIP model: (a) two-segment leg; (b) SLIP.

in (7.1)–(7.3) and transforming the resulting dynamics under the change of coordinates (7.5), yields

$$\begin{aligned} m_\mathrm{t} \left\{ \begin{bmatrix} \hat{x}_2^2 & 0 \\ 0 & 1 \end{bmatrix} \begin{pmatrix} \ddot{\hat{x}}_1 \\ \ddot{\hat{x}}_2 \end{pmatrix} + \hat{x}_2 \begin{bmatrix} \dot{\hat{x}}_2 & \dot{\hat{x}}_1 \\ -\dot{\hat{x}}_1 & 0 \end{bmatrix} \begin{pmatrix} \dot{\hat{x}}_1 \\ \dot{\hat{x}}_2 \end{pmatrix} + g_0 \begin{pmatrix} -\sin(\hat{x}_1)\,\hat{x}_2 \\ \cos(\hat{x}_1) \end{pmatrix} \right\} \\ = -k \begin{pmatrix} 2\,[\hat{x}_1 - \theta_1^\mathrm{x}] \\ \frac{1}{\sqrt{4a^2 - \hat{x}_2^2}}\,[\rho(\hat{x}_2) - \rho(\theta_2^\mathrm{x})] \end{pmatrix}, \end{aligned} \tag{7.6}$$

where

$$\rho(y) := \mp \arccos\left(1 - \frac{y^2}{2a^2}\right) \tag{7.7}$$

represents an abbreviation related to the knee angle $q_3 = q_2 - q_1 = \mp\left[\arccos\left(1 - \frac{\hat{x}_2^2}{2a^2}\right) - \pi\right]$, of which the negative or positive sign selects the solutions $q_3 > 0$ or $q_3 < 0$, respectively, and $\boldsymbol{\theta}^\mathrm{x} = \boldsymbol{f}(\boldsymbol{\theta})$ denotes the transformed control input. Indeed, by equating $m_\mathrm{t} = m_C$ and $\hat{\boldsymbol{x}} = \boldsymbol{x}$, it can be seen that the inertial dynamics of the matched two-segment leg model (7.6) and the slip model (7.4) are equivalent. This is not very surprising, since the inertia of the leg segments is set to zero, i. e., $m_\mathrm{l} = 0$. Note that the example of Sect. 5.2.2 does not require to make this assumption, but the mechanism is significantly more complex. The assumption of zero leg mass, as made in (7.6), is consistent with the common wisdom of designing the leg segments as light-weight as possible, and results in a much less complex mechanical design (compared to the example of Sect. 5.2.2). In particular, the decoupled structure of the elasticity as in the SLIP model (7.4) is maintained for the segmented leg, cf. (7.6). For $\theta_1^\mathrm{x} = 0$, the nonlinear dynamics of the two-segment leg (7.6) features an eigenmode $\hat{\mathcal{W}} := \{\hat{\boldsymbol{x}} \in \mathbb{R} \times [0; 2a] \,|\, \hat{x}_1 = 0\}$ for any $\theta_2^\mathrm{x} \in [0; 2a]$. Note that for a symmetric positioning of legs and a symmetric distribution of the trunk inertia, the eigenmode $\hat{\mathcal{W}}$ can be maintained for the complete quadruped, even in case of two-segment legs with non-zero inertias. This will be validated later after introducing the quadrupedal system design.

(a)

(b)

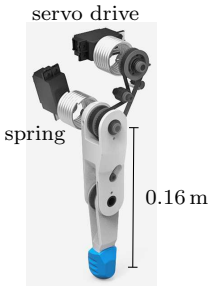

(c)

total mass	2.5 kg
mass of a leg	0.1 kg
spring stiffness	2 Nm/rad
max. energy spring	4 J
joint range hip (foreleg)	$-75\,\text{deg} \geq q_1 \geq 105\,\text{deg}$
joint range knee (foreleg)	$-120\,\text{deg} \geq q_2 - q_1 \geq 120\,\text{deg}$
joint range hindleg	symmetric

(d)

Figure 7.2.: Compliantly actuated quadrupedal robot Bert: (a) complete robotic system; (b) dimensions; (c) leg mechanism.

Quadrupedal system design

The complete quadrupedal system is dimensioned in view of dynamic locomotion capabilities. To this end, the task of vertical jumping serves as a reference. For the dimensioning, a single leg is considered. First, the servo motor of the series elastic actuators (SEA) are selected. This yields the maximum torque and velocity of the actuator (on motor side) and an estimate of the main body weight. Then, the leg-segment lengths and spring stiffnesses are determined in a series of computer simulation based optimizations of the jumping height. In this procedure, the insights of the modal leg design, as derived above, are taken into account such that only two parameters (i. e., the length of thigh and shank a and the stiffness of both actuated degrees of freedom k) need to be found. In order to maximally exploit the potential energy storing capabilities of SEAs, it is assumed that very low, viscous damping acts only at link side. This assumption reveals the requirement to implement the SEA with as few friction as possible in parallel to the spring. In order to satisfy also the low weight assumption made for the simulation model, the SEA is realized by a torsional spring. The resulting mechanical implementation of the compliantly actuated, modal leg design, as shown in Fig. 7.2c, is also advantageous regarding the installation space, and determines the width of shoulder and hip of the quadruped (Fig. 7.2b). The length of the quadrupedal system is selected such that the gallop gait is possible, i. e., fore-feet and hind-feet motions can intersect.

The arrangement of the legs as well as the inertial properties of the main body are chosen to be symmetric such that the complete quadrupedal system features an eigenmode, which can be exploited for vertical bouncing motions. This can be validated by inves-

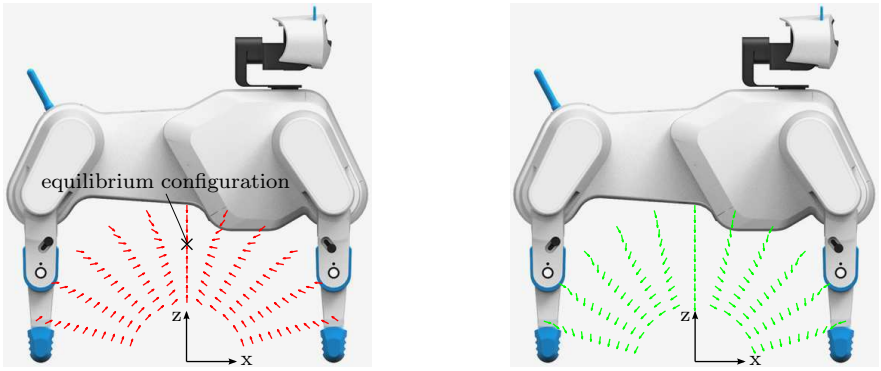

(a) (b)

Figure 7.3.: Acceleration field of the compliantly actuated quadruped Bert in stance: (a) due to potential forces; (b) Coriolis/centrifugal accelerations.

tigating the acceleration fields for displacements w. r. t. to an equilibrium configuration of the eigenmode and the field of Coriolis/centrifugal accelerations as shown in Fig. 7.3a and 7.3b, respectively. In more detail, the task dynamics of the complete quadrupedal system is considered in the formulation of Sect. 6.4.1, where all four feet are constrained at positions on the ground perpendicular to hip and shoulder rotation axes[5]. A symmetric equilibrium configuration is selected, in which the main body is parallel to the ground plane. The condition of Definition 5.1 related to potential forces is tested by analyzing the direction of acceleration for translational displacements of the trunk w. r. t. a ground fixed coordinate system (Fig. 7.3a). The condition of Definition 5.1 related to Coriolis/centrifugal forces needs to be satisfied simultaneously to the one corresponding to the potential forces. Therefore, the Coriolis/centrifugal acceleration is tested for different velocities expressed in polar coordinates at several configurations (Fig. 7.3b). The directions of the velocities correspond to the relative displacements of the robot w. r. t. the initial configuration considered for the potential force test. For instance, if the relative displacement is solely polar (angular), then also the tested velocity consists only of a polar component, etc. Both fields display vertical lines of accelerations such that the existence of an eigenmode can be deduced (according to Definition 5.1 and Theorem 5.1).

Servo motors

The quadruped Bert is designed to perform energetically efficient locomotion. A significant source of energy consumption (in electrically driven robotic systems) is given by the servo motors. Especially the implementation of the corresponding control system might have a large impact on the stand-by power consumption. As such, the mechatronic design of Bert builds upon a customized solution of electrical servo drives. The starting point is the off-the-shelf high torque servo Savöx SV-1270TG. This servo contains a core-less, brushed, direct current (DC) motor, which is designed to produce high torques and velocities. Brushed DC motors can be controlled with computationally cheaper control algorithms than, e. g., the brush-less DC motors (which are commonly used in robotic systems), since the electric commutation is implemented mechanically. This in turn requires less powerful

[5]Since all contact points of the legs can move only in parallel planes, only 10 rather than 12 constraints are feasible, i. e., all four contact points are constrained in vertical and forward/backward direction, but only either the two left or right feet are constrained in lateral direction.

max. active torque	1.3 Nm
max. stall torque	3.0 Nm
max. velocity	10.0 rad/s
mech. efficiency: output / motor power	0.6
elect. efficiency: output / elect. input power	0.4
communication rate of USB isochronous transfers	1 kHz

Table 7.1.: Technical characteristics of the customized servo unit.

and power-consuming central processing units (CPU) for their control. In order to satisfy the requirements from a control perspective such as the capability to implement link-side damping via the motors, the build-in electronics of the off-the-shelf servo is replaced by a customized one. The developed electronics has the option to connect an additional position sensor, which can be utilized to implement control loops based on measurements of the spring deflection on board. The technical characteristics of the developed servo unit are listed in Table 7.1.

7.1.2. Control of dynamic locomotion gaits

The dynamics of multi-legged locomotion such as pronking and trotting can be approximated by a spring-mass model [BF93]. As validated above (cf. Fig. 7.3a and 7.3b), for symmetric leg configurations and contact situation, the compliant quadruped at hand features an oscillation mode, which corresponds to such bouncing motions. This intrinsic dynamics behavior can be directly exploited in the stance phase and combined with well-studied foot-placement strategies [Rai86] to achieve dynamic locomotion gaits. However, the spring-mass or SLIP model is conservative, while the dynamics of the real quadrupedal system is subject to energetic losses due to impacts and friction in the joints. To excite and sustain the intrinsic oscillatory behavior of the real plant, a control method based on switching of motor positions, as introduced in Chapt. 4, can be applied along the eigenmodes. Accordingly, the locomotion controllers presented in the following switch the position of the motors triggered by events which depend solely on states at position level.

Pronking

A fundamental difference of the SLIP and the modal leg dynamics is that for the latter, the polar angle $\hat{x}_1$ is statically controllable during stance (cf. the right hand sides of (7.4) and (7.6)). This additional input variable θ_1^{x} can be utilized to control the pendulum motion of the trunk in a pronking gait. In [LSFAS15], it has been demonstrated for a single-leg system that the simple switching law

$$\boldsymbol{\theta}(\boldsymbol{\theta}_-, \boldsymbol{q}) = \begin{cases} \boldsymbol{f}^{-1}(-\alpha_\mathrm{l}, r_0) + \boldsymbol{w}\hat{s} & \text{if} \quad \boldsymbol{w}^T \frac{\partial U_\mathrm{e}(\boldsymbol{\theta}_-, \boldsymbol{q})}{\partial \boldsymbol{q}}^T > \epsilon_{\tau_\mathrm{w}} \\ \boldsymbol{f}^{-1}(\alpha_\mathrm{l}, r_0) & \text{if} \quad \boldsymbol{w}^T \frac{\partial U_\mathrm{e}(\boldsymbol{\theta}_-, \boldsymbol{q})}{\partial \boldsymbol{q}}^T < \epsilon_{\tau_\mathrm{w}} \end{cases}, \tag{7.8}$$

(where $\boldsymbol{f}^{-1}$ denotes the inverse mapping of (7.5) and $\boldsymbol{\theta}_-$ is the state of $\boldsymbol{\theta}$ before the switching instance) suffices to stabilize a periodic hopping motion. The control (7.8) switches only between two equilibrium configurations. The corresponding motor positions are parametrized in polar coordinates by the landing angle $\alpha_\mathrm{l} \in (-\pi/2; \pi/2)$, the radial

rest length $r_0 > 0$, and the switching amplitude $\hat{s} > 0$ along the eigenvector

$$\boldsymbol{w} = \text{sign}(q_2 - q_1) \begin{pmatrix} 1 \\ -1 \end{pmatrix} . \tag{7.9}$$

The transitions between the two controller states are triggered by approximating the touchdown and takeoff event by thresholding the generalized elastic force on the eigenmode $\boldsymbol{w}^T \frac{\partial U_\text{e}(\boldsymbol{\theta}_-, \boldsymbol{q})}{\partial \boldsymbol{q}}^T$ w. r. t. a constant $\epsilon_{\tau_\text{w}} > 0$ from below (touchdown) and above (takeoff), respectively. Therefore, the complete control is determined by only four, intuitive parameters. In particular, the parameter corresponding to the angle of attack α_l can be considered to regulate the average locomotion velocity v w. r. t. a desired value v_des, e. g., by an iterative law of the form

$$\alpha_\text{l}(j) = \alpha_\text{l}(j-1) + k_\text{v}(v(j) - v_\text{des}) , \tag{7.10}$$

which updates α_l once per jumping cycle j with a low gain $k_\text{v} > 0$. The control (7.10) is similar to the step-length adaptation as proposed by *Raibert* [Rai85]. The difference w. r. t. *Raibert's* controller is that (7.10) cumulates the control-error instead of considering a proportional and feed-forward term, as proposed in [Rai86].

The single-leg hopping control (7.8) can be directly transfered to the quadrupedal system by "linking" the input of all legs to a single, "virtual" leg, as proposed in [Rai86]. In case of pronking on spot, this results in a motion, which evolves ideally in the eigenmode of the plant, although the quadrupedal system is composed of articulated legs with non-zero mass.[6] As such, this pronking control is potentially efficient w. r. t. the jumping height. However, if the goal is to travel forward, there are different quadrupedal gaits, which are way more efficient depending on the desired locomotion speed [HT81].

Trotting

The trot control, which will be proposed in the following, serves as an example to show how the natural oscillatory dynamics of the quadrupedal system can be exploited to achieve forward locomotion. The running trot is a dynamic gait, where diagonal pairs of legs move in phase. While one leg pair is in stance and transports the COM forward in locomotion direction, the other leg pair swings towards the touchdown configuration. The gait can display a flight phase in between the alternation of these functionalities. In that case, the total COM need to oscillate in vertical direction, since during the flight phase, the height of the total COM cannot be constant due to gravity. However, from a view point of energetic efficiency (regarding forward locomotion), the vertical oscillation amplitude needs to be kept as low as possible, since due to friction (which is present in any physical system), any radial motion of the stance legs is subject to energetic losses, although kinetic energy (of the flight phase) is partially stored in the corresponding springs. This consideration reveals that a potential source to gain efficiency is given in the generation of the polar leg motion, and motivates a controller design based upon the natural oscillatory dynamics predominantly in this polar direction of the legs, cf. (7.6).[7]

The gait control can be described by a finite state machine (FSM), which switches the equilibrium configurations of the legs (Fig. 7.4). The link and motor positions of all legs

[6] This is based on the assumption that the quadrupedal system is symmetric w. r. t. the vertical axis.

[7] Note that for implementation based on the SLIP dynamics, e. g., via virtual model control [PDP97], the motors performing the polar leg motion would require to move as fast as the corresponding links, since there is no elasticity acting in the polar direction to perform the movement.

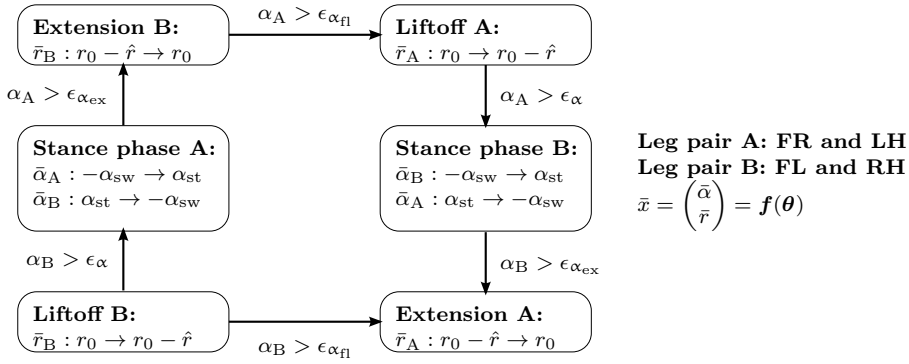

Figure 7.4.: Finite state machine controlling quadrupedal trot.

are expressed in polar coordinates (7.5). Diagonal leg pairs are considered as "linked". The gait generation is based on the idea to excite an antiphasic, elastic pendulum motion of the stance and swing leg pair by moving the motors as few as possible. This can be achieved by switching the polar equilibrium configuration of the stance and swing legs to α_st and $-\alpha_\mathrm{sw}$, respectively. Thereby, the sum of the parameters $\alpha_\mathrm{st} \geq 0$ and $\alpha_\mathrm{sw} \geq 0$ determines the *static* polar step length. The current stance phase is initiated depending on the polar angle of the previous leg pair in stance. Thereby, the threshold $\epsilon_\alpha > 0$ determines also the actual *dynamic* step length. It becomes evident that there might be an optimal value for ϵ_α, which for a given static step length (which determines the switching amplitude) maximizes the actual dynamic step length. In between the main two (finite) states of the stance phase, two more states are required, which initiate the radial extension and flexion of the swing and stance leg, respectively. Since, the effective inertia of the stance legs is much greater than of the swing legs but the stiffness is equal, also the time constant of oscillation of the former is greater. Loosely speaking, this means that the swing legs move faster than the one in stance. As such, the extension of the swing legs need to be initiated before the legs in stance are lifted. This can be achieved by setting the rest length of the swing legs to the initial leg length $r_0 \in (0; r_\mathrm{max}]$, when the polar angle of the legs in stance hits the threshold $\epsilon_{\alpha_\mathrm{ex}} < \epsilon_\alpha$ from below. The liftoff is initiated by reducing the initial rest length of the stance legs by an amount of $\hat{r} \in (0; r_0)$, when the polar angle of the same leg pair crosses the threshold $\epsilon_{\alpha_\mathrm{fl}} > \epsilon_{\alpha_\mathrm{ex}}$ (where $\epsilon_{\alpha_\mathrm{fl}} < \epsilon_\alpha$) from below. Note that for the legs in stance, their rest length is only decreased, which means that at most the potential energy is removed in the radial direction. However, although the radial oscillation is not directly excited, the energy storing capabilities in vertical direction can be exploited by selecting $\alpha_\mathrm{st} > \alpha_\mathrm{sw}$.

7.1.3. Experiments

The performance and efficiency of the quadrupedal pronk and trot controllers, as proposed in Sect. 7.1.2, are validated in real hardware experiments with the compliantly actuated quadruped Bert (Sect. 7.1.1). Thereby, the focus is on the energetic efficiency of the gait generation, which can be measured by the cost of transport (COT).

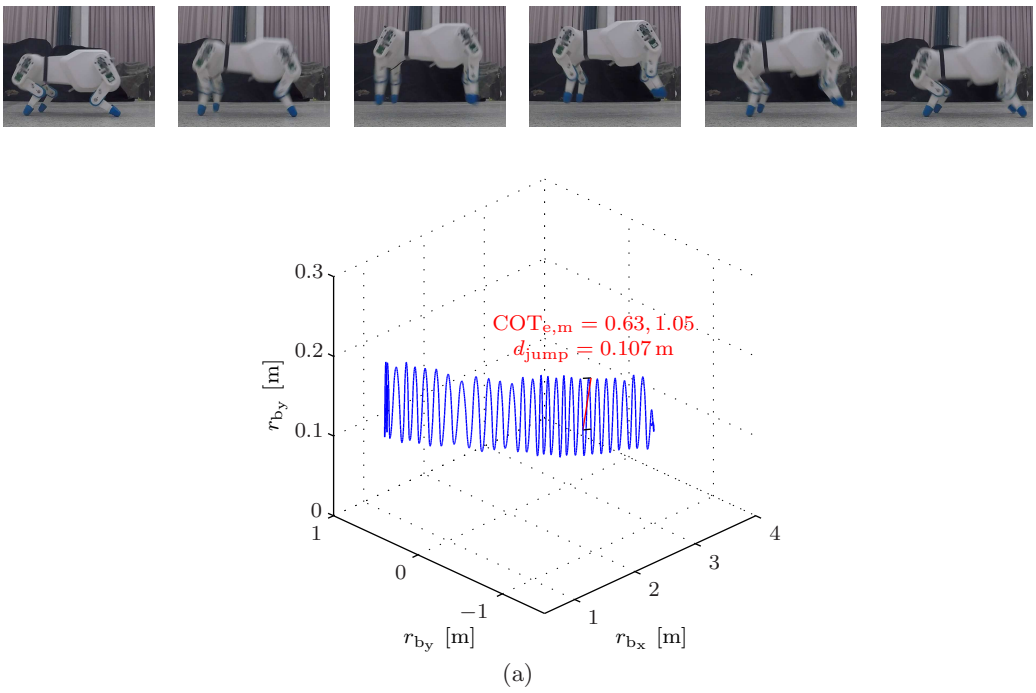

(a)

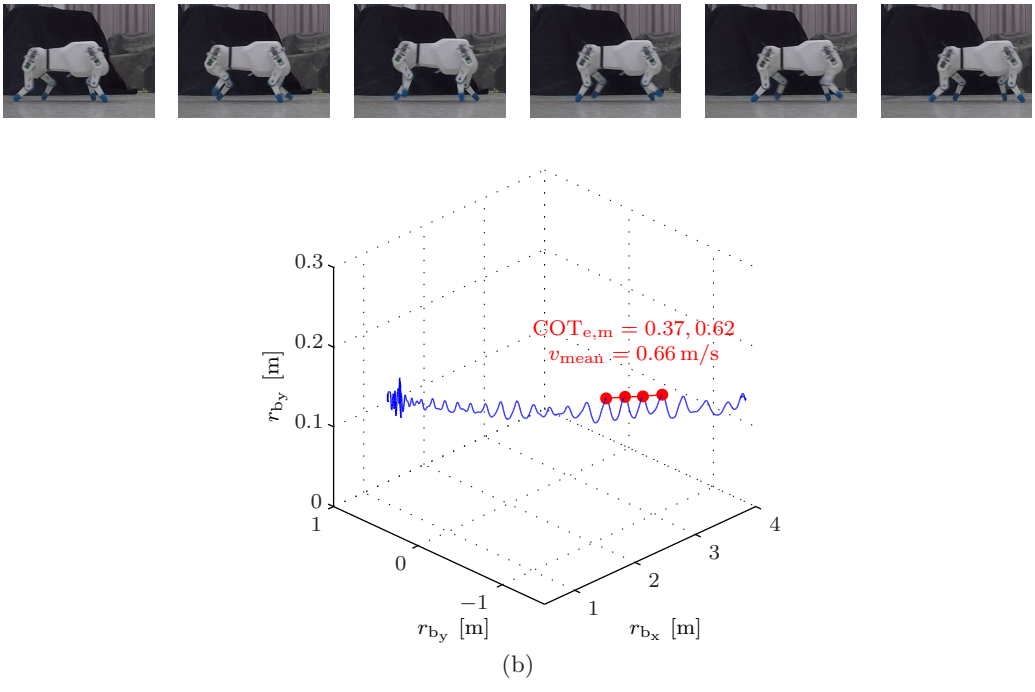

(b)

Figure 7.5.: Performance and efficiency of locomotion controllers tested in experiments with the quadrupedal robot Bert. The absolute position of the main body $\boldsymbol{r}_\mathrm{b}$ is plotted for (a) pronking; (b)trotting.

Cost of transport

The COT is defined as *the energy expenditure per unit weight of moving at a given velocity on a level path for a unit distance* [Tuc75], i. e.,

$$\mathrm{COT} = \frac{P_{\mathrm{in}}}{m_{\mathrm{tot}} g_0 v}\,, \tag{7.11}$$

where P_{in} is the power required to move the unit mass $m_{\mathrm{tot}} g_0$ (weight times gravitational constant) at a velocity v. In general, the power P_{in} as well as the velocity of movement v are varying over time. In particular, v can be zero such that the COT, as defined by (7.11) is undefined. Therefore, it is advantageous to average the power P_{in} and the velocity v over time such that (7.11) can be redefined as

$$\mathrm{COT} = \frac{\int_0^T P_{\mathrm{in}}(t)\mathrm{d}t}{m_{\mathrm{tot}} g_0 \int_0^T v(t)\mathrm{d}t} = \frac{E_{\mathrm{in}}}{m_{\mathrm{tot}} g_0 d}\,, \tag{7.12}$$

where $E_{\mathrm{in}} > 0$ is the energy required to transport the unit mass $m_{\mathrm{tot}} g_0$ over the distance $d > 0$, and $T > 0$ denotes the duration of observation. The COT has been introduced in [Tuc75] to compare the efficiency of locomotion among gaits and species of biological systems. Thereby, the power input is estimated by measuring rates of exchange of oxygen and carbon dioxide. To compare (mobile) robotic and biological systems, for the former, one need to consider the total power which is supplied to the complete system, e. g., the electrical power provided by the batteries. A further important efficiency measure is given by the "intermediate" COT based on the mechanical power input by the motors, i. e., $P_{\mathrm{m}} = \boldsymbol{\tau}_{\mathrm{m}}^T \dot{\boldsymbol{\theta}}$, where $\boldsymbol{\tau}_{\mathrm{m}}$ denotes the motor torques. It can be considered to compare different control methods, actuator principles (e. g., rigid versus compliant actuation), and design concepts of multibody systems such as the class of dynamics featuring oscillation modes.

Although it is planned for future versions, the current prototype of the quadrupedal robot Bert features no synchronized measurement of the electrical input power, nor of the motor torques. The total electrical power required for static stance, can be estimated from averaged voltage and current measurement of the power supply ($P_{\mathrm{el}} \approx 10.8\,\mathrm{W}$). However, for the highly dynamical power consumption, as expected for the generation of dynamic locomotion gaits, this method would not lead to reasonable results. A common method to estimate the (fluxgate) torque of electrical motors is done by measuring the current of the motor windings. However, in case of the coreless motors used in the servo drives, the electrical time constant is in the order of $5\,\mu\mathrm{s}$, which makes the observation of the current unrealizable. Thus, the mechanical power input generated by the motors is approximated by using the power input in the elasticities $P_{\mathrm{e}} = \boldsymbol{\tau}_{\mathrm{e}}^T \dot{\boldsymbol{\theta}}$ (where $\boldsymbol{\tau}_{\mathrm{e}}^T = -\partial U_{\mathrm{e}}(\boldsymbol{\theta}, \boldsymbol{q})/\partial \boldsymbol{q}$) and an estimate of the mechanical efficiency $\eta_{\mathrm{m}} \approx 0.6$ of motor and gearbox based on estimates of the acting friction, i. e., $P_{\mathrm{m}} \approx P_{\mathrm{e}}/\eta_{\mathrm{m}}$. Since energy recuperation is not implemented in the servo electronics yet, only positive power is taken into account. Therefore, the measures considered to evaluate the energetic efficiency of the quadrupedal locomotion controllers are

$$\mathrm{COT}_{\mathrm{m}} \approx \frac{1}{\eta_{\mathrm{m}}} \mathrm{COT}_{\mathrm{e}}\,, \tag{7.13}$$

$$\mathrm{COT}_{\mathrm{e}} = \frac{\int_0^T \max(\boldsymbol{\tau}_{\mathrm{e}}(t)^T \dot{\boldsymbol{\theta}}(t), 0)\mathrm{d}t}{m_{\mathrm{tot}} g_0 d}\,. \tag{7.14}$$

They will be referred to as the (approximated) mechanical and elastic COT, respectively.

Pronking

The pronk gait can be used to overcome obstacles. A reasonable performance and efficiency measure takes also the jumping height into account. In the experimental evaluation of the pronking controller, the jumping distance is considered as performance measure and reference length for the COT. It is defined as the geometric mean of the horizontally traveled distance d and the jumping height $h = h_{\max} - \bar{h}$ of the considered stride, where $\bar{h}$ denotes the height of the main body in static stance, i. e., $d_{\text{jump}} = \sqrt{d^2 + h^2}$. To this end, the controller parameters are tuned manually to maximize the jumping distance d_{jump}: the landing angle is selected to be $\alpha_{\text{l}} = -0.04\,\text{rad}$, the initial rest length is set to $r_0 = 0.15\,\text{m}$, the modal switching amplitude and threshold are chosen to be $\hat{s} = 0.6\,\text{rad}$ and $\epsilon_{\tau_{\text{w}}} = 0.35\,\text{Nm}$, respectively. This results in a jumping distance of $d_{\text{jump}} = 0.107$ as indicated in Fig. 7.5a. An elastic and mechanical COT of 0.63 and 1.05 are achieved for this jump, respectively.

Trotting

The experiment presented in the following aims at validating the performance and efficiency of the natural dynamics based trot control. Thereby the focus is on steady state locomotion. In order to approach a phase with approximately constant movement velocity, the polar angle of the swing leg pair is initially increased step-by-step until a desired value is reached, i. e., $\alpha_{\text{sw}} = 0.025\,\text{rad} + j0.005\,\text{rad} \leq 0.525\,\text{rad}$, where $j \in \mathbb{N}$ iterates over the steps. All remaining controller parameters are selected as a function of α_{sw}: To exploit the natural radial oscillation properties, the polar equilibrium angle of the stance legs is set to $\alpha_{\text{st}} = 1.25\alpha_{\text{sw}}$. The displacement of the initial rest length is selected by $\hat{r} = 0.035\,\text{m} + 0.03\frac{\text{m}}{\text{rad}}\alpha_{\text{sw}}$. Especially, it turned out that a larger displacement for the hindleg, i. e., $\hat{r}_{\text{hind}} = 1.3\hat{r}$ while $\hat{r}_{\text{fore}} = \hat{r}$, has a stabilizing effect on the pitch motion of the main body. The thresholds of the swing leg extension and stance leg flexion are chosen to be $\epsilon_{\alpha_{\text{ex}}} = 0.1\alpha_{\text{sw}}$ and $\epsilon_{\alpha_{\text{fl}}} = 0.3\alpha_{\text{sw}}$, respectively, such that both switchings occur after mid-stance, while the swing legs extend before the stance legs flex. The threshold for the interchange of swing and stance leg pairs is selected as a quadratic function of the static polar angle of the legs in swing (with minimum at $\alpha_{\text{sw}} = 0$), i. e., $\epsilon_{\alpha} = 0.6\alpha_{\text{sw}} + 0.3\frac{1}{\text{rad}}\alpha_{\text{sw}}^2$. This results in an locomotion velocity (as averaged over three steps) of $v_{\text{mean}} = 0.66\,\text{m/s}$ (Fig. 7.5b). Thereby, an elastic and mechanical COT of 0.37 and 0.62 are achieved, respectively.

A preliminary estimate of the total COT can be obtained based upon the mean efficiency for the conversion from electrical to elastic power, which for the servo units is $\eta_{\text{el}} \approx 0.4$. Considering further the electrical power consumption of the main computer, which is $P_{\text{CPU}} \approx 10\,\text{W}$, the total COT of the trot with the quadruped Bert can be approximated by $\int_0^T (P_{\text{e}}/\eta_{\text{el}} + P_{\text{CPU}})\text{d}t/(m_{\text{tot}} g_0 d) = 1.53$. Compared to other legged robots such as BigDog (COT = 15) and ASIMO (COT = 2), this value is already significantly lower. The COT of the compliantly actuated robot iSprawl is with 1.7 also higher than the value of Bert at hand. However, the MIT Cheetah achieves a COT of 0.51, which is the result of a very optimized mechatronic design [SWC+13].[8] Note that the current COT values estimated for Bert will be verified with a new version of the power supply and motor-controller electronics, which will permit direct measurement of the input power.

[8] The COT values are taken from [SWC+13].

7.2. Bipedal locomotion

The main difference in the dynamics of bipedal and quadrupedal systems is the distribution of inertias between the main body and the legs. A single leg of a human contributes to the total body mass with about 15% [HCH76], while the fore- and hindleg of a cheetah weights only about 4.3% and 8.6% of the total body mass [HH85], [KH13], respectively. As such in human like locomotion, the relatively slow motion of the leg segments contributes significantly to the dynamics of the gait. This motivates to investigate how the concept of oscillation modes (Chapt. 5) can be exploited in the design and control of compliantly actuated bipedal robots.

In the last decades, numerous bipedal robots and methods to control these systems have been developed. Achievements in the design of humanoid robots can be traced back to WABOT-1 (one of the first modern humanoids) [YSIT99], which formed the basis of many subsequent bipedal systems such as ASIMO [HHHT98],[HO07], the HRP series [AKK$^+$05], or Wabian-2R [OAS$^+$06] (just to mention a representative selection). These rigidly actuated robotic systems have been demonstrated to successfully perform bipedal walking gaits. Thereby, classical control approaches based on the inverted pendulum model and the zero moment point (ZMP) [VB05], [KT91], [Wie06] have been utilized. Since rigid robots cannot handle high peak forces on the one hand, but also the ZMP is a static criterion for balancing on the other hand, these systems are mainly able to perform only quasi-static rather than dynamic walking gaits. In order to overcome the limitations regarding mechanical robustness, but also to increase the energetic efficiency respectively performance of the locomotion gait, *Alexander* [Ale90] suggests the introduction of elastic elements. They help to reduce the impact forces at the gear-box of the drives and offer the capabilities of saving energy during weight bearing and for the generation of swing motions of the legs [Ale90]. On the basis of these insights, several bipedal robots built upon compliant actuators have been introduced [HCR07], [GHM$^+$09], [TLSC11], [ESNV12], [GH12], [TMD$^+$13]. Thereby, the dynamic locomotion gaits are realized, e. g., by virtual model control [PDP97], [PP98], [HRHS10], or the compliant hybrid zero dynamics framework of *Sreenath et al.* [SPG13].

For all of the mentioned bipedal systems, walking or even running have been demonstrated so far. However, the natural oscillatory behavior of the plant has not been explicitly taken into account neither in the mechanical design nor in the control. In this section, novel concepts are proposed, which allow to analyze, design, and control the natural oscillatory behavior of compliantly actuated bipedal systems w. r. t. task-relevant decoupled elasticities and oscillation modes.

7.2.1. C-Runner: a compliantly actuated biped

The main purpose of C-Runner is the investigation of different concepts of compliant actuation in bipedal locomotion. Therefore, the mechanical design is modular rather than highly integrated. This allows to realize several elastic couplings such as mono- and biarticular springs on the same basic test platform. In order to enable the comparison of performance and efficiency with its biological counterpart, the size and weight of the robotic system is in a human-like scale. The main focus is on the basic dynamics of bipedal locomotion. Therefore, all joint axes (including the main body rotation) are parallel and the system is guided to move on a circle. All technical characteristics of C-Runner (which are relevant for this thesis) are provided in Fig. 7.6. A comprehensive system description is given in [LWL$^+$16].

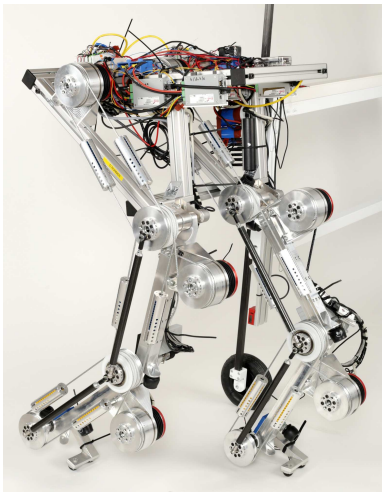

total mass	54 kg
mass of thigh, shank, foot	6, 6, 1.3 kg
segment lengths of thigh, shank, foot	0.4, 0.4, 0.17 m
distance ankle joint and heel	0.05 m
max. motor velocity (gear output)	5.2 rad/s
max. motor torque (gear output)	145 Nm
possible stiffness of springs	240, 500, 670 Nm/rad

Figure 7.6.: Compliantly actuated bipedal robot DLR C-Runner.

7.2.2. Task-oriented coordinates

In this section, a set of task-oriented coordinates is introduced, which aim at simplifying the analysis and the control of the natural oscillatory dynamics of the compliantly actuated bipedal system.

Single leg coordinates

The kinematics of a single leg can be described by a serial chain of main body, thigh, shank, and foot (Fig. 7.7a). The thigh is connected to the main body by the rotational hip joint, where the relative angle is denoted by q_1. The shank is hinged to the thigh and the foot is rotationally connected to the thigh, where the relative knee and ankle joint angles are denoted by q_2 and q_3, respectively. The joint angles are all zero, when the foot is parallel on the ground and the ankle, knee, and hip joints are vertically aligned with the COM of the main body (in the mentioned order). Assuming equal lengths of shank and thigh, the set of task-oriented coordinates of the single leg,

$$\boldsymbol{x}(\boldsymbol{q}) = \begin{pmatrix} q_1 + \frac{1}{2}q_2 \\ l(q_2) \\ \frac{1}{2}q_2 + q_3 \end{pmatrix} \tag{7.15}$$

can be considered (Fig. 7.7b). These coordinates are based on the line linking the hip and ankle joint, which is referred to as the leg axis. The first task coordinate $x_1 \in \mathbb{R}$ represents the relative angle of the leg axis and the main body. It is zero, if the COM of the main body, the hip and ankle joint are aligned in the mentioned order. The second

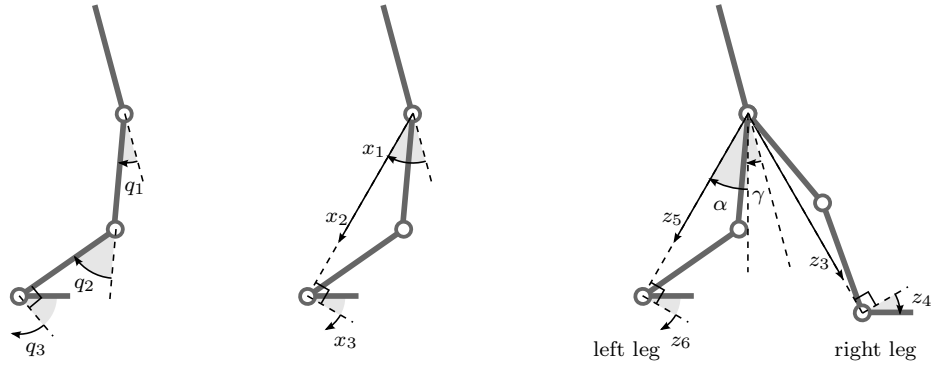

(a) (b) (c)

Figure 7.7.: Task-oriented coordinates: (a) joint configuration of a single leg; (b) task-oriented coordinates of a single leg; (c) bipedal task coordinates.

task coordinate $x_2 \in \mathbb{R}$ is any representation of the "length" of the leg axis $l(q_2)$. A natural choice is given by the Euclidean distance

$$l(q_2) = a\sqrt{2 + 2\cos(q_2)}\,, \tag{7.16}$$

where $a > 0$ denotes the equal segment lengths of thigh and shank. However, the mapping (7.16) is not bijective. As such, for some applications it can be advantageous to simply select the identity mapping $l(q_2) = q_2$. The third task-coordinate $x_3 \in \mathbb{R}$ represents the relative angle of the foot and the leg axis. It is zero, if the leg axis is perpendicular to the contact line of the foot (and the hip is above the ground).

In Sect. 7.2.4, a compliant actuation design will be proposed, which achieves an input and output decoupling of the elastic forces expressed in these task-oriented coordinates (7.15).

Bipedal coordinates

On the basis of the task-oriented representation of the configuration for the single leg (7.15), coordinates can be introduced for the bipedal system, which decouple the polar step length and the orientation of the legs w. r. t. the main body. To this end, assume that the task-oriented coordinates of the right and left leg are defined as

$$\boldsymbol{y}(\boldsymbol{q}) = \begin{pmatrix} \boldsymbol{x}(\boldsymbol{q}_{1\ldots3}) \\ \boldsymbol{x}(\boldsymbol{q}_{4\ldots6}) \end{pmatrix} = \begin{pmatrix} q_1 + \frac{1}{2}q_2 \\ l(q_2) \\ \frac{1}{2}q_2 + q_3 \\ q_4 + \frac{1}{2}q_5 \\ l(q_5) \\ \frac{1}{2}q_5 + q_6 \end{pmatrix}. \tag{7.17}$$

Then, the proposed set of bipedal task-oriented coordinates considers the relative angle between the leg axes

$$\alpha = \frac{y_4 - y_1}{2} \tag{7.18}$$

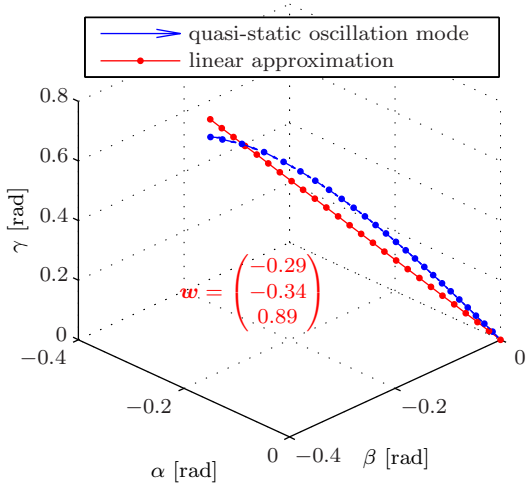

Figure 7.8.: Quasi-static oscillation mode of the bipedal system in the single support phase.

and the mean of the angles of the leg axes w. r. t. the main body

$$\gamma = \frac{y_1 + y_4}{2}\,, \tag{7.19}$$

such that the complete change of coordinates takes the form (Fig. 7.7c)

$$\boldsymbol{z}(\boldsymbol{q}) = \begin{pmatrix} \alpha \\ \gamma \\ z_3 \\ z_4 \\ z_5 \\ z_6 \end{pmatrix} = \begin{pmatrix} \frac{1}{2}\left(q_4 + \frac{1}{2}q_5 - q_1 - \frac{1}{2}q_2\right) \\ \frac{1}{2}\left(q_1 + \frac{1}{2}q_2 + q_4 + \frac{1}{2}q_5\right) \\ l(q_2) \\ \frac{1}{2}q_2 + q_3 \\ l(q_5) \\ \frac{1}{2}q_5 + q_6 \end{pmatrix}. \tag{7.20}$$

These coordinates form the basis to design an 1-manifold of the single support phase, which will be considered for the dynamic walking control presented next.

7.2.3. Dynamic walking

Walking is a gait, where at least one of the feet is in contact with the ground. Bipedal walking consists of a single and double support phase: In the single support phase, the stance leg bears and transports the total center of mass (COM) in walking direction. At the same time, the swing leg moves towards the configuration, which the stance leg had at the beginning of the step. During the double support phase, the functionalities of the previous stance and swing leg are interchanged. This phase is often modeled as instantaneous, see, e. g., [GAP01], such that walking can be regarded as concatenation of single support phases. The basic idea of the proposed dynamic walking control is to exploit the natural dynamics of the compliantly actuated bipedal system for the generation of motion during the single support phase. This presumes that the plant features a corresponding oscillation mode.

Quasi-static single support mode

A (planar) bipedal system with feet consisting of two contact points (corresponding to heel and toe) can display single support situations, where either only one or both contact

points are constrained to the walking surface. In particular, the contact situation may also change during stance. This would result in a structural change of the continuous dynamics such that the natural oscillatory behavior cannot evolve in a single oscillation mode. For simplicity, although not required from a theoretical point of view[9], in the following exemplary analysis the case is considered, where the stance foot is completely fixed to the ground. Additionally the stiffness of the elastic potential is assumed to be sufficiently high, such that the configuration $\boldsymbol{q} \in \mathbb{R}^6$ of the single support dynamics is statically controllable via the motor position $\boldsymbol{\theta} \in \mathbb{R}^6$ in the entire "relevant" configuration space (cf. Definition 3.4 and Proposition 3.1). The resulting compliantly actuated fixed-base system can be expressed in terms of the bipedal task coordinates (7.20), i. e.,

$$\bar{\boldsymbol{M}}(\boldsymbol{z})\ddot{\boldsymbol{z}} + \bar{\boldsymbol{b}}(\boldsymbol{z}, \dot{\boldsymbol{z}}) + \frac{\partial U(\boldsymbol{\theta}, \boldsymbol{z})}{\partial \boldsymbol{z}}^T = \boldsymbol{0}\,. \tag{7.21}$$

This step is not essential, but simplifies the geometric interpretation of possible modes.

To identify a quasi-static oscillation mode of such a system, the following procedure can be applied:

1. Select an equilibrium configuration $\boldsymbol{z}_0$ and fix the corresponding actuator configuration $\boldsymbol{\theta}_0 = \bar{\boldsymbol{z}}^{-1}(\boldsymbol{z}_0)$ (Definition 3.4);

2. Select a step size $\Delta r > 0$;

3. Find displacements $\Delta\boldsymbol{z}(j) = \sum_{i=1}^{j} \boldsymbol{w}(i)\Delta r$, where $\boldsymbol{w}(i) \in \mathbb{R}^n$ satisfying $\|\boldsymbol{w}(i)\| = 1$ represents the direction of a vector in $\mathbb{R}^n$, such that for any $j = 1 \ldots N_{\text{steps}}$, the quasi-static acceleration is aligned with the incremental displacement of step j. That is, for all $j = 1 \ldots N_{\text{steps}}$, there exists a scalar $\ddot{r}(j) \in \mathbb{R}$ such that

$$-\boldsymbol{M}(\boldsymbol{z}_0 + \Delta\boldsymbol{z}(j))^{-1} \left.\frac{\partial U(\boldsymbol{\theta}_0, \boldsymbol{z})}{\partial \boldsymbol{z}}\right|_{\boldsymbol{z}=\boldsymbol{z}_0+\Delta\boldsymbol{z}(j)}^{T} = \boldsymbol{w}_j \ddot{r}(j) \tag{7.22}$$

   is satisfied. If for a desired numerical accuracy, the condition (7.22) cannot be satisfied, the step size Δr can be decreased (for the current iteration step).

This procedure yields a discrete approximation of a quasi-static oscillation mode expressed by the sequence $\boldsymbol{z}(j) = \boldsymbol{z}_0 + \Delta\boldsymbol{z}(j)$, which represents a (discrete) curve in the configuration space of the system.

Remark 7.1. *The term "quasi-static oscillation mode" refers to the assumption that the velocity is zero, i. e., $\dot{\boldsymbol{z}} = \boldsymbol{0}$. In other words, the curve represents an invariant subset of static displacements. In order to obtain a "dynamic" oscillation mode, further requirements on the Coriolis/centrifugal acceleration need to be satisfied. However, for rather low velocities, this is a good approximation of the system.*

In case of the example at hand, the above procedure yields the quasi-static oscillation mode as depicted in Fig. 7.8 (which is denoted by $\hat{\mathcal{Z}}$). The inertial model of the compliantly actuated biped C-Runner, as introduced in Sect. 7.2.1, is considered (i. e., the inertial parameters appearing in the gravitational potential and in the inertia matrix are derived

[9] Oscillation modes require the existence of an equilibrium configuration. But this fixed point needs not to be stable (cf. Definition 5.2).

from the mechanical design data). In the knee and ankle joints, linear springs with implementable stiffness values of $k_2 = 670\,\mathrm{Nm/rad}$ and $k_3 = 500\,\mathrm{Nm/rad}$ are considered, respectively.[10]. For the spring in the hip joints a stiffness value of $k_1 = 50\,\mathrm{Nm/rad}$ is determined by utilizing the eigenvector matching procedure as proposed in Sect. 5.2.[11] As such the considered elastic potential has the form $U_\mathrm{e}(\boldsymbol{q}-\boldsymbol{\theta}) = \frac{1}{2}\sum_{i=1}^{3} k_i(q_i-\theta_i)^2 + \frac{1}{2}\sum_{i=4}^{6} k_{i-3}(q_i-\theta_i)^2$. The foot of the right leg is assumed to be fixed to the ground.[12] Due to this fixation, the relative angle of the stance leg w. r. t. to the vertical line β equals the corresponding angle of the ankle joint (in task coordinates), i. e., $\beta = z_4$. The equilibrium configuration is set to $\alpha_0 = \beta_0 = \gamma_0 = z_{0,3} = z_{0,6} = 0$ and $z_{0,5} = 5\,\mathrm{deg}$. This corresponds approximately to the mid-stance configuration (i. e., where the total COM is vertically aligned with the ankle joint of the stance foot). Due to the high ratio of stiffness and inertia in the knee and ankle joint of the swing leg, and since the stance leg is set to a singular rest configuration, it can be expected that oscillations contribute mainly to the degrees of freedom measured by α, β and γ. As such, only displacements in these directions are considered in the identification procedure of the quasi-static oscillation mode. The estimated curve of displacements which cause exclusively tangential accelerations is weakly nonlinear (Fig. 7.8). The nonlinearity is mainly a result of gravity (since the generalized inertia matrix is almost constant and the stiffness of the elastic potential is exactly constant). The vector corresponding to the major principal component of the curve is $w_\alpha = -0.29$, $w_\beta = -0.34$ and $w_\gamma = 0.89$. This reveals that the quasi-static oscillation of the mode contributes approximately equally to the relative and absolute leg angle. By presuming that the swing foot is kept parallel to the walking surface, such a behavior corresponds to a symmetric step, where the takeoff and touchdown angle of the swing leg differs only in the sign. The contribution of the main body oscillation in the mode is dominant. This can be observed in the experimental validation of the dynamic walking controller introduced next. The main differences between the conceptual model investigated above and the experimental implementation are: firstly, the stance foot cannot be assumed to be fixed in experiments. Secondly, the mode is assumed to be linear in the experiment (which is a rather weak assumption, since the oscillation mode is almost linear).

Control of a dynamic walking gait

The dynamic walking control aims at exploiting the quasi-static single support mode $\hat{\mathcal{Z}}$ as identified above. Assuming that the system features additionally also a corresponding modal control manifold according to Definition 6.1, the system can be controlled to evolve in the mode by constraining $\bar{\boldsymbol{z}} = \bar{\boldsymbol{z}}(\boldsymbol{\theta}) := \boldsymbol{z}(\bar{\boldsymbol{q}}(\boldsymbol{\theta}))$ in $\hat{\mathcal{Z}}$. This can be achieved using a high gain motor PD control, e. g., of the form (3.31), and selecting $\boldsymbol{\theta}_\mathrm{des} = \bar{\boldsymbol{z}}^{-1}(\bar{\boldsymbol{z}}_\mathrm{des})$ such that $\bar{\boldsymbol{z}}_\mathrm{des}$ is in the mode.

The estimated single support mode contains approximately no contribution of motion in the leg axis and in the ankle joint of the swing leg (i. e., along z_5 and z_6 if the right leg is in stance). However, these degrees of freedom need to be controlled to obtain ground clearance and to ensure that at the interchange of leg functionalities, the foot of the swing leg is configured appropriately (e. g., parallel to the walking surface). A further important aspect for the realization in a real system is given by friction, which is present on the motor side (gear box), in the spring mechanism and in the joints. An approach to excite the single support motion in the quasi-static mode, which simultaneously achieves the

[10] Springs with these stiffness values are available for the real hardware system.
[11] The most compliant spring currently available for C-Runner has a stiffness of 240 Nm/rad.
[12] This choice is arbitrary by symmetry.

desired swing leg behavior, is proposed in the author's previous work [LASRL16]. To this end, an 1-manifold for the reference values is designed, which implements the constraints of the quasi-static single support mode as well as the "rigid body motion" of the swing leg axis and foot. This control manifold is parametrized by a single, motor configuration dependent variable. By controlling this variable, the complete step can be controlled. Possible choices of such a parametrization are given by virtual equilibrium position of the relative leg angle and the absolute angle of the stance leg, i. e., $\bar{\alpha}(\boldsymbol{\theta})$ or $\bar{\beta}(\boldsymbol{\theta})$, respectively. Both represent the "progress" of the step. However, the latter parametrization $\bar{\beta}(\boldsymbol{\theta})$ relies on the assumption that the stance foot is fixed to the ground, and therefore $\bar{\alpha}(\boldsymbol{\theta})$ represents a more robust choice. By considering the linear approximation of the nonlinear mode, the control of the single support takes the form

$$\bar{\boldsymbol{z}}_{\text{des}}^{\text{right}} = \begin{cases} \bar{\alpha}_{\text{des}} &= \alpha(\boldsymbol{q}) - u_\alpha \\ \bar{\gamma}_{\text{des}} &= -\varphi_{\text{des}} \\ \bar{z}_{3,\text{des}} &= \rho_0 \\ \bar{z}_{4,\text{des}} &= \bar{\alpha}(\boldsymbol{\theta}) \\ \bar{z}_{5,\text{des}} &= \rho_0 + \rho(\bar{\alpha}) \\ \bar{z}_{6,\text{des}} &= -\bar{\alpha}(\boldsymbol{\theta}) \end{cases} \tag{7.23}$$

if the right leg is in stance, and

$$\bar{\boldsymbol{z}}_{\text{des}}^{\text{left}} = \begin{cases} \bar{\alpha}_{\text{des}} &= \alpha(\boldsymbol{q}) + u_\alpha \\ \bar{\gamma}_{\text{des}} &= -\varphi_{\text{des}} \\ \bar{z}_{3,\text{des}} &= \rho_0 + \rho(\bar{\alpha}) \\ \bar{z}_{4,\text{des}} &= \bar{\alpha}(\boldsymbol{\theta}) \\ \bar{z}_{5,\text{des}} &= \rho_0 \\ \bar{z}_{6,\text{des}} &= -\bar{\alpha}(\boldsymbol{\theta}) \end{cases} \tag{7.24}$$

if the left leg is in stance. The progress of the step is controlled by the new control input $u_\alpha \in \mathbb{R}_{\geq 0}$, which "pushes" the system along the single support manifold. Note that the term $\bar{\alpha}_{\text{des}} = \alpha(\boldsymbol{q})$ in (7.23) and (7.24) implements "zero torque" for the degree of freedom of the relative leg angle.[13] The constants $\varphi_{\text{des}} \in \mathbb{R}$ and ρ_0 in (7.23) and (7.24) determine the equilibrium orientation of the main body and the rest length of the stance leg, respectively. The function $\rho(\bar{\alpha})$ implements the flexion of the swing leg to ensure ground clearance. As such, $\rho(\bar{\alpha})$ needs to be zero at the boundaries of the step and of maximum magnitude at the nominal mid-stance, i. e., $\rho(\bar{\alpha}) = 0$ if $|\bar{\alpha}| = \alpha_0$ and $|\rho(\bar{\alpha})| = \rho_{\max}$ if $\bar{\alpha} = 0$, where $\alpha_0 > 0$ denotes the nominal (polar) step length. If the mapping l in (7.20) is chosen unity, i. e., $l(q_{2,5}) = q_{2,5}$, the flexion of the swing leg can be implemented by

$$\rho(\bar{\alpha}) = \rho_{\text{flexion}} \cos\left(\max\left(\min\left(\bar{\alpha}\alpha_0 \frac{\pi}{2}, \alpha_0\right), -\alpha_0\right)\right), \tag{7.25}$$

where the constant ρ_{flexion} determines the flexion of the knee (at nominal mid-stance).

To generate the motion of the complete gait, the transition between the single support controls (7.23) and (7.24) need to be controlled. A continuous evolution of the reference values can be achieved by switching based on the manifold parameter $\bar{\alpha}$. In particular, if u_α is continuous and zero at the transition, the symmetry of the control manifolds (7.23)

[13] An exact implementation of the quasi-static single support mode would require a spring with stiffness of $k_1 = 50\,\text{Nm/rad}$ in the hip joints, which is not available for the hardware system yet. If the appropriate spring could be implemented in the system, the corresponding portion of the control would reduce to $\bar{\alpha} = u_\alpha$.

and (7.24), $\bar{\boldsymbol{z}}_{\text{des}}^{\text{right}}(-\bar{\alpha}) = \bar{\boldsymbol{z}}_{\text{des}}^{\text{left}}(\bar{\alpha})$ and vice versa, can be exploited by thresholding $\bar{\alpha}$ w. r. t. the nominal step length α_0, i. e., the transitions from right to left stance and from left to right stance are performed if $-\alpha_0$ and α_0 are crossed from above and below, respectively. However, a step should be initiated only if the corresponding leg is in stance. This can be achieved by holding the reference values at the end of the single support phase (i. e., when the threshold is reached) until the touchdown of the next stance foot is detected. This has the effect of (oscillatory) retraction. The motion of the single support phase can be initiated by setting the control input for the manifold parameter to a constant value $u_\alpha = u_\alpha^0$, when the touchdown is detected.

Note that in the gait control, as proposed above, there is neither feedback of the orientation of the bipedal system w. r. t. the gravitational acceleration nor the walking surface. Additionally, since the control is based on the concept of exploiting the natural dynamics of the plant, also the contact forces are not explicitly controlled. That is, there is no control mechanism implemented, which prevents the robot from falling. As such, a method is proposed, which enables to "dynamically balance" the system by a control action on the single support manifold. To this end, the state of mid-stance is detected, i. e., where the total COM is vertically aligned with ankle joint of the stance leg. Then, depending on the relative leg angle at this state $\alpha_{\text{mid-stance}}(\boldsymbol{q})$, the control input u_α is corrected according to

$$\Delta u_\alpha = k_{\text{mid-stance}} \frac{\alpha_{\text{mid-stance}}(\boldsymbol{q})}{|\alpha_0|} \Delta u_\alpha^{\max}, \tag{7.26}$$

where $k_{\text{mid-stance}}$ and $\Delta u_\alpha^{\max}$ are positive constants. The controller (7.26) updates the control input once per step (at mid-stance). Thereby, an adaption of the length of the *current step* is achieved. This low-gain control action is able to "dynamically balance" the bipedal system. In particular, it excites the system only on its quasi-static oscillation mode.

Experiments

The performance and efficiency of the dynamic walking control, as described above, is validated in experiments on the compliantly actuated, bipedal robot DLR C-Runner introduced in Sect. 7.2.1. To this end, the nominal (polar) step length is set to $\alpha_0 = 15\,\text{deg}$ and the rest angle of the knee joint is chosen to be $\rho_0 = 40\,\text{deg}$. In order to ensure ground clearance, the relative flexion angle of the swing leg is set to $\rho_{\text{flexion}} = 25\,\text{deg}$. Initial tests revealed that the gait can be sustained by setting the nominal input on the control manifold to $u_\alpha^0 = 8.5\,\text{deg}$ and by choosing the parameters of the mid-stance correction controller to be $\Delta u_\alpha^{\max} = 3\,\text{deg}$ and $k_{\text{mid-stance}} = 4$. The controlled system reaches a mean locomotion velocity (averaged over two steps) of $v_{\text{mean}} = 0.61\,\text{m/s}$. Thereby, a mechanical COT based upon the energy expenditure of the motors (i. e., $P_{\text{in}} = \boldsymbol{\tau}_{\text{m}}^T \dot{\boldsymbol{\theta}}$ in (7.12)) of 0.55 is estimated based on measurements of the motor velocities, the motor torques, and the absolute position of bodies (for the total COM motion). Fig. 7.9a depicts the motion of the total COM and the feet during two steps. The motion of the swing foot displays a retraction phase. Additionally, the foot strikes down with the heel, rolls over the foot during the stance phase, and lifts off with the toes. As can be seen in Fig. 7.9b, the travel distance of the links (dashed lines) substantially exceeds the travel distance of the motors (solid lines). In particular, during the retraction phase (where the motor position is constant), the distribution of oscillation amplitudes matches approximately with the

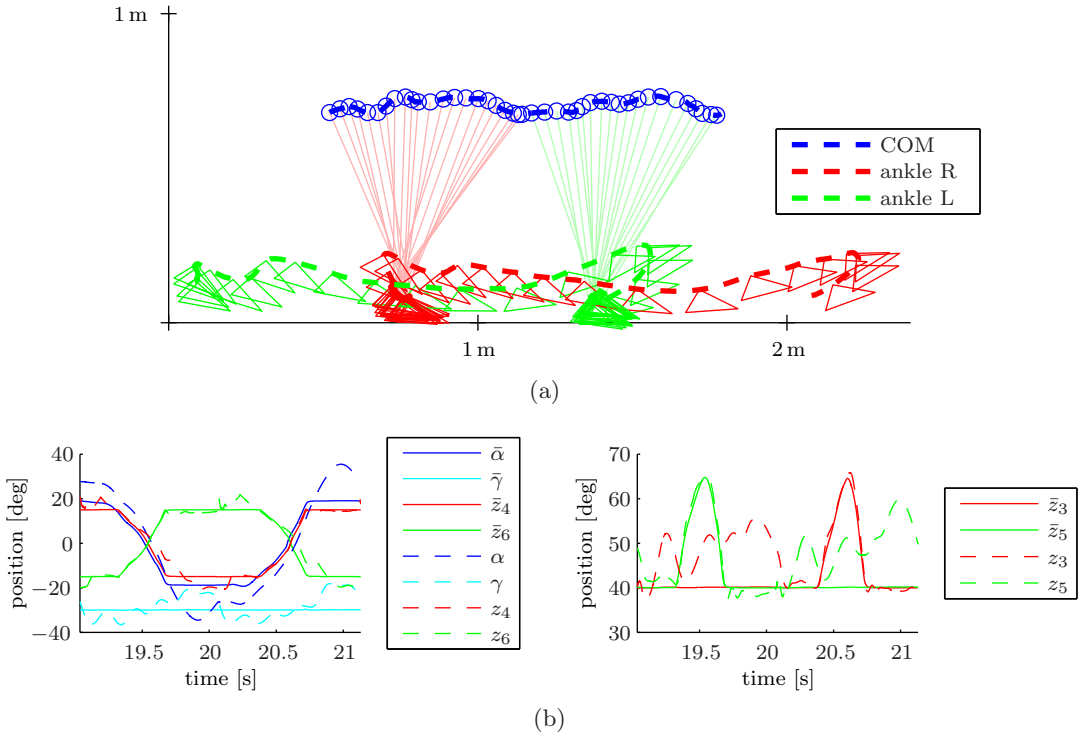

Figure 7.9.: Motion of a complete stride (two steps) recorded during a dynamic walking experiment on DLR C-Runner: (a) total COM and feet; (b) time evolution of virtual equilibrium and link configuration in bipedal task coordinates.

quasi-static single support mode, as identified above. This validates the exploitation of the natural oscillatory dynamics in the generation of the gait.

7.2.4. Running

Running is a dynamic locomotion gait with alternating stance and flight phases. This implies that the total COM oscillates in the direction of gravity. To achieve the locomotion, the legs need to swing forward as well as backward. Since, both motions are oscillatory, an energetically efficient implementation of the gait requires the usage of elastic elements [Ale90]. As proposed by *Raibert* in [Rai86], the bouncing oscillation of the COM can be realized by an elasticity in the direction of the leg axis. The swing leg motion can be implemented by a polar acting spring [Ale90]. In this section, a concept of bi-articular compliant actuation is introduced, for which the elastic behavior is decoupled w. r. t. these fundamental directions of the running gait. Based on this concept, a switching based control to generate a bipedal running gait is proposed [LRSAS14].

Bi-articular compliant actuator design

The bi-articular actuator design is based upon a kinematic structure of the three segment leg as treated in Sect. 7.2.2, i. e., where the segment length of thigh and shank is equal (cf. Fig. 7.7a). The key finding is a particular linkage of the actuator and joint configurations, which yields an input and output decoupled behavior in task-oriented coordinates (7.15) of the articulated leg. Simply speaking, each task-relevant direction is associated

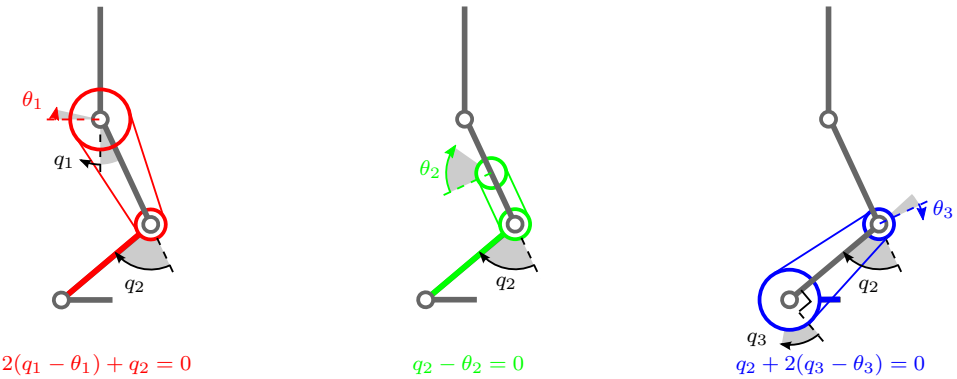

Figure 7.10.: Bi-articular coupling of a human-like three-segment leg which leads to decoupled properties in task-oriented coordinates.

with only a single actuator. To this end, consider the mapping $\boldsymbol{\phi} : \mathbb{R}^3 \times \mathbb{R}^3 \to \mathbb{R}^3$, where

$$\phi_1(\theta_1, q_1, q_2) = 2\,(q_1 - \theta_1) + q_2\,, \tag{7.27}$$
$$\phi_2(\theta_2, q_2) = q_2 - \theta_2\,, \tag{7.28}$$
$$\phi_3(\theta_3, q_2, q_3) = q_2 + 2\,(q_3 - \theta_3)\ . \tag{7.29}$$

The mapping (7.27)–(7.29) can be implemented as kinematic constraints, $\boldsymbol{\phi}(\boldsymbol{\theta}, \boldsymbol{q}) = \mathbf{0}$. This results in independent relations between each of the task-oriented coordinates x_i (defined by (7.15)) and the actuator configurations θ_i, i. e.,

$$x_1 = q_1 + \frac{1}{2}q_2 \overset{\phi_1=0}{=} \theta_1 - \frac{1}{2}q_2 + \frac{1}{2}q_2 = \theta_1\,,$$
$$x_2 = l(q_2) \overset{\phi_2=0}{=} l(\theta_2)\,,$$
$$x_3 = \frac{1}{2}q_2 + q_3 \overset{\phi_3=0}{=} \frac{1}{2}q_2 + \theta_3 - \frac{1}{2}q_2 = \theta_3\,.$$

As visualized by Fig. 7.10, the coupling (7.27) implements a 2 : 1-lever-arm ratio between the actuator in the hip and the knee joint. This leads to a decoupling of the leg angle (cf. Fig. 7.7b). The constraint (7.28) realizes a 1 : 1-lever-arm ratio between actuator and knee joint, which is responsible for actuating motions along the leg axis. The coupling (7.29) implements a 1 : 2-lever-arm ratio between the actuator in the knee and the ankle joint. This leads to a decoupled behavior of the angle of the ankle joint which is measured relative to the leg axis. In summary, to each actuator DOF, only one of the task-oriented coordinates (Fig. 7.7b) is related such that each task direction can be controlled independently. In particular, one can consider each of the mappings ϕ_i in (7.27)–(7.29) as deflections of independent elastic potential functions of the form

$$U_\mathrm{e}(\boldsymbol{\theta}, \boldsymbol{q}) = U_1(\phi_1(\theta_1, q_1, q_2)) + U_2(\phi_2(\theta_2, q_2)) + U_3(\phi_3(\theta_3, q_2, q_3))\,. \tag{7.30}$$

In that case, an input and output decoupled property of the elastic force is achieved. This can be proven by direct calculations, where the inverse of the change of coordinates (7.15) and its Jacobian matrix is utilized, which are provided here for readability:

$$\boldsymbol{q}(\boldsymbol{x}) = \begin{pmatrix} x_1 - \frac{1}{2}l^{-1}(x_2) \\ l^{-1}(x_2) \\ x_3 - \frac{1}{2}l^{-1}(x_2) \end{pmatrix}\,, \quad \frac{\partial \boldsymbol{q}(\boldsymbol{x})}{\partial \boldsymbol{x}} = \begin{bmatrix} 1 & -\frac{1}{2}\frac{\partial l^{-1}(x_2)}{\partial x_2} & 0 \\ 0 & \frac{\partial l^{-1}(x_2)}{\partial x_2} & 0 \\ 0 & -\frac{1}{2}\frac{\partial l^{-1}(x_2)}{\partial x_2} & 1 \end{bmatrix}\,. \tag{7.31}$$

To this end, consider the generalized elastic force in task coordinates, which by applying the chain rule takes the form

$$\frac{\partial U_{\mathrm{e}}(\boldsymbol{\theta}, \boldsymbol{q}(\boldsymbol{x}))}{\partial \boldsymbol{x}} = \frac{\partial U_{\mathrm{e}}(\boldsymbol{q})}{\partial \boldsymbol{q}} \frac{\partial \boldsymbol{q}(\boldsymbol{x})}{\partial \boldsymbol{x}} \,. \tag{7.32}$$

Due to the particular structure of the potential (7.30), the first factor on the right hand side of (7.32) can be rewritten as

$$\begin{aligned}
\frac{\partial U_{\mathrm{e}}(\boldsymbol{\theta}, \boldsymbol{q})}{\partial q_1} &= \frac{\partial U_1(\phi_1)}{\partial \phi_1} \frac{\partial \phi_1(\theta_1, q_1, q_2)}{\partial q_1} = 2 \frac{\partial U_1(\phi_1)}{\partial \phi_1} \\
\frac{\partial U_{\mathrm{e}}(\boldsymbol{\theta}, \boldsymbol{q})}{\partial q_2} &= \frac{\partial U_1(\phi_1)}{\partial \phi_1} \frac{\partial \phi_1(\theta_1, q_1, q_2)}{\partial q_2} + \frac{\partial U_2(\phi_2)}{\partial \phi_2} \frac{\partial \phi_2(\theta_2, q_2)}{\partial q_2} + \frac{\partial U_3(\phi_3)}{\partial \phi_3} \frac{\partial \phi_3(\theta_3, q_2, q_3)}{\partial q_2} \\
&= \frac{\partial U_1(\phi_1)}{\partial \phi_1} + \frac{\partial U_2(\phi_2)}{\partial \phi_2} + \frac{\partial U_3(\phi_3)}{\partial \phi_3} \\
\frac{\partial U_{\mathrm{e}}(\boldsymbol{\theta}, \boldsymbol{q})}{\partial q_3} &= \frac{\partial U_3(\phi_3)}{\partial \phi_3} \frac{\partial \phi_3(\theta_3, q_2, q_3)}{\partial q_3} = 2 \frac{\partial U_3(\phi_3)}{\partial \phi_3} \,.
\end{aligned}$$

Substituting this result together with the Jacobian matrix of (7.31) in (7.32), yields

$$\begin{aligned}
\frac{\partial U_{\mathrm{e}}(\boldsymbol{\theta}, \boldsymbol{q}(\boldsymbol{x}))}{\partial x_1} &= 2 \frac{\partial U_1(\phi_1)}{\partial \phi_1} \,, \\
\frac{\partial U_{\mathrm{e}}(\boldsymbol{\theta}, \boldsymbol{q}(\boldsymbol{x}))}{\partial x_2} &= \frac{\partial l^{-1}(x_2)}{\partial x_2} \left[- \frac{\partial U_1(\phi_1)}{\partial \phi_1} + \frac{\partial U_1(\phi_1)}{\partial \phi_1} + \frac{\partial U_2(\phi_2)}{\partial \phi_2} + \frac{\partial U_3(\phi_3)}{\partial \phi_3} - \frac{\partial U_3(\phi_3)}{\partial \phi_3} \right] \\
&= \frac{\partial l^{-1}(x_2)}{\partial x_2} \frac{\partial U_2(\phi_2)}{\partial \phi_2} \,, \\
\frac{\partial U_{\mathrm{e}}(\boldsymbol{\theta}, \boldsymbol{q}(\boldsymbol{x}))}{\partial x_3} &= 2 \frac{\partial U_3(\phi_3)}{\partial \phi_3} \,.
\end{aligned}$$

Then, by expressing (7.27)–(7.29) in terms of $\boldsymbol{x}$ (i. e., by utilizing $\boldsymbol{q}(\boldsymbol{x})$ of (7.31)), it can be finally seen that

$$\frac{\partial U_{\mathrm{e}}(\boldsymbol{\theta}, \boldsymbol{q}(\boldsymbol{x}))}{\partial x_1} = 2 \frac{\partial U_1(\phi_1)}{\partial \phi_1} \bigg|_{\phi_1 = 2(x_1 - \theta_1)} =: f_{\mathrm{x},1}(x_1 - \theta_1) \,, \tag{7.33}$$

$$\frac{\partial U_{\mathrm{e}}(\boldsymbol{\theta}, \boldsymbol{q}(\boldsymbol{x}))}{\partial x_2} = \frac{\partial l^{-1}(x_2)}{\partial x_2} \frac{\partial U_2(\phi_2)}{\partial \phi_2} \bigg|_{\phi_2 = l^{-1}(x_2) - \theta_2} =: f_{\mathrm{x},2}(l^{-1}(x_2) - \theta_2) \,, \tag{7.34}$$

$$\frac{\partial U_{\mathrm{e}}(\boldsymbol{\theta}, \boldsymbol{q}(\boldsymbol{x}))}{\partial x_3} = 2 \frac{\partial U_3(\phi_3)}{\partial \phi_3} \bigg|_{\phi_3 = 2(x_3 - \theta_3)} =: f_{\mathrm{x},3}(x_3 - \theta_3) \,. \tag{7.35}$$

This means that for each $i = 1, 2, 3$, the component of the generalized elastic force which is dual to $\dot{x}_i$, $f_{\mathrm{x},i}(x_i, \theta_i)$, depends only on x_i and θ_i.

Control of a running gait

Due to the input and output decoupled property of the generalized elastic force w. r. t. the task-oriented coordinates (7.15), as shown by (7.33)–(7.35), each of the subtask of a legged locomotion gait can be associated with a single control input θ_i. This will be exemplary shown for a bipedal running gait. The concept of the controller is to switch between simple time-continuous and constant control actions based on state dependent events. These events are either the touchdown TD, takeoff TO or an thresholding of

the elastic force along the axis of the stance leg, $\tau_{\mathrm{x},2}^{\mathrm{st}} := -f_{\mathrm{x},2}(l^{-1}(x_2^{\mathrm{st}}) - \theta_2^{\mathrm{st}})$. For the latter type of events, it is distinguished, whether $\tau_{\mathrm{x},2}^{\mathrm{st}}$ crosses the value of $\epsilon_{\tau_{\mathrm{x},2}\uparrow} > 0$ or $\epsilon_{\tau_{\mathrm{x},2}\downarrow} > 0$ from below or above, respectively. The corresponding events are referred to as *axial spring loading* or *unloading*, respectively. For simplicity, the effect of gravity on the virtual equilibrium configuration of the system is neglected, i. e., $\theta_1 = \bar{x}_1$, $\theta_2 = l^{-1}(\bar{x}_2)$ and $\theta_3 = \bar{x}_3$. This avoids to consider a contact state dependent gravity model in the feedback. In order to control the absolute orientation of the main body φ (and its time derivative $\dot{\varphi}$) only during the stance phase, the elastic torque (dual to $\dot{x}_1^{\mathrm{st}}$) is considered as control input instead of θ_1^{st}, i. e., $\theta_1^{\mathrm{st}} = (f_{\mathrm{x},1})^{-1}(\tau_{\mathrm{x},1}^{\mathrm{des}}) + x_1^{\mathrm{st}}$

A half cycle of the proposed running gait control (from the TD of one leg to the TD of the other leg) comprises five finite states: *spring loading, main body stabilization, mid-stance, pushoff initiation, and landing.* All quantities of the leg, which is in stance or swing phase during the considered half cycle, are denoted by the superscript $(\cdot)^{\mathrm{st}}$ or $(\cdot)^{\mathrm{sw}}$, respectively.

Spring loading The transition to that state is triggered by the touchdown event TD. The main purpose of this state is to assure the ground contact, which is required to stabilize the main body by control. This can be achieved by loading the spring along the leg axis w. r. t. the rest length $l_0 > 0$, which the current stance leg has displayed already during the last flight phase and by setting the rest angle of the stance foot to its configuration at TD, i. e., $\theta_2^{\mathrm{st}} = l^{-1}(l_0)$ and $\theta_3^{\mathrm{st}} = -\varphi(\mathrm{TD}^{\mathrm{st}}) - x_1^{\mathrm{st}}(\mathrm{TD}^{\mathrm{st}})$, respectively. Since in this phase, the contact state is not ensured, the hip torque of the stance leg compensates only for gravity, i. e., $\tau_{\mathrm{x},1}^{\mathrm{des}} = \tau_{\mathrm{g}}(\varphi)$, where $\tau_{\mathrm{g}}(\varphi)$ contains the model of the gravitational torque of the main body. The control inputs corresponding to the hip joint and axis of the stance leg are held to the constant values of the previous (finite) state, $\theta_1^{\mathrm{sw}} = x_1^{\mathrm{sw}}(\mathrm{TO}^{\mathrm{sw}})$ and $\theta_2^{\mathrm{sw}} = l^{-1}(l_{\mathrm{flexion}})$ with $0 < l_{\mathrm{flexion}} < l_0$, respectively. The swing foot is kept statically parallel to the ground, i. e., $\theta_3^{\mathrm{sw}} = -\varphi - x_1^{\mathrm{sw}}$. This control action is active over the duration of the complete step.

Main body stabilization The transition to this state occurs, when the ground contact is assured. This is detected by thresholding the axial spring compression $\tau_{\mathrm{x},2}^{\mathrm{st}}$ from below w. r. t. $\epsilon_{\tau_{\mathrm{x},2}\uparrow}$. During this phase, the main task of the stance leg is stabilizing the orientation of the main body w. r. t. a reference φ_{des}. This is achieved by PD control with gravity compensation $\tau_{\mathrm{x},1}^{\mathrm{des}} = \tau_{\mathrm{g}}(\varphi) + k_{\mathrm{P}}(\varphi - \varphi_{\mathrm{des}}) + k_{\mathrm{D}}\dot{\varphi}$, where $k_{\mathrm{P}} > 0$ and $k_{\mathrm{D}} > 0$ are constant controller gains. In order to bear the torque required for the stabilization of the main body, the resting angle of the ankle joint is adjusted such that the stance foot is statically parallel to the locomotion surface, i. e., $\theta_3^{\mathrm{st}} = -\varphi(\mathrm{EN}) - x_1^{\mathrm{st}}(\mathrm{EN})$, where EN denotes the time instance of the current (finite) state entry. At the same time, the angle of the swing leg is already prepared for the upcoming touchdown (although the bipedal system is still in stance). To this end, a foot placement algorithm similar to what was proposed in [Rai86] is considered. The "low gain" control is based upon measurements of the duration and averaged velocity of the previous stance phase, $T_{\mathrm{s}} = t(\mathrm{TO}) - t(\mathrm{TD})$ and $v_{\mathrm{mean}} = \frac{1}{T_{\mathrm{s}}} \int_{t(\mathrm{TD})}^{t(\mathrm{TO})} v_{\mathrm{b}}(r)\mathrm{d}r$, respectively:

$$\mathrm{fp}(v_{\mathrm{mean}}, v_{\mathrm{des}}, \varphi, x_2^{\mathrm{sw}}) = -\varphi - \arcsin\left(\frac{x_{\mathrm{f}}(T_{\mathrm{s}}, v_{\mathrm{mean}}, v_{\mathrm{des}})}{x_2^{\mathrm{sw}}}\right), \tag{7.36}$$

$$x_{\mathrm{f}}(T_{\mathrm{s}}, v_{\mathrm{mean}}, v_{\mathrm{des}}) = \frac{v_{\mathrm{mean}} T_{\mathrm{s}}}{2} + k_{\mathrm{v}}\left(v_{\mathrm{mean}} - v_{\mathrm{des}}\right). \tag{7.37}$$

The first term of the foot placement control (7.37) implements a feed-forward action, which is based on the assumption of a symmetric stance phase evolution. The latter term in (7.37) realizes a proportional control to regulate v_{mean} to v_{des}, where $k_{\text{v}} > 0$ denotes a constant gain. The algorithm is implemented in the hip joint of the swing leg, i. e., $\theta_1^{\text{sw}} = \text{fp}(v_{\text{mean}}, v_{\text{des}}, \varphi, x_2^{\text{sw}})$, according to (7.36) and (7.37). The foot-placement control remains active until the next touchdown event (of the current swing foot) occurs.

Mid-stance The mid-stance is detected by thresholding the axial spring compression $\tau_{\text{x},2}^{\text{st}}$ from below w. r. t. $\epsilon'_{\tau_{\text{x},2}\uparrow}$. Alternatively, the zero-crossing of the rate of change of $\tau_{\text{x},2}^{\text{st}}$ can be utilized. This (finite) controller state is responsible for preparing the pushoff by unloading the spring corresponding to the ankle of the stance leg. This is achieved by continuously adjusting the corresponding rest angle to $\theta_3^{\text{st}} = -\varphi - x_1^{\text{st}}$. Note that this has the effect of "zero torque" control.

Pushoff initiation The pushoff is initiated in the phase, where the axial spring of the stance leg decompresses. This can be detected by thresholding the corresponding elastic force $\tau_{\text{x},2}^{\text{st}}$ with $\epsilon_{\tau_{\text{x},2}\downarrow}$ from above. The control action, which initiates the pushoff, adds a constant offset $\hat{\beta} > 0$ to the resting angle, for which the stance foot is statically parallel to the locomotion surface, i. e., $\theta_3^{\text{st}} = \hat{\beta} - \varphi - x_1^{\text{st}}$. Simultaneously, the main body stabilization is deactivated, i. e., $\tau_{\text{x},1}^{\text{des}} = \tau_{\text{g}}(\varphi)$. All other control tasks remain unchanged.

Landing The flight phase is triggered by the takeoff event TO. At the entry instance of this (finite) state, the previous stance leg is flexed to prepare for the subsequent swing phase, and the previous swing leg is extended to prepare for the following stance phase, i. e., $\theta_2^{\text{st}} = l^{-1}(l_{\text{flexion}})$, and $\theta_2^{\text{sw}} = l^{-1}(l_0)$, respectively. Additionally, the rest angles of hip and ankle (of the previous stance leg) are set to their link-side values at the takeoff event, i. e., $\theta_1^{\text{st}} = x_1^{\text{st}}(\text{TO})$ and $\theta_3^{\text{st}} = \hat{\beta} - \varphi(\text{TO}) - x_1^{\text{st}}(\text{TO})$, respectively. At the exit instance of this controller state, i. e., at the touchdown event of the next stance leg, the labels $(\cdot)^{\text{st}}$ and $(\cdot)^{\text{sw}}$ can be considered as interchanged in between the legs.

Simulations

The bi-articular compliant actuator concept and its application to bipedal running is validated by simulations. To this end, a bipedal system is considered, which features a human-like mass distribution with a total body mass of $m = 80\,\text{kg}$, comprising $0.75m$ for the trunk, $0.0625m$ for each thigh, $0.0375m$ for each shank, and $0.025m$ for each foot. Thighs and shanks have segment lengths of $b = 0.5\,\text{m}$. Each foot has a segment length of $0.2\,\text{m}$. The ankle joint of each foot is located at 25% of the foot length measured w. r. t. the heel. The COM of the trunk is $0.3\,\text{m}$ above the hip. The COM of thighs and shanks are at 40% of the segments lengths (proximal) and the COM of each foot is at 30% of the forefoot length measured w. r. t. the ankle joint. For the bi-articular compliant actuators, quadratic potential functions of the form $U_{\text{e,leg}} = \frac{1}{2}\sum_{i=1}^{3} k_i \phi_i^2$ are considered for each leg. Thereby, initial simulation tests revealed that stable running can be achieved by selecting the stiffness values as $k_1 = 200\,\text{Nm/rad}$, $k_2 = 1000\,\text{Nm/rad}$, and $k_3 = 600\,\text{Nm/rad}$. For the link-side damping matrix, the same structure as for the stiffness matrix $\partial^2 U_{\text{e,leg}} / \partial \boldsymbol{q}_{\text{leg}}{}^2$ is assumed (where $\boldsymbol{q}_{\text{leg}} \in \mathbb{R}^3$ denotes the joint variables of one leg). Thereby, the linear, viscous friction coefficients are assumed to be $d_1 = d_3 = 10\,\text{Nms/rad}$, and $d_2 = 25\,\text{Nms/rad}$. The forward dynamics of the resulting system is computed based

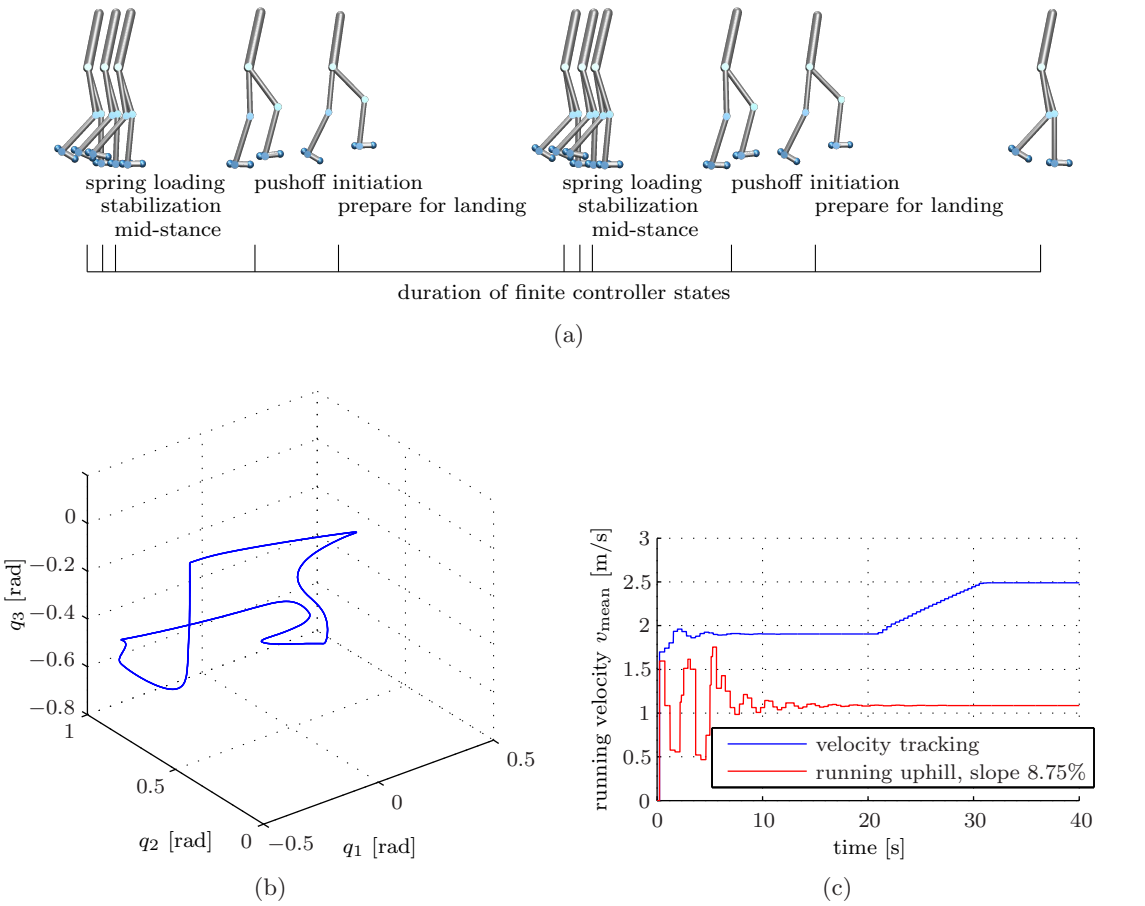

Figure 7.11.: Bipedal running based on the task-oriented, input and output decoupled bi-articular actuator design: (a) visualization of a complete gait cycle; (b) motion of joint configuration (five cycles); (c) velocity tracking and running uphill a constant slope with constant, desired velocity.

on the articulated body algorithm [Fea08] and a point version of the compliant contact model [AF10]. The resulting ordinary differential equations (including the control) are integrated in Matlab/Simulink® using a variable step solver.

The parameters of the stabilization controller for the main body are set to $k_{\text{P}} = 1000\,\text{Nm/rad}$ and $k_{\text{D}} = 200\,\text{Nms/rad}$, and the desired orientation is $\varphi_{\text{des}} = 0$. To indicate the axial spring loading, the maximum compression and the unloading, threshold values of $\epsilon_{\tau_{\text{x},2}\uparrow} = 400\,\text{N}$, $\epsilon'_{\tau_{\text{x},2}\uparrow} = 1150\,\text{N}$ and $\epsilon_{\tau_{\text{x},2}\downarrow} = 600\,\text{N}$ are found by manual search, respectively. Simulation tests revealed that by selecting a rest length for the stance leg of $l_0 = 0.99 \cdot 2b$ and for the swing leg of $l_{\text{flexion}} = 0.9 \cdot 2b$, ground clearance of the swing foot can be assured. The amplitude of the pushoff in the ankle is set to $\hat{\beta} = \frac{1}{6}\pi\,\text{rad}$. The proportional gain, as required for the control of the locomotion velocity (7.37), is chosen to be $k_{\text{v}} = 0.2\,\text{s}$ (which corresponds to almost the highest possible value).

All simulations started with an initial guess of the stance duration of $T_{\text{s}} = 0.2\,\text{s}$. On the basis of this initial guess and the reference values φ_{des} and v_{des}, the initial condition $x_1^{\text{st}}(0)$ is computed by (7.36) and (7.37). The remaining initial configurations are set to $x_2^{\text{st}}(0) = l_0$, $x_3^{\text{st}}(0) = -(\varphi_{\text{des}} + x_1^{\text{st}}(0))$, $x_1^{\text{sw}}(0) = -x_1^{\text{st}}(0)$, $x_2^{\text{sw}}(0) = l_{\text{flexion}}$, and $x_3^{\text{sw}}(0) = -(\varphi_{\text{des}} + x_1^{\text{sw}}(0))$. To obtain the corresponding joint angles, the inverse change of coordinates (7.31)

is considered. The initial actuator configurations result from (7.27)–(7.29). The initial conditions of the main body are chosen such that for $\varphi(0) = \varphi_{\text{des}} = 0$, the landing foot almost touches the ground. All initial conditions at velocity level except the vertical velocity of the main body are set to zero.

The first simulation test aims at investigating the steady-state behavior of the closed-loop system. To this end, a desired locomotion velocity of $v_{\text{des}} = 2\,\text{m/s}$ is selected. Fig. 7.11a shows a stroboscopic picture of a complete gait cycle. Fig. 7.11b shows the motion of the joint configuration of one leg. Five cycles in the steady-state phase of the running motion are plotted. The periodicity of the motion can be clearly seen. The following two simulations demonstrate the convergence behavior of the closed-loop system. Fig. 7.11c depicts the results of both simulations starting with the same initial conditions. In the first simulation, the desired locomotion velocity is linearly increased in the time interval of 20 s to 30 s from $v_{\text{des}} = 2\,\text{m/s}$ to $v_{\text{des}} = 3\,\text{m/s}$. In the second simulation, the system runs uphill a constant slope of 8.75 %, while the desired locomotion velocity is set to $v_{\text{des}} = 2\,\text{m/s}$. Both tests clearly demonstrate the ability of the system to converge to different periodic orbits of bipedal running, even in case of an inclination w. r. t. gravity.

7.3. Summary

In this chapter it is demonstrated that the concept of oscillation modes and corresponding control approaches, as proposed in this thesis, can be effectively applied to real world tasks of legged locomotion. Thereby, the contribution is twofold: the theory of oscillation modes supports the design of the mechanical system, and yields simple and robust yet effective controls to achieve the rather "complex" behavior of dynamic locomotion gaits. The concept of eigenmodes of nonlinear dynamics and the corresponding method of its embodiment forms the basis of the compliantly actuated quadruped Bert. On the basis of the quadrupedal pronk and trot gait, it is validated theoretically as well as experimentally that the dynamics of the fundamental SLIP model can be embodied in articulated legged multibody systems. The presented examples of bipedal dynamic walking (experimentally validated) and running (verified by simulation) show how the notion of nonlinear oscillation modes and input/output decoupling of elasticities can be exploited in the system (i. e., stiffness selection) as well as controller design, respectively. As the current quadrupedal and bipedal robotic systems serve only as test platforms for a first proof of concept, and since the parameters of the controllers are not tuned optimally yet, a substantial increase regarding performance and energetic efficiency can be expected in future versions of system designs and corresponding experimental tests. Moreover, a further application of a modal control approach to legged locomotion is presented in [SLOAS17]. Herein, the modally adaptive periodic motion, as presented in Sect. 6.3, is applied to a compliantly actuated single-leg hopper which features an oscillation mode. Thereby, it is shown by numerical optimal control as well as in a statistically significant experiment on the real-hardware that the proposed modally adaptive control (Sect. 6.3) is optimal w. r. t. the maximization of the jumping height for constant energy input. Finally, it is worth mentioning that in this thesis, the focus was on the high performance and energetically efficient tasks of legged locomotion. In parallel, a project has been initiated, which aims at validating versatility w. r. t. different gaits and movement in difficult terrain by means of the same robotic system as used for the high performance tasks. For example, the actuators of the quadruped Bert are currently revised such that a torque interface at joint-level can be provided, which is, e. g., required to realize the modal shaping approach (Sect. 6.2)

on the hardware. By showing performance and energetic efficiency as well as versatility on the same compliantly actuated legged system, a rigorous validation of the concept of oscillation modes will be obtained.

CHAPTER 8

Conclusion, Discussion and Outlook

The introduction of elastic elements in classically rigid robotic and mechanical systems yields a variety of potential advantages such as energetic efficiency, mechanical robustness, and realizability of versatile tasks. At the same time, the resulting nonlinear oscillatory behavior gives rise to fundamental research questions such as the existence or even the unpredictability of resonance-like motions in the single degree of freedom case. Intuitively and from simple considerations, it is clear that elastic multibody systems display periodic motions. However, the initial ideas that, e. g., linear modal analysis generalizes to the nonlinear case, had been merely a conjecture. As such, the theoretical evidence on how to efficiently control compliantly actuated systems was sparse. The ultimate goal of this thesis was to deepen the understanding and to learn how to control such nonlinear oscillatory systems strong focus on the practical feasibility and relevance w. r. t. robotic tasks. Thereby, the aim was to convert intuitive observations into theoretical foundations. Towards the vision to approach or even surpass the performance and energetic efficiency of biological systems by robots, the very basic insights and comprehensions of such nonlinear dynamics are indispensable. The approach of this dissertation is solving this holistic problem in the areas of *limit cycle generation*, *dimensionality reduction of nonlinear dynamics* and *robust modal control*. This closes the loop from intuitive observations over theoretical understanding to application and back to experimental verification.

8.1. Conclusion and discussion

In this section, the main findings and results reported in this thesis are summarized and discussed.

8.1.1. Limit cycle control

Due to the unpredictability of steady-state solutions of forced nonlinear oscillations, the generation of resonance-like limit cycles is already challenging in the single-DOF case. In Chapt. 4, a switching-based control principle is introduced, which is shown to be able to generate a unique and attractive closed orbit in a large class of physically relevant, planar Euler-Lagrange dynamics. The controller achieves that solely by a thresholding feedback

of state measurements at position level. By switching based on a non-zero threshold value, the controller is robust against sensor noise. In particular, the control principle can be implemented such that *no model-parameter knowledge is required in the feedback*. This stands in contrast to limit cycle controllers based on the Van der Pol oscillator respectively energy regulation principle. They need to feedback the full state (position and velocity). Additionally, they require at least the model-knowledge of dissipative and potential forces of the plant to compute the control. For the stability analysis of the switching-control-based closed-loop system, non-standard statements are proposed to prove the existence, uniqueness, and attractiveness of resulting hybrid closed orbits. The basic argument is a balance of energy input by the controller and energy dissipated by the plant along the continuous portion of the hybrid, periodic trajectory. The control principle is such that during the dissipative motion, the controller output is constant (natural oscillation). Therefore, by assuming that any motion of the motor (control input) is associated with energetic losses, it can be concluded that the proposed limit cycle control is energetically efficient in a sense that it injects the minimum amount of energy, which is required to sustain the limit cycle. The question of energetic efficiency of the controller principle can be (partially) answered by the finding that the structure of the proposed controller is similar to the optimal control which maximizes any unsigned linear combination of the state for a bounded control input (injected energy) [ÖH13]. In addition to solving the problem of energy-efficient limit cycle generation, novel existence, uniqueness and attractiveness statements are found. They may be regarded as extensions of the well-known Poincaré-Bendixson theorem and Lohmiller's contraction analysis for a particular but practically relevant class of planar, hybrid Euler-Lagrange systems.

8.1.2. Oscillation modes

Dimensionality reduction is a concept to ensure the existence of periodic motions in conservative multibody systems. Additionally, it suggests a way to control nonlinear-oscillations in non-conservative, compliantly actuated robotic systems. However, dimensionality reduction in case of the nonlinear dynamics at hand represents a highly challenging and mostly unresolved problem. As such, state-of-the-art methods are either not applicable or not feasible (w. r. t. obtaining closed-form solutions or sufficiently accurate approximations). In Chapt. 5, a novel concept has been proposed to describe the natural oscillatory or periodic behavior of multibody systems with elasticities. The general definition of what are called *oscillation modes* of nonlinear dynamics is introduced as invariant, one-dimensional and differentiable submanifolds of the configuration space. In a certain coordinate system, the one-dimensional curves of invariant configurations appear as straight lines. Such so-called modal lines have been shown to exist for systems of constant inertia but nonlinear and coupled springs. However, the algebraically testable conditions of the proposed theorem on oscillation modes allowed to introduce a methodology to embody desired one-dimensional dynamics of a given task in the mechanical design of elastic multibody systems. This way it was possible to find examples of such nonlinear dynamics featuring oscillation modes, which include also Coriolis/centrifugal effects. To the best of the author's knowledge, these are the first examples reported so far, in which the existence of one-dimensional, invariant manifolds for nonlinear, multibody systems with elasticities are validated. Nevertheless, from a theoretical point of view, the definition of oscillation modes is less general than the one of normal modes proposed by Shaw and Pierre in [SP93]. However, the conditions on the existence of oscillation modes are merely of algebraic form. This stands in marked contrast to the Shaw and Pierre definition of nor-

mal modes, where the proof of existence involves a system of nonlinear partial differential equations. In particular, as validated in the application from Chapt. 7, the proposed definition of oscillation modes captures a relevant class of system and task dynamics such as the mass-spring template model, which has been empirically shown to be fundamental in legged locomotion [Bli89]. The nonlinear dynamics of the pantograph leg, as presented in Sect. 5.2.2, is structurally equivalent to the dynamics of the SLIP model for a large range of realistic geometric and inertial parameters of the leg segments.

8.1.3. Modal control

The concept of oscillation modes forms a basis for natural oscillatory and periodic motions in compliantly actuated systems. However, the exploitation of such plant-inherent motions in robotic tasks demands appropriate control. This thesis contributes four approaches which achieve the generally opposing goals of feasibility, versatility, robustness, and energetic efficiency to different extent.

The concept of modal globalization (Sect. 6.1) is to consider the intrinsic oscillatory behavior of compliantly actuated systems locally (linearization) and to design the control such that it becomes valid globally. As such, by this control strategy, it is possible to realize decoupled, scalar, oscillatory dynamics for any statically controllable compliantly actuated system, since the method relies solely on the positive definiteness of the linearized plant dynamics. Although the controller performs dynamics shaping, energetic efficiency can be gained, as the plant-inherent inertia and the local stiffness matrix are maintained. This has been validated in experiments with the DLR Hand Arm System. An additional theoretical finding is the controller gain design and corresponding strict Lyapunov function approach, which allows to guarantee exponential decay of oscillations in undesired modes.

The method of modal shaping control, as introduced in Sect. 6.2, increases the versatility of possible tasks, where high performance and energetic efficiency are of paramount importance. The controller allows to realize any one-dimensional, attractive task manifold, as long as the shape of the embedded curve is diffeomorphic to a circle or a line. This comes generally at the price of performance and energy efficiency. However, it has been shown by simulation that the control method covers the case of stabilizing an inherent oscillation mode of the plant.

Oscillation modes are intrinsic properties of the plant. Even if their existence is guaranteed, e. g., by embodiment in the mechanical design, the knowledge of their exact geometric shape cannot be presumed due to model uncertainties. The method of what is called modally adaptive periodic motion control, as proposed in Sect. 6.3, solves this robustness issue, and represents therefore one of the core contributions of this thesis. The basic concept is to excite an oscillation based on an initial guess of the shape of the mode and then successively adapt to the oscillation mode and simultaneously improve the excitation by observations of resulting motions. This is achieved with at most the model knowledge of the potential function of the plant, and solely feedback of measurements of the state at position level. Several experiments with the DLR Hand Arm System revealed that even the model-parameter knowledge of the potential can be neglected in the controller implementation, i. e., merely the deflection of springs (instead of potential forces) can be considered in the control. Therefore, it can be concluded that the method is very robust against model uncertainties and sensor noise. In particular, investigations initiated and related to this thesis have shown by simulations and experiments for a task of a jumping leg, that the proposed modally adaptive periodic motion is closely optimal regarding the jumping height [SLOAS17].

Finally, the proposed methodology of modal matching (Sect. 6.4) exploits the nonlinear configuration dependency of the dynamics of multibody systems to match and control the direction of local eigenvectors to a desired task. On the basis of this concept, an effective method is introduced to control highly dynamic locomotion in compliantly actuated legs. The controller is conceptually validated by simulations of a jumping leg, where almost constant forward movement (instantaneous locomotion velocity) is achieved. Therefore, the method of modal matching closes the gap between the goals of task versatility and energetic efficiency.

8.1.4. Legged locomotion

Legged locomotion is an intrinsically oscillatory or even periodic task such that the application of the theory of oscillation modes, as introduced in Chapt. 5, and corresponding cyclic motion and modal control methods (Chapt. 4 and 6) potentially leads to high performance and energetic efficiency. The benefits of springs in legged locomotion have already been recognized by energetic considerations of Alexander [Ale90]. In particular, there is plenty of empirical evidence that high-dimensional, nonlinear dynamics of complex legged animals collapses to template models of highly reduced order. Additionally, such fundamental low-order dynamics models of locomotion such as the spring loaded inverted pendulum (SLIP) have been implemented in robotic systems by virtual model control. Nevertheless, the theoretical question, how the SLIP model (consisting of a constant point mass and a radially acting spring) can be intrinsically realized in the already geometrically nonlinear multibody system of an articulated leg, has not been answered yet. Section 5.2.2 provides a closed-form example, which validates that the dynamics of the SLIP model can be embodied in the mechanical design of a physically realizable mechanism of a pantograph leg. By this finding, the hypothesis of biologists about templates and anchors, as mentioned above, is substantiated from a theoretical point of view. Chapter 7 further validates the theoretical and methodological results by implementations in real robotic systems, applications to tasks of legged locomotion and finally by conducted experiments. Thereby, the contributions of Chapt. 7 are twofold: First, it is shown how the theory of oscillation modes can be applied to support the mechanical design of compliantly actuated quadrupedal and bipedal robotic systems. Secondly, simple and robust controllers are proposed, which exploit the embodiment of oscillation modes to implement the rather "complex" behavior of dynamic locomotion gaits, and their performance and efficiency is validated in a series of experiments. This closes the loop from empirical findings over theoretical foundations back to relevant applications and their experimental validation.

8.2. Outlook

The ultimate goals, as defined in the problem statement of this thesis (Sect. 1.2), were gaining the understanding for natural motions of highly nonlinear, elastic multibody systems and exploiting the acquired insights to increase performance and efficiency in the execution of robotic tasks. Towards these aims, it was possible to contribute to the research areas of limit cycles, dimensionality reduction of nonlinear dynamics, and multi-dimensional oscillatory and periodic motion control. In addition to these theoretical contributions, a first proof of concept of the introduced methodologies was performed by implementations in robotic systems and real-hardware experiments. Due to the richness and "complexity" of the nonlinear systems and tasks at hand, the problem of understanding and exploiting

natural nonlinear oscillations is for sure not completely solved yet. However, the investigations reported in this thesis yielded further relevant theoretical problem statements in the field of nonlinear system analysis and control, interdisciplinary hypotheses as well as engineering issues, which will be briefly discussed in the following paragraph.

The switching-based limit cycle control (Chapt. 4) has been derived from observations of human motor control and turned out to be a robust and efficient method to excite and sustain periodic motions in a broad class of one-dimensional nonlinear systems. Qualitative comparisons of the controller structure with analytical optimal control results suggest a matching of principles. Therefore, the mathematical proof of optimality would strongly impact the scientific relevance of the proposed control method on the one hand, but would possibly also help to derive other related feedback structures from existing feed-forward controls on the other hand. Section 5.3 addresses the existence of closed energy-level sets and the excitability of periodic orbits in non-conservative, nonlinear systems. To this end, a classification theorem for periodic motions is proposed, which is based on classical results of point-set topology. Utilizing this straightforwardly testable statement in a simulation study revealed that the multi-pendulum with elasticities in the joints displays also periodic motions, which cannot be described by the concept of a one-dimensional, differentiable manifold. In particular, it has been observed that the geometric shape of the curve of configuration evolutions depends on the magnitude of the applied initial velocity. This observation suggests a non-holonomic structure of resulting centres and raises the question of underlying physical principles which lead to the periodicity. Further related research issues have been initiated by the discovery of the modally adaptive periodic motion control, as introduced in Sect. 6.3. The equivalence of the modal adaptation law and the well studied recursive principle component analyzer, known as Oja's rule, in combination with the hybrid excitation control induct a fundamentally novel stability theory, which may combine the concepts of stochastic convergence, bounded-input-bounded-output stability, and the hybrid-dynamical-system statements proposed in Chapt. 4. Besides these theoretical outcomes, the finding of the modally adaptive concept initiated a hypothesis of motor control in biological systems, of which first conceptual validation results have been obtained within a doctoral research project launched in parallel to the investigations of this thesis [LAS14a], [SLAS16].

The experiments, as provided in the context of dynamic legged locomotion (Chapt. 7), serve as a first proof of concept. They reinforce the evidence that by the vigorous efforts currently put in the engineering part of the mechatronic design (e. g., in the development of the electrical drives), a rigorous validation of the proposed theory can be performed, such that versatile legged robots will become able to approach or even surpass the biological archetypes regarding performance and energetic efficiency. The author's vision is to contribute the theory to create a system being able to reach areas, where neither biological nor current technical system could go before. Maybe, one day, such a legged robot will support the discovery of *extra-terrestrial life* in planetary exploration missions.

APPENDIX A

Appendix

A.1. Proof of Proposition 4.1

Consider as candidate Lyapunov function the Hamiltonian $H(\boldsymbol{x})$ of the system (4.11), i. e.,

$$V(\boldsymbol{x}) := H(\boldsymbol{x}) = T(x_2) + U(x_1)\,, \tag{A.1}$$

where $T(x_2) = \frac{1}{2}Mx_2^2$. The function $V(\boldsymbol{x})$ is positive definite in $\boldsymbol{x}$ since $U(x_1)$ is positive definite in x_1 (cf. Assumption 4.1) and $T(x_2)$ is positive definite in x_2 by definition. The derivative along the solution of (4.11), $\dot{V}(\boldsymbol{x}) = -d(x_1, x_2)x_2 \leq 0$, is non-positive due to Assumption 4.2. As a result the origin $\boldsymbol{x} = \boldsymbol{0}$ is stable in a sense of Lyapunov [SL91, Theorem 3.2, p. 62]. By hypothesis of Assumption 4.2, $-d(x_1, x_2)x_2 = 0$ only if $x_2 = 0$. But $x_2 = 0$ implies that $\ddot{x}_1 = -\frac{1}{M}\partial U(x_1)/\partial x_1$ which is non-zero as long as $x_1 \neq 0$ according to Assumption 4.1. The system cannot remain in the set $\mathcal{R} = \{\boldsymbol{x} \in \mathbb{R}^2 \,|\, x_2 = 0\}$ except at $\boldsymbol{x} = \boldsymbol{0}$ since the largest invariant set in $\mathcal{R}$ is the origin $\boldsymbol{x} = \boldsymbol{0}$ itself. Therefore, the system is locally asymptotically stable according to La Salle's invariance principle [SL91, Theorem 3.4, p. 69]. Since $V(\boldsymbol{x})$ is radially unbounded, i. e., $V(\boldsymbol{x}) \to \infty$ if $\|\boldsymbol{x}\| \to \infty$, the above argumentation holds globally. As a result, the origin $\boldsymbol{x} = \boldsymbol{0}$ of the system (4.11) is globally asymptotically stable [SL91, Theorem 3.5, p. 73].

A.2. Algorithms

A.2.1. Solving the linearized modal matching problem

The problem (5.23) can be solved by applying Newton's method for nonlinear algebraic equations. Thereby, an iteration step $\Delta\boldsymbol{\zeta}_1$ is given by the solution of the system of linear equations

$$\begin{aligned}
&\sum_{i=1}^{N_\mathrm{q}} \sum_{j \in \mathcal{J}} \frac{1}{2} \boldsymbol{H}_j \left(\boldsymbol{w}_j(\boldsymbol{q}_i, \boldsymbol{\zeta}_1)\right) \left(\boldsymbol{w}_j(\boldsymbol{q}_i, \boldsymbol{\zeta}_1) - \boldsymbol{w}_j^{\mathrm{des}}\right) \\
&= \frac{1}{\gamma} \sum_{i=1}^{N_\mathrm{q}} \sum_{j \in \mathcal{J}} \frac{1}{2} \boldsymbol{H}_j \left(\boldsymbol{w}_j(\boldsymbol{q}_i, \boldsymbol{\zeta}_1)\right) \boldsymbol{G}_j(\boldsymbol{q}_i, \boldsymbol{\zeta}_1) \Delta\boldsymbol{\zeta}_1
\end{aligned}$$

where $\gamma > 0$ controls the step length and $\mathcal{J} \subseteq \{1, \ldots, n\}$. Due to the normalization condition (5.7), the Jacobian matrices

$$\boldsymbol{G}_j(\boldsymbol{q}_i, \boldsymbol{\zeta}_1) = \frac{\partial \boldsymbol{w}_j(\boldsymbol{q}_i, \boldsymbol{\zeta}_1)}{\partial \boldsymbol{\zeta}_1}\,. \tag{A.2}$$

are rank deficient, i. e., $\operatorname{rank}(\boldsymbol{G}_j(\boldsymbol{q}_i, \boldsymbol{\zeta}_1)) = n - 1$, even in cases $n \leq N_1$. This problem of rank deficiency can be solved by transforming the components of the eigenvectors to coordinates $\boldsymbol{y}_j = \boldsymbol{y}(\boldsymbol{w}_j) \in \mathbb{R}^{n-1}$ representing the direction of the eigenvector $\boldsymbol{w}_j$. The corresponding Jacobian matrix can be expressed as $\boldsymbol{H}(\boldsymbol{w}_j) = \partial \boldsymbol{y}(\boldsymbol{w})/\partial \boldsymbol{w}|_{\boldsymbol{w}=\boldsymbol{w}_j}$. Such a representation can be the angular part of n-spherical coordinates as given in Sect. A.2.2. Moreover, the computation of the Jacobian matrices defined in (A.2) requires to differentiate the eigenvectors $\boldsymbol{w}_j$ w. r. t. the optimization variables $\boldsymbol{\zeta}_1$. Therefore, a closed-form method is provided in Sect. A.2.3.

A.2.2. n-spherical coordinates

Given is the eigenvector $\boldsymbol{w} \in \mathbb{R}^n$. The components $\boldsymbol{w}$ can be expressed as the angular part of n-spherical coordinates $\boldsymbol{y} = \boldsymbol{y}(\boldsymbol{w}) \in \mathbb{R}^{n-1}$, where

$$y_i(\boldsymbol{w}) = \arccos\left(\frac{w_i}{\sqrt{\sum_{j=i}^{n} w_j^2}}\right)\,, \tag{A.3}$$

for $i = 1 \ldots (n-1)$. The corresponding Jacobian matrix can be computed by $\boldsymbol{H} = \partial \boldsymbol{y}(\boldsymbol{w})/\partial \boldsymbol{w} \in \mathbb{R}^{(n-1)\times n}$. The components of $\boldsymbol{H}$ are given by

$$H_{i,j} = \frac{\frac{w_i^2}{\left(\sum_{k=i}^{n} w_k^2\right)^{\frac{3}{2}}} - \frac{1}{\sqrt{\sum_{k=i}^{n} w_k^2}}}{\sqrt{1 - \frac{w_i^2}{\sum_{k=i}^{n} w_k^2}}}\,,$$

for $i = 1 \ldots (n-1)$ and $j = i$,

$$H_{i,j} = \frac{w_i w_j}{\left(\sum_{k=i}^{n} w_k^2\right)^{\frac{3}{2}} \sqrt{1 - \frac{w_i^2}{\sum_{k=i}^{n} w_k^2}}}\,,$$

for $i = 1 \ldots (n-2)$ and $j = (i+1) \ldots n$,

$$H_{n-1,n-1} = \operatorname{sign}(w_{n-1}) \frac{\frac{w_{n-1}^2}{\left(\sum_{k=n-1}^{n} w_k^2\right)^{\frac{3}{2}}} - \frac{1}{\sqrt{\sum_{k=n-1}^{n} w_k^2}}}{\sqrt{1 - \frac{w_{n-1}^2}{\sum_{k=n-1}^{n} w_k^2}}}\,,$$

$$H_{n-1,n} = \operatorname{sign}(w_{n-1}) \frac{w_{n-1} w_n}{\left(\sum_{k=n-1}^{n} w_k^2\right)^{\frac{3}{2}} \sqrt{1 - \frac{w_{n-1}^2}{\sum_{k=n-1}^{n} w_k^2}}}\,,$$

and $H_{i,j} = 0$, otherwise.

A.2.3. Derivatives of generalized eigenvectors

Given are two symmetric matrices $\boldsymbol{K}, \boldsymbol{M} \in \mathbb{R}^{n\times n}$ with $\boldsymbol{M}$ positive definite. Consider the generalized eigenvalue problem (5.6), (5.7), given in Sect. 5.1.1. Assume that all quantities in the above equations are functions of the variables $\boldsymbol{\zeta} = (\zeta_1, \ldots, \zeta_N)$. The goal is to compute the Jacobian matrix $\frac{\partial \boldsymbol{w}}{\partial \boldsymbol{\zeta}} = \begin{bmatrix} \frac{\partial \boldsymbol{w}}{\partial \zeta_1} & \ldots & \frac{\partial \boldsymbol{w}}{\partial \zeta_N} \end{bmatrix}$. Therefore, it is shown how to compute $\partial \boldsymbol{w}/\partial \zeta_i$: Derive both sides of (5.6) and rearrange the equation as

$$(\boldsymbol{K} - \lambda \boldsymbol{M}) \frac{\partial \boldsymbol{w}}{\partial \zeta_i} = \frac{\partial \lambda}{\partial \zeta_i} \boldsymbol{M}\boldsymbol{w} - \left(\frac{\partial \boldsymbol{K}}{\partial \zeta_i} - \lambda \frac{\partial \boldsymbol{M}}{\partial \zeta_i} \right) \boldsymbol{w} \tag{A.4}$$

Pre-multiplying (A.4) by $\boldsymbol{w}^T$ from the left and taking into account that $\boldsymbol{w}^T(\boldsymbol{K} - \lambda \boldsymbol{M}) = \boldsymbol{0}$ (cf. (5.6)), leads to the derivative of λ as

$$\frac{\partial \lambda}{\partial \zeta_i} = \frac{\boldsymbol{w}^T \left(\frac{\partial \boldsymbol{K}}{\partial \zeta_i} - \lambda \frac{\partial \boldsymbol{M}}{\partial \zeta_i} \right) \boldsymbol{w}}{\boldsymbol{w}^T \boldsymbol{M} \boldsymbol{w}} \,. \tag{A.5}$$

To compute $\partial \boldsymbol{w}/\partial \zeta_i$, (A.5) is substituted into (A.4):

$$(\boldsymbol{K} - \lambda \boldsymbol{M}) \frac{\partial \boldsymbol{w}}{\partial \zeta_i} = \left(\frac{\boldsymbol{M}\boldsymbol{w}\boldsymbol{w}^T}{\boldsymbol{w}^T \boldsymbol{M} \boldsymbol{w}} - \boldsymbol{I} \right) \left(\frac{\partial \boldsymbol{K}}{\partial \zeta_i} - \lambda \frac{\partial \boldsymbol{M}}{\partial \zeta_i} \right) \boldsymbol{w} \,. \tag{A.6}$$

Since the matrix $(\boldsymbol{K} - \lambda \boldsymbol{M})$ is singular by definition, one equation in (A.6) has to be replaced by the derivative of (5.7) in Sect. 5.1.1, $2\boldsymbol{w}^T \frac{\partial \boldsymbol{w}}{\partial \zeta_i} = -\frac{1}{2} \boldsymbol{w}^T \frac{\partial \boldsymbol{S}}{\partial \zeta_i} \boldsymbol{w}$ such that the resulting system of linear equations becomes regular.

A.3. Dynamics components of the pantograph leg featuring an eigenmode

The dynamics components provided in the following correspond to the three-segment pantograph-leg mechanism derived in Sect. 5.2.2. They are expressed w. r. t. configuration coordinates (joint angles).

$$\boldsymbol{M}(\boldsymbol{q}) = \begin{bmatrix} 2\left(1-\beta\right)\left[\Theta_1 + \Theta_2 \cos\left(\beta\left(q_2 - q_1\right)\right)\right] + \beta^2 \Theta_1 & \text{sym.} \\ \beta\left[\left(1-\beta\right)\Theta_1 + \Theta_2 \cos\left(\beta\left(q_2 - q_1\right)\right)\right] & \beta^2 \Theta_1 \end{bmatrix} \tag{A.7}$$

$$\boldsymbol{C}(\boldsymbol{q}, \dot{\boldsymbol{q}}) = \beta \Theta_2 \sin\left(\beta\left(q_2 - q_1\right)\right) \begin{bmatrix} \left(\beta - 1\right)\left(\dot{q}_2 - \dot{q}_1\right) & -\beta\left(\dot{q}_2 - \dot{q}_1\right) - \dot{q}_1 \\ \dot{q}_1 & 0 \end{bmatrix} \tag{A.8}$$

$$\frac{\partial U_{\mathrm{g}}(\boldsymbol{q})}{\partial \boldsymbol{q}}^T = \frac{\Theta_3}{l_1 + l_2} g_0 \begin{pmatrix} \left(\beta - 1\right)\sin\left(q_1 + \beta\left(q_2 - q_1\right)\right) - \sin\left(q_1\right) \\ -\beta \sin\left(q_1 + \beta\left(q_2 - q_1\right)\right) \end{pmatrix} \tag{A.9}$$

$$\frac{\partial U_{\mathrm{e}}(\boldsymbol{q} - \boldsymbol{\theta})}{\partial \boldsymbol{q}}^T = \begin{pmatrix} k_{\mathrm{lin}}\left(q_1 - \theta_1\right) + k_{\mathrm{cub}}\left(q_1 - \theta_1\right)^3 \\ \frac{\beta}{\beta - 2}\left[k_{\mathrm{lin}}\left(q_2 - \theta_2\right) + k_{\mathrm{cub}}\left(q_2 - \theta_2\right)^3\right] \end{pmatrix} \tag{A.10}$$

Herein, the following inertias are abbreviated:

$$\Theta_1 = \left(m_{\mathrm{t}} + m_1 + \frac{m_2}{4}\right)\left(l_1 + l_3\right)^2 + I_2^{\mathrm{c}} \tag{A.11}$$

$$\Theta_2 = \left(\left(m_{\mathrm{t}} + \frac{m_1}{2}\right) l_1 + \left(m_{\mathrm{t}} + m_1 + \frac{m_2}{2}\right) l_3\right)\left(l_1 + l_3\right) \tag{A.12}$$

$$\Theta_3 = \left(m_{\mathrm{t}} + m_1 + \frac{m_2}{2}\right)\left(l_1 + l_3\right)^2 \tag{A.13}$$

All geometric and inertial parameters are labeled in Fig. 5.2 and satisfy the conditions repeated in the following:

$$
\begin{aligned}
l_2 &= l_1 + l_3 \,, \\
I_1^{\mathrm{c}} + I_3^{\mathrm{c}} &= \frac{3m_1 + m_2}{4} l_1^2 + \frac{2m_1 + m_2}{2} l_1 l_3 \\
&\quad - \frac{3m_2 + m_3}{4} l_3^2 + I_2^{\mathrm{c}} \,, \\
\alpha &= \frac{\beta}{2 - \beta} \,, \\
m_3 &= \left(m_1 l_1 + m_2 \left(l_1 - l_3 \right) \right) / l_3 \,.
\end{aligned}
$$

Bibliography

[ACPS07] A. Alessandri, M. Cuneo, S. Pagnan, and M. Sanguineti. A recursive algorithm for nonlinear least-squares problems. *Computational Optimization and Applications*, 38(2):195–216, 2007.

[AF10] Morteza Azad and Roy Featherstone. Modeling the contact between a rolling sphere and a compliant ground plane. *ACRA, Brisbane, Australia*, 2010.

[AKK+05] Kazuhiko Akachi, Kenji Kaneko, Noriyuki Kanehira, Shigehiko Ota, Gou Miyamori, Masaru Hirata, Shuuji Kajita, and Fumio Kanehiro. Development of humanoid robot hrp-3p. In *Humanoid Robots, 2005 5th IEEE-RAS International Conference on*, pages 50–55. IEEE, 2005.

[Ale90] R. McN. Alexander. Three uses for springs in legged locomotion. *International Journal of Robotics Research*, 9(2):53–61, 1990.

[Arn13] Vladimir Igorevich Arnol'd. *Mathematical methods of classical mechanics*, volume 60. Springer Science & Business Media, 2013.

[ASEF+11] Alin Albu-Schäffer, Oliver Eiberger, Matthias Fuchs, Markus Grebenstein, Sami Haddadin, Christian Ott, Andreas Stemmer, Thomas Wimböck, Sebastian Wolf, Christoph Borst, and Gerd Hirzinger. Anthropomorphic soft robotics—from torque control to variable intrinsic compliance. In Cédric Pradalier, Roland Siegwart, and Gerhard Hirzinger, editors, *Robotics Research*, volume 70 of *Springer Tracts in Advanced Robotics*, pages 185–207. Springer, 2011.

[ASEG+08] Alin Albu-Schäffer, Oliver Eiberger, Markus Grebenstein, Sami Haddadin, Christian Ott, Thomas Wimböck, Sebastian Wolf, and Gerd Hirzinger. Soft robotics. *Robotics & Automation Magazine, IEEE*, 15(3):20–30, 2008.

[ASH01] Alin Albu-Schäffer and Gerd Hirzinger. A globally stable state feedback controller for flexible joint robots. *Advanced Robotics*, 15(8):799–814, 2001.

[ASOH04] Alin Albu-Schäffer, Christian Ott, and Gerd Hirzinger. A passivity based cartesian impedance controller for flexible joint robots-part ii: Full state feedback, impedance design and experiments. In *Proc. IEEE Int. Conf. on Robotics and Automation*, 2004.

[ASOP12] Alin Albu-Schäffer, Christian Ott, and Florian Petit. Constructive energie shaping control for a class of euler-lagrange systems. In *10th Int. IFAC Symposium on Robot Control*, 2012.

[ASWE+10] Alin Albu-Schäffer, S. Wolf, O. Eiberger, S. Haddadin, F. Petit, and M. Chalon. Dynamic modelling and control of variable stiffness actuators. In *IEEE Int. Conf. on Robotics and Automation*, 2010.

[BBM98] M. S. Branicky, V. S. Borkar, and S. K. Mitter. A unified framework for hybrid control: model and optimal control theory. *IEEE Transactions on Automatic Control*, 43(1):31–45, Jan 1998.

[BF93] Reinhard Blickhan and RJ Full. Similarity in multilegged locomotion: bouncing like a monopode. *Journal of Comparative Physiology A*, 173(5):509–517, 1993.

[BFDLZ16] A. Bisoffi, F. Forni, M. Da Lio, and L. Zaccarian. Global results on reset-induced periodic trajectories of planar systems. In *European Control Conference*, pages 2644–2649, 2016.

[BH89] Pierre Baldi and Kurt Hornik. Neural networks and principal component analysis: Learning from examples without local minima. *Neural networks*, 2(1):53–58, 1989.

[BHV11] D. J. Braun, M. Howard, and S. Vijayakumar. Exploiting variable stiffness in explosive movement tasks. In *Robotics: Science and Systems*, 2011.

[BI04] Jonas Buchli and Auke Jan Ijspeert. Distributed central pattern generator model for robotics application based on phase sensitivity analysis. In *BioADIT'04*, pages 333–349, 2004.

[BI08] J. Buchli and A.J. Ijspeert. Self-organized adaptive legged locomotion in a compliant quadruped robot. *Autonomous Robots*, 25(4):331–347, 2008.

[Bli89] Reinhard Blickhan. The spring-mass model for running and hopping. *Journal of Biomechanics*, 22:1217–1227, 1989.

[BOL95] B. Brogliato, R. Ortega, and R. Lozano. Global tracking controllers for flexible-joint manipulators: A comparative study. *Automatica*, 31(7):941–956, July 1995.

[BPH+12] D.J. Braun, F. Petit, F. Huber, S. Haddadin, P. van der Smagt, A. Albu-Schäffer, and S. Vijayakumar. Optimal torque and stiffness control in compliantly actuated robots. In *Proc. IEEE/RSJ Int. Conf. on Intelligent Robots and Systems*. IEEE, 2012.

[BPH+13] D.J. Braun, F. Petit, F. Huber, S. Haddadin, P. van der Smagt, A. Albu-Schäffer, and S. Vijayakumar. Robots driven by compliant actuators: Optimal control under actuation constraints. *Robotics, IEEE Transactions on*, 29(5):1085–1101, Oct 2013.

[BPS95] Nicolas Boivin, Christophe Pierre, and Steven W Shaw. Non-linear normal modes, invariance, and modal dynamics approximations of non-linear systems. *Nonlinear Dynamics*, 8(3):315–346, 1995.

[CEU02] Carlos Canudas-de-Wit, Bernard Espiau, and Claudio Urrea. Orbital stabilization of underactuated mechanical systems. In *Proc. of the 15th IFAC World Congress*, 2002.

[CVS90] TK Caughey, A Vakakis, and JM Sivo. Analytical study of similar normal modes and their bifurcations in a class of strongly non-linear systems. *International Journal of Non-Linear Mechanics*, 25(5):521–533, 1990.

[CVS12] Raffaella Carloni, Ludo C Visser, and Stefano Stramigioli. Variable stiffness actuators: A port-based power-flow analysis. *IEEE Transactions on Robotics*, 28(1):1–11, 2012.

[Cyb89] G. Cybenko. Approximation by superpositions of a sigmoidal function. *Mathematics of Control, Signals and Systems*, 2(4):303–314, 1989.

[DLF10] A. De Luca and F. Flacco. Dynamic gravity cancellation in robots with flexible transmissions. In *Decision and Control (CDC), 2010 49th IEEE Conference on*, pages 288–295, Dec 2010.

[DLL98] Alessandro De Luca and Pasquale Lucibello. A general algorithm for dynamic feedback linearization of robots with elastic joints. In *IEEE Int. Conf. on Robotics and Automation*, volume 1, pages 504–510, 1998.

[DS03] Vincent Duindam and Stefano Stramigioli. Passive asymptotic curve tracking. In *Proceedings of the IFAC Workshop on Lagrangian and Hamiltonian Methods for Nonlinear Control*, pages 229 – 234, 2003.

[DT96] A. De Luca and P. Tomei. *Theory of Robot Control*, chapter Elastic joints, pages 179–217. Springer Verlag, Berlin, 1996.

[Duf18] G. Duffing. *Erzwungene schwingungen bei veränderlicher eigenfrequenz und ihre technische bedeutung*. Sammlung Vieweg. F. Vieweg & sohn, 1918.

[ESNV12] Alexander Enoch, Andrius Sutas, Shinichiro Nakaoka, and Sethu Vijayakumar. Blue: A bipedal robot with variable stiffness and damping. In *Humanoid Robots (Humanoids), 2012 12th IEEE-RAS International Conference on*, pages 487–494. IEEE, 2012.

[Fea08] Roy Featherstone. *Rigid body dynamics algorithms*, volume 49. Springer Berlin, 2008.

[FK99] R.J. Full and D.E. Koditschek. Templates and anchors: neuromechanical hypotheses of legged locomotion on land. *J. Exp. Biol.*, 202(15):3325–3332, 1999.

[Fra03] Theodore Frankel. *The Geometry of Physics: An Introduction*. Cambridge University Press, 2 edition, 2003.

[FvdSS14] G.A. Folkertsma, A.J. van der Schaft, and S. Stramigioli. Power-continuous synchronisation of oscillators: A novel, energy-free way to synchronise dynamical systems. In *IEEE Int. Conf. on Robotics and Automation*, pages 1493–1498, May 2014.

[Gal87] David Gale. The classification of 1-manifolds: a take-home exam. *The American Mathematical Monthly*, 94(2):170–175, 1987.

[GAP01] Jessy W Grizzle, Gabriel Abba, and Franck Plestan. Asymptotically stable walking for biped robots: Analysis via systems with impulse effects. *IEEE Transactions on automatic control*, 46(1):51–64, 2001.

[GASB+11] Markus Grebenstein, Alin Albu-Schäffer, Thomas Bahls, Maxime Chalon, Oliver Eiberger, Werner Friedl, Robin Gruber, Sami Haddadin, Ulrich Hagn, Robert Haslinger, Hannes Höppner, Stefan Jörg, Matthias Nickl, Alexander Nothhelfer, Florian Petit, Joseph Reill, Nikolaus Seitz, Thomas Wimböck, Sebastian Wolf, Tilo Wüsthoff, and Gerd Hirzinger. The DLR Hand Arm System. In *Proc. IEEE Int. Conf. on Robotics and Automation*, 2011.

[GCH+13] C. Gehring, S. Coros, M. Hutter, M. Bloesch, M.A. Hoepflinger, and R. Siegwart. Control of dynamic gaits for a quadrupedal robot. In *IEEE Int. Conf. on Robotics and Automation*, pages 3287–3292, May 2013.

[GCH+14] Christian Gehring, Stelian Coros, Marco Hutter, Michael Bloesch, Péter Fankhauser, Markus A Hoepflinger, and Roland Siegwart. Towards automatic discovery of agile gaits for quadrupedal robots. In *Robotics and Automation (ICRA), 2014 IEEE International Conference on*, pages 4243–4248. IEEE, 2014.

[GH83] John Guckenheimer and Philip Holmes. *Nonlinear Oscillations, Dynamical Systems, and Bifurcations of Vector Fields*. Springer, 1983.

[GH12] Jesse A Grimes and Jonathan W Hurst. The design of ATRIAS 1.0 a unique monopod, hopping robot. In *Proceedings of the 2012 International Conference on Climbing and Walking Robots and the Support Technologies for Mobile Machines*, pages 548–554, 2012.

[GHM+09] JW Grizzle, Jonathan Hurst, Benjamin Morris, Hae-Won Park, and Koushil Sreenath. MABEL, a new robotic bipedal walker and runner. In *American Control Conference, 2009. ACC'09.*, pages 2030–2036. IEEE, 2009.

[GO16] Gianluca Garofalo and Christian Ott. Energy based limit cycle control of elastically actuated robots. *IEEE Transactions on Automatic Control*, 2016.

[GOAS13] Gianluca Garofalo, Christian Ott, and Alin Albu-Schäffer. Orbital stabilization of mechanical systems through semidefinite lyapunov functions. In *Proc. American Control Conference*, pages 5715–5721, 2013.

[Gol65] Herbert Goldstein. *Classical mechanics*. Pearson Education India, 1965.

[GSB06] Hartmut Geyer, Andre Seyfarth, and Reinhard Blickhan. Compliant leg behavior explains basic dynamics of walking and running. *Proc. R. Soc. B*, 273(1603):2861–2867, 2006.

[HASH+01] Gerd Hirzinger, A Albu-Schäffer, M Hahnle, Ingo Schaefer, and Norbert Sporer. On a new generation of torque controlled light-weight robots. In *IEEE Int. Conf. on Robotics and Automation*, volume 4, pages 3356–3363. IEEE, 2001.

[HCH76] RE Herron, JR Cuzzi, and J Hugg. Mass distribution of the human body using biostereometrics. Technical report, DTIC Document, 1976.

[HCR07] Jonathan W Hurst, Joel E Chestnutt, and Alfred A Rizzi. Design and philosophy of the BiMASC, a highly dynamic biped. In *Robotics and Automation, 2007 IEEE International Conference on*, pages 1863–1868. IEEE, 2007.

[HFKG06] P. Holmes, R.J. Full, D. Koditschek, and J. Guckenheimer. The dynamics of legged locomotion: Models, analyses and challenges. *SIAM Review*, 48(2):207–304, 2006.

[HGB+12] M. Hutter, C. Gehring, M. Bloesch, M.A. Hoepflinger, C.D. Remy, and R. Siegwart. Starleth: A compliant quadrupedal robot for fast, efficient, and versatile locomotion. In *Int. Conf. on Climbing and Walking Robots (CLAWAR)*, 2012.

[HGH+14] Marco Hutter, Christian Gehring, Mark A Höpflinger, Michael Blösch, and Roland Siegwart. Toward combining speed, efficiency, versatility, and robustness in an autonomous quadruped. *IEEE Trans. Robotics*, 30(6):1427–1440, 2014.

[HGJ+16] Marco Hutter, Christian Gehring, Dominic Jud, Andreas Lauber, C Dario Bellicoso, Vassilios Tsounis, Jemin Hwangbo, Karen Bodie, Peter Fankhauser, Michael Bloesch, et al. Anymal-a highly mobile and dynamic quadrupedal robot. In *Intelligent Robots and Systems (IROS), 2016 IEEE/RSJ International Conference on*, pages 38–44. IEEE, 2016.

[HH85] Milton Hildebrand and James P Hurley. Energy of the oscillating legs of a fast-moving cheetah, pronghorn, jackrabbit, and elephant. *Journal of morphology*, 184(1):23–31, 1985.

[HHAS12] Sami Haddadin, Felix Huber, and Alin Albu-Schäffer. Optimal control for exploiting the natural dynamics of variable stiffness robots. In *IEEE Int. Conf. on Robotics and Automation*, 2012.

[HHHT98] Kazuo Hirai, Masato Hirose, Yuji Haikawa, and Toru Takenaka. The development of honda humanoid robot. In *Robotics and Automation, 1998. Proceedings. 1998 IEEE International Conference on*, volume 2, pages 1321–1326. IEEE, 1998.

[HJ85] R.A. Horn and C.R. Johnson. *Matrix Analysis*. Cambridge University Press, 1985.

[HO07] Masato Hirose and Kenichi Ogawa. Honda humanoid robots development. *Philosophical Transactions of the Royal Society of London A: Mathematical, Physical and Engineering Sciences*, 365(1850):11–19, 2007.

[Hog85] Neville Hogan. Impedance Control: An Approach to Manipulation: Part I - Theory, Part II - Implementation, Part III - Applications. *Journal of Dynamic Systems, Measurement, and Control*, 107:1–24, March 1985.

[Hop42] Eberhard Hopf. Abzweigung einer periodischen lösung von einer stationären lösung eines differentialsystems. *Ber. Math.-Phys. Kl Sächs. Akad. Wiss. Leipzig*, 94:1–22, 1942.

[HRHS10] Marco Hutter, David Remy, Mark A. Höpflinger, and Roland Siegwart. Slip running with an articulated robotic leg. In *Proc. of IEEE/RSJ Int. Conf. on Intelligent Robots and Systems*, pages 4934–4939, 2010.

[HSH+96] JA Hoffer, RB Stein, MK Haugland, T Sinkjaer, WK Durfee, AB Schwartz, GE Loeb, and C Kantor. Neural signals for command control and feedback in functional neuromuscular stimulation: a review. *Journal of Rehabilitation Research and Development*, 33(2):145–157, 1996.

[HT81] Donald F Hoyt and C Richard Taylor. Gait and the energetics of locomotion in horses. *Nature*, 1981.

[IC07] A. J. Ijspeert and A. Crespi. Online trajectory generation in an amphibious snake robot using a lamprey-like central pattern generator model. In *IEEE Int. Conf. on Robotics and Automation*, pages 262–268, 2007.

[Ijs01] Auke Jan Ijspeert. A connectionist central pattern generator for the aquatic and terrestrial gaits of a simulated salamander. *Biological Cybernetics*, 84:331–348, 2001.

[Isi95] Alberto Isidori. *Nonlinear control systems*, volume 1. Springer Science & Business Media, 1995.

[JLJ98] Jürgen Jost and Xianqing Li-Jost. *Calculus of variations*, volume 64. Cambridge University Press, 1998.

[JS07] Dominic Jordan and Peter Smith. *Nonlinear Ordinary Differential Equations: An Introduction for Scientists and Engineers*. Oxford University Press, 2007.

[KH13] Brandon M. Kilbourne and Louwrens C. Hoffman. Scale effects between body size and limb design in quadrupedal mammals. *PLOS ONE*, 8(11):1–18, 11 2013.

[Kha02] H.K. Khalil. *Nonlinear Systems, 3rd edn.* Prentice Hall, Englewood Cliffs, 2002.

[KKO86] P.V. Kokotovic, H.K. Khalil, and J. O'Reilly. *Singular Perturbation Methods in Control: Analysis and Design*. Academic Press, London, 1986.

[KLO17] M. Keppler, D. Lakatos, and C. Ott. Verfahren und Vorrichtung zum Steuern und Regeln von Aktuatoren, die zum Antrieb eines seriellen, mehrgliedrigen mechanchischen Systems dienen, 2017.

[KLOAS16] M. Keppler, D. Lakatos, C. Ott, and A. Albu-Schäffer. A passivity-based approach for trajectory tracking and link-side damping of compliantly actuated robots. In *IEEE Int. Conf. on Robotics and Automation*, pages 1079–1086, May 2016. Best Automation Paper Award Finalist.

[KM94] Michael Kirby and Rick Miranda. Nonlinear reduction of high-dimensional dynamical systems via neural networks. *Physical Review Letters*, 72:1822–1825, Mar 1994.

[Kra91] Mark A Kramer. Nonlinear principal component analysis using autoassociative neural networks. *AIChE journal*, 37(2):233–243, 1991.

[KT91] S. Kajita and K. Tani. Study of dynamic biped locomotion on rugged terrain-derivation and application of the linear inverted pendulum mode. In *Proc. of IEEE Int. Conf. on Robotics and Automation*, 1991.

[LAS] D. Lakatos and A. Albu-Schäffer. Resonanz-/Modalanpassung für nichtlineare, schwingungsfähige Systeme mit multiplen Freiheitsgraden. German patent application No. 10 2016 200 394.1, filed on Jan. 14 2016.

[LAS14a] D. Lakatos and A. Albu-Schaffer. Neuron model interpretation of a cyclic motion control concept. In *IEEE RAS & EMBS Int. Conf. on Biomedical Robotics and Biomechatronics*, pages 905–910, Aug. 2014.

[LAS14b] D. Lakatos and A. Albu-Schäffer. Switching based limit cycle control for compliantly actuated second-order systems. In *Proc. of the IFAC World Congress*, pages 6392–6399, Aug. 2014.

[LAS16] D. Lakatos and A. Albu-Schäffer. Modal matching: An approach to natural compliant jumping control. *IEEE Robotics and Automation Letters*, 1(1):274–281, Jan. 2016.

[LASRL16] D. Lakatos, A. Albu-Schäffer, C. Rode, and F. Loeffl. Dynamic bipedal walking by controlling only the equilibrium of intrinsic elasticities. In *Proc. IEEE-RAS Int. Conf. on Humanoid Robots (Humanoids)*, pages 1282–1289, Nov. 2016.

[LFAS] D. Lakatos, W. Friedl, and A. Albu-Schäffer. Nichtlinearer schwingungsmechanismus. German patent application No. 10 2016 226 174.6 filled on 23. Dez. 2016.

[LFAS17] D. Lakatos, W. Friedl, and A. Albu-Schaffer. Eigenmodes of nonlinear dynamics: Definition, existence, and embodiment into legged robots with elastic elements. *IEEE Robotics and Automation Letters*, 2(2):1062–1069, Apr. 2017.

[LGDAS14] D. Lakatos, G. Garofalo, A. Dietrich, and A. Albu-Schäffer. Jumping control for compliantly actuated multilegged robots. In *IEEE Int. Conf. on Robotics and Automation*, pages 4562–4568, May 2014.

[LGP+13a] D. Lakatos, G. Garofalo, F. Petit, C. Ott, and A. Albu-Schäffer. Modal limit cycle control for variable stiffness actuated robots. In *IEEE Int. Conf. on Robotics and Automation*, pages 4934–4941, May 2013.

[LGP+13b] D. Lakatos, M. Görner, F. Petit, A. Dietrich, and A. Albu-Schäffer. A modally adaptive control for multi-contact cyclic motions in compliantly actuated robotic systems. In *Proc. IEEE/RSJ Int. Conf. on Intelligent Robots and Systems*, pages 5388–5395, Nov. 2013.

[LPAS13] D. Lakatos, F. Petit, and A. Albu-Schäffer. Nonlinear oscillations for cyclic movements in variable impedance actuated robotic arms. In *IEEE Int. Conf. on Robotics and Automation*, pages 508–515, May 2013.

[LPAS14] D. Lakatos, F. Petit, and A. Albu-Schäffer. Nonlinear oscillations for cyclic movements in human and robotic arms. *IEEE Transactions on Robotics*, 30(4):865–879, Aug. 2014.

[LR89] David Lovelock and Hanno Rund. *Tensors, differential forms, and variational principles*. Courier Dover Publications, 1989.

[LRSAS14] Dominic Lakatos, Christian Rode, Andre Seyfarth, and Alin Albu-Schäffer. Design and control of compliantly actuated bipedal running robots: Concepts to exploit natural system dynamics. In *Proc. IEEE-RAS Int. Conf. on Humanoid Robots (Humanoids)*, pages 930–937, Nov. 2014.

[LS98] W. Lohmiller and J.-J. E. Slotine. On contraction analysis for non-linear systems. *Automatica*, 34(6):683–696, 1998.

[LSFAS15] D. Lakatos, D. Seidel, W. Friedl, and A. Albu-Schäffer. Targeted jumping of compliantly actuated hoppers based on discrete planning and switching control. In *Proc. IEEE/RSJ Int. Conf. on Intelligent Robots and Systems*, pages 5802–5808, 2015.

[LWL+16] Florian Loeffl, Alexander Werner, Dominic Lakatos, Jens Reinecke, Sebastian Wolf, Robert Burger, Thomas Gumpert, Florian Schmidt, Christian Ott, Markus Grebenstein, et al. The dlr c-runner: Concept, design and experiments. In *Humanoid Robots (Humanoids), 2016 IEEE-RAS 16th International Conference on*, pages 758–765. IEEE, 2016.

[MLG+10] H-M Maus, SW Lipfert, M Gross, J Rummel, and A Seyfarth. Upright human gait did not provide a major mechanical challenge for our ancestors. *Nature communications*, 1:70, 2010.

[MRS08] Horst-Moritz Maus, Jürgen Rummel, and André Seyfarth. Stable upright walking and running using a simple pendulum based control scheme. In *Advances in Mobile Robotics: Proc. 11th Int. Conf. Climbing and Walking Robots. Coimbra, Portugal: World Scientific*, pages 623–629, 2008.

[Nay73] Ali Hasan Nayfeh. *Perturbation Methods*. John Wiley & Sons, 1973.

[NM79] Ali Hasan Nayfeh and Dean T. Mook. *Nonlinear Oscillations*. John Wiley & Sons, 1979.

[OAS+06] Yusuke Ogura, Hiroyuki Aikawa, Kazushi Shimomura, Akitoshi Morishima, Hun-ok Lim, and Atsuo Takanishi. Development of a new humanoid robot wabian-2. In *Robotics and Automation, 2006. ICRA 2006. Proceedings 2006 IEEE International Conference on*, pages 76–81. IEEE, 2006.

[OASK+04] Christian Ott, Alin Albu-Schäffer, Andreas Kugi, S Stamigioli, and Gerd Hirzinger. A passivity based cartesian impedance controller for flexible joint robots-part i: Torque feedback and gravity compensation. In *Proc. IEEE Int. Conf. on Robotics and Automation*, 2004.

[OASKH03] Christian Ott, Alin Albu-Schäffer, Andreas Kugi, and Gerd Hirzinger. Decoupling based cartesian impedance control of flexible joint robots. In *Proc. IEEE Int. Conf. on Robotics and Automation*, 2003.

[OBL00] Shan Ouyang, Zheng Bao, and Gui-Sheng Liao. Robust recursive least squares learning algorithm for principal component analysis. *IEEE Transactions on Neural Networks*, 11(1):215–221, Jan 2000.

[ÖH13] M. C. Özparpucu and S. Haddadin. Optimal control for maximizing link velocity of visco-elastic joints. In *2013 IEEE/RSJ International Conference on Intelligent Robots and Systems*, pages 3035–3042, Nov 2013.

[Oja82] Erkki Oja. Simplified neuron model as a principal component analyzer. *Journal of mathematical biology*, 15(3):267–273, 1982.

[OKL95] R. Ortega, R. Kelly, and A. Loria. A class of output feedback globally stabilizing controllers for flexible joints robots. *Robotics and Automation, IEEE Transactions on*, 11(5):766–770, Oct 1995.

[OL99] Jong H Oh and Jin S Lee. Control of flexible joint robot system by backstepping design approach. *Intelligent Automation & Soft Computing*, 5(4):267–278, 1999.

[Ott08] Christian Ott. *Cartesian Impedance Control of Redundant and Flexible-Joint Robots*. Springer, 2008.

[PAS11] Florian Petit and Alin Albu-Schäffer. State feedback damping control for a multi dof variable stiffness robot arm. In *Proc. IEEE Int. Conf. on Robotic and Automation*, 2011.

[PCY99] Jonghoon Park, Wankyun Chung, and Youngil Youm. On dynamical decoupling of kinematically redundant manipulators. In *IEEE/RSJ International Conference on Intelligent Robots and Systems*, pages 1495 –1500, 1999.

[PDP97] Jerry Pratt, Peter Dilworth, and Gill Pratt. Virtual model control of a bipedal walking robot. In *IEEE Int. Conf. on Robotics and Automation*, pages 193–198, 1997.

[PKB11] M. Pakdemirli, M.M.F. Karahan, and H. Boyaci. Forced vibrations of strongly nonlinear systems with multiple scales Lindstedt Poincare method. *Mathematical and Computational Applications*, 16(4):879–889, 2011.

[PMDL08] Gianluca Palli, Claudio Melchiorri, and Alessandro De Luca. On the feedback linearization of robots with variable joint stiffness. In *IEEE Int. Conf. on Robotics and Automation*, pages 1753–1759, 2008.

[PP98] Jerry Pratt and Gill Pratt. Intuitive control of a planar bipedal walking robot. In *IEEE Int. Conf. on Robotics and Automation*, pages 2014–2021, 1998.

[PPS02] E Pesheck, C Pierre, and SW Shaw. A new galerkin-based approach for accurate non-linear normal modes through invariant manifolds. *Journal of sound and vibration*, 249(5):971–993, 2002.

[PW95] Gill A Pratt and Matthew M Williamson. Series elastic actuators. In *Intelligent Robots and Systems 95.'Human Robot Interaction and Cooperative Robots', Proceedings. 1995 IEEE/RSJ International Conference on*, volume 1, pages 399–406. IEEE, 1995.

[Rai85] Marc H Raibert. Four-legged running with one-legged algorithms. In *Second International Symposium on Robotics Research*, pages 311–315. Cambridge: MIT Press, 1985.

[Rai86] Mark H. Raibert. *Legged Robots That Balance*. The MIT Press, 1986.

[Rai90] Marc H Raibert. Trotting, pacing and bounding by a quadruped robot. *Journal of biomechanics*, 23:7983–8198, 1990.

[Ran71] Richard H Rand. Nonlinear normal modes in two-degree-of-freedom systems. *Journal of Applied Mechanics*, 38(2):561–561, 1971.

[Ran74] Richard H Rand. A direct method for non-linear normal modes. *International journal of Non-linear Mechanics*, 9(5):363–368, 1974.

[RBM+10] Juergen Rummel, Yvonne Blum, Horst Moritz Maus, Christian Rode, and Andre Seyfarth. Stable and robust walking with compliant legs. In *Proc. of IEEE Int. Conf. on Robotics and Automation*, pages 5250–5255, 2010.

[RBN+08] Marc Raibert, Kevin Blankespoor, Gabriel Nelson, Rob Playter, and T Bigdog Team. Bigdog, the rough-terrain quadruped robot. In *Proceedings of the 17th world congress*, volume 17, pages 10822–10825. Proceedings Seoul, Korea, 2008.

[Rea94] Mark C Readman. *Flexible joint robots*. CRC press, 1994.

[Ros66] RM Rosenberg. On nonlinear vibrations of systems with many degrees of freedom. *Advances in applied mechanics*, 9:155–242, 1966.

[SBB+15] Claudio Semini, Victor Barasuol, Thiago Boaventura, Marco Frigerio, Michele Focchi, Darwin G Caldwell, and Jonas Buchli. Towards versatile legged robots through active impedance control. *The International Journal of Robotics Research*, 34(7):1003–1020, 2015.

[SC70] Eugene J Saletan and Alan H Cromer. A variational principle for nonholonomic systems. *American Journal of Physics*, 38(7):892–897, 1970.

[SD08] S. Stramigioli and M. Dijk. Energy conservative limit cycle oscillations. In *IFAC*, 2008.

[SFG10] Anton S Shiriaev, Leonid B Freidovich, and Sergei V Gusev. Transverse linearization for controlled mechanical systems with several passive degrees of freedom. *IEEE Transactions on Automatic Control*, 55(4):893–906, 2010.

[SGGB02] A. Seyfarth, H. Geyer, M. Günther, and R. Blickhan. A movement criterion for running. *Journal of Biomechanics*, 35(5):649–55, 2002.

[SL91] J.-J.E. Slotine and W. Li. *Applied Nonlinear Control*. Prentice-Hall, 1991.

[SLAS16] P. Stratmann, D. Lakatos, and A. Albu-Schäffer. Neuromodulation and synaptic plasticity for the control of fast periodic movement: Energy efficiency in coupled compliant joints via pca. *Frontiers in Neurorobotics*, 10(2):1–20, Mar. 2016.

[SLOAS17] P. Stratmann, D. Lakatos, M. C. Özparpucu, and A. Albu-Schäffer. Legged elastic multibody systems: Adjusting limit cycles to close-to-optimal energy efficiency. *IEEE Robotics and Automation Letters*, 2(2):436–443, Apr. 2017.

[SMCT+13] I. Sardellitti, G.A. Medrano-Cerda, N. Tsagarakis, A. Jafari, and D.G. Caldwell. Gain scheduling control for a class of variable stiffness actuators based on lever mechanisms. *Robotics, IEEE Transactions on*, 29(3):791–798, June 2013.

[SP93] S.W. Shaw and C. Pierre. Normal modes for non-linear vibratory systems. *Journal of Sound and Vibration*, 164(1):85–124, 1993.

[SP94] Steven W Shaw and Christophe Pierre. Normal modes of vibration for non-linear continuous systems. *Journal of Sound and Vibration*, 169:319–347, 1994.

[SPG13] Koushil Sreenath, Hae-Won Park, and Jessy W. Grizzle. Embedding active force control within the compliant hybrid zero dynamics to achieve stable, fast running on MABEL. *The International Journal of Robotics Research*, 2013.

[Spo87] M. W. Spong. Modeling and control of elastic joint robots. *Transactions of the ASME: Journal of Dynamic Systems, Measurement, and Control*, 109:310–319, 1987.

[Spo89] Mark W Spong. Adaptive control of flexible joint manipulators. *Systems & Control Letters*, 13(1):15–21, 1989.

[STG+11] Claudio Semini, Nikos G Tsagarakis, Emanuele Guglielmino, Michele Focchi, Ferdinando Cannella, and Darwin G Caldwell. Design of hyq–a hydraulically and electrically actuated quadruped robot. *Proceedings of the Institution of Mechanical Engineers, Part I: Journal of Systems and Control Engineering*, 225(6):831–849, 2011.

[Str94] Steven H. Strogatz. *Nonlinear Dynamics and Chaos*. Perseus Books, 1994.

[STV+13] Alexander Sproewitz, Alexandre Tuleu, Massimo Vespignani, Mostafa Ajallooeian, Emilie Badri, and Auke Ijspeert. Towards Dynamic Trot Gait Locomotion—Design, Control and Experiments with Cheetah-cub, a Compliant Quadruped Robot. *International Journal of Robotics Research*, 32(8):932–950, 2013.

[SW88] J-JE Slotine and Li Weiping. Adaptive manipulator control: A case study. *Automatic Control, IEEE Transactions on*, 33(11):995–1003, 1988.

[SWC+13] Sangok Seok, Albert Wang, Meng Yee Chuah, David Otten, Jeffrey Lang, and Sangbae Kim. Design principles for highly efficient quadrupeds and implementation on the mit cheetah robot. In *Robotics and Automation (ICRA), 2013 IEEE International Conference on*, pages 3307–3312. IEEE, 2013.

[SWC+15] Sangok Seok, Albert Wang, Meng Yee Michael Chuah, Dong Jin Hyun, Jongwoo Lee, David M Otten, Jeffrey H Lang, and Sangbae Kim. Design principles for energy-efficient legged locomotion and implementation on the mit cheetah robot. *IEEE/ASME Transactions on Mechatronics*, 20(3):1117–1129, 2015.

[TASLH08] L. Le Tien, A. Albu-Schäffer, A. De Luca, and G. Hirzinger. Friction observer and compensation for control of robots with joint torque measurement. In *2008 IEEE/RSJ International Conference on Intelligent Robots and Systems*, pages 3789–3795, Sept 2008.

[TLSC11] Nikos G Tsagarakis, Zhibin Li, Jody Saglia, and Darwin G Caldwell. The design of the lower body of the compliant humanoid robot "cCub". In *Robotics and Automation (ICRA), 2011 IEEE International Conference on*, pages 2035–2040. IEEE, 2011.

[TMD+13] Nikolaos G Tsagarakis, Stephen Morfey, Houman Dallali, Gustavo A Medrano-Cerda, and Darwin G Caldwell. An asymmetric compliant antagonistic joint design for high performance mobility. In *Intelligent Robots and Systems (IROS), 2013 IEEE/RSJ International Conference on*, pages 5512–5517. IEEE, 2013.

[Tom91] Patrizio Tomei. A simple pd controller for robots with elastic joints. *Automatic Control, IEEE Transactions on*, 36(10):1208–1213, 1991.

[Tuc75] Vance A Tucker. The energetic cost of moving about: walking and running are extremely inefficient forms of locomotion. much greater efficiency is achieved by birds, fish—and bicyclists. *American Scientist*, 63(4):413–419, 1975.

[UGK14] Mitsunori Uemura, Hidemasa Goya, and Sadao Kawamura. Motion control with stiffness adaptation for torque minimization in multijoint robots. *IEEE Transactions on Robotics*, 30(2):352–364, 2014.

[VASB+13] Bram Vanderborght, Alin Albu-Schäffer, Antonio Bicchi, Etienne Burdet, Darwin G Caldwell, Raffaella Carloni, M Catalano, Oliver Eiberger, Werner Friedl, Ganesh Ganesh, et al. Variable impedance actuators: A review. *Robotics and Autonomous Systems*, 61(12):1601–1614, 2013.

[VB05] Miomir Vukobratovic and Branislav Borovac. Zero-moment point - thirty five years of its life. *International Journal of Humanoid Robotics*, 2(2):225–227, 2005.

[VdP26] B. Van der Pol. On "relaxation-oscillations". *The London, Edinburgh, and Dublin Philosophical Magazine and Journal of Science*, 2(11):978–992, 1926.

[VdP27] B. Van der Pol. Forced oscillations in a circuit with non-linear resistance (receptance with reactive triode). *London, Edingburg and Dublin Phil*, pages 65–80, 1927.

[VdS12] Arjan Van der Schaft. *L2-gain and passivity techniques in nonlinear control*. Springer Science & Business Media, 2012.

[WGC+07] Eric R. Westervelt, Jessy W. Grizzle, Christine Chevallereau, Jun Ho Choi, and Benjamin Morris. *Feedback Control of Dynamic Bipedal Robot Locomotion*. CRC Press, 2007.

[WGE+16] Sebastian Wolf, Giorgio Grioli, Oliver Eiberger, Werner Friedl, Markus Grebenstein, Hannes Höppner, Etienne Burdet, Darwin G Caldwell, Raffaella Carloni, Manuel G Catalano, et al. Variable stiffness actuators: Review on design and components. *IEEE/ASME transactions on mechatronics*, 21(5):2418–2430, 2016.

[WGK03] Eric R Westervelt, Jessy W Grizzle, and Daniel E Koditschek. Hybrid zero dynamics of planar biped walkers. *IEEE transactions on automatic control*, 48(1):42–56, 2003.

[WH08] Sebastian Wolf and Gerd Hirzinger. A new variable stiffness design: Matching requirements of the next robot generation. In *Proc. IEEE Int. Conf. on Robotics and Automation*, 2008.

[WHI+00] H Witte, R Hackert, W Ilg, J Biltzinger, N Schilling, F Biedermann, M Jergas, H Preuschoft, MS Fischer, et al. Quadrupedal mammals as paragons for walking machines. In *Proceeding of the International Symposium on Adaptive Motion in Animals and Machines (AMAM), Montreal*, 2000.

[Wie06] Pierre-Brice Wieber. Trajectory free linear model predictive control for stable walking in the presence of strong perturbations. In *Proc. of IEEE/RAS Int. Conf. on Humanoid Robots*, 2006.

[YSIT99] Jin'ichi Yamaguchi, Eiji Soga, Sadatoshi Inoue, and Atsuo Takanishi. Development of a bipedal humanoid robot-control method of whole body cooperative dynamic biped walking. In *Robotics and Automation, 1999. Proceedings. 1999 IEEE International Conference on*, volume 1, pages 368–374. IEEE, 1999.

[ZDLS04] L. Zollo, A. De Luca, and B. Siciliano. Regulation with on-line gravity compensation for robots with elastic joints. In *Robotics and Automation, 2004. Proceedings. ICRA '04. 2004 IEEE International Conference on*, volume 3, pages 2687–2692, April 2004.

[Zei86] E. Zeidler. *Nonlinear Functional Analysis and its AApplication: Fixed-Point Theorems*, volume 1. Springer Science, 1986.